JAAVSO

Volume 41
Number 2
2013

The Journal of the American Association of Variable Star Observers

Discovery of Pulsating Components in Southern EB Systems

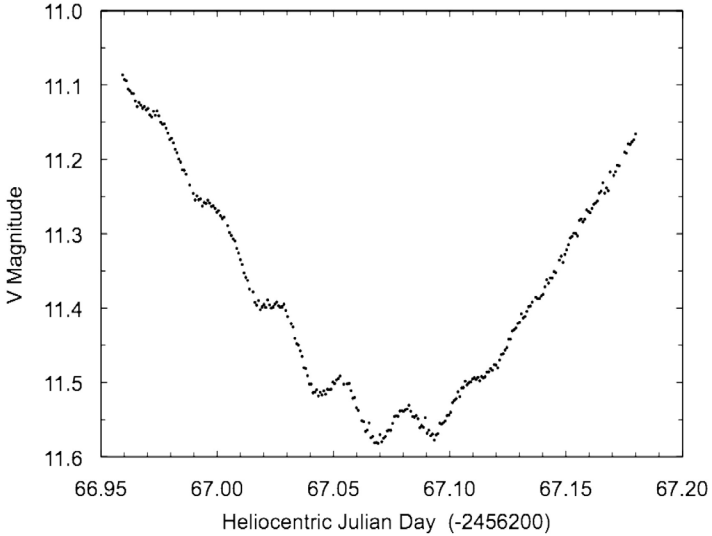

A primary eclipse of TT Hor with oscillations apparent in the descending phase and at the minimum of the eclipse

Also in this issue...

- The Naked-eye Optical Transient OT 120926
- Amplitude Variations in Pulsating Red Giants
- Comments on the UBV Photometric System's Defining Standard Stars

Complete table of contents inside...

THE AMERICAN ASSOCIATION OF VARIABLE STAR OBSERVERS
FOUNDED 1911

49 Bay State Road
Cambridge, MA 02138
U. S. A.

The Journal of the American Association of Variable Star Observers

ISSN 0271-9053

JAAVSO

The Journal of
The American Association
of Variable Star Observers

Volume 41
Number 2
2013

ISSN 0271-9053

49 Bay State Road
Cambridge, MA 02138
U. S. A.

The *Journal of the American Association of Variable Star Observers* is a refereed scientific journal published by the American Association of Variable Star Observers, 49 Bay State Road, Cambridge, Massachusetts 02138, USA. The *Journal* is made available to all AAVSO members and subscribers.

In order to speed the dissemination of scientific results, selected papers that have been refereed and accepted for publication in the *Journal* will be posted on the internet at the *eJAAVSO* website as soon as they have been typeset and edited. These electronic representations of the *JAAVSO* articles are automatically indexed and included in the NASA Astrophysics Data System (ADS). *eJAAVSO* papers may be referenced as *J. Amer. Assoc. Var. Star Obs., in press,* until they appear in the concatonated electronic issue of *JAAVSO*. The *Journal* cannot supply reprints of papers.

Page Charges

Unsolicited papers by non-Members will be assessed a charge of $15 per published page.

Instructions for Submissions

The *Journal* welcomes papers from all persons concerned with the study of variable stars and topics specifically related to variability. All manuscripts should be written in a style designed to provide clear expositions of the topic. Contributors are strongly encouraged to submit digitized text in MS WORD, LATEX+POSTSCRIPT, or plain-text format. Manuscripts may be mailed electronically to journal@aavso.org or submitted by postal mail to *JAAVSO*, 49 Bay State Road, Cambridge, MA 02138, USA.

Manuscripts must be submitted according to the following guidelines, or they will be returned to the author for correction:

Manuscripts must be:
1) original, unpublished material;
2) written in English;
3) accompanied by an abstract of no more than 100 words.
4) not more than 2,500–3,000 words in length (10–12 pages double-spaced).

Figures for publication must:
1) be camera-ready or in a high-contrast, high-resolution, standard digitized image format;
2) have all coordinates labeled with division marks on all four sides;
3) be accompanied by a caption that clearly explains all symbols and significance, so that the reader can understand the figure without reference to the text.

Maximum published figure space is 4.5" by 7". When submitting original figures, be sure to allow for reduction in size by making all symbols, letters, and division marks sufficiently large.

Photographs and halftone images will be considered for publication if they directly illustrate the text.

Tables should be:
1) provided separate from the main body of the text;
2) numbered sequentially and referred to by Arabic number in the text, e.g., Table 1.

References:
1) References should relate directly to the text.
2) References should be keyed into the text with the author's last name and the year of publication, e.g., (Smith 1974; Jones 1974) or Smith (1974) and Jones (1974).
3) In the case of three or more joint authors, the text reference should be written as follows: (Smith *et al.* 1976).
4) All references must be listed at the end of the text in alphabetical order by the author's last name and the year of publication, according to the following format:
   Brown, J., and Green, E. B. 1974, *Astrophys. J.*, **200**, 765.
   Thomas, K. 1982, *Phys. Rep.*, **33**, 96.
5) Abbreviations used in references should be based on recent issues of the Journal or the listing provided at the beginning of *Astronomy and Astrophysics Abstracts* (Springer-Verlag).

Miscellaneous:
1) Equations should be written on a separate line and given a sequential Arabic number in parentheses near the right-hand margin. Equations should be referred to in the text as, e.g., equation (1).
2) Magnitude will be assumed to be visual unless otherwise specified.
3) Manuscripts may be submitted to referees for review without obligation of publication.

Journal of the American Association of Variable Star Observers
Volume 41, Number 2, 2013

Table of Contents continued on following page

Editorial: The Unsung Heroes of the Scientific Publication Process—The Referees

John R. Percy, Editor, *Journal of the AAVSO*
Department of Astronomy and Astrophysics, University of Toronto, Toronto ON M5S 3H4, Canada; john.percy@utoronto.ca

You are aware (I hope) of the hard-working staff of this *Journal*—Production Editor Michael Saladyga (who does most of the work), Associate Editor Elizabeth Waagen and Assistant Editor Matthew Templeton, who review the submitted papers for general accuracy and from the perspective of the AAVSO and edit them for style, language, and content, and the less hard-working Editor (me). An Editorial Board provides sage advice from time to time. But there are several dozen others who make essential contributions to the publication process—the referees who read, consider, and assess every paper in this *Journal*, anonymously. For that reason, we do not list them here, but they are not unappreciated, or forgotten. The purpose of this editorial is to pay tribute and thanks to these people—almost a hundred since I became Editor.

Scientific journals are of many kinds. There are unrefereed, usually informal print or electronic publications which publish or post any appropriate material which they receive; the content may or may not be reliable. There are commercial journals whose main purpose is to make a profit—often by charging hefty subscription fees to libraries and/or page charges to authors. There are high-powered professional journals which publish papers by experts, for experts. There are prestigious general science journals such as *Nature* and *Science* which publish only a small fraction of all papers submitted.

This *Journal* is unusual in the sense that its authors are very diverse; they include professional astronomers and students, and the sort of skilled amateur astronomers who make and analyze variable star observations. The readers are even more diverse; they range from beginners to experts. Some readers complain that not all the papers are of interest to them but, since the *Journal* is on-line and open-access, readers can download and peruse any articles they want, and ignore the rest. But all the articles (we hope) have value to some readers—present or future.

The refereeing process must be both anonymous and confidential. In high-powered journals, especially in medical research, there are occasional cases in which the referee inadvertently or deliberately makes use of the content of a paper in their own work. Journals, and professional societies such as the American Astronomical Society have codes of ethics for their members, which deal with this and other issues (see, for example, http://aas.org/about/policies/aas-ethics-statement).

Refereeing isn't easy. In education, Bloom's Taxonomy is a way of classifying the depth of understanding of a topic. Evaluation is the highest level.

At least in academia, being asked to referee a paper is considered an honor, and counts for "Brownie points" at annual-report time. In sports, referees are usually called on to make a yes-or-no decision; in science, it is more complex. The referee must not only read and understand the paper, but they must also be able to provide useful, diplomatic, timely advice to the authors who, in the case of this *Journal*, may not be experienced at scientific publication. Our instructions to referees (http://www.aavso.org/instructions-referees-jaavso) are gentle and straightforward.

The ninety referees who have served us in the few years since I became Editor come from seventeen countries, on all continents except Antarctica. Most are professionals, but over ten percent are expert amateurs—one more illustration of the fact that amateurs can reach the status of "masters" in the field of variable star astronomy. The referees are chosen for both their expertise, and for their understanding of the special nature of this *Journal* and its readers and authors. Many are already associated with the AAVSO in some way. They are certainly kindred spirits.

Our referees play an essential role in maintaining the high scientific quality of the *Journal*, while providing guidance to a diverse authorship. On behalf of the AAVSO, the *Journal* staff, and the readers, I thank them, warmly and gratefully, for this important contribution.

Comments on the UBV Photometric System's Defining Standard Stars

Arlo U. Landolt
Department of Physics and Astronomy, Louisiana State University, Baton Rouge, LA 70803; landolt@phys.lsu.edu

Received August 2, 2013; accepted August 6, 2013

Abstract The purpose of this paper is to call the observing community's attention to the re-affirmation that a majority, 80 percent, of the basic UBV standard stars either are suspected or known variable stars. The elucidation of these stars' variability characteristics in exquisite detail is a task for which AAVSO observers are eminently qualified.

1. Introduction

The photometry portion of astronomy's observational community in particular is well aware of the fundamental nature of the UBV photometric system which was invented by Johnson and Morgan (1953) and Morgan (1988). A recent review of the UBV photometric system has appeared in Landolt (2011).

The basic steps in analyzing photometric data have been published in a number of places, including the well known books by Henden and Kaitchuck (1982, 1990) and Sterken and Manfroid (1992). Those books and other works in the astronomical literature, such as Landolt (2007), describe the use of stars of known magnitude and color to standardize data in a given observational program, thereby transforming the data onto a standard photometric system and enabling the inter-comparison of the photometric results with those of other observers as well as with theoretical models.

When one reduces all sky photometry, and accomplishes relative photometry, which is the kind of photometry that a vast majority of photometrists do, the results include the recovered magnitudes and color indices of the standard stars used in the processing. This author has wondered for years why the recovered standard star magnitudes and color errors for the stars defining the UBV photometric system (Johnson 1963) were larger than for the recovered errors when using, for example, standard star magnitudes from Cousins (1976), or from the author's papers (Landolt 1983, 1992, 2009).

Careful data acquisition and reduction techniques, over the past sixty years using photoelectric photometry techniques, and now CCDs, should provide photometric errors of data transformed to a standard photometric system, say, on the order of 0.005 magnitude. Such errors also were achievable through use of photoelectric photometers. However, the author's recovered photometry when

using the basic UBV standard stars normally featured errors more like 0.015 to 0.018 mangitude, or so. The exact numbers are not so important here. What is notable is that those errors are three to four times the size of achievable errors using Cousins and Landolt photoelectric photometer-based standard stars. The question, then, is why the difference in the size of the recoverable errors?

2. Stars omitted from original set

Johnson and Harris (1954) published the original set of 108 standard stars on the UBV photometric system. A final list of UBV standard stars was published by Johnson (1963), wherein he eliminated four stars: HR 753A, γ Tau, δ Tau, and α Lyr, without comment. The reasoning for their elimination from the original 108 UBV standard stars appears to be as indicated in the following paragraphs. Johnson (1963), in section 3, and Johnson and Iriarte (1959) do indicate that "some of the stars observed are more variable than others."

HR 753A: BD+06 398A, HD 16160, CCDM J02361+0653A, GJ 105 A, G73-70, 2MASS J02360498+0653140, UCAC4 485-003628, NLTT 8447; μ_α = 1807.8 ± 1.0 mas/yr, μ_δ = 1444.0 ± 1.0 mas/yr.

HR 753B: BD+06 398B, CCDM J02361+0653B, G73-71, GJ 105 B, NLTT 8455, BX Cet, variable of BY Dra type = 2MASS J02361535+0652191, UCAC4 485-003632; μ_α = 1813.0 ± 8.0 mas/yr, μ_δ = 1447.0 ± 8.0 mas/yr. Flare activity on HR 753B was predicted by Pettersen (1975) and remarked on by Petit (1980). Johnson's (1963) V magnitude differed from a V magnitude by Weistrop (1977) by 0.1 magnitude. Their (B–V) color index agreed well within their errors. The variability of HR 753B was announced by Weis (1994). The AAVSO database indicates a magnitude range 11.64 < V < 11.68.

It is interesting that Johnson retained HR 753B in his final publication of the UBV system (Johnson 1963), and not HR 753A. The latter appears to be constant in light, whereas HR 753B is not. Evidently Johnson's photometry did not convincingly show what is now known from the literature as a variation of a few percent for HR 753B through the V filter. The two stars appear in Giclas *et al.* (1961) as G 73-70 and G 73-71, with a separation of 2.8 arc minutes, and identified as a common proper motion pair. The stars' UCAC4 proper motions confirm that they are a common proper motion pair.

γ *Tauri*: 54 Tau, BD+15 612, HD 27371, CCDM J04198+1538AB, CSV 102439, NSV 1553, plus many names in SIMBAD. γ Tau is a double star whose components were separated by 0.4 arcsecond in position angle 179 degrees in 1979 (Dommanget and Nys (2002). Johnson and Harris (1954) were the first to identify the variability of the brighter component, γ Tau, of about 0.1 magnitude. The AAVSO archive indicates a range in V of 3.60–3.67 magnitudes.

δ *Tauri*: 61 Tau, BD+17 712A, HD 27697, CCDM J04229+1733A, CSV 102443, NSV 1582, plus many names in SIMBAD. δ Tau is a double star, the brighter component at V = 3.76, and the fainter at V = 12.6 magnitude.

The two stars were separated by 106.6 arcseconds, with a position angle of 341 degrees in 1909. Johnson and Harris (1954) were the first to identify the variability of the brighter component, δ Tau, of about 0.1 magnitude. The AAVSO archive indicates a range in V of 3.72–3.77 magnitudes.

α *Lyrae*: Vega, HR 7001, HD 172167, CSV 101745, NSV 11128, plus many more names via SIMBAD. α Lyr initially was reported as a variable star by Guthnick and Prager (1915), of the "δ Cephei-type." No individual data points were provided, other than to say that the amplitude of light variation was "on average" 0.04 magnitude, and that the period was short. Further note of the discovery appeared in the annual report of the Berlin-Babelsberg Observatory for 1915 (Struve 1916) and in Guthnick and Prager (1918). Photoelectric data were published by Johnson (Johnson *et al.* 1966) which indicated a total variation through the V filter of 0.129 magnitude. A periodic variation of 0.19 day in the radial velocity of α Lyr was reported by Belopolsky (1931), and was confirmed by Beardsley and Zizka (1980). The variation also was noted in Breger (1979). Note, though, that Neubauer and Farnsworth (1935) disputed the reported radial velocity variation.

3. The tables

Tables 1 and 2 contain the 104 UBV standard stars as published in a final form (Johnson 1963). Table 1 contains the ten primary UBV standard stars, and Table 2 lists the remaining original UBV standard stars, for a total of 104 stars. Information describing the many acronyms identifying a given star and the star catalogues in which useful information appears is provided in Appendix 1.

The first column in each table gives the star's HD number, while the second column provides the star's name by constellation, or HR, or BD, or Flamsteed number. Column three lists the star name from the UCAC4 catalogue (Zacharias *et al.* 2013). The fourth column provides a NSV identification (Kholopov *et al.* 1982) for stars suspected of variability. Columns five and six contain the Johnson V magnitude and B–V color index taken from Tables 1 and 2 (Johnson 1963). Columns seven and eight contain the J2000.0 right ascension and declinations from the UCAC4 catalogue (Zacharias *et al.* 2013), followed by columns nine through twelve which provide the proper motions and their errors in milli-arcseconds per year, also taken from the UCAC4 catlaogue. The last column indicates the presence of a footnote to the table containing a literature reference and/or additional comments pertaining to the star. The UCAC4 coordinates are the most recent highly accurate coordinates. A considerable number of these bright stars have large proper motions, and hence the proper motions given in columns nine through twelve will aid in centering these stars' positions for observing purposes.

The author went star by star through the tables, looking at each star's record in SIMBAD, in the AAVSO's VSX database, and elsewhere in the

literature, to determine whether there was information about that star's possible variability. The last columnn in both tables provides, via the footnotes for the tables, literature and variability information, the latter primarily via the NSV identification. One star, HD 47105, γ Gem, is listed as a spectroscopic binary, but nothing was found regarding its possible variability.

Eight of the ten primary UBV standard stars in Table 1 are variable. Seventy-five of the ninety-four UBV standard stars in Table 2 are variable. Hence, there are eighty-three variable stars among the 104 stars which define the UBV photometric standard star system. To put it another way, 80% of the stars which define the UBV photometric system now are known to be, or are suspected of being, variable in light.

4. A call for observations

The defining stars of the UBV photometric system are bright. Therefore, essentially only amateur astronomers have the equipment available to monitor these stars without saturating the images. Since modern light curves are not available, and in many instances light curves may not exist at all, here is an opportunity for careful observers to observe, preferably with a V filter, these variable and suspected stars over a time interval sufficiently long to obtain definitive light curves. Any observational effort for a given star should last long enough to thoroughly define the light curve, complete with a period (unless it becomes obvious that the star possesses non-periodic behavior). The observer's *goal* should be to reach both a precision and an accuracy of 0.001 magnitude in order to best understand these low amplitude variable stars. It must be emphasized that an undertaking of a study of these stars presupposes the greatest possible care and skill by the observer, for the suspected light variations are small, nearing the level of detectability, from ground-based observatories. Such attention to detail means that the observer must account for extinction effects, properly transform the data, and so on. Finally, the observer needs to be cognizant that variations are "suspected," remaining to be convincingly proven.

As the observer prepares to observe these stars, it is good to recall that the AAVSO's International Variable Star Index (VSX) database (www.aavso.org/vsx) is an excellent starting place for a wealth of information for these and other variable stars. The VSX database indicates the range in magnitude for many of the known or suspected variable stars, although the source of the information is not always clear. Tables 1 and 2 herein list the V magnitude and the (B–V) color index as aids in planning an observational program. Spectral types and the range in the known or suspected light variation is given in the footnotes. This information came from the VSX database, or from SIMBAD, if missing in the VSX database. The SIMBAD Astronomical Database (www.simbad.u-strasbg.fr/simbad) leads one to the majority of the modern literature for a given star.

Interpretation of one's data can be aided through reference to books, ordered by date of publication, such as those by Sterken and Jaschek (1996), Warner (2006), and Percy (2007). An explanation of the spectral type nomenclature may be found in Drilling and Landolt (1999).

It is to be noted that the MOST Microsatellite (Microvariability and Oscillations of STars) already has provided exquisite data for several of these stars (http://www.utias-sfl.net/microsatellites/MOST/)!

An obvious place to publish these definitive light curves, including the individual data points together with the heliocentric Julian Day for the observation(s)—such complete publication a highly desired *must*—is in the *Journal of the American Association of Variable Star Observers* (*JAAVSO*)!

5. Summary

This paper has shown that the majority of the original 104 UBV standard stars, 80 percent, either are known or suspected variable stars. The vast majority of these stars are very bright, many visible to the naked eye. Few modern observers have the capability of observing such bright stars, but most AAVSO observers do have such capabilities. Very, very careful and accurate light curves, appropriately defined by a Johnson V filter, at the minimum, are achievable by AAVSO observers. Such accurate and long-term studies of the light variations of these important stars would be of great value to the astronomical community.

6. Acknowledgements

The author extends his thanks to Elizabeth O. Waagen at AAVSO Headquarters for answering various questions, and to Brian Skiff for his limitless knowledge of the behavior of various stars and of their astronomical literature, and to Michael Saladyga for his counsel and editing efforts with the references. Karen Richard did the tedious job of LaTexing, for which the author is grateful! The author thanks the referee whose report added to the usefulness of the paper.

The author has been funded by NSF grant AST0803158.

This research has made use of the VizieR catalogue access service and of the SIMBAD database, both at CDS, Strasbourg, France. The original description of the VizieR service was published in *Astronomy and Astrophysics, Supplement Series*, 143, 23 (2000).

References

Aitken, R. G. 1932, *New General Catalogue of Double Stars Within 120° of the North Pole*, Publication 417, Carnegie Institution of Washington, Washington, DC.

Alfonso-Garzon, Domingo, J. A., Mas-Hesse, J. M., and Gimenez, A. 2012, arXiv:1210.0821.

Anon. 1879, *Observatory*, **2**, 420.

Anon. (G. Jackisch). 1958, *Sky & Telescope*, **18**, 73.

Argelander, F. W. A., Schönfeld, E., and Krüger, A. 1859, *Astronomische Beobachtungen auf der Sternwarte der Koeniglichen Rheinischen Freidrich-Wilhelms-Universitat zu Bonn*, *Bonner Sternverzeichnis (Bonner Durchmusterung),* volume 3 (–01 deg to +19 deg), A. Marcus und E. Weber's Verlag, Bonn.

Argelander, F. W. A., Schönfeld, E., and Krüger, A. 1861, *Astronomische Beobachtungen auf der Sternwarte der Koeniglichen Rheinischen Freidrich-Wilhelms-Universitat zu Bonn*, *Bonner Sternverzeichnis (Bonner Durchmusterung),* volume 4 (+20 deg to +40 deg), A. Marcus und E. Weber's Verlag, Bonn.

Argelander, F. W. A., Schönfeld, E., and Krüger, A. 1862, *Astronomische Beobachtungen auf der Sternwarte der Koeniglichen Rheinischen Freidrich-Wilhelms-Universitat zu Bonn*, *Bonner Sternverzeichnis (Bonner Durchmusterung),* volume 5 (+41 deg to +90 deg), A. Marcus und E. Weber's Verlag, Bonn.

Auwers, A. 1859, *Astron. Nachr.*, **50**, 99.

Baize, P. 1962, *J. Obs.*, **45**, 117.

Balona, L. A., and Engelbrecht, C. A. 1985, *Mon. Not. Roy. Astron. Soc.*, **214**, 559.

Bartolini, C., Dapergolas, A., and Piccioni, A. 1981, *Inf. Bull. Var. Stars*, No. 2010, 1.

Beardsley, W. R., Gatewood, G., and Kamper, K. W. 1974, *Astrophys. J.*, **194**, 637.

Beardsley, W. R., and Zizka, E. R. 1980, in *Current Problems in Stellar Pulsation Instabilities*, ed, D. Fischel, J. R. Lesh, and W. M. Sparks, NASA TM-80625, Astronomisches Rechen-Institut, Heidelberg, 421.

Belopolsky, A. 1931, *Z. Astrophys.*, **2**, 245.

Benedict, G. F. , *et al.* 1998, *Astron. J.*, **116**, 429.

Breger, M. 1979, *Publ. Astron. Soc. Pacific*, **91**, 5.

Buzasi, D. L., *et al.* 2005, *Astrophys. J.*, **619**, 1072.

Corben, P. M., Carter, B. S., Banfield, R. M., and Harvey, G. M. 1972, *Mon. Not. Astron. Soc. S. Afr.*, **31**, 7.

Cousins, A. W. J. 1966, *Roy. Obs. Bull., Ser. E*, No. 122, 59.

Cousins, A. W. J. 1976, *Mem. Roy. Astron. Soc.*, **81**, 25.

Cousins, A. W. J. 1980, *S. Afr. Astron. Obs. Circ.*, **1**, 234.

Cousins, A. W. J., and Stoy, H. R. 1962, *Roy. Obs. Bull.*, No. 64, 103.

Cutri, R. M., *et al.* 2003, *2MASS All-Sky Catalog of Point Sources*, VizieR Online Data Catalog, II/246.

Delgado, A. J., and Garrido, R. 1981, *Inf. Bull. Var. Stars*, No. 1992, 1.

Desmet, M., *et al.* 2009, in *Stellar Pulsation: Challenges for Theory and Observation*, AIP Conf. Proc. 1170, American Institute of Physics, Melville, NY, 376.

Dommanget, J., and Nys, O. 1994, *Commun. Obs. Roy. Belg.*, **115**, 1.
Dommanget, J., and Nys, O. 2002, *Catalog of components of Double and Multiple Stars* (CCDM), VizieR Online Data Catalog, I/274.
Drilling, J. S., and Landolt, A. U. 1999, in *Allen's Astrophysical Quantities*, 4th ed., ed. A. N. Cox, AIP Press, Springer-Verlag, New York, 381.
Durrant, C. J. 1970, *Mon. Not. Roy. Astron. Soc.*, **147**, 75.
Elst, E. W. 1979, *Inf. Bull. Var. Stars*, No. 1562, 1.
Engels, D., Sherwood, W. A., Wamsteker, W., and Schultz, G. V. 1981, *Astron. Astrophys, Suppl. Ser.*, **45**, 5.
FitzGerald, M. P. 1973, *Astron. Astrophys., Suppl. Ser.*, **9**, 297.
Fracastoro, G. M., and Catalano, S. 1965. *Mem. Soc. Astron. Ital.*, **36**, 99.
Frey, G. J., Hall, D. S., Mattingly, P., Robb, S., Wood, J., Zeigler, K., and Grim, B. 1991, *Astron. J.*, **102**, 1813.
Frolov, M. S. 1970, *Inf. Bull. Var. Stars*, No. 427, 1.
Giclas, H. L., Burnham, R., Jr., and Thomas, N. G. 1961, *Lowell Obs. Bull.*, **5**, 61.
Giclas, H. L., Burnham, R., Jr., and Thomas, N. G. 1971, *Lowell Proper Motion Survey Northern Hemisphere: The G Numbered Stars*, Lowell Observatory, Flagstaff, AZ.
Giclas, H. L., Burnham, R., Jr., and Thomas, N. G., 1978, *Lowell Obs. Bull.*, **8**, 89.
Giclas, H. L., Burnham, R., Jr., and Thomas, N. G. 1980, *Lowell Obs. Bull.*, **8**, 157.
Gliese, W., and Jahreiss, H. 1979, *Astron. Astrophys., Suppl. Ser.*, **38**, 423.
Golay, M. 1973, in *Problems of Calibration of Absolute Magnitudes and Temperature of Stars*, IAU Symp. 54, Reidel, Dordrecht, 275.
Gore, J. E. 1884, *Proc. Roy. Irish Acad. (II)*, **4**, 267.
Gould, B. A. 1879, *Resultados del Observatorio Nacional Argentino en Cordoba*, **1**, 1.
Gray, D. F., Baliunas, S. L., Lockwood, G. W., and Skiff, B. A. 1996, *Astrophys. J.*, **456**, 365.
Gray, R. O., *et al.* 2006, *Astron. J.*, **132**, 161.
Guthnick, P. 1917, *Astron. Nachr.*, **205**, 97.
Guthnick, P., and Pavel, F. 1922, *Astron. Nachr.*, **215**, 395.
Guthnick, P., and Prager, R. 1915, *Astron. Nachr.*, **201**, 443.
Guthnick, P., and Prager, R. 1918, *Veroff. K. Sternw. Berlin-Babelsberg*, **2**, No. 3, 1 (see pages 91, 112, 114, 116).
Gutierrez–Moreno, A., Moreno, H., Stock, J., Torres, C., and Wroblewski, H. 1966, *Cerro Tololo Inter–Amer. Obs. Contrib.*, No. 9, 1.
Gutierrez-Moreno, A., Moreno, H., Stock, J., Torres, C., and Wroblewski, H. 1966, *Publ. Obs. Astron. Natl. Cerro Calan*, No. 1, 1.
Handler, G. *et al.* 2009, *Astrophys. J., Lett.*, **698**, L56.
Heck, A. 1977, *Astron. Astrophys., Suppl. Ser.*, **27**, 47.
Heintz, W. D. 1984, *Publ. Astron. Soc. Pacific*, **96**, 557.
Henden, A. A., and Kaitchuck, R. H. 1982, *Astronomical Photometry*, Van Nostrand Reinhold, New York.

Henden, A. A., and Kaitchuck, R. H. 1990, *Astronomical Photometry*, Willmann-Bell, Richmond, VA.

Herschel, J. F. W. 1847, *Results of astronomical observations made during the years 1834, 5, 6, 7, 8, at the Cape of Good Hope; being the completion of a telescopic survey of the whole surface of the visible heavens, commenced in 1825*, Smith, Elder and Co., London, pages 341, 343, 349, 350.

Hill, G. , Morris, S. C., and Walker, G. A. H. 1971, *Astron. J.*, **76**, 246.

Hiltner, W. A. 1954, *Astrophys. J.*, **120**, 41.

Hoffleit, D., and Jaschek, C. 1982, *The Bright Star Catlaogue*, 4th ed., Yale Univ. Observatory, New Haven.

Jackisch, G. 1963, *Veroff. Sternw. Sonneberg*, **5**, 227.

Jeffers, H. M., van den Bos, W. H., and Greeby, F. M. 1963, *Publ. Lick Obs.*, **21**, 1.

Johnson, H. L. 1963, in *Basic Astronomical Data*, ed. K. Aa. Strand, Univ. Chicago Press, Chicago, 204.

Johnson, H. L., and Harris, III, D. L. 1954, *Astrophys. J.*, **120**, 196.

Johnson, H. L., and Iriarte, B. 1959, *Lowell Obs. Bull.*, **4**, 99.

Johnson, H. L., Mitchell, R. I., Iriarte, B., and Wisniewski, W. Z. 1966, *Commun. Lunar Planet. Lab.*, No. 63, 33.

Johnson, H. L., and Morgan, W. W. 1953, *Astrophys. J.*, **117**, 313.

Kholopov, P. N., *et al.* 1982, *New Catalogue of Suspected Variable Stars* (NSV), Moscow.

Kiraga, M., and Stepien, K. 2007, *Acta Astron.*, **57**, 149.

Koen, C., and Eyer, L. 2002, *Mon. Not. Roy. Astron. Soc.*, **331**, 45.

Kornilov, V. G., *et al.* 1991, *Tr. Gos. Astron. Inst. Sternberg*, **63**, 1 (see page 3).

Kron, G. E., Guetter, H. H., and Riepe, B. Y. 1972, *Publ. U.S. Naval Obs., Second Ser.*, **20**, Part 5 (pages 54 and 70).

Kukarkin, B. V., Kholopov, P. N., Efremov, Y. N., and Kurochkin, N. E. 1965, in *Second Catalogue of Suspected Variable Stars* (CSV; star nos. 102300–103137), Acad. Sci., USSR and Sternberg State Astron. Inst., Moscow.

Kukarkin, B. V., Parenago, P. P., Efremov, Y. N., and Kholopov, P. N. 1951, in *Catalogue of Suspected Variables* (CSV; star nos. 100000–102299), Acad. Sci., USSR and Sternberg State Astron. Inst., Moscow.

Kusakin, A. V. 1992, manuscript only, see AAVSO VSX database.

Landolt, A. U. 1983, *Astron. J.*, **88**, 439.

Landolt, A. U. 1992, *Astron. J.*, **104**, 340.

Landolt, A. U. 2007, in *The Future of Photometric, Spectrophotometric, and Polarimetric Standardization*, ed. C. Sterken, ASP Conf. Ser. 364, Astron. Soc. Pacific, San Francisco, 27.

Landolt, A. U. 2009, *Astron. J.*, **137**, 4186.

Landolt, A. U. 2011, in *Astronomical Photometry: Past, Present and Future*, eds. E. F. Milone and C. Sterken, Astrophysics Space Science Library 373, Springer, Berlin, 107.

Larsson-Leander, G. 1959, *Ark. Astron.*, **2**, 283.

Lau, H. E. 1914, *Astron. Nachr.*, **196**, 425.
Lub, J., and Pel, J. W. 1977, *Astron. Astrophys.*, **54**, 137.
Luyten, W. J. 1963, in *Basic Astronomical Data*, ed. K. Aa. Strand, Univ. Chicago Press, Chicago, 46.
Luyten, W. J. 1976, *A Catalogue of 1849 Stars with Proper Motions greater than 0.5" annually* (LHS), Univ. Minnesota, Minneapolis.
Luyten, W. J. 1979a, *LHS Catalogue*, 2nd ed., Univ. Minnesota, Minneapolis.
Luyten, W. J. 1979b, *New Luyten Catalogue of Stars with Proper Motions Larger than Two Tenths of an Arcsecond* (NLTT), vol. 1, Univ. Minnesota, Minneapolis.
Luyten, W. J. 1979c, *New Luyten Catalogue of Stars with Proper Motions Larger than Two Tenths of an Arcsecond* (NLTT), vol. 2, Univ. Minnesota, Minneapolis.
Luyten, W. J. 1980a, *New Luyten Catalogue of Stars with Proper Motions Larger than Two Tenths of an Arcsecond* (NLTT), vol. 3, Univ. Minnesota, Minneapolis.
Luyten, W. J. 1980b, *New Luyten Catalogue of Stars with Proper Motions Larger than Two Tenths of an Arcsecond* (NLTT), vol. 4, Univ. Minnesota, Minneapolis.
Luyten, W. J., and Hughes, H. S. 1980, *Proper Motion Survey with the Forty-Eight Inch Schmidt Telescope LV. First Supplement to the NLTT Catalogue*, Univ. Minnesota, Minneapolis.
Lynds, C. R. 1959, *Astrophys. J.*, **130**, 577.
Mathys, G., and Manfroid, J. 1985, *Astron. Astrophys., Suppl. Ser.*, **60**, 17.
Monnier, J. D., Townsend, R. H. D., Che, X., Zhao, M., Kallinger, T., Matthews, J., and Moffat, A. F. J. 2010, *Astrophys. J.*, **725**, 1192.
Moreno, H. 1971, *Astron. Astrophys.*, **12**, 442.
Morgan, W. W. 1988, *Ann. Rev. Astron. Astrophys.*, **26**, 1.
Neubauer, F. J., and Farnsworth, A. H. 1935, *Lick Obs. Bul.*, **17**, 109.
Olsen, E. H. 1974, *Inf. Bull. Var. Stars*, No. 925, 1.
Percy, J. R. 2007, *Understanding Variable Stars*, Cambridge Univ. Press, Cambridge.
Perryman, M. A. C., European Space Agency Space Science Department, and the Hipparcos Science Team. 1997, *The Hipparcos and Tycho Catalogues*, ESA SP-1200 (VizieR On-line Data Catalog: I/239), ESA Publications Division, Noordwijk, The Netherlands.
Petit, M. 1968, *Inf. Bull. Var. Stars*, No. 320, 1.
Petit, M. 1975, *Inf. Bull. Var. Stars*, No. 1056, 1.
Petit, M. 1980, *Inf. Bull. Var. Stars*, No. 1788, 1.
Petit, M. 1990, *Astron. Astrophys., Suppl. Ser.*, **85**, 971.
Pettersen, B. R. 1975, *Astron. Astrophys.*, **41**, 87.
Pojmański, G. 2002, *Acta Astron.*, **52**, 397.
Rufener, F. 1976, *Astron. Astrophys., Suppl. Ser.*, **26**, 275.

Rufener, F. 1981, *Astron. Astrophys., Suppl. Ser.*, **45**, 207
Rufener, F., and Bartholdi, P. 1982, *Astron. Astrophys., Suppl. Ser.*, **48**, 503.
Schmidt, J. F. J. 1858, *Astron. Nachr.*, **47**, 312.
Schönfeld, E., 1886, *Astronomische Beobachtungen auf der Sternwarte der Koeniglichen Rheinischen Freidrich-Wilhelms-Universitat zu Bonn*, *Bonner Sternverzeichnis (Sudliche Bonner Durchmusterung),* volume 8 (–02 deg to –22 deg), Adolph Marcus, Bonn.
Shapley, H. 1914, *Astron. Nachr.*, **196**, 398.
Skiff, B., and Lockwood, W. 1986, *Publ. Astron. Soc. Pacific*, **98**, 338.
Skrutskie, M. F., *et al.* 2006, *Astron. J.*, **131**, 1163.
Sterken, C., and Jaschek, C. 1996, *Light Curves of Variable Stars, A Pictorial Atlas*, Cambridge Univ. Press, Cambridge.
Sterken, C., and Manfroid, J. 1992, *Astronomical Photometry: A Guide*, Springer-Verlag, Berlin.
Struve, H. 1916, *Vierteljahrsschr. Astron. Ges.*, **51**, 79.
Taylor, B. J., and Joner, M. D. 1992, *Publ. Astron. Soc. Pacific*, **104**, 911.
Tempesti, P., and Patriarca, R. 1976, *Inf. Bull. Var. Stars*, No. 1164, 1.
van Belle, G. T., and von Braun, K. 2009, *Astrophys. J.*, **694**, 1085.
Vogt, S. S., and Penrod, G. D. 1983, *Astrophys. J.*, **275**, 661.
Warner, B. D. 2006, *A Practical Guide to Lightcurve Photometry and Analysis*, Springer Science + Business Media, New York.
Warren, W. H., Jr., and Hesser, J. E. 1977, *Astrophys. J., Suppl. Ser.*, **34**, 115.
Watson, C., Henden, A. A., and Price, A. 2013, AAVSO International Variable Star Index VSX (Watson+, 2006–2013; http://www.aavso.org/vsx).
Weber, R. 1958, *J. Obs.*, **41**, 74.
Weis, E. W. 1994, *Astron. J.*, **107**, 1135.
Weistrop, D. 1977, *Astrophys. J.*, **215**, 845.
Widorn, T. 1959, *Mitt. Univ. Sternw. Wien*, **10**, 3.
Wood, F. B. 1946, *Princeton Obs. Contrib.*, No. 21, 1.
Wylie, C. C. 1922, *Astrophys. J.*, **56**, 217.
Zacharias, N., Finch, C. T., Girard, T. M., Henden, A., Bartlett, J. L., Monet, D. G., and Zacharias, M. I. 2013, *Astron. J.*, **145**, 44.
Zinner, E. 1929, *Astron. Abh., Erganzungshefte zu den Astron. Nachr.*, **8**, No. 1, 1.
Zverev, M. S. 1936, *Tr. Gos. Astron. Inst. Shternberg*, **8**, No. 1, pages 90, 150.

Table 1. The ten primary standard stars of the UBV system.

HD (1)	*Name* (2)	*UCAC4* (3)	*NSV* (4)	*V* (5)	*B–V* (6)	*R.A. (J2000.0)* (7) *h m s*	*Dec. (J2000.0)* (8) ° ′ ″	*pm/a* (9)	*e/a* (10)	*pm/d* (11)	*e/d* (12)	*Note* (13)
12929	α Ari	568–004324	725	2.00	+1.15	02 07 10.407	+23 27 44.71	191.0	1.0	–147.1	1.0	note, ref.
18331	HR 875	432–003634	—	5.17	+0.08	02 56 37.424	–03 42 44.36	–36.6	1.0	–44.2	1.0	
69267	β Cnc	496–050763	3973	3.52	+1.48	08 16 30.921	+09 11 07.96	–46.8	1.0	–49.3	1.0	ref.
74280	η Hya	467–040291	4212	4.30	–0.20	08 43 13.476	+03 23 55.18	–18.5	1.0	–1.5	1.0	note, ref.
135742	β Lib	404–059971	7009	2.61	–0.11	15 17 00.414	–09 22 58.50	–97.6	1.0	–20.0	1.0	note, ref.
140573	α Ser	483–060001	20391	2.65	+1.17	15 44 16.074	+06 25 32.26	133.8	1.0	44.8	1.0	note, ref.
143107	ε CrB	585–052496	—	4.15	+1.23	15 57 35.251	+26 52 40.36	–77.1	1.0	–60.6	1.0	
147394	τ Her	682–056339	7641	3.89	–0.15	16 19 44.437	+46 18 48.11	–13.3	1.0	38.5	1.0	note, ref.
214680	10 Lac	646–115008	25932	4.88	–0.20	22 39 15.679	+39 03 00.98	–0.3	1.0	–5.0	1.0	note, ref.
219134	HR 8832	736–099538	14458	5.57	+1.01	23 13 16.976	+57 10 06.08	2075.0	1.0	294.7	1.0	note, ref.

Notes:

HD 12929: H. Moreno, Astron. Astrophys.*, 12, 442, 1971 (only says possible variable, no numbers); B. A.Gould,* Resultados del Observatorio Nacional Argentino en Cordoba*, 1, 1, 1879 (see pages 128–342); K2 IIIab; 1.98 < V < 2.04.*

HD 69267: A. Gutierrez–Moreno et al., Cerro Tololo Inter–Amer. Obs. Contrib.*, No. 9, 1966; also see M. P. FitzGerald,* Astron. Astrophys., Suppl. Ser.*, 9, 297, 1973; K4 III; 3.53 (0.005)V.*

HD 74280: variable star of β *Cep type; E. W. Elst,* Inf. Bull. Var. Stars*, No. 1562, 1, 1979; B3 V; 4.27 < V < 4.33.*

HD 135742: M. Golay, IAU Symp. No. 54, 275, 1973; B8 V; 2.60 < V < 2.63.

HD 140573: in double system; variable type, SR; magnitude range 0.2 magnitude; microvariable in V? via F. Rufener, Astron. Astrophys., Suppl. Ser.*. 45, 207, 1981; also, M. Petit,* Inf. Bull. Var. Stars*, No. 1788, 1980; K2 IIIe; 2.64 (0.2)V.*

HD 147394: variable type SPB; Perryman, M. A. C. et al., The Hipparcos and Tycho Ctalogues*, ESA SP–1200, European Space Agency, 1997; B5 IV; 3.83 < V < 3.86.*

HD 214680: HR 8622; variability discovered by A. J. Delgado and R. Garrido, Inf. Bull. Var. Stars*, No. 1992, 1981; variability verified by B. J. Taylor and M. D. Joner,* Publ. Astron. Soc. Pacific*; 104, 911, 1992;* O9 V; 4.86 (0.03)B.

HR 8832: flare star; H. Moreno, Astron. Astrophys.*, 12, 442, 1971; also, W. A. Hiltner,* Astrophys. J.*, 120, 41, 1954 (suggests that HR 8832 might be variable by 0.02 magnitude); K3; 5.52 < V < 5.61.*

Table 2. The photometric standards of the UBV system.

HD (1)	Name (2)	UCAC4 (3)	NSV (4)	V (5)	B–V (6)	R.A. (J2000.0) (7) h m s	Dec. (J2000.0) (8) ° ′ ″	pm/a (9)	e/a (10)	pm/d (11)	e/d (12)	Note (13)
886	γ Peg	526–000414	—	2.83	–0.23	00 13 14.151	+15 11 00.94	1.9	1.0	–9.4	1.0	note, ref.
1280	θ And	644–001051	116	4.61	+0.06	00 17 05.499	+38 40 53.89	–49.4	1.0	–17.7	1.0	note, ref.
4727	ν And	656–003126	15178	4.53	–0.15	00 49 48.847	+41 04 44.08	22.8	1.0	–18.4	1.0	note, ref.
6961	θ Cas	726–010067	423	4.33	+0.17	01 11 06.162	+55 08 59.65	226.8	1.0	–18.8	1.0	note, ref.
8538	δ Cas	752–016413	—	2.68	+0.13	01 25 48.952	+60 14 07.02	296.6	1.0	–49.6	1.0	note, ref.
9270	η Psc	527–002693	532	3.62	+0.97	01 31 29.042	+15 20 45.41	25.7	1.0	–3.3	1.0	note, ref.
10476	107 Psc	552–003413	600	5.23	+0.83	01 42 29.762	+20 16 06.60	–302.4	1.0	–678.9	1.0	note, ref.
10700	τ Cet	371–001883	15373	3.50	+0.72	01 44 04.084	–15 56 14.92	–1720.5	1.0	855.3	1.0	note, ref.
11636	β Ari	555–003766	658	2.65	+0.13	01 54 38.411	+20 48 28.91	98.7	1.0	–110.4	1.0	note, ref.
—	–18 359	362–002344	15436	10.18	+1.53	02 05 04.814	–17 36 52.61	1317.5	8.0	–173.9	8.0	note, ref.
—	+2 348	468–002996	—	10.03	+1.44	02 12 20.917	+03 34 31.11	–1761.1	8.0	1852.8	8.0	
15318	ξ^2 Cet	493–003597	—	4.28	–0.06	02 28 09.543	+08 27 36.20	41.8	1.0	–13.6	1.0	
—	HR 753B	485–003632	—	11.65	+1.61	02 36 15.344	+06 52 18.99	1813.0	8.0	1447.0	8.0	note, ref.
20630	κ Cet	467–004501	1100	4.82	+0.68	03 19 21.697	+03 22 12.71	270.5	1.0	93.7	1.0	note, ref.
21120	ο Tau	496–005017	1134	3.59	+0.89	03 24 48.798	+09 01 43.95	–67.0	1.0	–78.0	1.0	note, ref.
21447	HR 1046	728–028717	1159	5.08	+0.05	03 30 00.183	+55 27 06.52	–46.1	1.0	–11.1	1.0	note, ref.
22049	ε Eri	403–004235	—	3.73	+0.89	03 32 55.845	–09 27 29.73	–975.2	1.0	19.5	1.0	note, ref.
28305	ε Tau	546–009607	—	3.54	+1.02	04 28 37.000	+19 10 49.56	108.0	1.0	–36.2	1.0	
30652	π^3 Ori	485–008472	1731	3.19	+0.45	04 49 50.411	+06 57 40.60	464.7	1.0	12.0	1.0	note, ref.
30836	π^4 Ori	479–008295	1742	3.69	–0.17	04 51 12.365	+05 36 18.37	–2.2	1.0	0.8	1.0	note, ref.

Table continued on following pages

Table 2. The photometric standards of the UBV system, cont.

HD (1)	Name (2)	UCAC4 (3)	NSV (4)	V (5)	B–V (6)	R.A. (J2000.0) (7) h m s	Dec. (J2000.0) (8) ° ′ ″	pm/a (9)	e/a (10)	pm/d (11)	e/d (12)	Note (13)
32630	η Aur	657–029789	1822	3.17	–0.18	05 06 30.892	+41 14 04.11	30.2	1.0	–68.3	1.0	note, ref.
33111	β Eri	425–008420	1841	2.80	+0.13	05 07 50.980	–05 05 11.25	–92.9	1.0	–80.4	1.0	note, ref.
35299	–0 936	450–010142	16300	5.70	–0.22	05 23 42.310	–00 09 35.35	2.1	1.0	–2.6	1.0	note, ref.
35468	γ Ori	482–011583	1972	1.64	–0.23	05 25 07.863	+06 20 58.94	–8.2	1.0	–12.2	1.0	note, ref.
35497	β Tau	594–018583	—	1.65	–0.13	05 26 17.513	+28 36 26.83	22.7	1.0	–173.6	1.0	note
36395	–3 1123	432–009930	2075	7.97	+1.47	05 31 27.396	–03 40 38.03	761.9	1.0	–2093.6	1.0	note, ref.
36512	υ Ori	414–009336	16333	4.63	–0.26	05 31 55.860	–07 18 05.54	–0.1	1.0	–4.9	1.0	note, ref.
36591	–1 935	443–010496	2107	5.35	–0.20	05 32 41.353	–01 35 30.59	–2.0	1.0	0.8	1.0	note, ref.
37043	ι Ori	421–010083	—	2.77	–0.25	05 35 25.982	–05 54 35.64	1.4	1.0	–0.5	1.0	note
37128	ε Ori	444–010753	—	1.70	–0.19	05 36 12.813	–01 12 06.92	1.4	1.0	–1.5	1.0	note, ref.
38678	ζ Lep	376–009566	—	3.55	+0.10	05 46 57.341	–14 49 19.02	–15.0	1.0	–0.6	1.0	
38899	134 Tau	514–015191	—	4.90	–0.07	05 49 32.930	+12 39 04.76	–23.0	1.0	–18.2	1.0	note
—	+17 1320	538–030603	—	9.63	+1.50	06 37 10.739	+17 33 53.61	–775.5	8.0	331.8	8.0	
47105	γ Gem	532–029305	—	1.93	0.00	06 37 42.711	+16 23 57.41	13.8	1.0	–54.9	1.0	note
—	+5 1668	477–036219	—	9.82	+1.56	07 27 24.506	+05 13 32.14	571.3	8.0	–3694.3	8.0	
56537	λ Gem	533–040057	3512	3.58	+0.11	07 18 05.580	+16 32 25.39	–44.5	1.0	–36.6	1.0	note, ref.
58946	ρ Gem	609–039674	17482	4.16	+0.32	07 29 06.719	+31 47 04.38	159.1	1.0	193.3	1.0	note, ref.
62345	κ Gem	572–041547	—	3.57	+0.93	07 44 26.854	+24 23 52.79	–23.4	1.0	–54.6	1.0	
71155	HR 3314	431–046612	17882	3.90	–0.02	08 25 39.632	–03 54 23.12	–66.6	1.0	–23.5	1.0	note, ref.
76644	ι UMa	691–048807	4329	3.14	+0.18	08 59 12.454	+48 02 30.58	–441.3	1.0	–215.3	1.0	note, ref.

Table continued on following pages

Table 2. The photometric standards of the UBV system, cont.

HD (1)	Name (2)	UCAC4 (3)	NSV (4)	V (5)	B–V (6)	R.A. (J2000.0) (7) h m s	Dec. (J2000.0) (8) ° ′ ″	pm/a (9)	e/a (10)	pm/d (11)	e/d (12)	Note (13)
79469	θ Hya	462–044140	4425	3.88	–0.06	09 14 21.860	+02 18 51.34	114.6	1.0	–313.9	1.0	note, ref.
—	–12 2918	383–056111	4515	10.06	+1.53	09 31 19.433	–13 29 19.33	722.9	8.0	53.5	1.0	note, ref.
82885	11 LMi	630–044785	—	5.41	+0.77	09 35 39.503	+35 48 36.49	–728.7	1.0	–259.8	1.0	note
87696	21 LMi	627–045317	4736	4.48	+0.18	10 07 25.762	+35 14 40.89	51.4	1.0	0.3	1.0	note, ref.
87901	α Leo	510–051462	4750	1.36	–0.11	10 08 22.311	+11 58 01.95	–248.7	1.0	5.6	1.0	note, ref.
89021	λ UMa	665–055971	—	3.45	+0.03	10 17 05.783	+42 54 51.68	–180.7	1.0	–46.1	1.0	
—	+1 2447	455–050081	18415	9.63	+1.52	10 28 55.545	+00 50 27.49	–602.3	8.0	–731.9	8.0	note, ref.
91316	ρ Leo	497–055273	—	3.85	–0.14	10 32 48.672	+09 18 23.71	–5.9	1.0	–3.4	1.0	note. ref.
100600	90 Leo AB	534–051686	—	5.95	–0.16	11 34 42.492	+16 47 48.89	–8.8	1.0	–0.6	1.0	note
102647	β Leo	523–054144	5349	2.14	+0.09	11 49 03.578	+14 34 19.41	–497.7	1.0	–114.7	1.0	note, ref.
102870	β Vir	459–049231	—	3.61	+0.55	11 50 41.719	+01 45 52.99	741.9	1.0	–270.6	1.0	
103095	HR 4550	639–046031	5374	6.45	+0.75	11 52 58.769	+37 43 07.24	4003.3	1.0	–5815.1	1.0	note, ref.
103287	γ UMa	719–051426	5379	2.44	0.00	11 53 49.839	+53 41 41.12	98.9	1.0	9.1	1.0	note, ref.
106591	δ UMa	736–053984	5513	3.31	+0.08	12 15 25.561	+57 01 57.42	103.8	1.0	8.1	1.0	note, ref.
106625	γ Crv	363–062247	5515	2.60	–0.11	12 15 48.370	–17 32 30.95	–159.4	1.0	21.9	1.0	note, ref.
111631	+0 2989	447–054239	19498	8.49	+1.41	12 50 43.566	–00 46 05.24	–32.0	1.0	–393.8	2.8	note, ref.
113139	78 UMa	732–051636	6058	4.93	+0.36	13 00 43.700	+56 21 58.82	108.4	1.0	2.7	1.0	note, ref.
114710	β Com	590–051410	19648	4.28	+0.57	13 11 52.394	+27 52 41.45	–801.2	1.0	881.8	1.0	note, ref.
115617	61 Vir	359–064461	—	4.75	+0.71	13 18 24.315	–18 18 40.31	–1068.7	1.0	–1064.1	1.0	
116658	α Vir	395–055656	—	0.96	–0.23	13 25 11.579	–11 09 40.75	–42.4	1.0	–30.7	1.0	note, ref.

Table continued on following pages

Table 2. The photometric standards of the UBV system, cont.

HD (1)	Name (2)	UCAC4 (3)	NSV (4)	V (5)	B–V (6)	R.A. (J2000.0) (7) h m s	Dec. (J2000.0) (8) ° ′ ″	pm/a (9)	e/a (10)	pm/d (11)	e/d (12)	Note (13)
116842	80 UMa	725–051101	6238	4.01	+0.16	13 25 13.538	+54 59 16.66	120.2	1.0	–16.0	1.0	note, ref.
117176	70 Vir	519–054549	—	4.98	+0.71	13 28 25.809	+13 46 43.64	–235.7	1.0	–576.0	1.0	
121370	η Boo	542–053388	19993	2.69	+0.58	13 54 41.079	+18 23 51.80	–61.0	1.0	–356.3	1.0	note, ref.
130109	109 Vir	460–053938	6794	3.74	0.00	14 46 14.924	+01 53 34.37	–116.4	1.0	–24.2	1.0	note, ref.
130819	α^1 Lib	371–068727	—	5.16	+0.41	14 50 41.181	–15 59 50.05	–136.4	1.0	–59.0	1.0	
130841	α^2 Lib	370–069040	6827	2.75	+0.15	14 50 52.713	–16 02 30.40	–105.7	1.0	–68.4	1.0	note, ref.
—	–7 4003	412–059591	7023	10.56	+1.61	15 19 26.806	–07 43 20.23	–1224.6	8.0	–99.5	8.0	note, ref.
141003	β Ser A	528–059498	20396	3.67	+0.06	15 46 11.254	+15 25 18.60	65.4	1.0	–38.6	1.0	note, ref.
141004	λ Ser	487–059560	7246	4.43	+0.60	15 46 26.614	+07 21 11.04	–224.0	1.0	–70.7	1.0	note, ref.
142860	γ Ser	529–057946	7350	3.85	+0.48	15 56 27.183	+15 39 41.82	310.8	1.0	–1282.8	1.0	note, ref.
—	–12 4523	387–070731	7768	10.13	+1.60	16 30 18.061	–12 39 44.88	–93.6	8.0	–1184.9	8.0	note, ref.
149757	ζ Oph	398–065625	—	2.56	+0.02	16 37 09.537	–10 34 01.52	12.1	1.0	25.6	1.0	note, ref.
154363	–4 4225	425–069303	—	7.73	+1.16	17 05 03.394	–05 03 59.44	–917.1	1.0	–1139.3	1.0	note
154363B	–4 4226	425–069319	8176	10.07	+1.43	17 05 13.752	–05 05 39.70	–921.2	8.0	–1128.2	8.0	note, ref.
157881	+2 3312	461–067140	21919	7.54	+1.36	17 25 45.233	+02 06 41.12	–579.7	1.0	–1184.8	1.0	note, ref.
159561	α Oph	513–067491	9189	2.08	+0.15	17 34 56.069	+12 33 36.13	108.1	1.0	–221.6	1.0	note, ref.
161096	β Oph	473–066890	23613	2.77	+1.16	17 43 28.352	+04 34 02.29	–42.0	1.0	159.3	1.0	note, ref.
161868	γ Oph	464–066593	—	3.75	+0.04	17 47 53.560	+02 42 26.20	–23.5	1.0	–74.4	1.0	
—	+4 3561	472–067401	9910	9.54	+1.74	17 57 56.930	+04 14 52.07	3.6	1.0	4.6	0.9	note, ref.
—	–3 4233	435–075468	10167	9.38	+1.52	18 05 07.601	–03 01 52.94	570.1	8.0	–332.6	8.0	note, ref.

Table continued on following pages

Table 2. The photometric standards of the UBV system, cont.

HD (1)	Name (2)	UCAC4 (3)	NSV (4)	V (5)	B–V (6)	R.A. (J2000.0) (7) h m s	Dec. (J2000.0) (8) ° ′ ″	pm/a (9)	e/a (10)	pm/d (11)	e/d (12)	Note (13)
176437	γ Lyr	614–066016	11624	3.25	–0.05	18 58 56.622	+32 41 22.40	–3.1	1.0	1.1	1.0	note, ref.
177724	ζ Aql	520–091451	11724	2.99	0.00	19 05 24.608	+13 51 48.52	–7.3	1.0	–95.6	1.0	note, ref.
180617	+4 4048	476–093846	—	9.13	+1.49	19 16 55.230	+05 10 07.12	–578.9	8.0	–1331.7	8.0	note, ref.
184279	+3 4065	469–106653	—	6.82	+0.02	19 33 36.919	+03 45 40.78	0.0	1.0	–3.0	1.0	note, ref.
184915	κ Aql	415–127824	12204	4.96	–0.01	19 36 53.449	–07 01 38.92	0.3	1.0	–3.2	1.0	note, ref.
187642	α Aql	495–118192	24910	0.77	+0.22	19 50 46.999	+08 52 05.96	536.2	1.0	385.3	1.0	note, ref.
188512	β Aql	483–118413	12557	3.71	+0.86	19 55 18.793	+06 24 24.34	45.3	1.0	–481.9	1.0	note, ref.
196867	α Del	530–136721	13207	3.77	–0.06	20 39 38.287	+15 54 43.49	52.8	1.0	9.7	1.0	note
198001	ε Aqr	403–132292	—	3.77	+0.01	20 47 40.552	–09 29 44.79	32.6	1.0	–35.5	1.0	note
—	–15 6290	379–165686	—	10.17	+1.60	22 53 16.717	–14 15 49.14	960.3	8.0	–675.6	8.0	note, ref.
216494	74 Aqr	392–129365	—	5.81	–0.08	22 53 28.703	–11 36 59.45	20.8	1.0	1.7	1.0	note, ref.
218045	α Peg	527–148659	14417	2.49	–0.05	23 04 45.654	+15 12 18.96	61.6	1.0	–41.5	1.0	note, ref.
222368	ι Psc	479–133082	14657	4.13	+0.51	23 39 57.041	+05 37 34.65	376.8	1.0	–436.6	1.0	note, ref.
—	+1 4774	463–135261	14719	8.98	+1.48	23 49 12.570	+02 24 03.77	995.1	8.0	–968.3	8.0	note, ref.

Notes:

HD 886: HR 39, CSV 100009; variable star of β Cep type, G. Handler et al., Astrophys. J., Lett., 698, L56, 2009; B2 IV; 2.82–2.86V.
HD 1280: HR 63; double or multiple star; NSV 116; M. Golay, IAU Symp. 54, 275, 1973; A2 V; 4.58–4.62V.
HD 4727: HR 226; magnitude range in V unknown; V. G. Kornilov et al., Tr. Sternberg Astron. Inst., 63, 1, 1991 (see page 3); B5 V + F8 V; 4.53–?V.
HD 6961: HR 343, NLTT 3919; M. S. Zverev, Tr. Gos. Astron. Inst. Sternberg, 8, No. 1, 1936 (pages 90, 150); A7 V; 4.32–4.36V.
HD 8538: HR 403, NLTT 4718; eclipsing binary of Algol type, P. Guthnick, and R. Prager, Veroff. K. Sternw. Berlin-Babelsberg, 2, 112 (H.3), 1918; AAVSO's VSX database notes the period still is to be confirmed; A5 V; 2.68–2.76V.

Table continued on following pages

Table 2. The photometric standards of the UBV system, cont.

Notes (continued):

HD 9270: HR 437, CSV 100120, NSV 532; J. F. J. Schmidt, Astron. Nachr.*, 47, 314, 1858; P. Baize,* J. Obs.*, 45, No. 6–7, 117, 1962; G7 IIIa; 3.59–3.65V.*

HD 10476: NSV 600, GJ 68, CCDM J01425+2016A; A. Gutierrez-Moreno et al., Publ. Obs. Astron. Natl. Cerro Calan*, No. 1, 1966; K1 V; 5.14–5.26V.*

HD 10700: τ Cet, HR 509; suspected variable, F. Rufener and P. Bartholdi, Astron. Astrophys, Suppl. Ser.*, 48, 503, 1982; G8 Vp; 3.5–?V.*

HD 11636: CSV 100146, HR 553; P. Guthnick and R. Prager, Veroff. K. Sternw. Berlin-Babelsberg*, 2, 114 (H.3), 1918; A4 V; 2.56–2.70V.*

BD–18 359: GJ 84, G 272-148; suspected variable, E. W. Weis, Astron. J.*, 107, 1135, 1994; amplitude of 0.026 magnitude, M. Kiraga and K. Stepien,* Acta Astron.*, 57, 149, 2007; M2.5; 10.19(0.026)V.*

HR 753B: BD+06 398B; see text above; the variable star BX Cet.

HD 20630: HR 996, CSV 6022; variable of BY Dra type; M. A. C. Perryman et al., The Hipparcos and Tycho Ctalogues*, ESA SP-1200, European Space Agency, 1997; G5 Vvar; 4.95–4.99Hp.*

HD 21120: HR 1030, CSV 100272; E. Zinner, Astron. Abh., Erganzungshefte zu den Astron. Nachr.*, 8, No. 1, 1929; G6 III; 23.57–3.62V.*

HD 21447: CSV 100281; G. Hill et al., Astron. J.*, 76, 246, 1971; also, H. E. Lau,* Astron. Nachr.*, 196, 425, 1914; A1 V; 5.06–5.13V.*

HD 22049: HR 1084, CCDM J03329-0927A; variable of BY Dra type, G. J. Frey et al., Astron. J.*, 102, 1813, 1991; stellar rotation period between 10 and 12 days; magnitude range about 0.05 magnitude; K2 Vk, R. O. Gray et al.* Astron. J.*, 132, 161, 2006 (Table 2); 3.73(0.05)V.*

HD 30652: HR 1543, CSV 100411; H. Moreno, Astron. Astrophys.*, 12, 442, 1971; F6 V; 3.15–3.21V.*

HD 30836: HR 1552, CSV 100415; spectroscopic binary; E. Zinner, Astron. Abh., Erganzungshefte zu den Astron. Nachr.*, 8, No. 1, 1929; C. Koen and L. Eyer,* Mon. Not. Roy. Astron. Soc.*, 331, 45, 2002, give an amplitude of 0.0032 magnitude for HIP 22549 = HD 30836; B2 III; 3.68(0.003)V.*

HD 32630: HR 1641, CSV 100441; P. Guthnick and F. Pavel, Astron. Nachr.*, 215, 395, 1922; Var?, G. Larsson-Leander,* Ark. Astron.*, 2, 283, 1959; G. M. Fracastoro and S. Catalano,* Mem. Soc. Astron. Ital.*, 36, 99, 1965, T. Widorn,* Mitt. Univ. Sternw. Wien*, 10, 3 (No. 2), 1959; C. Koen and L. Eyer,* Mon. Not. Roy. Astron. Soc.*, 331, 45, 2002, find for V = 3.18, an amplitude of 0.0053 magnitude for HIP 23767 = HD 32630; B3 V; 3.18(0.005)V.*

HD 33111: HR 1666, CSV 100450, IDS 05030-0513 A; B. A. Gould, Resultados del Observatorio Nacional Argentino en Cordoba*, 1, 1, 1879 (see pages 128-342); A3 III; 2.72–2.80V.*

HD 35299: HR 1781; suspected variable, W. H. Warren, Jr. and J. E. Hesser, Astrophys. J., Suppl. Ser.*, 34, 115, 1977; B2 V; 5.69–5.72V.*

HD 35468: HR 1790, CSV 100483; J. F. W. Herschel, Results of Astronomical Observations made during the years 1834, 5, 6, 7, 8 at the Cape of Good Hope*, pp.341, 343, 349, 350, 1847; A. W. J.Cousins and H. R. Stoy,* Roy. Obs. Bull.*, No. 64, 103, 1962., A.Gutierrez-Moreno et al.,* Cerro Tololo Inter-Amer. Obs. Contrib.*, No. 9, 1966; B2 III; 1.59–1.64V.*

HD 35497: HR 1791, double star, IDS 05200+2831 A, CCDM J05263+2836A.

HD 36395: CSV 6182, GJ 205; BY Dra type variable; V = 7.96 magnitude with an amplitude of 0.008 magnitude, period 33.61 days; M. Kiraga and K. Stepien, Acta Astron.*, 57, 149, 2007; R. Weber,* J. Obs.*, 41, 74, 1958; M1.5; 7.96(0.008)V.*

Table continued on following pages

Table 2. The photometric standards of the UBV system, cont.

Notes (continued):

HD 36512: HR 1855; line profile variable of 0.009 magn. amplitude; perhaps a β *Cep star, L. A.Balona and C. A. Engelbrecht,* Mon. Not. Roy. Astron. Soc.*, 214, 559, 1985; B0 V; 4.62–?V.*

HD 36591: HR 1861, CSV 100504, ADS 4141; F. B.Wood, Princeton Obs. Contrib.*, 21, 1946; B1 IV; 5.31–5.38V.*

HD 37043: HR 1899, ADS 4193 A, CCDM J05355-0555A, IDS 05305-0559 A.

HD 37128: HR 1903, CCDM J05363-0112A; pulsating variable, A. W. J. Cousins, Roy. Obs. Bull.*, No. 122, E59, 1966; W. H. Warren., Jr. and J. E. Hesser,* Astrophys. J., Suppl. Ser.*, 34, 115, 1977; B0.5 Iabea; 1.64–1.74V.*

HD 38899: HR 2010, CCDM J05495+1239A, IDS 05439+1237 A.

HD 47105: HR 2421, IDS 06319+1629 A, CCDM J06377+1624A, spectroscopic binary.

HD 56537: HR 2763, CSV 100844, ADS 5961 A, IDS 07124+1643 A; H. L. Johnson et al., 1966; A3 V; 3.52–3.62V.

HD 58946: ρ *Gem, HR 2852, GJ 274.0; suspected variable, A. V. Kusakin, 1992, manuscript only, see VSX database; F0 V; 4.18–?V.*

HD 71155: suspected variations in H Beta, A. Heck, Astron. Astrophys., Suppl. Ser.*, 27, 47, 1977; A0 V; 3.9–?V.*

HD 76644: HR 3569; spectroscopic binary, short period A-star, G. Jackisch, Veroff. Sternw. Sonneberg, 5, 271 (H. 5), 1963; A7 IV; 3.12–3.18V.

HD 79469: θ *Hya, HR 3665, ADS 7253 A; H. E. Lau,* Astron. Nachr.*, 196, 425, 1914; suspected variable, C. J. Durant,* Mon. Not. Roy. Astron. Soc.*, 147, 75, 1970; B9.5 V; 3.88–3.91V.*

BD–12 2918: double or multiple, IDS 09265-1303 AB, CCDM J09313-1329AB, GJ 352, NLTT 21974, Ross 440; sp type M2; V 10.05–?; P. M.Corben et al., Mon. Not. Astron. Soc. S. Africa*, 31, No.1–2, 7, 1972, change in (U–B) = 0.18; J. Alfonso-Garzon et al., 2012, arXiv:1210.0821 [astro-ph.IM] (online info); M.Petit,* Inf. Bull. Var. Stars*, No. 320, 1, 1968.*

HD 82885: NLTT 22117; SV LMi, a variable of RS CVn type, amplitude in Stromgren y *of 0.033 magnitude, with period of 18.0 days, B. Skiff and W. Lockwood,* Publ. Astron. Soc. Pacific*, 98, 338, 1986; G8 IIIv; 5.39(0.004)V.*

HD 87696: discovered by G. Jackisch, Sky & Telescope*, 18, 73, 1958; also G. Jackisch, Veroff. Sternw. Sonneberg, 5, 1963, variable of* δ *Scuti type, P = ~0.1 day; suspected variable, G. Hill et al.,* Astron. J.*, 76, 246, 1971; A7 V; 4.47–4.52V.*

HD 87901: Regulus; double, ADS 7654 A, HR 3982; A. Gutierrez-Moreno et al., Cerro Tololo Inter-Amer. Obs. Contrib.*, No. 9, 1966; P. Guthnick and R. Prager,* Veroff. K. Sternw. Berlin-Babelsberg*, 2, 116 (H.3), 1918; B7 V; 1.33–1.40V.*

BD+01 2447: GJ 393.0, G 55-24, Ross 446; H. L. Giclas et al., Lowell Obs. Bull.*, 5, 61, 1961; suspected variable, E. W. Weis,* Astron. J.*, 107, 1135, 1994; M2.5 V; 9.63–9.68V.*

HD 91316: pulsating variable of amplitude 0.07 magnitude, E. H. Olsen, Inf. Bull. Var. Stars*, No. 925, 1, 1974; illustrated light curve with period 3.4271 days in* The Hipparcos and Tycho Catalogues, Variability Annex*: periodic variables, HIP 51624, SP-1200, vol. 12, page A236; B1 Ib; 3.83–3.9V.*

Table continued on following pages

Table 2. The photometric standards of the UBV system, cont.

Notes (continued):

HD 100600: double star, ADS 8220 AB, CCDM J11347+1648AB, IDS 11295+1721, component B also spectroscopic binary via D. Hoffleit and C. Jaschek, The Bright Star Catalogue, *1982.*

HD 102647: Denebola, β Leo, ADS 8314 A; predicted variable of δ Scuti type, M. S. Frolov, Inf. Bull. Var. Stars, *No. 427, 1, 1970; found to have approximate amplitude of 0.025 magnitude and period about 0.05 day by C. Bartolini et al.,* Inf. Bull. Var. Stars., *No. 2010, 1, 1981; A3 Va, G. T. van Belle and K. von Braun,* Astrophys. J., *694, 1085, 2009; 2.14(0.025)V.*

HD 103095: Groombridge 1830A, high proper motion star and metal-poor subdwarf; NLTT 28839; flare caused change in photographic magnitude from 6.6 to 7.2 on secondary component, named CF UMa, W. R. Beardsley et al., Astrophys. J., *194, 637, 1974; W. D. Heintz,* Publ. Astron. Soc. Pacific, *96, 557, 1984, casts strong doubt on the reality of the flare star, CF UMa; G8 Vp; 6.6–7.20B.*

HD 103287: emission line star; CSV 101229, HR 4554; short period variation with up to 0.03 magnitude variation, P. Guthnick, Astron. Nachr., *205, 97, 1917 (see page 112); A0 Ve; 2.41–2.45V.*

HD 106591: HR 4660, CSV 101249, CCDM J12155+5702A; possible micro-variable, F. Rufener, Astron. Astrophys., Suppl. Ser., *26, 275, 1976; A3 V; 3.27–3.34V.*

HD 106625: HR 4662, CSV 101250; discoverer Ferrero; E. Zinner, Astron. Abh., Erganzungshefte Astron. Nachr., *8, No. 1, 1929; B8 III; 2.56–2.60V.*

HD 111631: GJ 488.0, G 14-6, NLTT 32069; suspected variable, F. Rufener and P. Bartholdi, Astron. Astrophys., Suppl. Ser., *48, 503, 1982; M0.5 Ve; 8.46–?V.*

HD 113139: ADS 8739 AB, CCDM J13007+5622AB, IDS 12564+5654, HR 4931; P. Baize, J. Obs., *45, 117, 1962; G6 V; 7.4–10.5V (note: this range in magnitude is huge; correct?).*

HD 114710: β Com, HR 4983, GJ 502.0; variable, D. F. Gray et al., Astrophys. J., *456, 365, 1996; F9.5 V; 4.26(0.02)V.*

HD 116658: Spica, α Vir, IDS 13200-1038 A,; an eclipsing binary with the primary component a β Cep type variable star, M. Desmet et al., Amer. Inst. Physics Conf. Proc. 1170, page 376, 2009; B1 III-IV; 0.95(0.1)V.

HD 116842: HR 5062, CSV 101383; variability suspected by H. Shapley, Astron. Nachr., *196, 398, 1914; A5 Vn; 3.93–4.03V.*

HD 121370: η Boo, HR 5235; 0.1 magnitude variation in V, M. Petit, Astron. Astrophys., Suppl. Ser., *85, 971, 1990; G0 IV; 2.68(0.1)V.*

HD 130109: 109 Vir, HR 5511; A. Gutierrez-Moreno et al., Publ. Obs. Astron. Natl. Cerro Calan, *No. 1, 1966; A0 V; 3.70–3.75V.*

HD 130841: α Lib 2, HR 5531, A. Gutierrez-Moreno et al., Publ. Obs. Astron. Natl. Cerro Calan, *No.1, 1966; A3 V; 2.72–2.75V.*

BD–07 4003: HO Lib; variable of BY Dra type; E. W. Weis, Astron. J., *107, 1135, 1994; J. Alfonso-Garzon et al., 2012, arXiv:1210.0821 [astro-ph.IM] (online info); M5.0 V; 10.56–10.58V.*

HD 141003: β Ser, 28 Ser, HR 5867, double star, ADS 9778 A; micro-variable, F. Rufener, Astron. Astrophys., Suppl. Ser., *45, 207, 1981; A1 V; 3.65–?V.*

HD 141004: 27 Ser, HR 5868; J. E. Gore, A Catalogue of Suspected Variable Stars, Proc. Roy. Irish Acad. (II), *4, 267, 1884; suspected variablility in Kukarkin et al., 1951; A.Gutierrez-Moreno et al.,* Cerro Tololo Inter-Amer. Obs. Contrib., *No. 9, 1966.; and G. Hill et al.,* Astron. J., *76, 246, 1971; G0 V; 4.39–4.44V.*

Table continued on following pages

Table 2. The photometric standards of the UBV system, cont.

Notes (continued):

HD 142860: γ Ser, 41 Ser, HR 5933; suspected variable, M. Golay, IAU Symp. 54, 275, 1973; F6 V; 3.79–3.88V.

BD–12 4523: GJ 628, V2306 Oph, a variable of BY Dra type; suspected variable, E. W. Weis, Astron. J.*, 107, 1135, 1994; J. Alfonso-Garzon et al., 2012, arXiv:1210.0821 [astro-ph.IM] (online info); M3.5 V; 10.05–10.1V.*

HD 149757: ζ Oph, 13 Oph, HR 6175; Be star; S. S. Vogt and G. D. Penrod, Astrophys. J.*, 275, 661, 1983; O9.5 V(e); 2.56–2.58V.*

HD 154363: double star, Wolf 635, CCDM J17051-0504A, GJ 653, IDS 16597-0456 A, NLTT 44127.

HD 154363B: variable in (U–B), P. M.Corben, B. S.Carter, R. M.Banfield, G. M. Harvey, Mon. Not. Astron. Soc. S. Africa*, 31, 7, 1972; M4 V; 10.06–?V.*

HD 157881: G 19-24, GJ 673.0; V magnitude only marked as a weak determination in A. W. J. Cousins, S. Afr. Astron. Obs. Circ.*, 1, 234, 1980 (Table 1); K7 V; 7.51–7.56:V.*

HD 159561: α Oph, HR 6556, CSV 101982, CCDM J173449+1234A, NLTT 45084; found in minimum once, H. E. Lau, Astron. Nachr.*, 196, 425, 1914; DSCT+GDOR; "Rotationally-modulated g-modes in the rapidly-rotating δ Scuti star Rasalhague (α Ophiuchi)," J. D. Monnier et al.,* Astrophys. J.*, 725, 1192, 2010; has a low mass companion; A5 IV; 2.08V(0.006).*

HD 161096: HR 6603; suspected variable in near-infrared, D. Engels et al., Astron. Astrophys., Suppl. Ser.*, 45, 5, 1981; K2 III; 2.75–2.77V.*

BD+04 3561: V2500 Oph, Barnard's Star, G 140-24, GJ 699.0; G. F. Benedict et al., Astron. J.*, 116, 429, 1998; M. Kiraga and K. Stepien,* Acta Astron.*, 57, 149, 2007; M4; 9.55(0.02)V.*

BD–03 4233: HD 165222, G 20-22; variable, M. P. FitzGerald, Astron. Astrophys., Suppl. Ser.*, 9, 297, 1973; M. Petit,* Inf. Bull. Var. Stars*, No. 1056, 1, 1975; M2; 9.28–9.43V.*

HD 176437: γ Lyr, ADS 11980 A, HR 7178; variable in P. Guthnick and R. Prager, Astron. Nachr.*, 201, 443, 1915; B9; 3.23–3.26V.*

HD 177724: ζ Aql, HR 7235, double star, ADS 12026 A; suspected variable, A.Gutierrez-Moreno et al., Publ. Obs. Astron. Natl. Cerro Calan*, No.1, 1966; A0; 2.98–2.99V.*

HD 180617: Ross 652, CCDM J19169+0510A, NLTT 47619, suspected variable, E. W. Weis, Astron. J.*, 107, 1135, 1994; V1428 Aql, a BY Dra type variable star, J. Alfonso-Garzon et al., 2012, arXiv:1210.0821 [astro-ph.IM] (online info); M3.5 V; 9.09–9.13V.*

HD 184279: V1294 Aql; Be star; variable in P. Tempesti and R. Patriarca, Inf. Bull. Var. Stars*, No. 1164, 1, 1976; G. Pojmański,* Acta Astron.*, 52, 397, 2002; J. Alfonso-Garzon et al., 2012, arXiv:1210.0821 [astro-ph.IM] (online info); B0.5 IVe; 6.78–7.59V.*

HD 184915: κ Aql, HR 7446; possibly variable, 0.02 magnitude or less, C. R. Lynds, Astrophys. J.*, 130, 577, 1959; B1; 4.94–4.98V.*

HD 187642: Altair, HR 7557, ADS 13009 A; δ Scuti type variable, demonstrated by D. L. Buzasi et al., Astrophys. J.*, 619, 1072, 2005; A7 IV/V; 0.77(0.004)V.*

HD 188512: β Aql, HR 7602, ADS 13110 A, CSV 101909; variable, H. E. Lau, Astron. Nachr. *196, 425, 1914; C. Wylie,* Astrophys. J.*, 56, 217, 1922; A. Gutierrez-Moreno et al.,* Publ. Obs. Astron. Natl. Cerro Calan*, No.1, 1966; G8; 3.68–3.74V.*

Table continued on next page

Table 2. The photometric standards of the UBV system, cont.

Notes (continued):

HD 196867: α Del, HR 7906, ADS 14121 A, CCDM J20396+1555A, described as suspected variable in A. Auwers, Astron. Nachr.*, 50, 99, 1859 (see page 105), but seems unrealistic based on modern possible variation in I, G. E. Kron et al.,* Publ. U.S. Naval Obs., Second Ser.*, 20, part 5, 1972, pages 54 and 70; B9; 3.77–3.80V.*

HD 196867: α Del, HR 7906, ADS 14121 A, CCDM J20396+1555A, described as suspected variable in A. Auwers, Astron. Nachr.*, 50, 99, 1859 (see page 105), but seems unrealistic based on modern possible variation in I, G. E. Kron et al.,* Publ. U.S. Naval Obs., Second Ser.*, 20, part 5, 1972, pages 54 and 70; B9; 3.77–3.80V.HD 198001: ε Aqr, HR 7950 suspected of variability, but by whom?*

BD–15 6290: NLTT 55130, GJ 876.0, suspected variable, E. W. Weis, Astron. J.*, 107, 1135, 1994; IL Aqr, a variable of BY Dra type, J. Alfonso-Garzon et al., 2012, arXiv:1210.0821 [astro-ph.IM] (online info); M4 V; 10.15–10.21V.*

HD 216494: 74 Aqr, HR 8704, HI Aqr, a variable star of α2 CVn type, G. Mathys and J. Manfroid, Astron. Astrophys., Suppl. Ser.*, 60, 17, 1985, with period 0.724 day; B9 pHgMn; 5.80(0.01)V.*

HD 218045: α Peg, HR 8781, variable star, Anon., Observatory*, 2, 420, 1879; J. Lub and J. W. Pel,* Astron. Astrophys.*, 54, 137, 1977 (Table 13); B9; 2.47–2.52V.*

HD 222368: ι Psc, HR 8969; M.Golay, IAU Symp. 54, 275, 1973 (Table 4.2); F7; 4.11–4.14V.

BD+01 4774, GJ 908, NLTT 58069: BR Psc, a BY Dra type var.; E. W. Weis, Astron. J.*, 107, 1135, 1994; M2 V; 8.93–9.03V.*

Appendix A: Notes on stellar nomenclature

Most of the stars in Tables 1 and 2 have additional identifications. Therefore a description follows next of the stellar nomenclature which the reader will encounter. These different star naming systems and catalogues are given in alphabetical order.

2MASS: The 2 Micron All-Sky Survey (Skrutskie *et al.* 2006) is a survey of the sky in the near-infrared. There is an online catalogue, VizieR, II/246, Cutri, *et al.* (2003).

ADS: An Aitken double star (Aitken 1932).

BD: The *Bonner Durchmusterung* is a multiple-volume star catalogue published between 1852 and 1859 by F. W. A. Argelander, A. Krüger, and E. Schönfeld (1859, 1861, 1862). It is a visual survey of stars in declination zones from +90 to –01 Degrees. The *Sudliche Bonner Durchmusterung* covers the declination range from –02 to –22 degrees (Schönfeld 1886).

CCDM: A catalogue of the components of double and multiple stars by J. Dommanget and Nys (1994; online version, CDS Catalogue I/211), first edition.

CSV: An acronym used for stars in the *Catalogue of Suspected Variable Stars* (Kukarkin *et al.* (1951) and in the *Second Catalogue of Suspected Variable Stars* (Kukarkin *et al.* 1965).

G and GD: Proper motion stars published by Giclas and colleagues in the *Lowell Observatory Bulletins* (Giclas *et al.* 1971)—Northern Hemisphere, the G numbered stars; Giclas *et al.* (1978)—Southern Hemisphere Catalogue; Giclas *et al.* (1980)—Summary catalogue of the GD and GR stars. This latter group contained very blue (GD) or very red (GR) stars of little or no proper motion.

GD: A list of white dwarf suspects compiled by Giclas and colleagues in *Lowell Observatory Bulletins* (Giclas, Burnham, and Thomas, 1980).

GJ: The nomenclature GJ pertains to stars in the Gliese and Jahreiss (1979) catalogue of nearby stars.

HD: *The Henry Draper Catalogue* was published in the *Annals of the Harvard College Observatory*, vols. 91–99 in the time interval 1918–1924.

IDS: *The Index Catalogue of Double Stars* was published in 1963 (Jeffers, van den Bos, and Greeby 1963).

Luyten devised several numbering systems for the white dwarf and high proper motion stars that he discovered (Luyten 1963, 1976).

NLTT: *The New Luyten Two Tenths Catalogue* (Luyten, 1979a,b,c; 1980a,b; Luyten and Hughes 1980); includes stars in the LTT from Luyten publications in the 1954–1969 era.

NSV: The NSV terminology began with the *New Catalogue of Suspected Variable Stars* (Kholopov *et al.* 1982). One can now most easily access variable and suspected variable star information by entering the Sternberg Astronomical

Institute's web page, clicking on the "GCVS Research Group" (*General Catalogue of Variable Stars*), and then going to the appropriate catalogue; see http://www.sai.msu.su.

Ross: The Ross stars numbers arise from a series of papers in the *Astronomical Journal* by F. E. Ross on high proper motion stars. The papers appeared in the time interval 1925–1939.

UCAC4: A catalogue of accurate coordinates and proper motions for stars around the sky (Zacharias *et al.* 2103). The photometry is by the AAVSO, on its APASS photometric system.

VSX: The American Association of Variable Star Observers' International Variable Star Index (Watson, Henden, and Price 2013).

Wolf: Wolf star numbers are stars catalogued by M. Wolf in his studies of high proper motion stars. These papers appeared in the *Astronomische Nachrichten* in the time interval 1919–1931.

Discovery of Pulsating Components in the Southern Eclipsing Binary Systems AW Velorum, HM Puppis, and TT Horologii

David J. W. Moriarty
315 Main Road, Wellington Point, Queensland 4160, Australia; send email correspondence to djwmoriarty@bigpond.com

Terry Bohlsen
Mirranook, Armidale, NSW 2350, Australia

Bernard Heathcote
269 Domain Road, South Yarra, Victoria 3141, Australia

Tom Richards
P.O. Box 323, Kangaroo Ground, Victoria 3097, Australia

Margaret Streamer
3 Lupin Place, Murrumbateman, NSW 2582, Australia

Received June 4, 2013; revised July 15, 2013; accepted August 6, 2013

Abstract Eclipsing binary stars with pulsating components are especially valuable for studies of stellar evolution. We have discovered that three eclipsing binary stars in the southern sky have a pulsating component with oscillations similar to those of δ Scuti stars. The systems are: AW Velorum, HM Puppis, and TT Horologii. Their spectral types were determined as A7 for AW Vel and HM Pup and F0-F2 for TT Hor. The dominant pulsation frequencies are 15–38 cycles per day with amplitudes of 10–60 millimagnitudes.

1. Introduction

The interiors of stars cannot be observed directly, but they can be studied by observing and interpreting the frequency spectra of pulsating stars. This is the field of asteroseismology. In recent years there has been great interest in single δ Scuti stars, which pulsate with typical frequencies of 20–50 cycles per day. Such pulsating stars may also be found in eclipsing binary systems where the absolute masses and sizes of the two components can be determined accurately from radial velocity spectrometry and eclipse photometry. This information can only be derived indirectly for single δ Scuti stars. Furthermore, the passage of the secondary star in front of the primary during a primary eclipse provides a spatial filter, accentuating or repressing the visibility of different pulsation modes. Accordingly, the study of δ Scuti stars in binary systems yields considerably more information than for isolated δ Scuti stars (see for example

Creevey *et al.* 2011; Liakos *et al.* 2012; Mkrtichian *et al.* 2004; Soydugan *et al.* 2006).

Two types of binary systems with pulsating components are recognized:

a) detached systems, in which both stars do not fill their Roche lobes and thus there is no mass exchange; the pulsator is a typical δ Scuti star. Such systems are at an early stage of binary evolution, where neither component has evolved away from the main sequence to swell to the sub-giant stage and fill its Roche lobe, thus initiating mass transfer. These types of systems are traditionally classified as EA/DSCT.

b) semi-detached systems, in which the (primary) pulsating component is undergoing mass accretion from the larger secondary that has filled its Roche lobe. Its properties and evolutionary history are considerably different from isolated δ Scuti stars. These types of eclipsing Algol (EA) binaries are classified as oscillating EA systems (oEA) (Mkrtichian *et al.* 2002, 2004).

The Southern Eclipsing Binaries Programme of Variable Stars South is a multi-purpose and ongoing campaign to observe and analyze bright eclipsing binary stars accessible to Southern Hemisphere observers. Despite their importance and ease of observation, many of them have not been observed in detail since their discovery, and many more require follow-up work to extend and check existing studies (Richards 2013). During studies to obtain accurate eclipse timings and update ephemeris elements, we have found that AW Vel, HM Pup, and TT Hor each contain a component with short periodic oscillations in magnitude. In this paper, we provide a brief summary of their properties. Further observations are in progress and are planned to obtain full light curves and radial velocities.

None of the three eclipsing binaries that we report on here were listed by Soydugan *et al.* (2006) in their catalogue as candidates for eclipsing binaries with δ Scuti components.

2. Observations and analysis

2.1. Time series photometry

The instruments used for photometry were a 350-mm Meade Schmidt-Cassegrain with a SBIG ST8 CCD camera (Streamer), a 356-mm Celestron Edge HD 1400 aplanatic Schmidt Cassegrain with a Moravian G3-6303 CCD camera (Moriarty), and a 410-mm RCOS Ritchey-Chrétien with an Apogee U9 CCD camera (Richards). All imaging was done with Johnson V filters. The images were reduced using aperture photometry; details of the comparison stars are given in Table 1. The resulting magnitude data are un-transformed.

Examples of primary and secondary eclipses of each target are shown in the figures.

The ephemeris light elements were updated from the data available from the GCVS and AAVSO/VSX. Times of minima were determined using the Kwee and van Woerden algorithm or Polynomial fit in PERANSO, with at least three minima analysed for each system (Vanmunster 2013). A linear regression analysis was applied to obtain improved light elements and errors. Pulsation frequencies were analysed after subtraction of the eclipse curves using Fourier methods in PERIOD04 (Lenz and Breger 2005).

2.2. Spectra

The spectra of TT Hor were obtained using an Lhires spectrograph with 150 g/mm grating on a 280-mm SCT, with an Atik 314L CCD, giving a resolution of 10 Angstroms (R=590) (Heathcote). Spectra of AW Vel and HM Pup were obtained with a LISA spectrograph on a Celestron C11 SCT using a SBIG ST8XME CCD with a resolution of R = 900 and a S/N of approximately 50 (Bohlsen). Each spectrum was calibrated using a neon calibration light.

The spectra were compared to known standards in the MK Spectral classification system with a resolution of 3.6 Angstroms from the Dark Sky Observatory at the Appalachian State University (Gray 2013). The accuracy of the spectral types that we determined was limited by the resolution and the S/N of equipment and observing sites.

3. Results and discussion

3.1. AW Vel

AW Vel (V mag. = 10.7, P = 1.9924566 days) is an EA system with a 1.54-magnitude primary eclipse and a 0.05-magnitude secondary eclipse. Oscillations similar to those of δ Scuti stars were most apparent during the secondary eclipse (Figure 1). The oscillations were also observed in the out-of-eclipse sections of the light curve, but less apparent during the primary eclipse (Figure 2). This may be due to a spatial filtering effect as discussed by Mrktichian *et al.* (2002). The dominant frequency was 15.2 ± 0.3 cycles/day with an amplitude of 58 ± 1 millimagnitudes (Table 2); other frequencies were not significant. We determined the combined spectral type to be A7 (Table 2). This can be taken as the spectral type of the primary, as the shallow secondary eclipse indicates that the luminosity of the secondary component is relatively weak. The spectral type of A7 lies at the hot end of the intersection of the instability strip and the main sequence. In the catalogue of Svechnikov and Kuznetsova (1990), it is recorded as a semi-detached system with spectral types as (A4)+[G2IV].

3.2. HM Pup

HM Pup (V mag. = 10.9, P = 2.589715 days) is an EA system with a very

deep, flat-bottomed (total) primary eclipse to V magnitude 14.2 and a weak 0.05-magnitude secondary eclipse. Uneclipsed portions of the light curve are slightly convex. The primary eclipse lasts for about 43 minutes, during which no oscillations were apparent (Figure 3). Oscillations similar to those of δ Scuti stars were recorded during the intervals between eclipses and during the secondary eclipse (Figures 4, 5). The amplitude of the pulsations was small, in summation no greater than 20 millimagnitudes (mmag.) when the maxima were in phase with each other, as seen in an out-of-eclipse portion of the light curve. Analysis of the secondary eclipses and the out-of-eclipse phases showed the dominant frequency to be 31.9 ± 1.2 cycles/day with an amplitude of 10 ± 4 mmag. A second frequency of 38.0 ± 0.4 cycles/day had an amplitude of 6 ± 2 mmag. Other frequencies could be extracted from the data, but were unreliable given the limits of detection for our instruments. We determined that the spectral type for HM Pup is A7 (Table 2), whereas Svechnikov and Kuznetsova (1990) show it as (A2)+[G6IV] and semi-detached.

3.3. TT Hor

TT Hor (V mag. = 11.0, P = 2.6082044 days) is an EA system with a 0.65-magnitude primary eclipse and a very weak 0.03-magnitude secondary eclipse. The system shows oscillations during the primary eclipses, as well as in the secondary eclipses and the intervals between eclipses (Figures 6a, 7a, 8). The amplitudes of the pulsations varied during the eclipse cycle, but were greater during the primary eclipses. For example, on HJD 2456267 the oscillations had a greater amplitude before and during the primary minimum than after it (Figure 6b), whereas on HJD 2456280, the oscillation amplitude was greater after the primary eclipse (Figure 7b). The same primary eclipse (HJD 2456280) was recorded from two different locations and the pattern of oscillations was identical, indicating that these were not due to equipment or differences in seeing conditions. The frequency analysis showed pulsations with several frequencies. The dominant frequency was 38.7 ± 0.4 cycles/day, with two others of 33.4 ± 0.7 and 42.3 ± 0.3 cycles/day (Table 2). We determined the spectral type of TT Hor to be in the range of F0–F2 (Table 2), whereas Svechnikov and Kuznetsova (1990) catalogued it as (A2)+[G6IV)] and semi-detached.

4. Conclusions

The pulsating components of eclipsing binary systems are usually the brighter, primary, components of the systems, as evidenced by the data in the catalogue of Soydugan *et al.* (2006), where the primary component was the pulsator in 23 of 25 confirmed eclipsing binaries with an oscillating component. Our photometric data for these three systems indicate that the primary components are the pulsators. Furthermore, the spectral classifications indicate that the primaries are in the instability strip of the H-R diagram. Whether all

three can be classified as semi-detached is not certain. In the case of TT Hor, the amplitudes of the oscillations during the (partial) primary eclipse were greater than those observed during the secondary eclipses and in the intervals between the eclipses. We suggest that the observed amplitude changes during the primary eclipses were due to beating between the frequencies noted above. A spatial filtering effect may also be present.

As our data shown in Figure 5 indicate that the light curve of HM Pup is not flat, we conclude that it is most likely to be an oEA system as defined by Mkrtichian *et al.* (2002). Although ASAS data (Pojmański 1997) indicate that the three targets have substantially flat light curves between eclipses, there is considerable scatter in those observations. We are planning more detailed observations to determine the precise shape of the full light curves in several pass bands for these systems.

The spectral types that we determined for these stars are the first record of their actual spectra and differ from those given in the catalogue of Svechnikov and Kuznetsova (1990). Their designations were inferred from statistical analysis of data given in GCVS IV and are, therefore, approximate.

Additional photometric studies combined with radial velocity measurements are needed for a better understanding of each of these targets.

5. Acknowledgements

David Moriarty acknowledges the support of a grant for the purchase of a telescope from the Edward Corbould Research Fund of the Astronomical Association of Queensland. Margaret Streamer and David Moriarty acknowledge grants from Variable Stars South to purchase software. We thank the referee for his or her helpful comments.

References

Creevey, O. L., Metcalfe, T. S., Brown, T. M., Jiménez-Reyes, S., and Belmonte, J. A. 2011, *Astrophys. J.*, **733**, 38.

Gray, R. O. 2013, A Digital Spectral Classification Atlas (http://stellar.phys.appstate.edu/Standards/stdindex.html; http://ned.ipac.caltech.edu/level5/Gray/frames.html).

Lenz, P., and Breger, M. 2005. *Commun. Asteroseismology*, **146**, 53.

Liakos, A., Niarchos, P., Soydugan, E., and Zasche, P. 2012, *Mon. Not. Roy. Astron. Soc.*, **422**, 1250.

Mkrtichian, D. E., Kusakin, A. V., Gamarova, A. Yu., and Nazarenko, V. 2002, in *Radial and Nonradial Pulsations as Probes of Stellar Physics*, eds. C. Aerts, T. R. Bedding, and J. Christensen-Dalsgaard, ASP Conf. Ser. 259, 96.

Mkrtichian, D. E., *et al.* 2004, *Astron. Astrophys.*, **419**, 1015.

Pojmański, G. 1997, *Acta Astron.*, **47**, 467.

Richards, T. 2013, Southern Eclipsing Binaries Programme of the Variable Stars South group (http://www.variablestarssouth.org/index.php/research/eclipsing-binaries).

Soydugan, E., Soydugan, F., Demircan, O., and İbanoğlu, C. 2006, *Mon. Not. Roy. Astron. Soc.*, **370**, 2013.

Svechnikov, M. A., and Kuznetsova, E. F. 1990, *Katalog priblizhennykh fotometricheskikh i absoliutnykh elementov zatmennykh peremennykh zvezd* (Catalogue of *Approximate Photometric and Absolute Elements of Eclipsing Variable Stars*), A. M. Gorky University of the Urals, Sverdlovsk, Russia.

Vanmunster, T. 2013, Light Curve and Period Analysis Software, PERANSO v.2.50 (http://www.peranso.com/).

Table 1. Photometry and updated ephemeris elements of AW Vel, HM Pup, and TT Hor. The numbers of primary minima with accurate timings that were used to calculate new periods are shown for each star.

Parameter	*AW Vel*	*HM Pup*	*TT Hor*
Comparison star	GSC 7671 1482	GSC 8124 0271	GSC 8059 0284
Magnitude (V)	10.459	10.905	10.755
Epoch (HJD)	2456274.15028	2455991.0535	2456267.0770
Epoch error	0.0003135	0.00193	0.004035
No. of primary minima	6	2	3
Period (days)	1.9924566	2.589715	2.6082044
Period error	0.0000037	0.000002	0.000607

Table 2. Oscillation parameters and spectral types of AW Vel, HM Pup, and TT Hor. The oscillation frequencies are cycles/day and the amplitude of the dominant frequency is in millimagnitudes.

Parameter	*AW Vel*	*HM Pup*	*TT Hor*
Oscillation Frequency 1	15.2±0.3	31.9±1.2	38.7±0.4
Oscillation Frequency 2	—	38.0±0.4	33.4±0.7
Oscillation Frequency 3	—	—	42.3±0.3
Oscillation Amplitude 1	58±1	10±4	20±4
Oscillation Amplitude 2	—	6±2	10±2
Oscillation Amplitude 3	—	—	14±2
Spectral Type	A7	A7	F0-F2

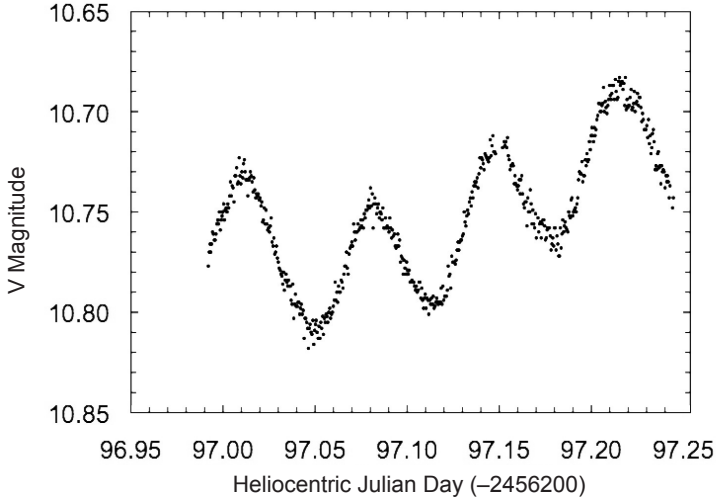

Figure 1. A secondary eclipse of AW Vel, with oscillations of 50–70 millimagnitudes.

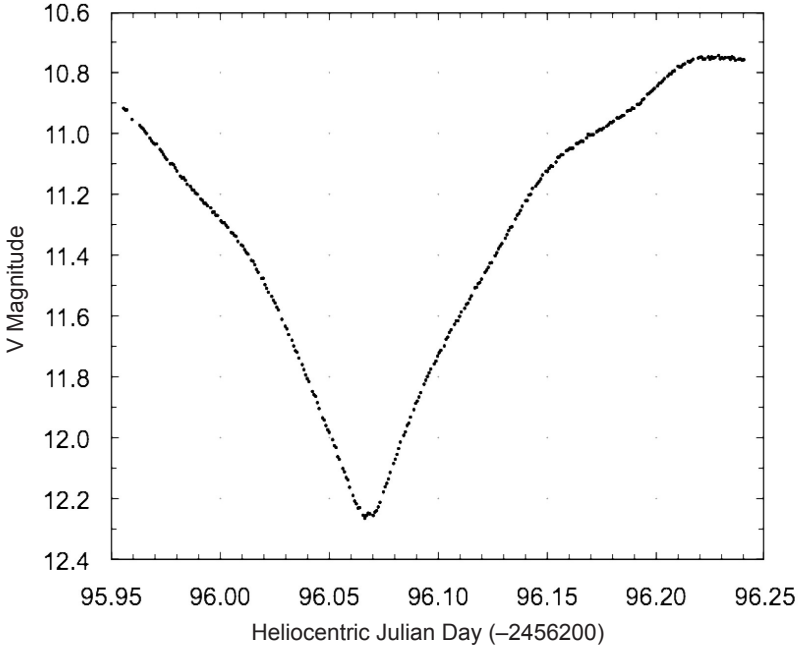

Figure 2. A primary eclipse of AW Vel.

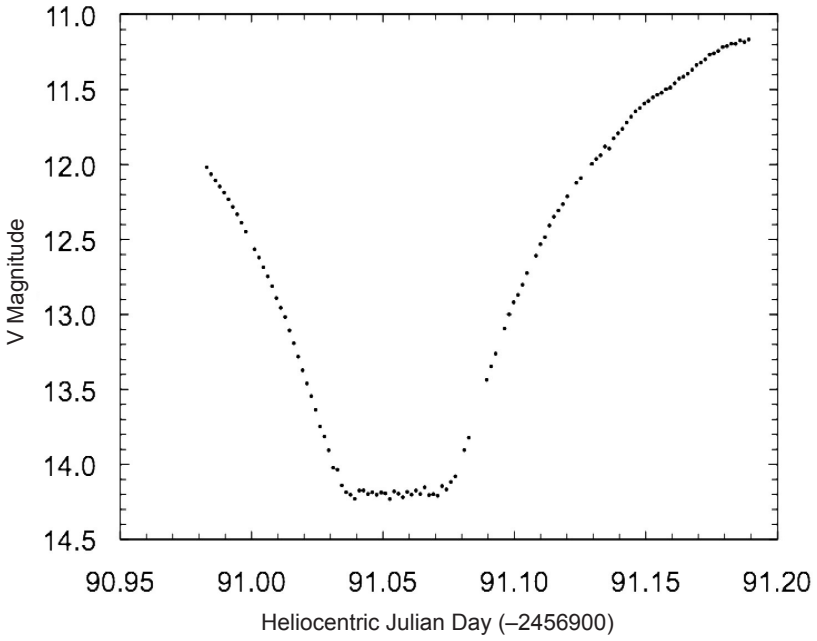

Figure 3. A primary eclipse of HM Pup.

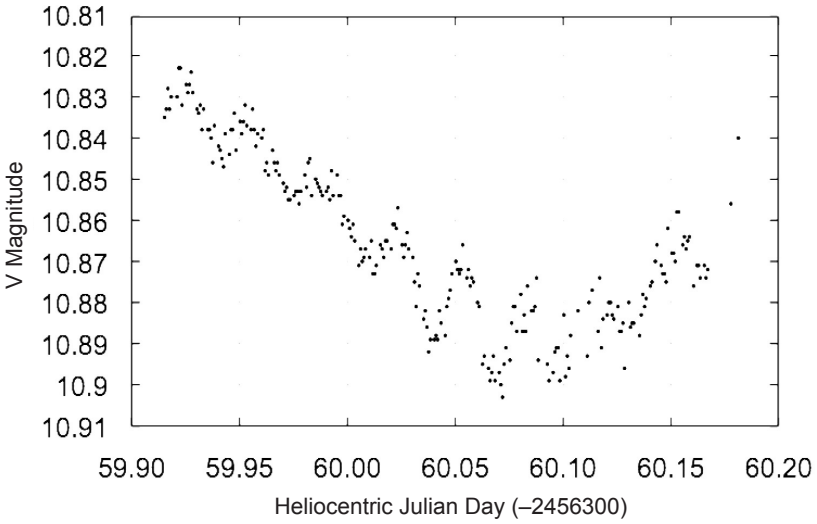

Figure 4. A secondary eclipse of HM Pup with oscillations of 20–30 mmag.

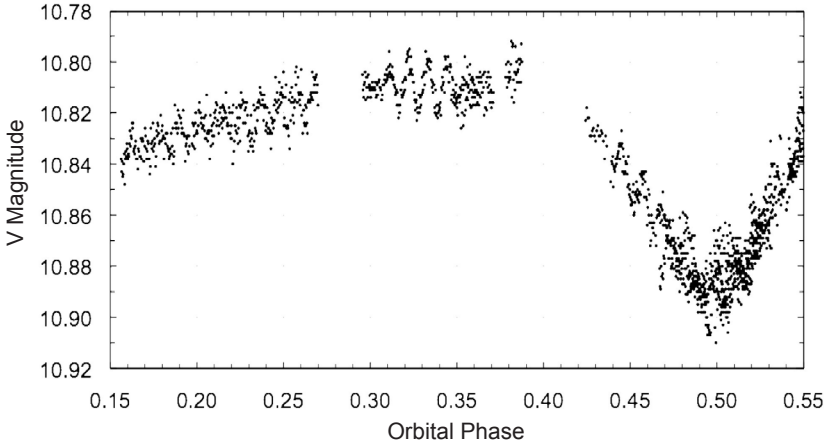

Figure 5. A portion of the phased light curve of HM Pup showing the oscillations during the secondary eclipse and the interval between eclipses.

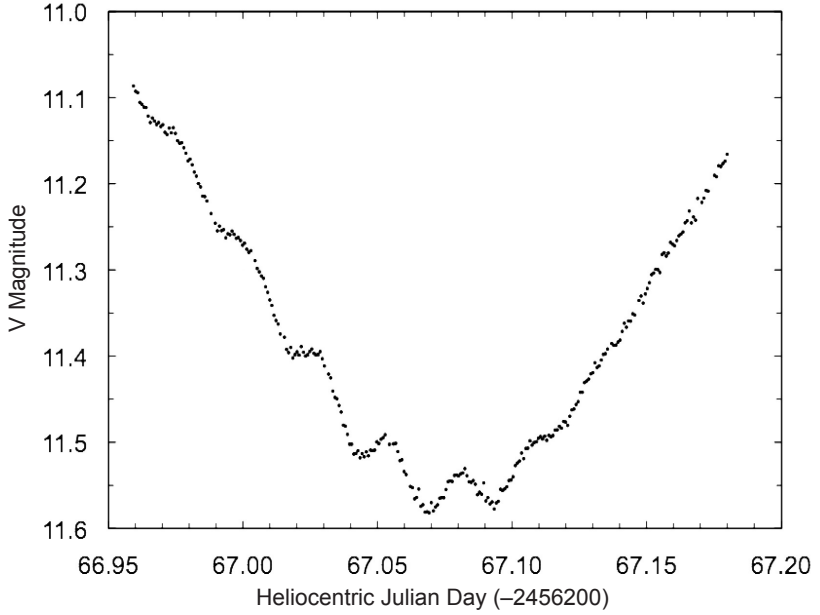

Figure 6a. A primary eclipse of TT Hor with oscillations apparent in the descending phase and at the minimum of the eclipse.

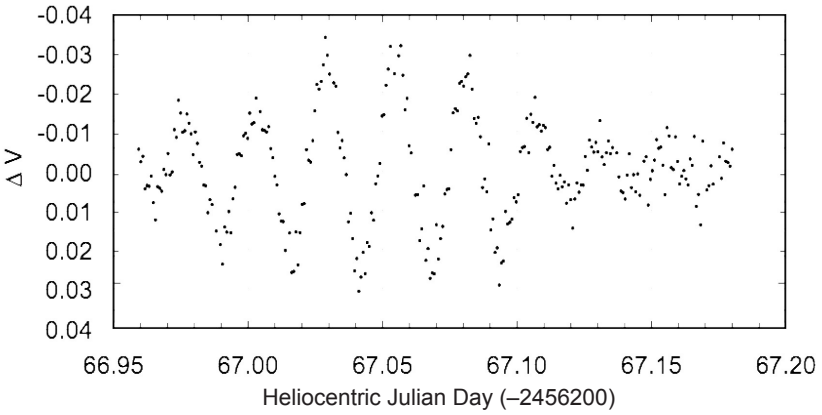

Figure 6b. Oscillations during the primary eclipse of TT Hor in Figure 6a with the primary eclipse light curve subtracted.

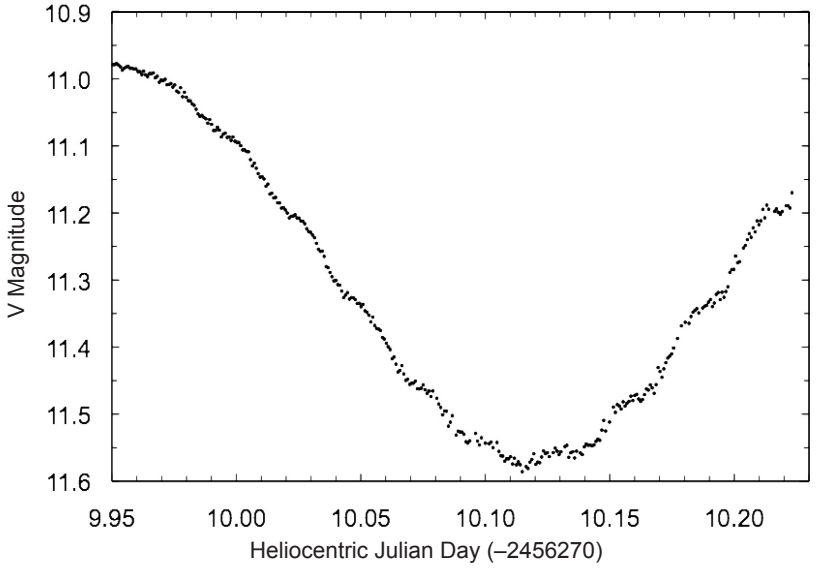

Figure 7a. A primary eclipse of TT Hor 70 days later than that shown in Figure 6, with oscillations more prominent on the ascending phase of the light curve than observed earlier.

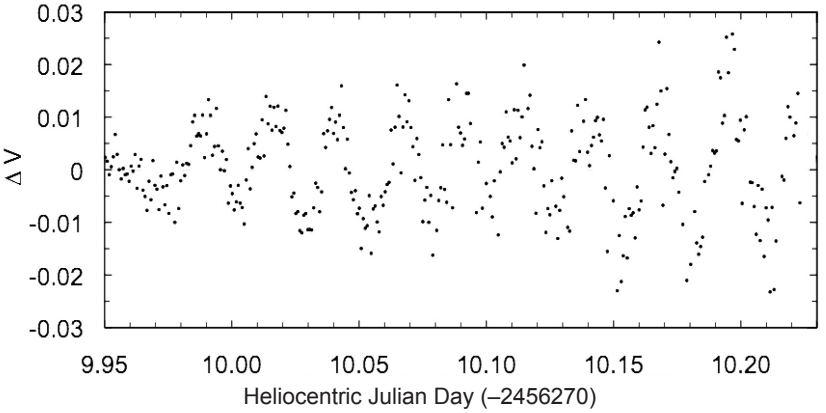

Figure 7b. Oscillations during the primary eclipse of TT Hor in Figure 7a with the primary eclipse light curve subtracted.

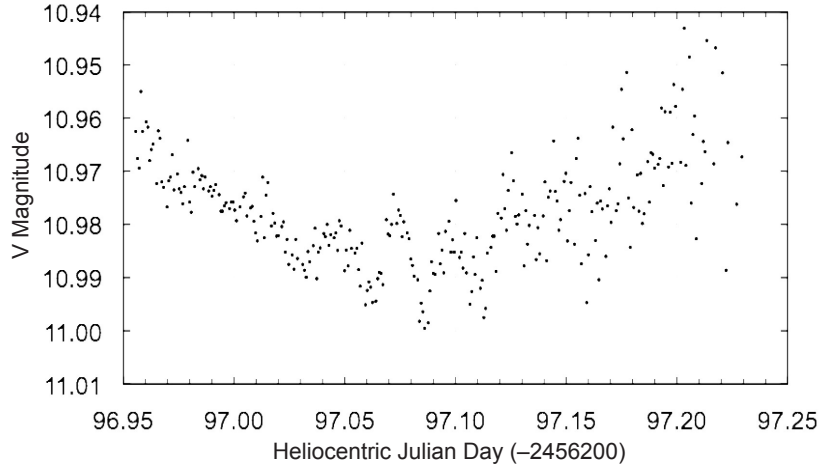

Figure 8. A secondary eclipse of TT Hor.

Amplitude Variations in Pulsating Red Giants

John R. Percy
Romina Abachi
Department of Astronomy and Astrophysics, University of Toronto, Toronto, ON M5S 3H4, Canada; address email correspondence to john.percy@utoronto.ca

Received June 6, 2013; revised August 7, 2013; accepted August 13, 2013

Abstract We have used long-term AAVSO visual observations and Fourier and wavelet analysis to study the long-term amplitude variations in 29 single-mode and 30 double-mode semiregular (SR) pulsating red giants, in the "long secondary periods" (LSPs) of 26 SR stars, and in 10 Mira stars. The amplitudes of the single-mode SR stars vary by factors of 2 to over 10, on time scales of 18 to 170 (median 44) pulsation periods. The amplitudes of the *individual* modes in double-mode SR stars behave similarly; the median time scale is 31 pulsation periods, with half lying between 24 and 42. The amplitudes of the two modes seem to vary independently, rather than varying in phase or anti-phase. The amplitudes of the Mira stars vary by typically factors of 1.1 to 1.3, on time scales of about 35 pulsation periods. The amplitudes of the LSPs, in most stars, vary by up to a factor of 2, on time scales of about 30 LSPs or greater. In view of the uncertainty in determining the time scales, we conclude that the time scales of the amplitude variability are similar in each of these four samples. These results should assist theorists in understanding the nature and cause of the amplitudes and their variations.

1. Introduction

The amplitudes of pulsating variable stars display a wide range of behavior with time. Most Cepheids have constant amplitudes; those with changing amplitudes, such as Polaris (Arellano Ferro 1983) are the object of special study. Many RR Lyrae stars have constant amplitudes, but some show slow, cyclic amplitude variations called the *Blazhko effect* (Kolenberg 2012) which is also of special interest. This paper deals with the amplitude behavior of pulsating red giants, especially non-Mira ones.

Pulsating red giants are classified in the *General Catalogue of Variable Stars* (GCVS; Kholopov *et al.* 1985) as Mira (M) variables if their visual amplitude is greater than 2.5 magnitudes, and semiregular (SR) or irregular (L) variables if their visual amplitude is less than that value. SR variables are subdivided into SRa and SRb (both giants), where SRb have less obvious periodicity than SRa, and SRc (supergiants). Irregular (L) variables nominally show little or no periodicity; see Percy and Terziev (2011) and references therein for comprehensive studies of a large sample of L variables. The M-SRa/SRb-L

classification is an arbitrary one; there is a continuum of behavior from small-amplitude to large, and from periodic to irregular.

Many Mira variables are known to have variable amplitudes (for example, Percy *et al.* 1990); Mira itself ranges, in maximum visual magnitude, from 3 to 6. SR variables have been studied especially by Kiss *et al.* (1999) and by Percy and Tan (2013) and Percy and Kojar (2013). They found that many of these stars show at least two radial pulsation modes, and sometimes a "long secondary period" whose nature and cause are uncertain (Nicholls *et al.* 2009). These studies carried out Fourier analysis of the entire datasets, so did not study possible amplitude variations, except as noted below.

The present paper was initially motivated by the possibility that some of the double-mode SR variables would exhibit *mode switching*, in which the amplitudes of the two modes vary in anti-phase. This is shown in the interesting behavior of R Dor (Bedding *et al.* 1998), though the actual behavior is a bit more complicated than simple mode switching, as described below. In mode switching, pulsation energy may be transferred from one mode to the other, and back again, with the total pulsation energy remaining roughly constant.

Kiss *et al.* (1999) noted that the SR variable RY UMa (period 310 days) varied in amplitude on a time scale of 4000 days, and V Boo, RU Cyg, and Y Per had decreased in amplitude, as had R Dor. Kiss *et al.* (2000) followed up their earlier paper with a study of systematic amplitude variations in a sample of eight pulsating red giants. Y Per slowly reduced its amplitude, nominally changing from a Mira star to an SR variable. RX UMa, RY Leo, and V CVn apparently vary in amplitude due to beating between closely-spaced periods. In RY UMa and possibly RS Aur, the authors model the amplitude modulation in terms of the interaction between pulsation and rotation. In W Cyg and AF Cyg, they propose that the variations are due to mode switching (as in the case of R Dor).

We realized, however, that no systematic study had been carried out of the amplitude behavior of single-mode SR variables. We also analyzed a small sample of Mira stars, using the same procedure, to compare their amplitude behavior with that of the SR variables. We then studied a sample of LSPs to study their amplitude behavior, in the hope that it would shed light on their nature. Our study has been made much easier by the availability of the user-friendly time-series package VSTAR (Benn 2013)—freely available on the AAVSO website—and by the availability of the AAVSO International Database, of course.

2. Data and analysis

We used visual observations, from the AAVSO International Database (AID), of some of the single-mode and double-mode SR variables studied by Kiss *et al.* (1999), Mattei *et al.* (1997), and Percy and Tan (2013). A few of these have LSPs but, with the exception of the ones discussed below, we did not study these LSPs. The observations extend over many decades, thanks to the work of

AAVSO and other observers. They are, however, subject to some limitations. Since there are seasonal gaps in the data, there are alias frequencies in the Fourier spectra, separated from the true frequencies by an integral number of cycles per year. There is also a physiological effect, the Ceraski effect, which produces spurious one-year periods in the Fourier spectra; the amplitudes are generally a few hundredths of a magnitude at most. These alias and spurious periods are especially problematic for pulsating red giants, since their time scales are similar to the stars' true periods. There may also be small, spurious long-term variability if the visual reference stars or their assumed magnitudes have changed, though the AAVSO endeavors to minimize any such effects. Finally: we should point out that visual observation of red stars is particularly challenging because of the different color sensitivities of observers' eyes, and the fact that the visual reference stars are generally less red than the variables.

The data, extending from JD(1) (as given in the tables) to about JD 2456300, were analyzed using the VSTAR package (www.aavso.org/vstar-overview), especially the Fourier analysis and wavelet analysis routines. For the wavelet analysis, the default values were used for the decay time c (0.001) and time division Δt (50 days). The results are sensitive to the former, but not to the latter. Templeton *et al.* (2005) used c = 0.001. For the single-mode SR variables, Mira stars, and LSPs, periods between 0.9 and 1.1 times the published periods were scanned at 0.1 to 1-day resolution, using the range of JDs given in the Tables. Within these ranges, the data were sufficiently dense and continuous for analysis. Especially for the double-mode pulsators, we inspected the power spectra and wavelet plots to identify possible alias periods.

3. Results

3.1. Single-mode variables

Table 1 lists single-mode variables from Kiss *et al.* (1999). All of the stars showed variability of amplitude by typically a factor of 2 to 10 or more. The variations were not strictly periodic, but it was possible to define the approximate number N and length L of the "cycles" of increase and decrease. The amplitude plots were not sinusoids (see Figures 1–8) so the definition of the cycle lengths was somewhat subjective, but we have tried to be consistent in analyzing our four samples of stars. Figure 1 shows an example of amplitude as a function of JD. In this and the other figures, we have also shown the raw light curve. If preferred, light curves with *mean* values of the magnitudes can be constructed, using the Light Curve Generator function on the AAVSO website. The light curves show, for instance, that changes in amplitude include changes in both maximum brightness and minimum brightness. In the table: P is the period in days; JD(1) is the Julian Date of the first observation used; ΔJD is the total length of the dataset; A is the mean amplitude in magnitudes as given by Kiss *et al.* (1999); A Range is the range of amplitudes, in magnitudes, from the wavelet

analysis; N is the number of cycles of amplitude increase and decrease; L is the average length in days of the N cycles; and L/P is the average length of the N cycles expressed in pulsation periods.

The ratio L/P is rather uniform, considering the uncertainty in determining L, though the ratio decreases slightly with increasing P. It ranges from 18 to 170; the median value is 44.

3.2. Mira stars

Out of curiosity, we analyzed a small number of Mira stars in exactly the same way as the single-mode SR variables; they are listed in Table 2. They were taken from the 2013 edition of the RASC *Observer's Handbook* (Chapman 2012), and cover a range of periods. The results are given in Table 2, where the columns are the same as in Table 1. The amplitudes vary by factors of 1.1 to 1.3, with one star (R And) showing only an abrupt change at the beginning of the dataset. The cycle lengths L for increase and decrease in amplitude, in units of the pulsation period P, have a median value of 35, which is not unlike that (44) for the SR variables. Figure 7 shows the amplitude variation in one star, S Hya.

3.3. Double-mode variables

The results for double-mode variables are given in Table 3, where the values of the period P in days, the mean amplitude A in magnitudes, the range R in magnitudes, and amplitude cycle length L in days and periods are given for both mode 1 (the longer) and mode 2 (the shorter). Because of the multiple periods, alias periods, and possible Ceraski periods, these stars required careful analysis, and further notes are provided in section 3.5. The amplitudes of each of the two modes were analyzed both together (that is, by scanning from below the short period to above the longer one) and separately (that is, around each period), using VSTAR.

We began by analyzing R Dor, to reproduce the results of Bedding *et al.* (1998), which we did successfully; the results are shown in Figure 2. The amplitude of the longer period is initially largest, then that of the shorter period, then the longer, and finally the shorter. But there are epochs (for example, JD 2437000–2439000) when one amplitude is largest, even though it is near the minimum in its cycle of variability, so "mode switching" is a somewhat misleading term.

In RS Cam (Figure 3), the amplitudes of the two modes are sometimes in phase, sometimes in antiphase. V CVn has two close periods, and it was not possible to separate them using wavelet analysis; Figure 4 shows the amplitude variability of the combined periods; see section 3.5 below. In RZ Cyg (Figure 5), it is clear that the amplitude of the long period varies more slowly than that of the shorter period, as is the case with R Dor (Figure 2). In W Vul (Figure 6), the amplitudes of the two modes also vary independently.

Many of the stars mode-switch in the sense that the modes alternate in *dominance*, even though they are not necessarily varying in anti-phase.

3.4. Long secondary periods

The results are given in Table 4, where the columns are the same as in Table 1, except that the pulsation period P and the long secondary period LSP, both in days, are given separately. Long secondary periods are typically an order of magnitude longer than radial pulsation periods, so our datasets of 20,000+ days are essential for this study. We found that, in most stars in our sample, the amplitudes of the LSPs varied by up to a factor of 2, though 4 of the 26 stars showed no significant variation (0.01 magnitude or less). Figure 8 shows the amplitude variation in one star, V UMi.

Even with our long datasets, few of the stars showed a full cycle of amplitude increase and decrease and, for those which did, it was obviously not possible to know whether the variation in amplitude was truly cyclic (or periodic). We could only define a "characteristic time" L for increase or decrease. For stars which showed less than a full cycle of increase or decrease, we have defined a crude lower limit for L (Table 4). We have then expressed this in units of the LSP in the last column of Table 4. The median value of L/LSP (obviously a lower limit) is about 30. It is interesting to note that this is approximately equal to the value of L/P for the single-mode and double-mode radial pulsation periods.

Several stars show no significant variability in LSP amplitude. They tend to be stars with longer pulsation periods.

3.5. Notes on individual stars

These are listed in the order that they appear in the four tables and are marked in the tables with an asterisk.

RV And: the amplitude variability is quasi-periodic.

GY Aql: note the large amplitude.

RV Boo: note the small amplitude.

T Cnc: the amplitude variability is irregular.

T Cen: the amplitude variability is irregular.

DM Cep: the data are sparse; the amplitude is small.

V460 Cyg: note the small amplitude.

U Hya: note the small amplitude.

UZ Per: only about a quarter of a cycle of amplitude variability is observed.

W Tau: note the very large range in amplitude.

R And: the amplitude is constant, except for an abrupt change at the beginning of the dataset.

W And: there is an abrupt change in amplitude at the end of the dataset.

R Tri: there is an abrupt change in the amplitude at the beginning of the dataset.

TV And: the short period is clearly separated from the aliases of the longer period, but is rather weak. The longer period varies in amplitude, but is dominant throughout the dataset.

V Aql: the overall amplitude decreases throughout the dataset.

V Boo: the overall amplitude decreases throughout the dataset, as Kiss *et al.* (1999) found, so the star has technically ceased to be a Mira star and is now an SR. The long period is dominant.

RX Boo: the Fourier spectrum is indistinct, and the amplitudes of the modes are very small at times.

U Cam: the dataset is initially sparse. The amplitude of the shorter period actually varies more slowly than that of the longer period—a rarity in our sample.

RS Cam: the data are sparse, and are only usable for the last 10,000 days.

V CVn: this is one of the stars in which Kiss *et al.* (2000) identified beating behavior. In our study, it was not possible to separate the amplitude behavior of the two close periods, 186.45 and 192.73 days, using wavelet analysis; Figure 4 shows the amplitude behavior of the combined periods. We subdivided the data into four segments, and used Fourier analysis. The amplitude of the shorter period remained approximately constant (about 0.2) but the amplitude of the longer period decreased substantially in the last quarter of the dataset—from about 0.48 to about 0.16. The beat period between the two close periods is 5,721 days, or about 30 times the mean period.

SV Cas: the data are somewhat sparse. The longer period initially has a low amplitude, but is dominant in the second half of the dataset.

RS CrB: there is some confusion between the shorter period, and an alias of the longer one, which is dominant. The data are somewhat sparse. There is a noticeable slow variation of the mean magnitude, on a time scale of 10,000 days.

W Cyg: Kiss *et al.* (2000) considered this star to undergo mode-switching, but the situation is more complicated. The shorter period has the larger mean amplitude but, for the first half of the dataset, the amplitudes are comparable and variable, so they switch dominance ("mode-switch") several times. The amplitude of the shorter period becomes much larger toward the end of the dataset.

RU Cyg: although the shorter period has the largest mean amplitude, it is highly variable, and the two periods switch "dominance" several times.

RZ Cyg: the amplitude of the 540-day period declined slowly from 0.9 to 0.4, with four small (0.1) cycles of amplitude variation superimposed.

T Eri: note that the amplitude of the longer period is dominant and greater than 2.5; this is technically a Mira star.

RS Gem: there is some confusion between the shorter period, and an alias of the longer one. The two periods have comparable amplitudes, and do indeed mode-switch (in the sense of alternating in having the largest amplitude) several times.

g Her: there appears to be a second radial period of about 60 days (also found by Lebzelter and Kiss (2001)).

SW Mon: the periods have comparable amplitudes, and do mode-switch.

BQ Ori: the data are somewhat sparse. The modes have comparable and

variable amplitudes, and switch dominance several times.

RU Per: the 170-day period may be mixed with an alias of the 316-day period. The two periods have comparable amplitudes, and do alternate in dominance several times.

S Tri: the data are sparse. The longer period is variable in amplitude, but always dominant.

V UMa: the longer period has a variable amplitude, but is almost always dominant.

V UMi: the amplitudes of the two modes are initially very small, but the amplitude of the shorter-period one becomes significant towards the end of the dataset.

SW Vir: the amplitudes of the two close periods seem to vary in phase.

W Vul: the data are sparse, and the Fourier spectrum is indistinct.

RU Vul: the amplitude decreases abruptly around JD 2439000. This decrease is associated primarily with the shorter period.

RS Cam: the data are sparse; the variability in amplitude is large, though we only observe a small fraction of the cycle of amplitude variability.

RW Eri: the data are sparse.

V Hya: this is an extremely complex star, with a large-amplitude, eclipse-like light curve. It shows bipolar outflows which appear to come from an accretion disk in an inferred binary system.

4. Discussion

Although there have been no systematic studies of amplitude changes in SR stars, there have been a few studies of small samples, including those mentioned in the introduction. Also, Percy *et al.* (2003) used long-term *photoelectric* photometry to detect cyclic amplitude variations in five small-amplitude multiperiodic pulsating red giants which are classified as SR. When the amplitude variations were re-analyzed in the same way as in this paper (and with the same uncertainties), the mean value of the cycle length L was 34P, for the twelve different periods of these five stars—consistent with the results of the present paper.

The question now arises: what is the cause of the amplitude variations, and why are the time scales consistently a few tens of pulsation periods? First: is it plausible that the actual pulsation energy increases and decreases on time scales of tens of periods? Non-linear models for pulsating red giants (Olivier and Wood 2005) and *supergiants* (Fadeyev 2012) indicate growth times of a few tens of periods, so it is possible that the pulsation energy, and hence amplitude, could vary on this time scale.

Wood (2013) has pointed out that, if a star were to dissipate its pulsation energy, then its mean brightness might increase as the amplitude was decreasing. Observing such an effect in these stars is complicated by the presence of LSPs in some of the stars, and by other long-term changes in mean brightness. SS Vir,

for instance, has large changes in mean brightness, but these do not appear to correlate with the changing amplitude of the pulsation. We have looked at a number of single-mode stars with large amplitude decreases, and we find no evidence of correlations between changing amplitude and changing mean brightness—with one possible exception: SS Vir, as revealed by the photoelectric V data on this star in the last 5000 days. It shows a significant brightening as the amplitude decreases.

In the RR Lyrae stars which show the Blazhko effect, the ratio L/P is about 100; Kolenberg (2012) has described several mechanisms which might explain the effect; she leans slightly toward a model involving a resonant interaction between two radial modes.

One potentially-relevant process in SR stars might be the presence of large convection cells ("supergranular convection"). These are predicted to cause large "spots" on the photospheres of red *supergiants* (for example, Chiavassa *et al.* 2011). They have also been suggested as a cause of the "red noise" observed in the power spectra of pulsating red supergiants (Kiss *et al.* 2006) and giants (Templeton and Karovska 2009; Templeton *et al.* 2012) and also as a possible cause of the LSPs. If large convection cells caused the amplitude to vary across the face of the star, then *rotation*—which undoubtedly occurs in the stars—would modulate the observed amplitude. The constancy of L/P (at least within an order of magnitude) suggests that whatever modulates the amplitude should scale as the period, and the rotation period would do this via the radius of the star.

A simple calculation of the ratio of the rotation period to the pulsation period (the latter determined from the pulsation constant Q) shows that, for a star of two solar masses, a rotation velocity $v \sin i = 1$ km/s, a pulsation period of 300 days, and a pulsation constant Q = 0.08, gives a ratio of 33, which is very close to the median value observed. Specifically:

$$P_{rot} / P_{puls} = 32.2 \, ((m/m_{\odot})^{0.33} / Q^{0.67} \, P_{puls}^{0.33}) \, v \sin i \qquad (1)$$

According to this calculation, the ratio should be larger for the first-overtone mode; indeed, the ratio of L2/P2 to L1/P1 from Table 3 has a median value of 1.33. This calculation also predicts that, for a given pulsation mode, the ratio should be smaller for larger pulsation periods. We do not find this correlation in Table 3.

Amplitude changes could thus occur if there were large convective regions which rotated around the star, and varied in time and position so as to produce the more irregular rise and fall of the amplitude. On the other hand, the rotational hypothesis does not explain why the time scales of the amplitude variations in the double-mode SR stars are different for the two modes, so we cannot tell, at this point, whether the amplitude changes are a physical effect or a geometrical effect. Bedding (2013) has suggested a plausible alternative: the amplitude variations are due to growth and decay of stochastically-excited pulsations. Christensen-Dalsgaard, *et al.* (2001) showed that SR stars have amplitude scatter which is consistent with this mechanism; they showed a

simulated time series, based on this mechanism, with amplitude variations very similar to those of some of the stars in Table 1.

On a different topic: in the linear (small-amplitude) approximation, the period of a vibrating object such as a star is independent of the amplitude. It is possible, however, that the changes in amplitude that we have observed might produce observable non-linear increases in period (Bedding *et al.* 2000; Zijlstra *et al.* 2004). Because period changes produce a *cumulative* effect, they can be observable, even if they are very small. Bedding *et al.* (2000) and Zijlstra *et al.* (2004) used wavelet analysis to show that R Aql, BH Cru, and S Ori show matching amplitude and period changes. It is not known, however, whether the observed period changes are a direct result of the amplitude changes, or whether both are the result of some change in the physical properties of the stars. Also, Mira stars show apparent period changes due to random cycle-to-cycle period fluctuations (Eddington and Plakidis 1929; Percy and Colivas 1999). We have examined the period and amplitude plots for a few of our stars, and there is a general—but not exact—correspondence between the variations of the two.

5. Conclusions

We have studied the changing amplitudes of the pulsation modes in 29 single- and 30 double-mode SR stars, and a small sample of 10 Miras. We have also studied the changing amplitudes of the LSPs in 26 SR stars. Almost all of the stars show variable amplitudes and, despite the uncertainty in determining the time scales of the amplitude variability, the time scales are 30 to 45 periods in most stars in each of the four samples. This time scale is consistent with the rotation period of the stars, but the hypothesis that the changes in amplitude are connected with the rotation of the star is only partly supported by our data. There is no evidence for *systematic* mode switching in the double-mode SR stars; the amplitudes of the two modes seem to vary independently, though they may alternate in dominance. These new results raise some intriguing questions, and should provide useful information for theoreticians in understanding the pulsations and the LSPs in pulsating red giants.

6. Acknowledgements

We thank the hundreds of AAVSO observers who made the observations which were used in this project, and we thank the AAVSO staff for processing and archiving the measurements. We also thank the team which developed the VSTAR package, and made it user-friendly and publicly available. We are grateful to Professors Tim Bedding and Peter Wood for reading and commenting on a draft of this paper, and additionally to Professor Bedding for his important contribution to Section 4. This project was supported by the University of Toronto Work-Study Program. It made use of the SIMBAD database, which is operated by CDS, Strasbourg, France.

References

Arellano Ferro, A. 1983, *Astrophys. J.*, **274**, 755.
Bedding, T. R. 2013, private communication (November).
Bedding, T. R., Conn, B. C., and Zijlstra, A. A. 2000, in *The Impact of Large-Scale Surveys on Pulsating Star Research*, eds. L. Szabados and D. W. Kurtz, ASP Conf. Ser., 203, Astron. Soc. Pacific, San Francisco, 96.
Bedding, T. R., Zijlstra, A. A., Jones, A., and Foster, G. 1998, *Mon. Not. Roy. Astron. Soc.*, **301**, 1073.
Benn, D. 2013, VSTAR data analysis software (http://www.aavso.org/node/803).
Chapman, D. M. F., ed. 2013, *Observer's Handbook*, Royal Astronomical Society of Canada, Toronto.
Chiavassa, A. *et al.* 2011, *Astron. Astrophys.*, **528A**, 120.
Christensen-Dalsgaard, J., Kjeldsen, H., and Mattei, J. A. 2001, *Astrophys. J.*, **562**, L141.
Eddington, A. S., and Plakidis, S. 1929, *Mon. Not. Roy. Astron. Soc.*, **90**, 65.
Fadeyev, Y. A. 2012, *Astron. Lett.*, **38**, 260.
Kholopov, P. N. *et al.*, 1985, *General Catalogue of Variable Stars*, 4th ed., Moscow.
Kiss, L. L., Szabó, G. M., and Bedding, T. R. 2006, *Mon. Not. Roy. Astron. Soc.*, **372**, 1721.
Kiss, L. L., Szatmáry, K., Cadmus, R. R., Jr., and Mattei, J. A. 1999, *Astron. Astrophys.*, **346**, 542.
Kiss, L. L., Szatmáry, K., Szabó, G. M., and Mattei, J. A. 2000, *Astron. Astrophys., Suppl. Ser.*, **145**, 283.
Kolenberg, K. 2012, *J. Amer. Assoc. Var. Star Obs.*, **40**, 481.
Lebzelter, T., and Kiss, L. L. 2001, *Astron. Astrophys.*, **380**, 388.
Mattei, J. A., Foster, G., Hurwitz, L. A., Malatesta, K. H., Willson, L. A., and Mennessier, M. O. 1997, in *Proceedings of the ESA Symposium "Hipparcos—Venice '97"*, ESA SP-402, ESA Publ. Div., Noordwijk, The Netherlands, 269.
Nicholls, C. P., Wood, P. R., Cioni, M.-R. L., and Soszyński, I. 2009, *Mon. Not. Roy. Astron. Soc.*, **399**, 2063.
Olivier, E. A., and Wood, P. R. 2005, *Mon. Not. Roy. Astron. Soc.*, **362**, 1396.
Percy, J. R., Besla, G., Velocci, V., and Henry, G. W. 2003, *Publ. Astron. Soc. Pacific*, **115**, 479.
Percy, J. R., and Colivas, T. 1999, *Publ. Astron. Soc. Pacific*, **111**, 94.
Percy, J. R., Colivas, T., Sloan, W. B., and Mattei, J. A. 1990, in *Confrontation between Stellar Pulsation and Evolution*, eds. C. Cacciari and G. Clementini, ASP Conf. Ser., 11, Astron. Soc. Pacific, San Francisco, 446.
Percy, J. R., and Kojar, T. 2013, *J. Amer. Assoc. Var. Star Obs.*, **41**, 15.
Percy, J. R., and Tan, P. J. 2013, *J. Amer. Assoc. Var. Star Obs.*, **41**, 1.
Percy, J. R., and Terziev, E. 2011, *J. Amer. Assoc. Var. Star Obs.*, **39**, 1.
Templeton, M. R., and Karovska, M. 2009, in *Stellar Pulsation: Challenges for Theory and Observation*, ed . J. A. Guzik and P. A. Bradley, AIP CP1170,

American Institute of Physics, Melville, NY, 164.
Templeton, M. R., Karovska, M., and Waagen, E. O. 2012, *Bull. Amer. Astron. Soc.*, **44**, 348.16.
Templeton, M. R., Mattei, J. A., and Willson, L. A., 2005, *Astron. J.*, **130**, 776.
Wood, P. R. 2013, private communication (May 31).
Zijlstra, A. A. *et al.* 2004, *Mon. Not. Roy. Astron. Soc.*, **352**, 325.

Table 1. Amplitude variability of monoperiodic pulsating red giants.

*Star**	*P(d)*	*JD(1)*	*ΔJD*	*A*	*A Range*	*N*	*L(d)*	*L/P*
RV And*	165	2428000	28300	0.30	0.20–0.60	4	7075	43
S Aql	143	2420000	36300	0.98	0.65–1.20	10:	3630:	25
GY Aql*	464	2447000	9300	2.35	1.90–2.20	1	9300	20
T Ari	320	2428000	28300	0.91	0.70–1.35	1.5	18867	59
S Aur	596	2416000	40300	0.61	0.45–0.85	2.5	16120	27
U Boo	204	2420000	49300	0.62	0.35–0.80	6	8216	40
RV Boo*	144	2434000	22300	0.09	0.05–0.15	5	4460	31
S Cam	327	2417000	39300	0.34	0.23–1.00	5	7860	24
RY Cam	134	2435000	21300	0.16	0.10–0.40	1.5	14200	106
T Cnc*	488	2417000	39300	0.34	0.23–0.47	3	13100	27
RT Cap	400	2417000	39300	0.31	0.25–0.45	1	39300	98
T Cen*	91	2413000	43300	0.62	0.50–1.20	10	4330	48
DM Cep*	367	2435000	21300	0.12	0.05–0.10	3	7100	18
RS CrB	331	2435000	21300	0.19	0.13–0.38	0.5	42600	129
AI Cyg	146	2450000	5700	0.18	0.17–0.52	1.5	3800	26
GY Cyg	143	2440000	16300	0.13	0.08–0.43	1	16300	114
V460 Cyg*	160	2435000	21300	0.08	0.04–0.14	3	7100	44
V930 Cyg	247	2442000	14300	0.72	0.30–0.70	2	7150	29
EU Del	62	2435000	21300	0.08	0.05–0.17	4	5325	86
SW Gem	700	2427500	28800	0.10	0.05–0.35	0.5	57600	82
RR Her	250	2435000	21300	0.54	0.10–0.70	1	21300	85
RT Hya	255	2415000	41300	0.20	0.20–1.00	2.5	16520	65
U Hya*	791	2420000	36300	0.06	0.04–0.16	0.5	72600	92
X Mon	148	2415000	41300	0.59	0.25–0.85	4	10325	70
SY Per	477	2446000	10300	0.89	0.67–0.92	1	10300	22
UZ Per*	850	2448000	8300	0.25	0.23–0.29	0.25	33200	39
W Tau*	243	2415000	41300	0.27	0.10–1.50	1	41300	170
V UMa	198	2420000	36300	0.19	0.15–0.50	6.5:	5585	28
SS Vir	361	2420000	36300	0.81	0.60–1.15	3.5	10371	29

**Note in section 3.5*

Table 2. Amplitude variability of a small set of Mira stars.

*Star**	*P(d)*	*JD(1)*	*ΔJD*	*A Range*	*N*	*L(d)*	*L/P*
R And*	409	2420000	36300	constant	—	—	—
W And*	397	2420000	36300	2.95–3.15	6	6050	15
R Aur	459	2420000	36300	2.05–2.80	2	18150	40
T Cam	374	2420000	36300	2.15–2.75	3	12100	32
V Cnc	272	2420000	36300	2.00–2.45	3.5	10371	38
T Cas	445	2410000	46300	1.40–1.95	3:	15433	35
U Cet	235	2420000	36300	2.05–2.65	3.5	10371	44
S Hya	257	2420000	36300	2.10–2.55	4.5	8067	31
R Tri*	266	2420000	36300	2.40–2.65	3	12100	45
R UMa	302	2420000	36300	2.55–2.90	5	7260	24

**Note in section 3.5*

Table 3. Amplitude variability of double–mode semiregular variable stars.

*Star**	*P1/A1, P2/A2*	*JD(1)*	*L1/P1*	*R1*	*L2/P2*	*R2*
TV And*	112/0.71, 62/0.31	2427500	37	0.15–0.65	42	0.10–0.40
V Aql*	400/0.10, 215/0.11	2423000	21	0.28–0.04	26	0.31–0.04
V Boo*	258/1.20, 134/0.47	2419000	36	0.10–1.50	40	0.15–0.50
RX Boo*	305/0.14, 162/0.17	2434000	15	0.02–0.19	20	0.03–0.22
U Cam*	400/0.09, 220/0.09	2427500	29	0.04–0.19	53	0.05–0.23
RR Cam	223/0.09, 124/0.10	2427500	20	0.10–0.30	29	0.08–0.28
RS Cam*	160/0.15, 90/0.12	2445000	25	0.07–0.28	17	0.15–0.50
V CVn*	194/0.42, 186/0.13	2433000	30	0.07–0.17	42:	0.11–0.58
SV Cas*	460/0.48, 262/0.32	2435000	62	0.25–0.75	23	0.20–0.85
WZ Cas	373/0.16, 187/0.09	2430000	24	0.07–0.28	24	0.06–0.29
T Col	225/3.95, 116/0.36	2415000	61	1.75–2.40	178	0.35–1.15
RS CrB*	332/0.34, 183/0.10	2435000	16:	0.03–0.16	13:	0.03–0.13
W Cyg*	237/0.23, 131/0.54	2420000	31	0.07–0.40	56:	0.07–0.43
RU Cyg*	434/0.30, 235/0.69	2420000	42	0.05–0.42	52	0.11–0.76
RZ Cyg*	537/0.63, 271/0.86	2415000	19	0.90–0.40	33	0.40–1.40
R Dor	330/0.15, 176/0.10	2430000	100	0.13–0.48	95	0.05–0.35
S Dra	311/0.12, 172/0.12	2420000	78:	0.10–0.55	141	0.05–0.75
TX Dra	136/0.13, 77/0.31	2432000	30	0.06–0.20	33	0.05–0.37
T Eri*	254/4.49, 132/0.25	2428000	28	2.00–2.50	43	0.20–0.95
RS Gem*	271/0.25, 148/0.22	2427000	18	0.15–0.65	40	0.11–0.65
g Her*	90/0.16, 60/0.05	2432000	25	0.03–0.19	37	0.03–0.15
SW Mon*	194/0.40, 103/0.30	2428000	24	0.13–0.46	23	0.13–0.47
BQ Ori*	240/0.14, 127/0.10	2434000	23	0.12–0.40	25	0.09–0.51
RU Per*	329/0.38, 170/0.42	2428000	29	0.05–0.60	37	0.06–0.43

Table continued on next page

Table 3. Amplitude variability of double–mode semiregular variable stars, cont.

*Star**	*P1/A1, P2/A2*	*JD(1)*	*L1/P1*	*R1*	*L2/P2*	*R2*
S Tri*	250/1.06, 131/0.29	2440000	33	0.25–0.70	31	0.17–0.46
V UMa*	199/0.49, 109/0.16	2420000	15	0.07–0.38	74	0.06–0.52
V UMi*	127/0.10, 73/0.14	2432000	21	0.03–0.17	33	0.04–0.29
SW Vir*	164/0.13, 154/0.20	2434000	34	0.05–0.55	29	0.10–0.62
W Vul*	242/0.34, 126/0.35	2436000	22	0.10–0.45	30	0.10–0.37
RU Vul*	369/0.13, 136/0.11	2428000	38	0.03–0.23	104:	0.06–0.80

**Note in section 3.5*

Table 4. Amplitude variability of long secondary period in SR variables.

*Star**	*P(d)*	*LSP(d)*	*A*	*JD(1)*	*A Range*	*ΔJD*	*L(d)*	*L/LSP*
U Cam	400, 220	2800	0.13	2427000	0.15–0.18	28800	≥115200	≥41
RS Cam*	160, 90	966	0.17	2445000	0.09–0.25	11300	45200	47
ST Cam	372, 202	1580	0.10	2435000	constant	21300	—	—
X Cnc	350, 193	1870	0.08	2433000	0.03–0.05	23300	46600	25
Y CVn	273, 160	3000	0.08	2432000	constant	24300	48600	—
V465 Cas	97	898	0.16	2440000	0.13–0.25	16300	≥32600	≥36
AF Cyg	163, 93	921	0.08	2425000	0.05–0.20	31300	41733	45
AW Cyg	387	3700	0.10	2435000	constant	21300	—	—
V927 Cyg	229:	2900	0.25	2450000	constant	2700	—	—
U Del	110:	1146	0.21	2430000	0.14–0.26	26300	43833	38
RY Dra	200–300	1150	0.20	2435000	0.08–0.14	21300	28400	25
TX Dra	137, 77	706	0.10	2432000	0.09–0.19	24300	24300	34
Z Eri	74	729	0.15	2432000	0.08–0.19	24300	18692	26
RW Eri*	91	950	0.15	2435000	0.09–0.19	21300	≥42600	≥26
TU Gem	215	2406	0.10	2433000	0.10–0.12	23300	≥46600	≥19
g Her	90	887	0.20	2432000	0.14–0.22	24300	32400	37
UW Her	172, 107	1000	0.09	2435000	0.09–0.12	21300	14200	14
V Hya*	531	6400	1.22	2416000	1.09–1.16	40300	—	—
S Lep	97	856	0.24	2435000	0.19–0.35	21300	28400	33
W Ori	208	2390	0.15	2433000	0.18–0.23	23300	≥58250	≥24
V431 Ori	273:	2400	0.18	2440000	0.17–0.20	16300	≥65200	≥27
BD Peg	78:	3300	0.18	2435000	0.11–0.21	21300	≥85200	≥26
τ^4 Ser	111	1240	0.10	2435000	0.07–0.12	21300	21300	17
ST UMa	615	5300	0.11	2432000	no result	24300	—	—
V UMi	126, 73	737	0.06	2433000	0.03–0.10	23300	23300	32
SW Vir	164, 154	1700	0.15	2434000	0.10–0.16	22300	27875	16

**Note in section 3.5*

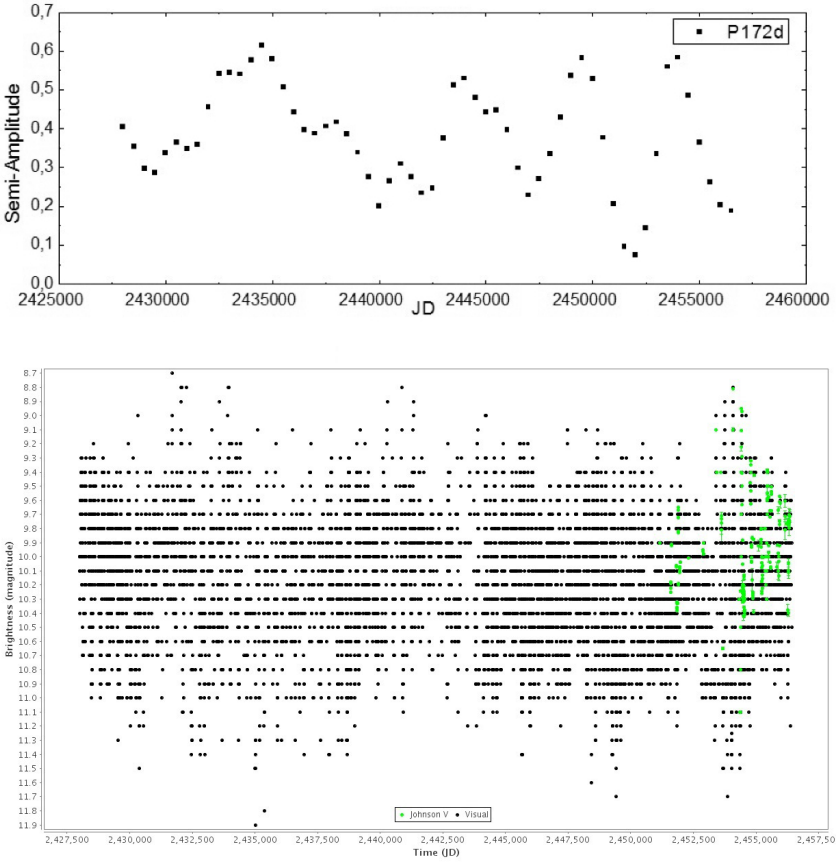

Figure 1. The changing amplitude of the single-mode semiregular variable RV And, determined by wavelet analysis (upper plot). The pulsation period is 172 days. The amplitude varies by a factor of six, and there are approximately four cycles of increase and decrease. The light curve from the AAVSO International Database (AID) is shown in the lower plot.

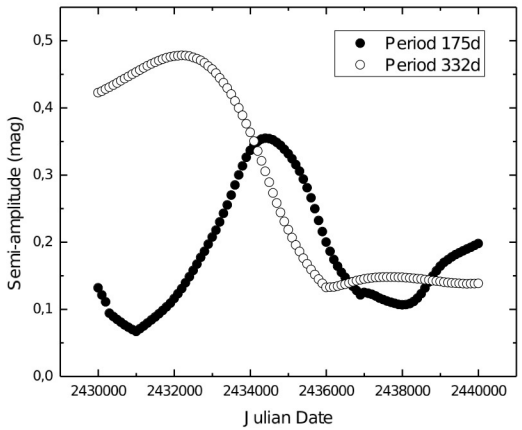

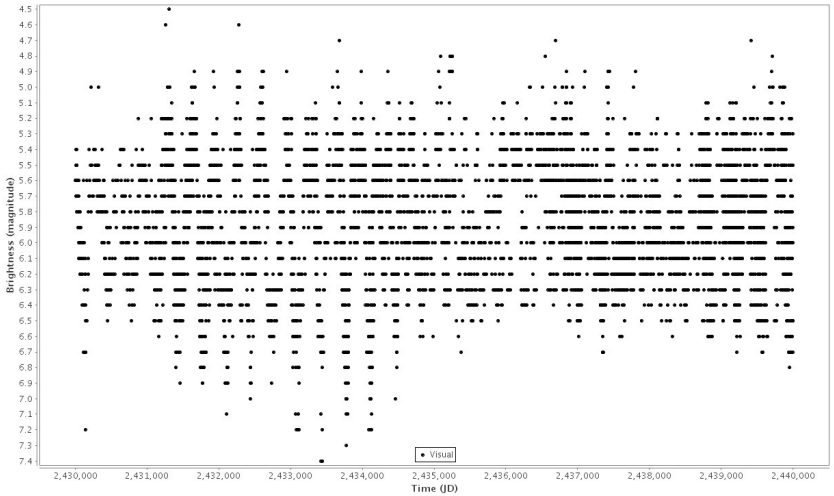

Figure 2. The changing amplitudes of the two pulsation modes in the double-mode SR star R Dor (upper plot). The amplitude of the shorter period varies more rapidly than that of the longer period. The star switches modes in the sense that the two modes alternate in dominance, but the longer period dominates, the second time, when it is at minimum amplitude. The light curve from the AID is shown in the lower plot.

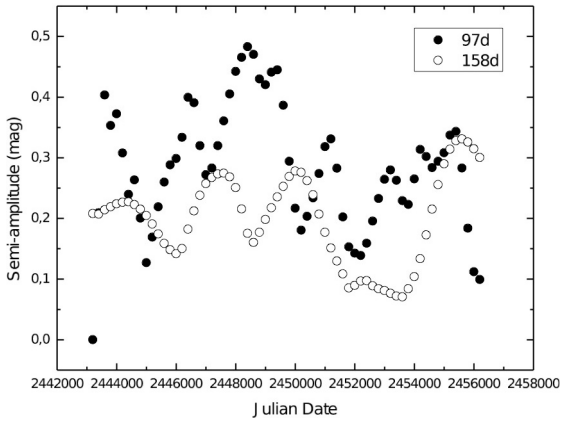

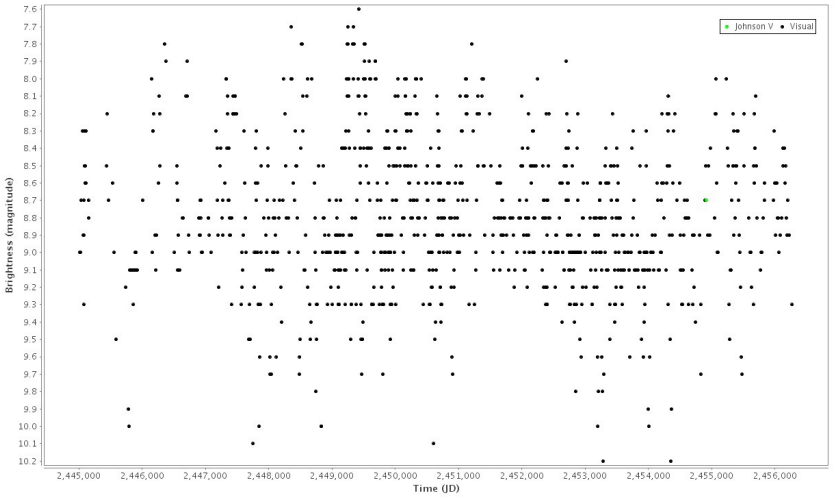

Figure 3. The changing amplitudes of the two pulsation modes in the double-mode SR star RS Cam (upper plot). The shorter period varies in amplitude more rapidly than the longer one. The light curve from the AID is shown in the lower plot.

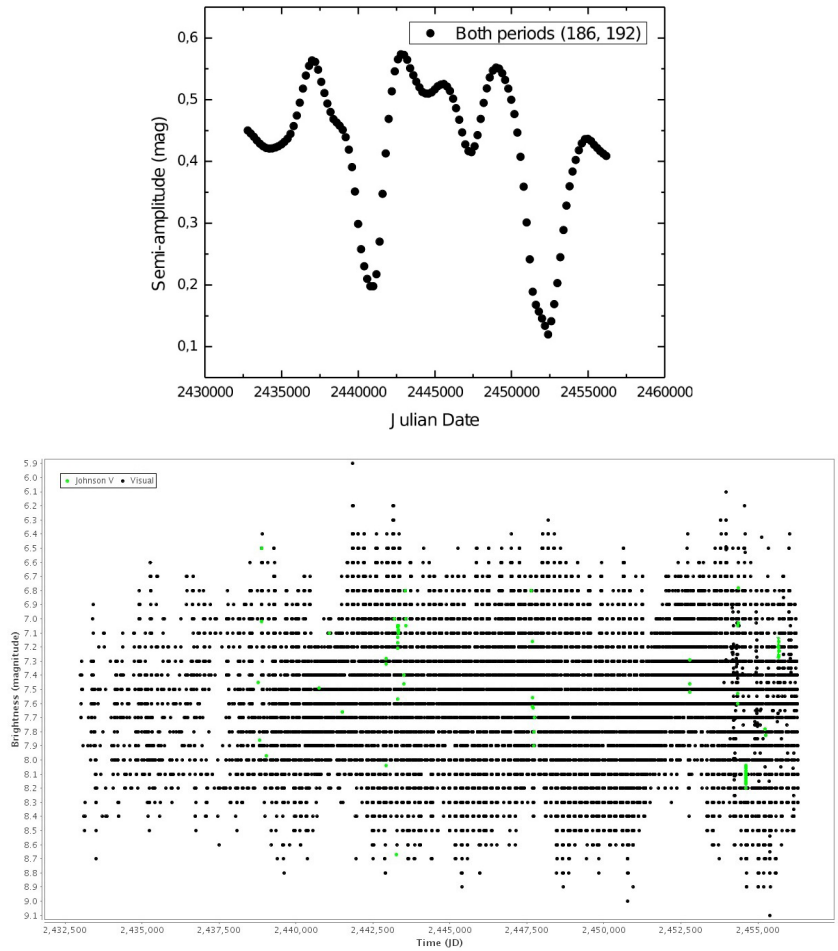

Figure 4. The changing amplitudes of the two pulsation modes in the double-mode SR star V CVn (upper plot). The amplitude variations of the two close periods could not be individually followed. The light curve from the AID is shown in the lower plot.

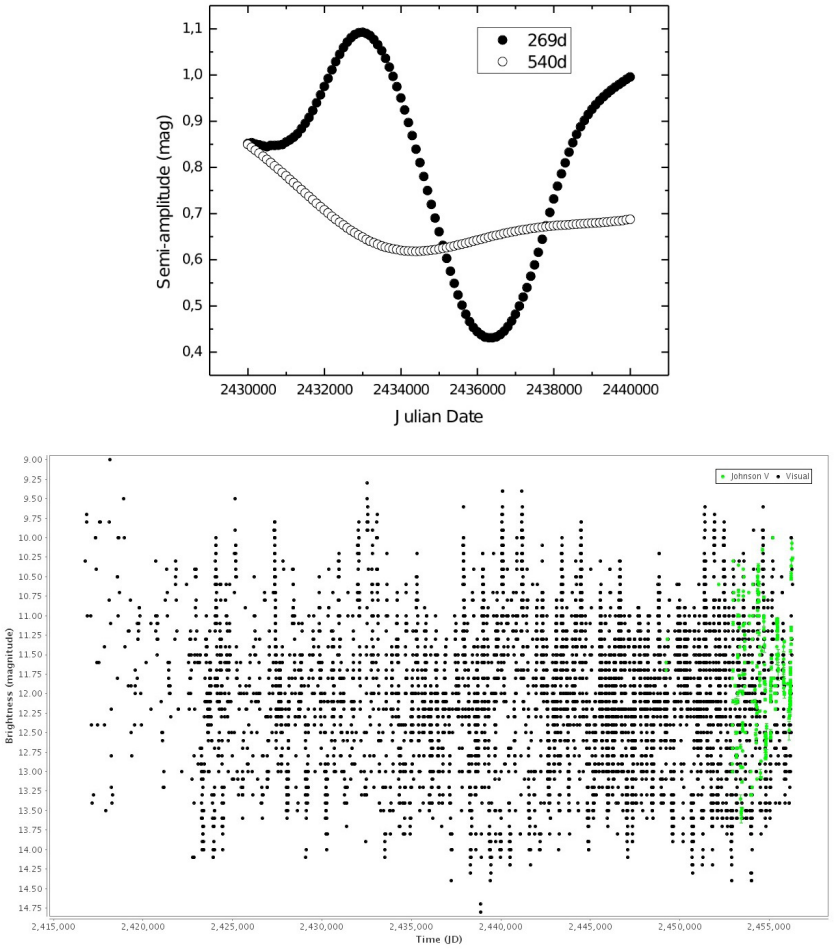

Figure 5. The changing amplitudes of the two pulsation modes in the double-mode SR star RZ Cyg (upper plot). The amplitude of the shorter period varies more rapidly than that of the longer one. The light curve from the AID is shown in the lower plot.

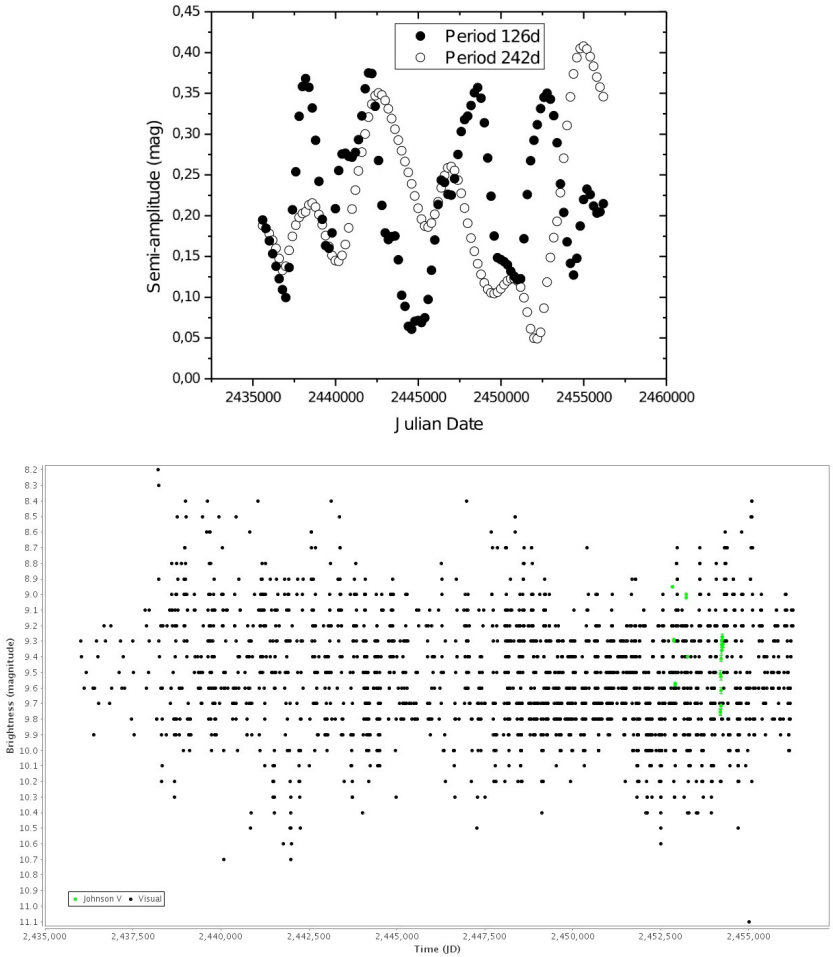

Figure 6. The changing amplitudes of the two pulsation modes in the double-mode SR star W Vul (upper plot). Note that the amplitude variations of the two modes are sometimes in phase, sometimes in anti-phase, and sometimes neither. The light curve from the AID is shown in the lower plot.

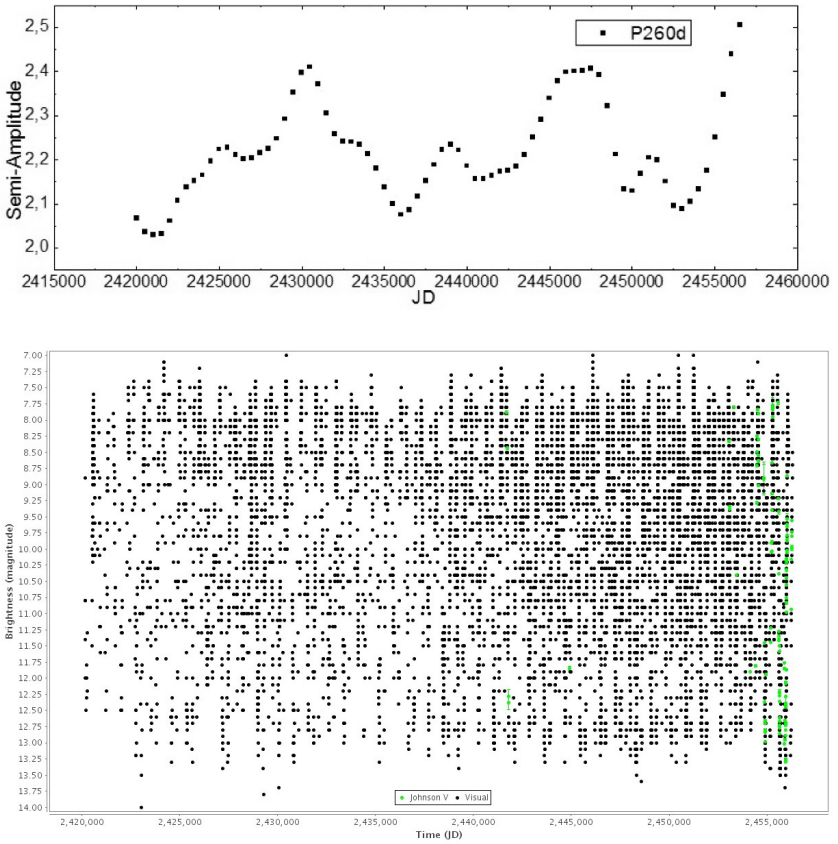

Figure 7. The changing amplitude of the Mira star S Hya, determined by wavelet analysis (upper plot). The pulsation period is 260 days. The light curve from the AID is shown in the lower plot.

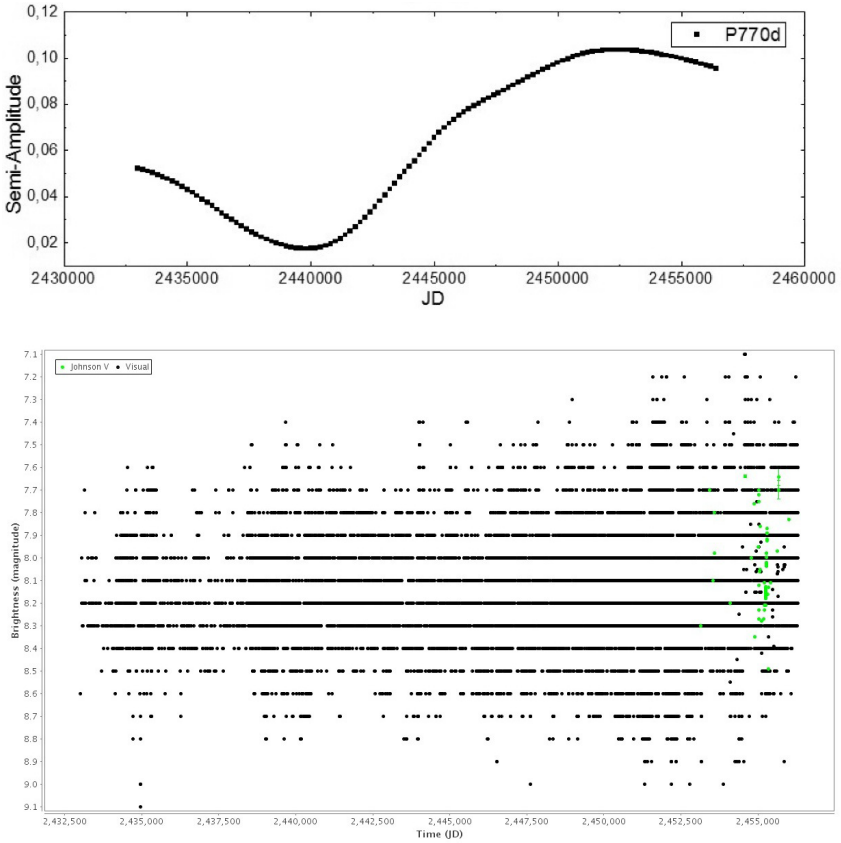

Figure 8. The changing amplitude of the long secondary period of the semiregular variable V UMi, determined by wavelet analysis (upper plot). The long secondary period is 770 days. It is not possible to know whether the amplitude variation is actually cyclic; only a fraction of a "cycle" can be observed. The light curve from the AID is shown in the lower plot.

V784 Ophiuchi: an RR Lyrae Star With Multiple Blazhko Modulations

Pierre de Ponthière
15 Rue Pré Mathy, Lesve, Profondeville 5170, Belgium; address email correspondence to pierredeponthiere@gmail.com

Franz-Josef Hambsch
12 Oude Bleken, Mol, 2400, Belgium

Tom Krajci
P.O. Box 1351, Cloudcroft, NM 88317

Kenneth Menzies
318A Potter Road, Framingham, MA 01701

Received May 15, 2013; revised June 14, 2013; accepted June 24, 2013

Abstract The results of an observation campaign of V784 Ophiuchi over a time span of two years have revealed a multi-periodic Blazhko effect. A Blazhko effect for V784 Oph has not been reported previously. From the observed light curves, 60 pulsation maxima have been measured. The Fourier analyses of the (O–C) values and of magnitudes at maximum light (M_{max}) have revealed a main Blazhko period of 24.51 days but also two other secondary Blazhko modulations with periods of 34.29 and 31.07 days. A complete light curve Fourier analysis with PERIOD04 has shown triplet structures based on main and secondary Blazhko frequencies close to the reciprocal of Blazhko periods measured from the 60 pulsation maxima.

1. Introduction

In the *General Catalogue of Variable Stars* (GCVS; Samus *et al.* 2011) V784 Ophiuchi is correctly classified as an RR Lyr (RRab) variable star but with an incorrect period of 0.3762746 day as pointed out by Wils *et al.* (2006). They corrected the period to 0.60336 day but did not detect a Blazhko effect from the Northern Sky Variability Survey data (Wozniak *et al.* 2004) due to the paucity of available datasets.

The current data were gathered during 238 nights between June 2011 and October 2012. During this period of 488 days, a total of 15,223 magnitude measurements covering 18 Blazhko cycles were collected. The observations were made by Krajci and Hambsch using 30- and 40-cm telescopes located in Cloudcroft (New Mexico), Mol (Belgium), and mainly in San Pedro de Atacama (Chile). The numbers of observations for the different locations are 1,986 for Cloudcroft, 470 for Mol, and 12,767 for San Pedro de Atacama.

The comparison stars are given in Table 1. The star coordinates and magnitudes in B and V bands were obtained from the NOMAD catalogue (Zacharias *et al.* 2011). C1 was used as a magnitude reference and C2 as a check star. The Johnson V magnitudes from different instruments have not been transformed to the standard system since measurements were performed with a V filter only. However, two simultaneous maximum measurements from the instruments in Cloudcroft and San Pedro de Atacama were observed to differ by only 0.034 and 0.042 mag. Dark and flat field corrections were performed with MAXIMDL software (Diffraction Limited 2004), and aperture photometry was performed using LESVEPHOTOMETRY (de Ponthière 2010), a custom software which also evaluates the SNR and estimates magnitude errors.

2. Light curve maxima analysis

The times of maxima of the light curves have been evaluated with custom software (de Ponthiere 2010) fitting the light curve with a smoothing spline function (Reinsch 1967). Table 2 provides the list of 60 observed maxima and Figures 1a and 1b show the (O–C) and M_{max} (Magnitude at Maximum) values. For clarity only the most intensive part of the observation campaign is included in Figures 1a and 1b. From a simple inspection of the M_{max} graph the Blazhko effect is obvious as well as the presence of a second modulation frequency. The Blazhko effect is itself apparently modulated by a lower frequency component.

A linear regression of all available (O–C) values has provided a pulsation period of 0.6033557 d (1.657397 d^{-1}). The (O–C) values have been re-evaluated with this new pulsation period and the pulsation ephemeris origin has been set to the highest recorded maximum: HJD 2456047.7942. The new derived pulsation elements are:

$$HJD_{Pulsation} = (2456047.7942 \pm 0.0015) + (0.6033557 \pm 0.0000078)\, E_{Pulsation} \quad (1)$$

The derived pulsation period is in good agreement with the value of 0.60336 d published by Wils *et al.* (2006). The folded light curve on this pulsation period is shown in Figure 2.

To determine the Blazhko effect, Fourier analyses and sine-wave fittings of the (O–C) values and M_{max} (Magnitude at Maximum) values were performed with PERIOD04 (Lenz and Breger 2005). These analyses were limited to the first two frequency components and are tabulated in Table 3.

The frequency uncertainties have been evaluated from the Least-Square fittings. The obtained periods (24.56 and 24.51 days) for the first Blazhko effect agree within the errors. However, the periods (34.29 and 31.07 days) of the second Blazhko modulation are statistically different and in the next section it will be shown that they are also found in the complete light curve Fourier analysis. To dismiss the possible effect of minor amplitude differences between

the non-standardized observations, the Blazhko spectral components from M_{max} have been re-evaluated with only the observations from San Pedro de Atacama (Chile). The resulting frequencies (0.04081 and 0.03215 c/d) are within the uncertainties of the complete dataset.

The (O–C) and magnitude at maximum curves folded with the Blazhko period are given in Figures 3a and 4a. In these diagrams, the scatter of the data is mainly due to the presence of the second Blazhko modulation. These data were folded using the period of 24.56 days for the (O–C) values and 24.51 days for the M_{max} values. When a pre-whitening with the frequency of 0.02916 c/d is applied to the (O–C) dataset, the scatter is reduced significantly as is shown in Figure 3b. The scatter of the M_{max} data is also reduced after a pre-whitening with the corresponding frequency of 0.03219 c/d (Figure 4b).

On this basis the best Blazhko ephemeris is

$$HJD_{Blazhko} = 2456047.7942 + (24.51 \pm 0.02)\, E_{Blazhko} \qquad (2)$$

where the origin has been selected as the epoch of the highest recorded maximum.

The peak-to-peak magnitude variation during the night of highest recorded maximum is 1.34 mag. Over the Blazhko period, the magnitude at maximum brightness differs by about 0.66 mag., that is, 49% of the light curve peak-to-peak variations. The (O–C) values differ in a range of 0.046 day, that is, 7.7% of the pulsation period.

3. Frequency spectrum analysis of the light curve

From the light curve maxima analysis, the pulsation and Blazhko frequencies and other frequencies modulating the Blazhko effect have been identified. It is interesting to note that these modulating frequencies are clearly present in the spectrum of the complete light curve.

The Blazhko effect can be seen as an amplitude and phase modulation of the periodic pulsation with the modulation frequency being the Blazhko frequency (Szeidl and Jurcsik 2009). The spectrum of a signal modulated in amplitude and phase is characterized by a pattern of peaks called multiplets at the positions $kf_0 \pm nf_B$ with k and n being integers corresponding respectively to the harmonic and multiplet orders. The frequencies, amplitudes, and phases of the multiplets can be measured by a succession of Fourier analyses, pre-whitenings, and sine-wave fittings.

This analysis has been performed with PERIOD04. Only the harmonic and multiplet components having a signal-to-noise ratio (SNR) greater than 4 have been retained as significant signals.

Besides the pulsation frequency f_0, harmonics nf_0, and series of triplets $nf_0 \pm f_B$ based on the principal Blazhko frequency f_B, other triplets have also been found and are tabulated in Table 4. They are based on two other secondary

modulation frequencies, f_{B2} and f_{B3}, which are close to the secondary modulation components identified in the (O–C) and M_{max} analyses.

It is interesting to note that the period ($1/f_{B2}$) of 34.70 days is close to the second period 34.29 days found in the (O–C) analysis. The period ($1/f_{B3}$) of 29.99 days can be compared to the second period 31.07 days found in the magnitude at maximum (M_{max}) analysis. Table 5 provides the complete list of Fourier components with their amplitudes, phases, and uncertainties. During the sine-wave fitting, the fundamental frequency f_0 and largest triplets f_0+f_B, f_0+f_{B2}, and f_0-f_{B3} have been left unconstrained and the other frequencies have been entered as combinations of these four frequencies. The uncertainties of frequencies, amplitudes, and phases have been estimated by Monte Carlo simulations. The amplitude and phase uncertainties have been multiplied by a factor of two as it is known that the Monte Carlo simulations underestimate these uncertainties (Kolenberg *et al.* 2009). The two Blazhko modulation frequencies, f_B (0.040544) and f_{B2} (0.028820), are close to a 7:5 resonance ratio and the corresponding beat period is around 173 days. Calculations based on Blazhko periods (24.56 and 34.29 days) obtained with the (O–C) analysis provide the same resonance ratio. The other pair of frequencies, f_B (0.040544) and f_{B3} (0.033346), is close to a 5:6 resonance ratio with a beat period around 149 days, but a different resonance ratio of 5:4 with a beat period of 123 days is obtained from the periods (24.51 and 31.07 days) found in the M_{max} analysis. This discrepancy is probably due to the greater uncertainty (124 E^{-6}) of the f_{B3} side lobes. In CZ Lacertae, Sódor *et al.* (2011) have also detected two modulation components with a resonance ratio of 5:4 during a first observing season but a different resonance ratio of 4:3 during the next season.

Table 6 lists for each harmonic the amplitude ratios A_i/A_1 and the ratios usually used to characterize the Blazhko effect, that is, A_i^+/A_1 ; A_i^-/A_1 ; $R_i=A_{i1}^+/A_{i1}^-$; and asymmetries $Q_i=(A_{i1}^+-A_{i1}^-)/(A_{i1}^++A_{i1}^-)$. Szeidl and Jurcsik (2009) have shown that the asymmetry of the side lobe amplitudes depends on the phase difference between the amplitude and the phase modulation. If the Blazhko effect is limited to amplitude or phase modulation the asymmetry vanishes. In the present case the side lobe A_{i1}^+ is the strongest one, which is generally the case for stars showing a Blazhko effect. The asymmetry ratios Q_i around 0.32 are a sign of both strong amplitude and phase modulations. The R_i and Q_i ratios for triplets around the secondary Blazhko frequency f_{B2} are also given in Table 6. The f_{B2} frequency is close to the secondary frequency detected in the (O–C) analysis and thus likely related to a phase modulation effect. The f_{B2} frequency seems to act only on phase modulation, and this could explain the low asymmetry values (0.03) of the f_{B2} side lobes.

4. Light curve variations over Blazhko cycle

Subdividing the data set into temporal subsets is a classical method to

analyze the light curve variations over the Blazhko cycle. Ten temporal subsets corresponding to the different Blazhko phase intervals Ψ_i $(i = 0, 9)$ have been created using the epoch of the highest recorded maximum (2456047.7942) as the origin of the first subset. Fortunately, the data points are relatively well distributed over the subsets with the number of data points varying between 1,126 and 1,715. Figure 5 presents the folded light curve for the ten subsets. Despite the subdivision over the Blazhko cycle, a scatter still remains in the light curves. The light curves are folded with the primary Blazhko frequency, and the secondary Blazhko frequencies are creating the observed scatter.

Fourier analyses and Least-Square fittings have been performed on the different temporal subsets. For the fundamental and the first four harmonics the amplitude A_i and the epoch-independent phase differences ($\Phi_{k1} = \Phi_k - k\Phi_1$) are given in Table 7 and plotted in Figure 6. The number of data points belonging to each subset is also given in this table. The amplitudes of the fundamental and harmonics show smooth sinusoidal variations with the minima occurring around Blazhko phase 0.5, that is, when the light curve amplitude variation on the pulsation is weaker. The ratio of harmonic A_4 to fundamental A_1 is at maximum at Blazhko phase 1.0, when the ascending branch of the light curve is steeper. The difference between maximum and minimum Φ_1 phases is a measure of the phase modulation strength and is equal to 0.453 radian, or 0.072 cycle, which corresponds roughly to the value of 7.7% noted for the peak-to-peak deviation of (O–C). The epoch-independent phase differences Φ_{31} and Φ_{41} vary as smooth sinusoids, with the maximum phase differences occurring at Blazhko phase 0.5. However, Φ_{21} variations, if any, are small. This weak Φ_{21} variation has been also noted for MW Lyr (Jurcsik *et al.* 2008) and V1820 Ori (de Ponthiere *et al.* 2013).

5. Conclusions

The effects of three Blazhko modulations have been detected by measurements of (O–C) values and amplitude of light curve maxima and confirmed by complete light curve Fourier analysis. The main Blazhko period $(1/f_B)$ is 24.51 days. The secondary Blazhko period $(1/f_{B2})$ of 34.70 days is apparently related to phase modulation, as it is detected in the (O–C) analysis, and f_B and f_{B2} are close to a 7:5 resonance ratio. The tertiary modulation $(1/f_{B3})$ is weaker in the Fourier analysis and the period values are slightly different from magnitude at maximum and light curve Fourier analysis (31.07 and 29.99 days, respectively). The resonance ratios of f_B and f_{B3} are approximately 5:4 or 5:6 in function of the analysis method. This discrepancy is probably due to the weakness of the corresponding Fourier multiplet values and their larger uncertainties.

6. Acknowledgements

AAVSO Director Dr. Arne A. Henden and the AAVSO are acknowledged for the use of AAVSOnet telescopes at Cloudcroft (New Mexico). The authors thank the referee for constructive comments which have helped to clarify and improve the paper. This work has made use of The International Variable Star Index (VSX) maintained by the AAVSO and of the SIMBAD astronomical database (http://simbad.u-strasbg.fr)

References

de Ponthière, P. 2010, LESVEPHOTOMETRY, automatic photometry software (http://www.dppobservatory.net).

de Ponthière, P. , Hambsch, F.-J., Krajci, T., Menzies, K., and Wils, P. 2013, *J. Amer. Assoc. Var. Star Obs.*, **41**, 58.

Diffraction Limited. 2004, MAXIMDL image processing software (http://www.cyanogen.com).

Jurcsik, J., *et al.* 2008, *Mon. Not. Roy. Astron. Soc.*, **391**, 164.

Kolenberg, K., *et al.* 2009, *Mon. Not. Roy. Astron. Soc.*, **396**, 263.

Lenz, P., and Breger, M. 2005, *Commun. Asteroseismology*, **146**, 53.

Reinsch, C. H. 1967, *Numer. Math.*, **10**, 177.

Samus, N. N., *et al.* 2011, *General Catalogue of Variable Stars* (GCVS database, Version 2011 January, http://www.sai.msu.su/gcvs/gcvs/index.htm).

Sódor, Á., *et al.* 2011, *Mon. Not. Roy. Astron. Soc.*, **411**, 1585.

Szeidl, B., and Jurcsik, J. 2009, *Commun. Asteroseismology*, **160**, 17.

Wils, P., Lloyd, C., and Bernhard, K. 2006, *Mon. Not. Roy. Astron. Soc.*, **368**, 1757.

Wozniak, P., *et al.* 2004, *Astron. J.*, **127**, 2436.

Zacharias, N., Monet, D., Levine, S., Urban, S., Gaume, R., and Wycoff, G. 2011, The Naval Observatory Merged Astrometric Dataset (NOMAD, http://www.usno.navy.mil/USNO/astrometry/optical-IR-prod/nomad/the-nomad1-catalogue).

Table 1. Comparison stars for V784 Oph.

Identification	*R.A. (2000)* h m s	*Dec. (2000)* ° ′ ″	*B*	*V*	*B–V*	
GSC 992-1617	17 35 18.037	+07 40 58.97	13.24	12.32	0.92	C1
TYC 992-1203	17 35 35.883	+07 41 29.21	11.491	10.442	1.049	C2

Table 2. List of measured maxima of V784 Oph.

Maximum HJD	*Error*	*O–C (day)*	*E*	*Magnitude*	*Error*	*Location**
2455778.6910	0.0014	–0.0066	–446	11.692	0.004	1
2455780.5024	0.0021	–0.0052	–443	11.841	0.004	1
2455783.5146	0.0035	–0.0098	–438	12.043	0.005	1
2455792.5913	0.0055	0.0166	–423	11.952	0.022	1
2455795.6064	0.0023	0.0149	–418	11.757	0.005	1
2455798.6121	0.0022	0.0038	–413	11.581	0.004	1
2455801.6283	0.0012	0.0032	–408	11.580	0.004	1
2455804.6413	0.0018	–0.0006	–403	11.747	0.004	1
2455815.5203	0.0062	0.0180	–385	12.139	0.005	1
2455818.5302	0.0040	0.0112	–380	11.998	0.005	1
2455989.8824	0.0030	0.0103	–96	11.897	0.006	1
2455992.8923	0.0021	0.0035	–91	11.762	0.007	1
2456009.8043	0.0036	0.0215	–63	11.971	0.008	1
2456012.8109	0.0027	0.01133	–58	11.830	0.007	1
2456015.8195	0.0018	0.00315	–53	11.683	0.006	1
2456018.8292	0.0015	–0.00393	–48	11.569	0.006	1
2456024.8557	0.0014	–0.01098	–38	11.751	0.009	1
2456027.8774	0.0026	–0.00606	–33	11.965	0.009	1
2456035.7338	0.0025	0.00671	–20	12.028	0.007	1
2456038.7570	0.0033	0.01314	–15	11.898	0.007	1
2456038.7570	0.0033	0.01314	–15	11.898	0.007	1
2456047.7942	0.0019	0.00000	0	11.512	0.006	1
2456050.8100	0.0019	–0.00098	5	11.753	0.007	1
2456053.8208	0.0025	–0.00696	10	11.931	0.010	1
2456056.8352	0.0041	–0.00934	15	12.120	0.008	1
2456059.8458	0.0071	–0.01551	20	12.172	0.011	1
2456062.8785	0.0082	0.00041	25	12.091	0.007	1
2456064.6946	0.0034	0.00644	28	11.939	0.007	1
2456065.8972	0.0029	0.00233	30	11.856	0.008	1
2456067.7028	0.0019	–0.00214	33	11.709	0.007	1
2456068.9082	0.0009	–0.00345	35	11.624	0.008	1
2456070.7195	0.0016	–0.00222	38	11.555	0.006	1
2456073.7360	0.0014	–0.00249	43	11.563	0.007	1
2456076.7611	0.0021	0.00583	48	11.764	0.007	1
2456076.7625	0.0032	0.00723	48	11.806	0.015	2
2456079.7870	0.0026	0.01495	53	11.922	0.008	1
2456081.6018	0.0037	0.01968	56	11.980	0.010	1
2456082.8111	0.0090	0.02227	58	12.060	0.013	1
2456084.6218	0.0046	0.02290	61	12.036	0.010	1

Table continued on next page

Table 2. List of measured maxima of V784 Oph, cont.

Maximum HJD	*Error*	*O–C (day)*	*E*	*Magnitude*	*Error*	*Location**
2456085.8238	0.0052	0.01819	63	12.044	0.009	1
2456087.6345	0.0045	0.01882	66	11.997	0.008	1
2456088.8314	0.0043	0.00901	68	11.966	0.008	1
2456088.8321	0.0045	0.00971	68	12.000	0.012	2
2456091.8378	0.0024	–0.00137	73	11.906	0.013	2
2456093.6474	0.0026	–0.00183	76	11.771	0.007	1
2456096.6554	0.0015	–0.01061	81	11.712	0.007	1
2456102.6891	0.0051	–0.01047	91	11.870	0.012	2
2456105.7166	0.0036	0.00025	96	11.961	0.010	2
2456108.7536	0.0033	0.02048	101	11.932	0.009	1
2456110.5743	0.0040	0.03111	104	11.895	0.010	1
2456111.7694	0.0030	0.01950	106	11.824	0.012	1
2456113.5785	0.0027	0.01853	109	11.783	0.010	1
2456114.7832	0.0024	0.01652	111	11.727	0.009	1
2456116.5854	0.0012	0.00865	114	11.631	0.007	1
2456122.6012	0.0018	–0.00911	124	11.673	0.006	1
2456125.6160	0.0028	–0.01108	129	11.821	0.007	1
2456131.6492	0.0068	–0.01144	139	12.059	0.008	1
2456134.6806	0.0037	0.00318	144	11.988	0.008	1
2456145.5391	0.0008	0.00128	162	11.572	0.007	1
2456227.5864	0.0027	–0.00780	298	11.955	0.006	2

**Locations : 1—San Pedro de Atacama (Chile); 2—Cloudcroft (New Mexico).*

Table 3. Blazhko spectral components.

From (O–C) values					
Frequency (cycle/days)	$\sigma(d^{-1})$	*Period (days)*	$\sigma(d)$	*Amplitude (days)*	ϕ *(cycle)*
0.04071	13 E–5	24.56	0.08	0.0098	0.502
0.02916	14 E–5	34.29	0.17	0.0091	0.195
From M_{max}					
Frequency (cycle/days)	$\sigma(d^{-1})$	*Period (days)*	$\sigma(d)$	*Amplitude (mag.)*	ϕ *(cycle)*
0.04080	4 E–5	24.51	0.02	0.229	0.622
0.03219	8 E–5	31.07	0.08	0.112	0.620

Table 4. Triplet component frequencies and periods.

Component	*Derived from*	*Frequency* (d^{-1})	$\sigma(d^{-1})$	*Period* (d)	σ(d)
f_0	—	1.657399	3.2 E^{-6}	0.6033551	1.16 E^{-6}
f_B	$f_0 + f_B$	0.040544	29 E^{-6}	24.66	0.02
f_{B2}	$f_0 + f_{B2}$	0.028820	35 E^{-6}	34.70	0.04
f_{B3}	$f_0 - f_{B3}$	0.033346	124 E^{-6}	29.99	0.11

Table 5. Multi-frequency fit results for V784 Oph.

Component	$f(d^{-1})$	$\sigma(f)$	A_i (mag)	$\sigma(A_i)$	ϕ_i(cycle)	$\sigma(\phi_i)$	*SNR*
f_0	1.657399	3.2 E–06	0.3594	0.0017	0.01810	0.0007	140.8
$2f_0$	3.314798		0.1612	0.0016	0.42518	0.0017	71.9
$3f_0$	4.972196		0.0963	0.0016	0.87223	0.0024	47.6
$4f_0$	6.629595		0.0587	0.0013	0.32035	0.0049	31.3
$5f_0$	8.286994		0.0324	0.0017	0.77462	0.0080	18.1
$6f_0$	9.944393		0.0135	0.0018	0.17084	0.0207	7.9
$7f_0$	11.601792		0.0094	0.0016	0.56694	0.0289	6.0
$8f_0$	13.259190		0.0060	0.0017	0.99881	0.0358	4.2
f_0+f_B	1.697943	29 E–06	0.0516	0.0016	0.62414	0.0047	20.3
f_0-f_B	1.616855		0.0263	0.0017	0.40709	0.0113	10.4
$2f_0+f_B$	3.355341		0.0314	0.0017	0.00102	0.0082	14.0
$2f_0-f_B$	3.274254		0.0140	0.0016	0.77565	0.0204	6.2
$3f_0+f_B$	5.012740		0.0336	0.0018	0.42290	0.0083	16.6
$3f_0-f_B$	4.931653		0.0183	0.0015	0.21889	0.0130	9.0
$4f_0+f_B$	6.670139		0.0254	0.0016	0.85193	0.0111	13.6
$4f_0-f_B$	6.589051		0.0166	0.0018	0.67866	0.0166	8.9
$5f_0+f_B$	8.327538		0.0156	0.0015	0.30249	0.0178	8.7
$5f_0-f_B$	8.246450		0.0116	0.0017	0.11565	0.0214	6.5
$6f_0+f_B$	9.984937		0.0101	0.0016	0.73701	0.0248	5.9
$6f_0-f_B$	9.903849		0.0088	0.0016	0.60313	0.0297	5.1
$7f_0+f_B$	11.642335		0.0087	0.0016	0.19222	0.0299	5.5
f_0+f_{B2}	1.686218	35 E–06	0.0237	0.0018	0.77081	0.0114	9.3
f_0-f_{B2}	1.628579		0.0224	0.0018	0.94771	0.0133	8.8
$2f_0+f_{B2}$	3.343617		0.0187	0.0016	0.19953	0.0119	8.3
$2f_0-f_{B2}$	3.285978		0.0175	0.0016	0.32003	0.0155	7.8
$3f_0+f_{B2}$	5.001016		0.0185	0.0017	0.62995	0.0148	9.1
$3f_0-f_{B2}$	4.943377		0.0149	0.0016	0.75635	0.0183	7.4
$4f_0+f_{B2}$	6.658415		0.0133	0.0018	0.08536	0.0206	7.1
$4f_0-f_{B2}$	6.600776		0.0152	0.0017	0.19267	0.0172	8.1
$5f_0+f_{B2}$	8.315814		0.0098	0.0017	0.52105	0.0276	5.5
$5f_0-f_{B2}$	8.258174		0.0104	0.0018	0.61650	0.0246	5.8
f_0-f_{B3}	1.624053	124 E–06	0.0178	0.0022	0.90174	0.0147	8.1
f_0+f_{B3}	1.690744		0.0112	0.0019	0.11617	0.0246	5.4

Table 6. V784 Oph harmonic, triplet amplitudes, ratios, and asymmetry parameters.

i	A_i/A_1	A_i^+/A_1	A_i^-/A_1	R_i	Q_i	$R_i\,(f_{B2})$	$Q_i\,(f_{B2})$
1	1.00	0.14	0.07	1.96	0.32	1.06	0.03
2	0.45	0.09	0.04	2.24	0.38	1.07	0.03
3	0.27	0.09	0.05	1.84	0.30	1.24	0.11
4	0.16	0.07	0.05	1.53	0.21	0.88	–0.07
5	0.09	0.04	0.03	1.35	0.15	0.94	–0.03
6	0.04	0.03	0.02	1.15	0.07	—	—
7	0.03	0.02	—	—	—	—	—
8	0.02	—	—	—	—	—	—

Table 7. V784 Oph Fourier coefficients over Blazhko cycles.

Ψ *(cycle)*	A_1 *(mag)*	A_2 *(mag)*	A_3 *(mag)*	A_4 *(mag)*	A_4/A_1	Φ_1 *(rad)*	Φ_{21} *(rad)*	Φ_{31} *(rad)*	Φ_{41} *(rad)*
0.0–0.1	0.423	0.191	0.137	0.093	0.220	0.161	2.406	5.024	1.357
0.1–0.2	0.363	0.162	0.102	0.064	0.176	0.025	2.392	5.126	1.432
0.2–0.3	0.324	0.144	0.085	0.055	0.170	0.383	2.458	5.300	1.724
0.3–0.4	0.293	0.123	0.059	0.042	0.145	0.399	2.533	5.417	2.140
0.4–0.5	0.288	0.114	0.050	0.027	0.094	0.248	2.533	5.631	2.338
0.5–0.6	0.322	0.133	0.066	0.036	0.111	0.287	2.536	5.411	2.010
0.6–0.7	0.354	0.154	0.077	0.041	0.117	0.168	2.477	5.276	1.949
0.7–0.8	0.394	0.174	0.119	0.072	0.182	0.067	2.457	5.166	1.518
0.8–0.9	0.408	0.197	0.138	0.101	0.246	0.202	2.415	5.121	1.466
0.9–1.0	0.431	0.196	0.149	0.096	0.223	-0.054	2.234	4.797	1.127

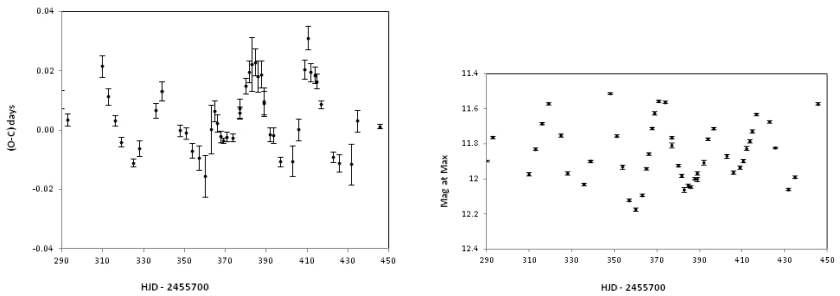

Figure 1a, b. V784 Oph O–C (days) and magnitude at maximum.

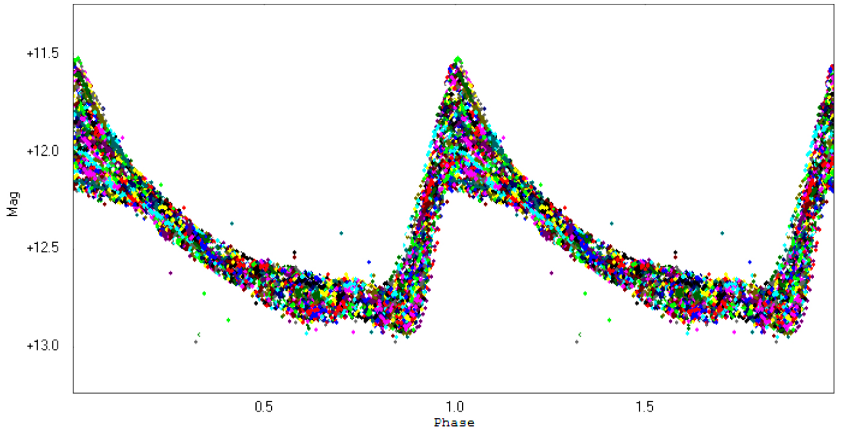

Figure 2. V784 Oph light curve folded with pulsation period.

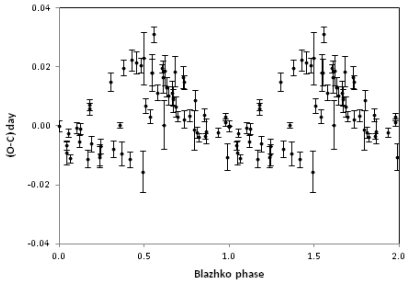

Figure 3a. O–C without pre-whitening.

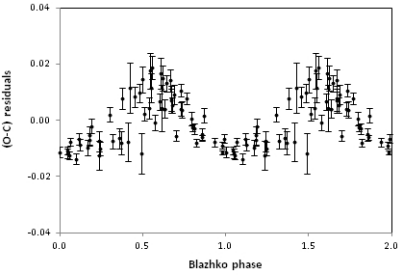

Figure 3b. O–C after pre-whitening.

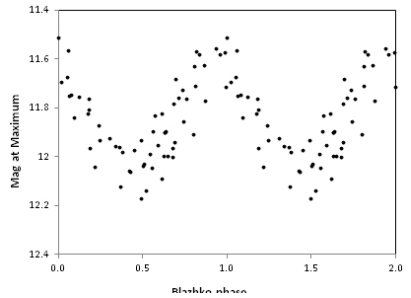

Figure 4a. Magnitude at maximum without pre-whitening.

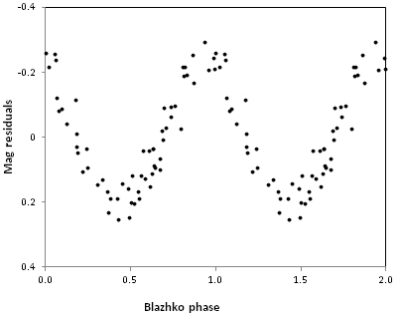

Figure 4b. Magnitude at maximum after pre-whitening.

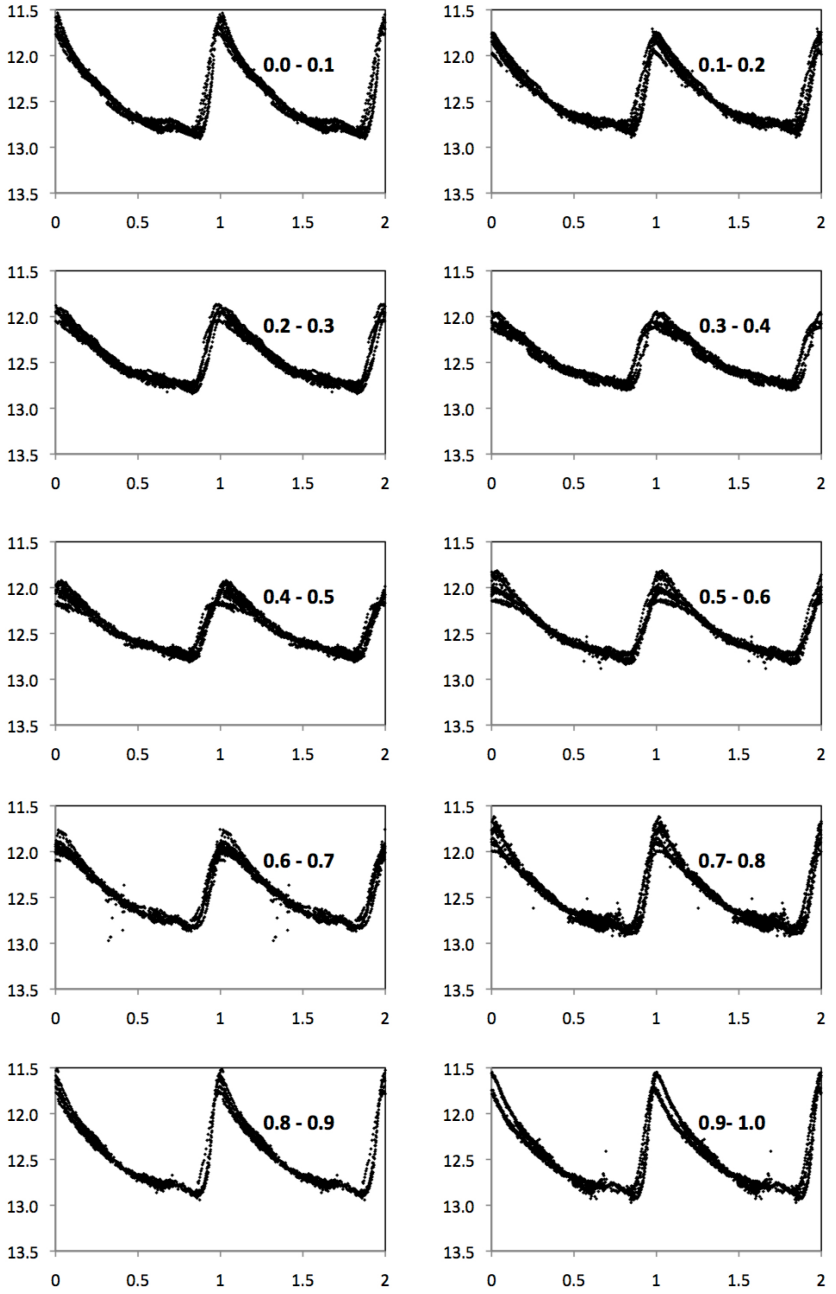

Figure 5. V784 Oph light curve for the ten temporal subsets (magnitude vs. pulsation phase).

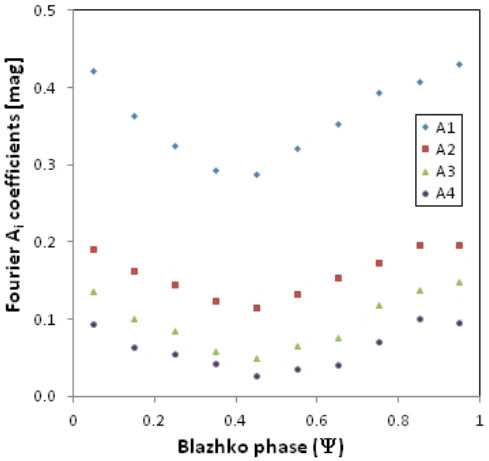

Figure 6a. V784 Oph Fourier A_i amplitude (mag.) for the ten temporal subsets.

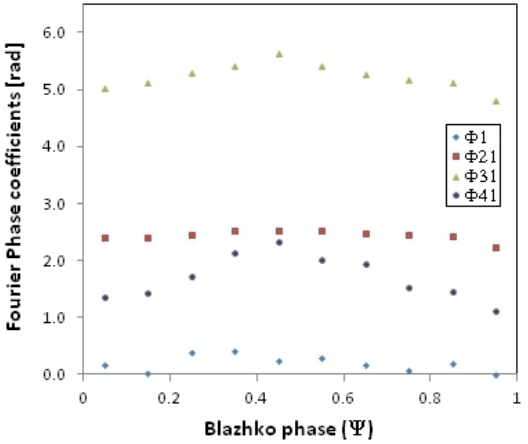

Figure 6b. V784 Oph Fourier Φ_i and Φ_{ki} phase (rad.) for the ten temporal subsets.

Simultaneous CCD Photometry of Two Eclipsing Binary Stars in Pegasus—Part 2: BX Pegasi

Kevin B. Alton
UnderOak Observatory, 70 Summit Avenue, Cedar Knolls, NJ 07927; kbalton@optonline.net

Received December 5, 2012; revised January 3, 2013; accepted January 3, 2013

Abstract BX Peg is an overcontact W UMa binary system (P = 0.280416 d) which has been rather well studied, but not fully understood due to complex changes in eclipse timings and light curve variations attributed to star spots. Photometric data collected in three bandpasses (B, V, and I_c) produced nineteen new times of minimum for BX Peg. These were used to update the linear ephemeris and further analyze potential changes in orbital periodicity by examining long-term changes in eclipse timings. In addition, synthetic fitting of light curves by Roche modeling was accomplished with the assistance of three different programs, two of which employ the Wilson-Devinney code. Different spotted solutions were necessary to achieve the best Roche model fits for BX Peg light curves collected in 2008 and 2011. Overall, the long-term decrease (9.66×10^{-3} sec y^{-1}) in orbital period defined by the parabolic fit of eclipse timing data could arise from mass transfer or angular momentum loss. The remaining residuals from observed minus predicted eclipse timings for BX Peg exhibit complex but non-random behavior. These may be related to magnetic activity cycles and/or the presence of an unseen mass influencing the times of minimum, however, additional minima need to be collected over a much longer timescale to resolve the nature of these complex changes.

1. Introduction

The variable behavior of BX Peg was first discovered by Shapley and Hughes (1934) and thereafter studied by numerous investigators. Briefly, BX Peg belongs to the W UMa class of eclipsing binaries whose component main sequence stars (spectral type A–F to early K) rotate rapidly (P < 1 day) while in contact with each other. The spectral type of this overcontact binary has been variously assigned between G4V and G9V. Light curves and/or refined photoelectric- or CCD-derived light elements for BX Peg have been reported by Zhai and Zhang (1979), Hoffmann (1982), Kaluzny (1984), Samec (1990), Leung *et al.* (1985), Samec and Bookmyer (1987), De Young *et al.* (1991), Samec and Hube (1991), Lee *et al.* (2004), and Lee *et al.* (2009). A radial velocity study (Samec and Hube 1991) yielded a spectroscopic mass ratio value ($q_{sp} = 0.372$); based solely upon these data, BX Peg belongs to the W-type classification where the smaller secondary is somewhat hotter than the more

massive primary star. This system also exhibits asymmetry at maximum light which is ascribed to the so-called O'Connell effect frequently observed with W UMa variables. Only the photoelectric V-band light curve collected in 1979 (Hoffmann 1982) and the 1978 B-band curve produced by Zhai and Zhang (1979) convincingly exhibited a positive O'Connell effect (Max I > Max II). Aside from a few examples where Max I ≈ Max II (Samec and Bookmyer 1987), the majority of the published light curves show a negative O'Connell effect (Max II > Max I). In most cases investigators invoked the addition of cool or hot starspots in order to obtain the best light curve fits with Roche modeling. The high orbital inclination angle (i ~88°) indicates that our view of this eclipsing binary is very close to edge-on.

2. Observations and data reduction

Session dates in 2008 and 2011, along with the photometric equipment, acquisition parameters, and image processing, were exactly as described in the companion paper (Part I; Alton 2013) for KW Peg, which is in the same field-of-view (FOV) as BX Peg.

Roche-type modeling was performed using BINARY MAKER 3 (BM3; Bradstreet and Steelman 2002), WDWINT v5.6a (Nelson 2009), and PHOEBE v.31a (Prša and Zwitter 2005), the latter two of which employ the Wilson-Devinney (W-D) code (Wilson and Devinney 1971; Wilson 1979). 3-D spatial renderings of BX Peg were also produced by BM3 once each model fit was finalized. Times of minimum (ToM) were estimated using the method of Kwee and van Woerden (1956) as implemented in Minima V25c (Nelson 2007).

3. Results and discussion

3.1. Photometry

Five stars in the same FOV as BX Peg were used to derive catalogue-based (MPOSC3) magnitudes in MPO CANOPUS (Minor Planet Observer 2010; Table 1). Comparison stars showed no evidence of inherent variability over the period of image acquisition and stayed within ±0.015 magnitude for V and I_c filters and ±0.03 for the B passband.

3.2. Ephemerides

3.2.1. Light curves from 2008 Campaign

Photometric values in B (n = 873), V (n = 863), and I_c (n = 885) were folded by filter to produce light curves that spanned 23 days in October 2008 (Figure 1). These determinations produced eight new ToM values in each bandpass. No meaningful color dependencies emerged; therefore the timings from all three filters were averaged for each session (Table 2). The Fourier routine (FALC) in MPO CANOPUS provided a period solution for all the data after

initially seeding the analysis with the orbital period derived by Kreiner (2004). The corresponding linear ephemeris (Equation 1) was determined as follows using the latest primary epoch from this dataset:

$$\text{Min. I (hel.)} = 2454770.5181\ (8) + 0.2804259\ (1)\ E \quad (1)$$

3.2.2. Light curves from 2011 Campaign

Photometric values in B (n = 638), V (n = 646), and I_c (n = 649) were folded by filter to produce light curves that spanned 32 days (Figure 2) in October and November 2011. These observations produced eleven new ToM values in each bandpass (Table 2). As described above for the 2008 data, the linear ephemeris (Equation 2) for the last primary epoch captured in 2011 was as follows:

$$\text{Min. I (hel.)} = 2455868.6282\ (8) + 0.2804197\ (1)\ E \quad (2)$$

The overall accuracy of the orbital period can be improved by pooling the light curve data from 2008 and 2011 which extends the time baseline for Fourier analysis from less than 33 days to 1,126 days. As a result, the composite linear ephemeris (Equation 3) was determined to be:

$$\text{Min. I (hel.)} = 2455868.6282\ (8) + 0.2804164\ (5)\ E \quad (3)$$

which compares more favorably with values reported over the past five decades. As is standard practice at UnderOak Observatory (UO), all period determinations were independently confirmed using PERANSO v2.5 (CBA Belgium Observatory 2011) by applying periodic orthogonals (Schwarzenberg-Czerny 1996) to fit observations and analysis of variance (ANOVA) to evaluate fit quality. In toto, eleven new secondary (s) and eight primary (p) minima were recorded during this investigation of BX Peg. These nineteen new minima along with published values starting in 1960 (Table 3) were used to assess eclipse timing (ET) over the past fifty-one years. The reference epoch (Kreiner 2004) employed for calculating ET residuals (ETR) was defined by the following linear ephemeris (Equation 4):

$$\text{Min. I (hel.)} = 2452500.2563\ (8) + 0.2804177\ (2)\ E \quad (4)$$

To visualize the progression of orbital periodicity over time the difference between the observed eclipse times and those predicted by the reference epoch are plotted against period cycle number (Figure 3). Although commonly called an observed minus computed, or O–C diagram, this generalized term fails to exactly inform the reader about which variables are being plotted. Going forward, the term ET diagram will be used instead. The top panel in Figure 3 chronicles a very complex pattern of eclipse timings for BX Peg over the past fifty-one years. Collectively all of the ETR values describe a parabola as a function of time, however, there is significant scatter which complicates any cogent interpretation about the periodic behavior of this system. Due to the very

apparent variability associated with visual (vis) and photographic (pg) values, photoelectric- (PE) and CCD-derived observations were weighted eight-fold while curve fitting. As indicated by the downwardly turned parabolic relationship ($c + a_1x - a_2x^2$) between ETR and time, the corresponding period decrease is similar irrespective of whether all data (Figure 3, top) or just the CCD/PE data are evaluated (Figure 3, middle). This leads to an updated quadratic ephemeris (Equation 5) as follows:

$$\text{Min. I (hel.)} = 2455873.4019\ (4) + 0.28041753\ (4)\ E - 4.29\ (17) \times 10^{-11}\ E^2 \quad (5)$$

In this case the orbital period rate of decrease ($\Delta p/p = 2a_2 = 8.585 \pm 0.169 \times 10^{-11}$) of this system, which is equivalent to a period decrease rate of $dP/dt = +0.00966$ sec y^{-1}, has lasted from at least 1960. The secular, or long-term period change associated with a parabola-shaped ET diagram is often attributed to mass transfer or by angular momentum loss (AML) due to magnetic stellar wind. The first systematic examination of period and light variations for BX Peg was conducted by Lee *et al.* (2004) and included ET data up through mid-2003 (cycle 1124). Essentially their analysis suggests the continuous period decrease is most likely related to mass transfer from the primary to secondary star or a combination of AML and mass transfer. Quadratic residuals derived from the CCD and PE data (Figure 3, bottom) reveal a potential quasi-sinusoidal change up through 2003 as described by Lee *et al.* (2004). Thereafter, new eclipse timings reveal what appears to additional cyclic changes of shorter duration. Further attempts to mathematically model all the CCD and PE eclipse timing data using non-linear polynomial regression with and without a sine term did not lead to a good fit of the data. Cyclic changes of eclipse timings are also attributed to the light-time effect of a third unseen body and/or cyclical changes in the magnetic activity of either binary constituent. Beyond speculation there presently are not enough supporting data which could be used to confidently explain the complex behavior of this binary system.

A near-term linear ephemeris (Equation 6) from the present investigation was projected from a straight line segment (Figure 3, middle inset) covering observations from 2008 to 2011; calculated least-squares fit residuals over this period of time are provided in Table 4.

$$\text{Min. I (hel.)} = 2455873.3958\ (8) + 0.28041636\ (8)\ E \quad (6)$$

Not surprisingly, this near term orbital period is consistent with the linear ephemeris (Equation 3) determined directly from Fourier analysis of the pooled (2008 and 2011) light curves. Given the complex changes in orbital period for this system, revised ephemerides for BX Peg should be determined on a regular basis to maintain an accurate record about the behavior of this overcontact variable system.

3.3. Light curve behavior

Individual light curves from 2008 (Figure 1) and 2011 (Figure 2) show that minima are separated by 0.5 phase and as might be expected from a contact binary system, are consistent with a circular orbit. Similar to most published light curves for BX Peg (Samec 1990, De Young *et al.* 1991, Lee *et al.* 2004, and Lee *et al.* 2009), a negative, albeit modest O'Connell effect (Max I fainter than Max II) was observed with all passbands during the 2008 campaign. The so-called O'Connell effect is believed to involve the presence of cool starspot(s), hot regions, gas stream impact on one or both of the binary components, and/or other unknown phenomena which distort surface homogeneity and can produce unequal heights during quadrature (Yakut and Eggleton 2005). In 2008 this asymmetry was most noticeable in B-band. By comparison the 2011 light curves exhibited a positive (Max I brighter than Max II) O'Connell effect but in this case the asymmetry was more prominent in V-band (Table 5). Brighter measurements during first quadrature (Max I) had only been sporadically reported (Hoffmann 1982; Zhai and Zhang 1979) in the past.

3.4. Spectral classification

The effective temperature (Teff) of the primary was estimated from the mean observed color index (B–V = 0.716) determined during quadrature (0.25 P and 0.75 P) in 2008 and 2011. Since W UMa systems are invariably comprised of main sequence stars, this corresponds to the effective temperature (5613 K) associated with spectral class G7V (Flower 1996; Harmanec 1988). Similarly, other investigators (Kaluzny 1984, Samec 1990, Samec and Hube 1991, Leung *et al.* 1985, Maceroni and van't Veer 1996, Lee *et al.* 2004, and Lee *et al.* 2009) report that BX Peg ranges between G4 (5807 K) and G9V (5330 K). Supporting color index (B–V) data from other surveys (Table 6) indicate a system ranging between G3 and G9V. For Roche modeling, the average Teff (5520 K; G7-G8V) from this tabulation was adopted for the more massive but cooler star. Assignment of this temperature to the cooler component in a W-type W UMa variable at first glance seemed counter-intuitive. Although the luminosity of a star is proportional to the fourth power of its effective temperature according to the Stefan-Boltzmann law ($L = 4\pi R^2 \alpha T^4$), brightness also increases with surface area or radius squared (R^2). As is the case with most W UMa type variable stars, the temperature difference between each main sequence component rarely exceeds 500 K. It follows that the overall luminosity of BX Peg is dominated by the nearly three-fold mass difference between the primary and secondary components, which, according to the mass-radius relationship ($R = M^{0.8}$) for main sequence stars, also corresponds to more than a two-fold difference in size. A heads-up comparison from a 500 K difference in temperature $(6020/5520)^4$ versus the putative radius ratio $(1/0.38)^{0.8}$ from radial velocity data reveals that overall luminosity increases 1.4-fold with a hotter secondary but by a greater amount (2.2-fold) due to the increased size of the primary. This "size-beats-

temperature-difference" luminosity relationship for BX Peg is confirmed in the next section where the relevant attributes ($Teff_1$, $Teff_2$, R_1, and R_2) for this binary system are defined in more detail after Roche modeling.

3.5. Roche Modeling

3.5.1. 2008 Light Curves

Coincidently, Lee *et al.* (2009) also recorded light curve data (B-, V-, and R_c-band) for BX Peg in the fall of 2008. Different starspots were used by these investigators to model data collected between September 27 and October 22 (Group 1; Max I < Max II) and on two consecutive nights (15th and 16th) in November (Group 2; Max I > Max II). Group 1 data were fit with a single cool spot on the more massive star, whereas Group 2 also required a hot spot on either star. Since the 2008 data collected at UO only included values from October, a photometric solution using PHOEBE was initially attempted by adopting all of the parameters described for Group 1 (Lee *et al.* 2009). Roche modeling proceeded with phased B-, V-, and I_c-band data which had been transformed into catalogue-based magnitudes. Mode 3 (an overcontact binary system not in thermal contact) with synchronous rotation and circular orbits were employed in PHOEBE. Each model fit of data from the present study incorporated individual observations assigned an equal weight of 1. All Group 1 parameters from Lee *et al.* (2009) remained fixed whereas phase shift and passband specific luminosity corrections were iteratively adjusted using differential corrections (DC) to achieve a simultaneous minimum residual fit of all (B, V, and I_c) photometric observations. The best simultaneous solution provided a reasonable synthesis of the B-band light curve (Figure 4), but less than acceptable in V- (Figure 5) and I_c-bands (Figure 6) due to marginal fits around Min I and Min II.

Significant improvement in the synthetic fit for all filters was ultimately achieved but this required modification of many modeling parameters. When setting up W-type W UMa eclipsing binaries for Roche modeling according to the Wilson-Devinney code, the reader should be aware of different approaches that appear in the literature regarding the assignment of effective temperatures for $Teff_1$ and $Teff_2$ as well as the calculations for mass ratio (q). By convention, the primary star in an eclipsing binary system is the one being eclipsed that produces the deeper minimum. In most cases but not all it is the most massive and therefore the brightest and hottest as might be predicted from luminosity-mass relationship established in Hertzsprung-Russell type diagrams. The primary star in an A-type W UMa eclipsing variable is more massive, hotter, and therefore brighter than its secondary companion. As would be expected, in this case $Teff_1$ is assigned to the primary and $Teff_2$ to the secondary, while the mass ratio (q) corresponds to m_2/m_1, a value that is less than one. It follows that the deepest minimum (Min I) or dimmest photometric reading on an A-type light curve occurs when the secondary star either transits or partially

eclipses the brighter primary star. By contrast, the effective temperature of the more massive star in a W-type W UMa binary system is somewhat cooler than its less massive stellar cohort. In this case the deepest minimum (Min I) or dimmest photometric reading on a W-type light curve occurs when the primary star either occults or partially eclipses the hotter secondary star. Under these circumstances, in order to properly execute the Wilson-Devinney code during Roche lobe modeling, an adjustment from standard convention can be made using one of two different approaches. For example, in the paper by Lee *et al.* (2009), the authors chose to define the mass ratio (q) as m_1/m_2, which in this case is 2.6897, or the reciprocal of q_{sp} (0.372), which was based upon initial radial velocity experiments by Samec and Hube (1991). This approach also requires re-defining the primary star as the hottest ($Teff_1$), rather than the most massive, and the secondary star as the coolest ($Teff_2$). The equivalent strategy taken herein, maintains the convention whereby the primary is still defined as the most massive (m_1) star, however, in this case $Teff_1 < Teff_2$ and model fitting starts by shifting the phase of the folded light curve data by 0.5. This approach where $q < 1$ is also employed by Samec and Hube (1991) and mathematically leads to a different value for the dimensionless Roche potential ($\Omega_1 = \Omega_2$) which defines the common envelope in overcontact binary systems.

Given other differences (for example, R vs. I_c filters) from the dataset produced by Lee *et al.* (2009), modeling the 2008 light curves (B, V, and I_c) collected at UO essentially started with a clean slate except for the spectroscopically determined mass ratio ($q_{sp} = 0.372$) reported by Samec and Hube (1991) and the orbital inclination ($i \approx 88°$) which is fairly consistent across all BX Peg publications. The putative effective temperature ($Teff_1$ = 5520 K) of the cooler star was based on the G7-G8V spectral classification proposed herein. BM3 requires normalized flux that has been phased; this was accomplished by MPO CANOPUS, which has a feature to prepare light curve data for BM3. Bolometric albedo ($A_{1,2} = 0.5$) and gravity darkening coefficients ($g_{1,2} = 0.32$) for cooler stars with convective envelopes were assigned according to Rucinski (1969) and Lucy (1967), respectively. Following any Teff change to either star, new logarithmic limb darkening coefficients (x_1, x_2, y_1, y_2) were interpolated according to van Hamme (1993). Values for $Teff_1$ (5520 K) and the spectroscopic mass ratio (0.372) were initially held constant while iteratively adjusting the effective temperature of the secondary ($Teff_2$), inclination (*i*), and common envelope surface potential ($\Omega_1 = \Omega_2$) until an acceptable fit of the model in a single bandpass (V) was initially obtained.

Not unexpectedly, the first iterations leading to an unspotted solution clearly indicated a marginal synthetic fit, especially during quadrature where the O'Connell effect is largely observed. To rectify this shortcoming, a cool spot on the more massive star was introduced into the model. Thereafter, model fitting with PHOEBE employed phased data that had been transformed into catalogue-based magnitudes. A_1, A_2, g_1, g_2, and $Teff_1$ were fixed parameters whereas initial

values for Ω_1 (2.60), i (88°), and $Teff_2$ (5800 K) from BM3 along with passband specific luminosity, phase shift, x_1, x_2, y_1, and y_2 were iteratively adjusted using differential corrections (DC) to achieve a simultaneous minimum residual fit of all (B, V, and I_c) photometric observations. Although Lee *et al.* (2004) had proposed the potential presence of additional mass around BX Peg based upon sinusoidal-like behavior of residuals in the ET diagram, invoking third light (l_3) in each bandpass during DC did not meaningfully improve the fit. A number of different spot solutions were attempted, most notably some which invoked the presence of an additional cool or hot spot on one or both stars. These solutions offered some improvement in the overall fits, however, they exemplify the slippery slope of trying to fit light curve data by the addition of multiple starspots. The additional degrees of freedom to the model allowed by multiple spots limits the possibility that a unique fit can be found. This was notably obvious by the increased number of iterations required to reach convergence and by the much broader error estimates for Ω_1, i, $Teff_2$, and q obtained from heuristic scanning (Prša and Zwitter 2005).

Sticking with the simplest model, the final proposed location of a single cool spot which accounts for most of the asymmetry is shown in a spatial representation for BX Peg (Figure 7). Associated unspotted and spotted light curve fits from the present study (2008) are reproduced in Figures 8 (B mag.), 9 (V mag.), and 10 (I_c mag.) while a comparison of light curve parameters and geometric elements obtained from Lee *et al.* (2009) and those collected at UO are summarized in Table 8. Importantly, excellent agreement between the spectroscopically determined (Samec and Hube 1991) mass ratio (q_{sp} = 0.372 ± 0.002) and the photometrically derived value (q_{ph} = 0.370 ± 0.005) was obtained in the present study. This is not unexpected in cases where the high orbital inclination of a contact binary leads to a total eclipse (Terrell and Wilson 2005).

3.5.2. 2011 light curves

As had been previously mentioned, in contrast to 2008 the light curves from 2011 exhibited a positive O'Connell effect where Max I was brighter than Max II. Roche model fitting with BM3 and PHOEBE was attempted using the same geometric and physical parameters derived from the 2008 light curves collected at UO, but initially without any spots. Incorporation of a single cool spot on the primary (Figure 11) facing the observer during primary minimum ultimately provided the best model fit in each filter (Figures 12–14). A comparison between light curve parameters and geometric elements obtained from Roche modeling the 2008 and 2011 light curves collected at UO is summarized in Table 6. Based upon a compilation of absolute dimensions of eclipsing binaries (Harmanec 1988), the mean stellar mass for an G7-G8 main sequence binary star (0.96 $M_\odot$) was used to derive M_1, M_2, R_1, R_2, and the semi-major axis (a) in solar units. These values (Table 7) compare favorably with those published by Samec and Hube (1991).

4. Conclusions

CCD-based photometric data collected in B, V, and I_c produced nineteen new times of minimum for BX Peg. The linear ephemeris for BX Peg was updated and potential changes in orbital periodicity were assessed through the use of ET diagrams. The ET diagram for BX Peg exhibited complex behaviors often attributed to mass transfer, magnetically active cycles, and/or the presence of an unseen mass influencing the times of minimum. However, no convincing single explanation for these periodic changes can be derived from the data extant. Different spotted solutions were necessary to achieve the best Roche model fits for BX Peg light curves collected in 2008 and 2011. Public access to any light curve data associated with this research can be obtained by request (mail@underoakobservatory.com)

5. Acknowledgements

This research has made use of the SIMBAD database, operated at Centre de Données astronomiques de Strasbourg, France. Time of minima data from the B.R.N.O., IBVS, AASVO, BAV, BBSAG, BAA VSS, and VSOLJ websites proved invaluable to the assessment of period changes experienced by this variable star. The diligence and dedication shown by all associated with these organizations is very much appreciated. I would also like to thank Professor Dirk Terrell and an unknown referee for reviewing this study report and suggesting changes which significantly improved the quality of this manuscript.

References

Agerer, F., and Hübscher, J. 2002, *Inf. Bull. Var. Stars*, No. 5296, 1.

Agerer, F., and Hübscher, J. 2003, *Inf. Bull. Var. Stars*, No. 5484, 1.

Alton, K. B. 2013, *J. Amer. Assoc. Var. Star Obs.*, **41**, in press.

Baldinelli, L., and Maitan, A. 2002, *Inf. Bull. Var. Stars*, No. 5220, 1.

Baldwin, M., and Samolyk, G. 1995, *Observed Minima Timings of Eclipsing Binaries: Number 2*, AAVSO, Cambridge, MA.

Baldwin, M., and Samolyk, G. 2004, *Observed Minima Timings of Eclipsing Binaries: Number 9*, AAVSO, Cambridge, MA.

Baldwin, M., and Samolyk, G. 2007, *Observed Minima Timings of Eclipsing Binaries: Number 12*, AAVSO, Cambridge, MA.

Beob. der Schweizerischen Astron. Ges. (BBSAG). 1987, *BBSAG Bull.*, No. 83, 1.

Beob. der Schweizerischen Astron. Ges. (BBSAG). 1988a, *BBSAG Bull.*, No. 86, 1.

Beob. der Schweizerischen Astron. Ges. (BBSAG). 1988b, *BBSAG Bull.*, No. 89, 1.

Beob. der Schweizerischen Astron. Ges. (BBSAG). 1989a, *BBSAG Bull.*, No. 90, 1.

Beob. der Schweizerischen Astron. Ges. (BBSAG). 1989b, *BBSAG Bull.*, No. 92, 1.

Beob. der Schweizerischen Astron. Ges. (BBSAG). 1990a, *BBSAG Bull.*, No. 93, 1.

Beob. der Schweizerischen Astron. Ges. (BBSAG). 1990b, *BBSAG Bull.*, No. 96, 1.
Beob. der Schweizerischen Astron. Ges. (BBSAG). 1991, *BBSAG Bull.*, No. 98, 1.
Beob. der Schweizerischen Astron. Ges. (BBSAG). 1992a, *BBSAG Bull.*, No. 99, 1.
Beob. der Schweizerischen Astron. Ges. (BBSAG). 1992b, *BBSAG Bull.*, No. 102, 1.
Beob. der Schweizerischen Astron. Ges. (BBSAG). 1994a, *BBSAG Bull.*, No. 105, 1.
Beob. der Schweizerischen Astron. Ges. (BBSAG). 1994b, *BBSAG Bull.*, No. 107, 1.
Beob. der Schweizerischen Astron. Ges. (BBSAG). 1995, *BBSAG Bull.*, No. 109, 1.
Beob. der Schweizerischen Astron. Ges. (BBSAG). 2001, *BBSAG Bull.*, No. 126, 1.
Beob. der Schweizerischen Astron. Ges. (BBSAG). 2002, *BBSAG Bull.*, No. 127, 1.
Bíró, I. B., *et al.* 2006, *Inf. Bull. Var. Stars*, No. 5684, 1.
Bradstreet, D. H., and Steelman D. P. 2002, *Bull. Amer. Astron. Soc.*, **34**, 1224.
Brát, L., Zejda, M., and Svoboda, P. 2007, *Open Eur. J. Var. Stars*, **74**, 1 (*B.R.N.O. Contrib.*, No. 34).
Brát, L., *et al.* 2011, *Open Eur. J. Var. Stars*, **137**, 1 (*B.R.N.O. Contrib.*, No. 37).
CBA Belgium Observatory. 2011, Flanders, Belgium (http://www.cbabelgium.com/).
De Young, J.A., Schmidt, R.E., and Gritz, L.I. 1991, *Inf. Bull. Var. Stars*, No. 3578.
Diethelm, R. 2003, *Inf. Bull. Var. Stars*, No. 5438, 1.
Diethelm, R. 2004, *Inf. Bull. Var. Stars*, No. 5543, 1.
Diethelm, R. 2005, *Inf. Bull. Var. Stars*, No. 5653, 1.
Diethelm, R. 2010, *Inf. Bull. Var. Stars*, No. 5920, 1.
Diethelm, R. 2011, *Inf. Bull. Var. Stars*, No. 5960, 1.
Diethelm, R. 2012, *Inf. Bull. Var. Stars*, No. 6011, 1.
Diethelm, R., Isles, J., and Locher, K. 1972, *Orion*, **30**, 60.
Doğru, S. S., Dönmez, A., Tüysüz, M., Doğru, D., Ozkardes, B., Soydugan, E., and Soydugan, F. 2007, *Inf. Bull. Var. Stars*, No. 5746, 1.
Flower, P. J. 1996, *Astrophys. J.*, **469**, 355.
Gürol, B., Gürdemir, L., Çaglar, A., Kirca, M., Akcay, U., Tunc, A., and Elmas, T. 2003, *Inf. Bull. Var. Stars*, No. 5443, 1.
Harmanec, P. 1988, *Bull. Astron. Inst. Czechoslovakia*, **39**, 329.
Hoffmann, M. 1982, *Acta Astron.*, **32**, 131.
Hübscher, J. 2005, *Inf. Bull. Var. Stars*, No. 5643, 1.
Hübscher, J. 2011, *Inf. Bull. Var. Stars*, No. 5984, 1.
Hübscher, J., Agerer F., Frank, P., and Wunder, E. 1994, *BAV Mitt.*, No. 68, 1.
Hübscher, J., Agerer F., and Wunder, E. 1992, *BAV Mitt.*, No. 60, 1.
Hübscher, J., Agerer F., and Wunder, E. 1993, *BAV Mitt.*, No. 62, 1 .
Hübscher, J., and Lichtenknecker, D. 1988, *BAV Mitt.*, No. 50, 1.
Hübscher, J., Lichtenknecker, D., and Meyer, J. 1986, *BAV Mitt.*, No. 43, 1.
Hübscher, J., Lichtenknecker, D., and Wunder, E. 1989, *BAV Mitt.*, No. 52, 1.
Hübscher, J., Lichtenknecker, D., and Wunder, E. 1990, *BAV Mitt.*, No. 56, 1.
Hübscher, J., and Mundry, E. 1984, *BAV Mitt.*, No. 38, 1.
Hübscher, J., Paschke, A., and Walter, F. 2005, *Inf. Bull. Var. Stars*, No. 5657, 1.

Hübscher, J., Paschke, A., and Walter, F. 2006, *Inf. Bull. Var. Stars*, No. 5731, 1.
Hübscher, J., Steinbach, H-M., and Walter, F. 2009, *Inf. Bull. Var. Stars*, No. 5889, 1.
Hübscher, J., and Walter, F. 2007, *Inf. Bull. Var. Stars*, No. 5761, 1.
Isles, J. 1985a, *Br. Astron. Assoc. Var. Star Sect. Circular*, No. 59, 14.
Isles, J. 1985b, *Br. Astron. Assoc. Var. Star Sect. Circular*, No. 60, 15.
Isles, J. 1985c, *Br. Astron. Assoc. Var. Star Sect. Circular*, No. 61, 14.
Isles, J. 1989, *Br. Astron. Assoc. Var. Star Sect. Circular*, No. 68, 30.
Isles, J. 1992, *Br. Astron. Assoc. Var. Star Sect. Circular*, No. 73, 13.
Kaluzny, J. 1984, *Acta Astron.*, **34**, 217.
Krajci, T. 2005, *Inf. Bull. Var. Stars*, No. 5592, 1.
Kreiner, J. M. 2004, *Acta Astron.*, **54**, 207.
Kwee, K. K., and van Woerden, H. 1956, *Bull. Astron. Inst. Netherlands*, **12**, 327.
Lee, J. W., Kim, C-H., Han, W., Kim, H-I., and Koch, R. H. 2004, *Mon. Not. Roy. Astron. Soc.*, **352**, 1041.
Lee, J. W., Kim, S-L., Lee, C-U., and Youn, J-H. 2009, *Publ. Astron. Soc. Pacific*, **886**, 1366.
Leung, K-C., Zhai, D., and Zhang, Y. 1985, *Astron. J.*, **90**, 515.
Lucy, L. B. 1967, *Z. Astrophys.*, **65**, 89.
Maceroni, C., and van't Veer, F. 1996, *Astron. Astrophys.*, **311**, 523.
Maciejewski, G., and Karska, A. 2004, *Inf. Bull. Var. Stars*, No. 5494.
Mikulášek, Z. (ed.). 1985, *Contrib. Nicholas Copernicus Obs. Planetarium Brno*, No. 26, 5.
Mikulášek, Z. (ed.). 1986, *Contrib. Nicholas Copernicus Obs. Planetarium Brno*, No. 27, 5.
Mikulášek, Z., and Šilhán, J. (eds.). 1988, *Contrib. Nicholas Copernicus Obs. Planetarium Brno*, No. 28, 6.
Mikulášek, Z., Šilhán, J., and Zejda, M. (eds.). 1992, *Contrib. Nicholas Copernicus Obs. Planetarium Brno*, No. 30, 4.
Mikulášek, Z., and Zejda, M. (eds.) 2002, *Contrib. Nicholas Copernicus Obs. Planetarium Brno*, No. 32, 5.
Minor Planet Observer. 2010, MPO Software Suite (http://www.minorplanetobserver.com), BDW Publishing, Colorado Springs.
Nagai, K. 2003, *VSOLJ Var. Star Bull.*, No. 40, 1.
Nagai, K. 2006, *VSOLJ Var. Star Bull.*, No. 44, 1.
Nagai, K. 2007, *VSOLJ Var. Star Bull.*, No. 45, 1.
Nagai, K. 2008, *VSOLJ Var. Star Bull.*, No. 46, 1.
Nagai, K. 2010, *VSOLJ Var. Star Bull.*, No. 50, 1.
Nagai, K. 2012, *VSOLJ Var. Star Bull.*, No. 53, 1.
Nelson, R. H. 2001, *Inf. Bull. Var. Stars*, No. 5040, 1.
Nelson, R. H. 2002, *Inf. Bull. Var. Stars*, No. 5224, 1.
Nelson, R. H. 2003, *Inf. Bull. Var. Stars*, No. 5371, 1.

Nelson, R. H. 2007, Minima©2002–2006: Astronomy Software by Bob Nelson (http://members.shaw.ca/bob.nelson/software1.htm).
Nelson, R. H. 2009, WDwint56a: Astronomy Software by Bob Nelson (http://members.shaw.ca/bob.nelson/software1.htm).
Ogloza, W., Niewiadomski, W., Barnacka, A., Biskup, M., Malek, K., and Sokolowski, M. 2008, *Inf. Bull. Var. Stars*, No. 5843, 1.
Parimucha, Š., Dubovský, P., Baludanský, D., Pribulla, T., Hambalek, L., Vanko, M., and Ogloza, W. 2009, *Inf. Bull. Var. Stars*, No. 5898, 1.
Parimucha, Š., Dubovský, P., Vanko, M., Pribulla, T., Kudzej, I., and Barsa, R. 2011, *Inf. Bull. Var. Stars*, No. 5980, 1.
Paschke, A. 2007, *Open Eur. J. Var. Stars*, **73**, 1.
Pribulla, T., *et al.* 2005, *Inf. Bull. Var. Stars*, No. 5668, 1.
Prša, A., and Harmanec, P. 2010, *PHOEBE Manual, Adopted for PHOEBE 0.32*, Villanova Univ., Radnor Township, PA.
Prša, A., and Zwitter, T. 2005, *Astrophys. J.*, **628**, 426.
Ruciński, S. M. 1969, *Acta Astron.*, **19**, 245.
Šafář, J., and Zejda, M. 2000a, *Inf. Bull. Var. Stars*, No. 4887, 1.
Šafář, J., and Zejda, M. 2000b, *Inf. Bull. Var. Stars*, No. 4888, 1.
Samec, R. G. 1989, *Inf. Bull. Var. Stars*, No. 3392, 1.
Samec, R. G. 1990, *Astron. J.*, **100**, 808.
Samec, R. G., and Bookmyer, B. B. 1987, *Inf. Bull. Var. Stars*, No. 2999, 1.
Samec, R. G., and Hube, D. P. 1991, *Astron. J.*, **102**, 1171.
Samolyk, G. 2008a, *J. Amer. Assoc. Var. Star Obs.*, **36**, 171.
Samolyk, G. 2008b, *J. Amer. Assoc. Var. Star Obs.*, **36**, 186.
Samolyk, G. 2009, *J. Amer. Assoc. Var. Star Obs.*, **37**, 44.
Samolyk, G. 2010, *J. Amer. Assoc. Var. Star Obs.*, **38**, 183.
Schwarzenberg-Czerny, A. 1996, *Astrophys. J., Lett.*, **460**, L107.
Shapley, H., and Hughes, E. M. 1934, *Ann. Harvard Coll. Obs.*, **90**, 163.
Terrell, D., and Wilson, R. E. 2005, *Astrophys. Space Sci.*, **296**, 221.
van Hamme, W. 1993, *Astron. J.*, **106**, 2096.
Warner, B. 2007, *Minor Planet Bull.*, **34**, 113.
Wilson, R. E. 1979, *Astrophys. J.*, **234**, 1054.
Wilson, R. E., and Devinney, E. J. 1971, *Astrophys. J.*, **166**, 605.
Yakut, K., and Eggleton, P. P. 2005, *Astrophys. J.*, **629**, 1055.
Zejda, M. (ed.). 1995, *Contrib. Nicholas Copernicus Obs. Planetarium Brno*, 31, 4.
Zejda, M. 2004, *Inf. Bull. Var. Stars*, No. 5583, 1.
Zejda, M., Mikulásek, Z., and Wolf, M. 2006, *Inf. Bull. Var. Stars*, No. 5741, 1.
Zhai, D-S., and Zhang, R-X. 1979, *Kexue Tongbao*, **24**, 986.

Table 1. Astrometric coordinates (J2000) and MPOSC3 catalogue magnitudes (V, B, and I_c) for BX Peg and five comparison stars used in this photometric study.

Star Identification	*R.A.* h m s	*Dec.* ° ′ ″	*MPOSC3*[a] *B mag.*	*MPOSC3 V mag.*	*MPOSC3 I_c mag.*	*MPOSC3 (B–V)*
BX Peg	21 38 49.39	26 41 34.2	11.54–12.29[b]	10.8–11.53	10.0–10.63	0.812
C1	21 38 57.74	26 36 51.4	13.154	12.694	12.145	0.460
C2	21 39 00.59	26 38 10.4	13.327 (13.51)[c]	12.678 (12.77)[c]	11.95	0.649
C3	21 39 02.87	26 38 43.0	13.384 (13.37)[c]	12.287 (12.34)[c]	11.16 (11.20)[c]	1.097
C4	21 39 07.72	26 44 37.4	13.219	12.736	12.164	0.483
C5	21 39 00.86	26 44 58.8	13.88	13.044	12.151	0.836

Notes: *a. MPOSC3 (Warner 2007) is a hybrid catalogue which includes a large subset of the Carlsberg Meridian Catalog (CMC–14) as well as data from the Sloan Digital Sky Survey (SDSS). b. Range of magnitudes in light curves for each variable. c. AAVSO comparison star magnitudes in parentheses.*

Table 2. New times of minimum for BX Peg acquired at UnderOak Observatory.

Mean Computed Time of Minimum (HJD–2400000)[a]	*Error ±*	*UT Date of Observations*	*Type of Minimum*[a]
54747.5240	0.0009	08 Oct 2008	p
54751.5902	0.0006	12 Oct 2008	s
54752.5717	0.0006	13 Oct 2008	p
54755.5162	0.0008	16 Oct 2008	s
54759.5823	0.0004	20 Oct 2008	p
54763.5074	0.0004	24 Oct 2008	p
54766.5924	0.0004	27 Oct 2008	p
54770.5181	0.0008	31 Oct 2008	p
55840.5864	0.0006	06 Oct 2011	p
55841.5688	0.0005	07 Oct 2011	s
55841.7066	0.0009	07 Oct 2011	p
55842.5496	0.0006	08 Oct 2011	p
55842.6906	0.0008	08 Oct 2011	s
55843.5316	0.0007	09 Oct 2011	s
55843.6709	0.0005	09 Oct 2011	p
55844.6535	0.0008	10 Oct 2011	s
55868.4890	0.0007	02 Nov 2011	s
55868.6282	0.0008	03 Nov 2011	p
55873.5372	0.0005	08 Nov 2011	s

Note: a. s = secondary; p = primary

Table 3. Visual, Photographic, Photoelectric, and CCD Times of Minimum (–2,400,000) for BX Peg from 1960 to 2011. Eclipse timing residuals $(ETR)_1$ are based on the linear elements defined by Kreiner (2004).

Time of Minimum	*Cycle Mumber*	*Source*	$(ETR)_1$	*Ref.**	*Time of Minimum*	*Cycle Mumber*	*Source*	$(ETR)_1$	*Ref.**
37225.6274	–54470.5	PE	–0.136572	1	44195.2373	–29616.5	PE	–0.028188	5
41249.276	–40122	vis	–0.061341	2	44195.3771	–29616	PE	–0.028597	5
43042.715	–33726.5	vis	–0.033741	3	44474.825	–28619.5	vis	–0.016935	3
43079.725	–33594.5	vis	–0.038877	3	44539.601	–28388.5	vis	–0.017424	3
43096.557	–33534.5	vis	–0.031939	3	44544.653	–28370.5	vis	–0.012942	3
43380.755	–32521	vis	–0.037278	3	44822.403	–27380	vis	–0.016674	6
43452.688	–32264.5	vis	–0.031418	3	44843.423	–27305	vis	–0.028001	7
43452.691	–32264.5	vis	–0.028418	3	44843.574	–27304.5	vis	–0.017210	7
43714.739	–31330	vis	–0.030759	3	44844.409	–27301.5	vis	–0.023463	7
43757.644	–31177	vis	–0.029667	3	44869.375	–27212.5	vis	–0.014639	7
43790.0303	–31061.5	PE	–0.031611	1	44880.730	–27172	vis	–0.016556	3
43790.1704	–31061	PE	–0.031720	1	44926.577	–27008.5	vis	–0.017850	3
43790.1708	–31061	PE	–0.031320	4	45175.460	–26121	vis	–0.005558	8
43791.0126	–31058	PE	–0.030773	1	45191.430	–26064	vis	–0.019367	8
43791.1524	–31057.5	PE	–0.031182	1	45195.500	–26049.5	vis	–0.015424	8
43802.650	–31016.5	vis	–0.030708	3	45197.456	–26042.5	vis	–0.022348	8
43840.0847	–30883	PE	–0.031771	1	45291.687	–25706.5	vis	–0.011695	3
43844.9908	–30865.5	PE	–0.032981	1	45561.446	–24744.5	vis	–0.014522	8
44101.724	–29950	vis	–0.022185	3	45566.487	–24726.5	vis	–0.021041	8
44128.648	–29854	vis	–0.018284	3	45573.374	–24702	vis	–0.004275	8

Table continued on following pages

Table 3. Visual, Photographic, Photoelectric, and CCD Times of Minimum (–2,400,000) for BX Peg from 1960 to 2011. Eclipse timing residuals $(ETR)_1$ are based on the linear elements defined by Kreiner (2004).

Time of Minimum	*Cycle Mumber*	*Source*	*$(ETR)_1$*	*Ref.**	*Time of Minimum*	*Cycle Mumber*	*Source*	*$(ETR)_1$*	*Ref.**
45576.451	–24691	vis	–0.011869	8	46028.626	–23078.5	vis	–0.010411	3
45577.443	–24687.5	vis	–0.001331	8	46028.636	–23078.5	vis	–0.000411	3
45605.335	–24588	vis	–0.010892	9	46271.4864	–22212.5	vis	0.008261	11
45605.476	–24587.5	vis	–0.010101	9	46289.4426	–22148.5	vis	0.017728	11
45621.317	–24531	vis	–0.012701	9	46292.5148	–22137.5	vis	0.005334	11
45621.458	–24530.5	vis	–0.011910	9	46292.5231	–22137.5	vis	0.013634	11
45640.2445	–24463.5	PE	–0.013396	9	46292.5252	–22137.5	vis	0.015734	11
45646.2746	–24442	PE	–0.012277	9	46292.5273	–22137.5	vis	0.017834	11
45651.3219	–24424	PE	–0.012495	9	46292.5273	–22137.5	vis	0.017834	11
45701.649	–24244.5	vis	–0.020372	3	46292.5273	–22137.5	vis	0.017834	11
45925.444	–23446.5	vis	0.001303	10	46292.5280	–22137.5	vis	0.018534	11
45932.441	–23421.5	vis	–0.012139	10	46292.5280	–22137.5	vis	0.018534	11
45933.428	–23418	vis	–0.006601	10	46293.6380	–22133.5	vis	0.006863	3
45942.407	–23386	vis	–0.000968	10	46297.414	–22120	vis	–0.002776	12
45945.769	–23374	vis	–0.003980	3	46318.311	–22045.5	vis	0.003105	13
45956.710	–23335	vis	0.000729	3	46319.422	–22041.5	pg	–0.007565	13
45959.655	–23324.5	vis	0.001344	3	46327.284	–22013.5	vis	0.002739	13
45962.591	–23314	vis	–0.007042	3	46351.400	–21927.5	vis	0.002817	12
45964.593	–23307	vis	0.032034	3	46352.286	–21924.5	vis	0.047564	12
45975.530	–23268	vis	0.032744	3	46380.278	–21824.5	vis	–0.002206	12

Table continued on following pages

Table 3. Visual, Photographic, Photoelectric, and CCD Times of Minimum (–2,400,000) for BX Peg from 1960 to 2011. Eclipse timing residuals $(ETR)_1$ are based on the linear elements defined by Kreiner (2004).

Time of Minimum	*Cycle Mumber*	*Source*	$(ETR)_1$	*Ref.**	*Time of Minimum*	*Cycle Mumber*	*Source*	$(ETR)_1$	*Ref.**
46612.4885	–20996.5	vis	0.022438	14	46728.284	–20583.5	vis	0.005428	14
46612.4899	–20996.5	vis	0.023838	14	46743.283	–20530	vis	0.002081	15
46619.4786	–20971.5	vis	0.002096	14	47039.548	–19473.5	pg	0.005781	16
46619.4793	–20971.5	vis	0.002796	14	47055.390	–19417	vis	0.004181	17
46619.4807	–20971.5	vis	0.004196	14	47056.360	–19413.5	vis	–0.007281	17
46641.487	–20893	vis	–0.002294	12	47057.348	–19410	vis	–0.000743	17
46659.435	–20829	vis	–0.001027	12	47333.8400	–18424	PE	–0.000595	4
46667.423	–20800.5	vis	–0.004931	12	47362.452	–18322	vis	0.008799	18
46678.3706	–20761.5	vis	0.006379	14	47374.360	–18279.5	vis	–0.000953	18
46678.3768	–20761.5	vis	0.012579	14	47378.432	–18265	vis	0.004990	18
46678.3831	–20761.5	vis	0.018879	14	47381.395	–18254.5	vis	0.023605	18
46678.5247	–20761	vis	0.020270	14	47387.5412	–18232.5	vis	0.000615	19
46678.5261	–20761	vis	0.021670	14	47389.5140	–18225.5	vis	0.010491	18
46678.5268	–20761	vis	0.022370	14	47405.491	–18168.5	pg	0.003682	20
46688.4580	–20725.5	vis	–0.001259	12	47450.6339	–18007.5	PE	–0.000667	1
46701.7787	–20678	PE	–0.000399	5	47451.7556	–18003.5	PE	–0.000638	1
46703.7409	–20671	PE	–0.001123	5	47469.293	–17941	vis	0.010656	3
46703.8797	–20670.5	PE	–0.002532	5	47524.242	–17745	vis	–0.002214	21
46704.7227	–20667.5	PE	–0.000785	5	47727.408	–17020.5	pg	0.001163	22
46709.640	–20650	vis	0.009205	3	47727.548	–17020	pg	0.000954	22

Table continued on following pages

Table 3. Visual, Photographic, Photoelectric, and CCD Times of Minimum (–2,400,000) for BX Peg from 1960 to 2011. Eclipse timing residuals $(ETR)_1$ are based on the linear elements defined by Kreiner (2004).

Time of Minimum	*Cycle Mumber*	*Source*	*$(ETR)_1$*	*Ref.**	*Time of Minimum*	*Cycle Mumber*	*Source*	*$(ETR)_1$*	*Ref.**
47734.448	–16995.5	vis	0.030720	19	48120.4212	–15619	vis	0.008956	26
47734.448	–16995.5	vis	0.030720	19	48120.4233	–15619	vis	0.011056	26
47742.442	–16967	vis	0.032816	23	48120.4302	–15619	vis	0.017956	26
47757.408	–16913.5	vis	–0.003531	24	48120.4316	–15619	vis	0.019356	26
47762.456	–16895.5	vis	–0.003050	24	48120.4323	–15619	vis	0.020056	26
47790.358	–16796	pg	–0.002611	22	48121.419	–15615.5	vis	0.025294	27
47813.354	–16714	vis	–0.000862	24	48126.459	–15597.5	vis	0.017776	27
47817.300	–16700	vis	0.019290	25	48147.330	–15523	vis	–0.002343	27
47822.327	–16682	pg	–0.001229	22	48174.274	–15427	vis	0.021558	27
47822.3275	–16682	PE	–0.000729	22	48174.5303	–15426	CCD	–0.002560	28
47822.3278	–16682	PE	–0.000429	22	48187.285	–15380.5	vis	–0.006865	27
47838.3310	–16625	vis	0.018962	25	48189.384	–15373	vis	–0.010998	27
47847.2843	–16593	PE	–0.001004	22	48191.4989	–15365.5	CCD	0.000769	28
47847.2844	–16593	PE	–0.001004	22	48213.5094	–15287	CCD	–0.001520	28
47847.2850	–16593	vis	–0.000404	24	48225.5672	–15244	CCD	–0.001681	28
47854.299	–16568	vis	0.003154	25	48225.5681	–15244	CCD	–0.000781	28
47859.360	–16550	vis	0.016635	25	48419.5004	–14552.5	vis	0.022679	26
47859.633	–16549	vis	0.009217	3	48438.454	–14485	vis	0.048084	29
48085.5081	–15743.5	vis	0.007860	26	48439.403	–14481.5	vis	0.015623	29
48120.4142	–15619	vis	0.001956	26	48444.451	–14463.5	vis	0.016104	29

Table continued on following pages

Table 3. Visual, Photographic, Photoelectric, and CCD Times of Minimum (–2,400,000) for BX Peg from 1960 to 2011. Eclipse timing residuals $(ETR)_1$ are based on the linear elements defined by Kreiner (2004).

Time of Minimum	*Cycle Mumber*	*Source*	$(ETR)_1$	*Ref.**	*Time of Minimum*	*Cycle Mumber*	*Source*	$(ETR)_1$	*Ref.**
48479.376	–14339	vis	0.029100	29	49171.5549	–11870.5	PE	–0.003092	34
48491.4017	–14296	PE	–0.003161	30	49214.4502	–11717.5	vis	–0.011700	26
48491.4023	–14296	PE	–0.002561	30	49218.5212	–11703	vis	–0.006757	26
48499.540	–14267	pg	0.003026	31	49228.3394	–11668	PE	–0.003176	34
48500.402	–14264	vis	0.023773	29	49250.3510	–11589.5	CCD	–0.004366	35
48507.420	–14239	vis	0.031330	32	49250.4910	–11589	CCD	–0.004575	35
48518.360	–14200	vis	0.035040	32	49317.2317	–11351	PE	–0.003287	34
48828.458	–13094	vis	–0.008936	26	49568.394	–10455.5	vis	0.044962	36
48834.4922	–13072.5	vis	–0.003717	26	49624.586	–10255	vis	0.013214	3
48834.4971	–13072.5	vis	0.001183	26	49897.459	–9282	vis	0.039791	37
48834.4984	–13072.5	vis	0.002483	26	49920.555	–9199.5	vis	0.001331	38
48837.480	–13062	vis	0.039697	33	49923.4918	–9189	vis	–0.006255	38
48862.418	–12973	vis	0.020522	33	50282.4339	–7909	vis	0.001189	38
48882.359	–12902	vis	0.051865	33	50282.4346	–7909	vis	0.001889	38
48883.338	–12898.5	vis	0.049403	33	50282.4373	–7909	vis	0.004589	38
48914.585	–12787	vis	0.029830	3	50282.4394	–7909	vis	0.006689	38
48922.565	–12758.5	vis	0.017925	3	50282.4429	–7909	vis	0.010189	38
48946.275	–12674	vis	0.032630	33	50316.3607	–7788	CCD	–0.002552	39
48954.529	–12644.5	vis	0.014308	3	50316.5003	–7787.5	CCD	–0.003161	39
49171.4142	–11871	PE	–0.003583	34	50376.671	–7573	vis	0.017942	40

Table continued on following pages

Table 3. Visual, Photographic, Photoelectric, and CCD Times of Minimum (–2,400,000) for BX Peg from 1960 to 2011. Eclipse timing residuals $(ETR)_1$ are based on the linear elements defined by Kreiner (2004).

Time of Minimum	*Cycle Mumber*	*Source*	*$(ETR)_1$*	*Ref.**	*Time of Minimum*	*Cycle Mumber*	*Source*	*$(ETR)_1$*	*Ref.**
50703.4593	–6407.5	vis	–0.020587	38	51434.5232	–3800.5	vis	–0.005631	38
50707.5502	–6393	CCD	0.004256	39	51470.0005	–3674	CCD	–0.001170	42
50713.2946	–6372.5	CCD	0.000093	39	51470.1399	–3673.5	CCD	–0.001979	42
50726.648	–6325	vis	0.033653	40	51477.0109	–3649	CCD	–0.001213	42
50829.2453	–5959	CCD	–0.001926	41	51477.1507	–3648.5	CCD	–0.001622	42
50990.4783	–5384	vis	–0.009103	38	51500.9856	–3563.5	CCD	–0.002226	42
51021.4704	–5273.5	vis	–0.003159	38	51758.4227	–2645.5	vis	0.011425	43
51021.4725	–5273.5	vis	–0.001059	38	51758.4234	–2645.5	vis	0.012125	43
51021.4753	–5273.5	vis	0.001741	38	51758.4269	–2645.5	vis	0.015625	43
51031.4291	–5238	vis	0.000713	38	51758.4317	–2645.5	vis	0.020425	43
51032.409	–5234.5	vis	–0.000849	38	51758.4352	–2645.5	vis	0.023925	43
51084.588	–5048.5	vis	0.020458	40	51761.9155	–2633	CCD	–0.001046	44
51156.505	–4792	vis	0.010318	40	51791.0798	–2529	CCD	–0.000137	42
51432.4232	–3808	vis	–0.002498	38	51791.2196	–2528.5	CCD	–0.000546	42
51432.4253	–3808	vis	–0.000398	38	51837.636	–2363	vis	0.006725	40
51432.4309	–3808	vis	0.005202	38	51899.3225	–2143	CCD	0.001331	43
51433.4059	–3804.5	vis	–0.001260	38	52015.9750	–1727	CCD	0.000068	45
51433.408	–3804.5	vis	0.000840	38	52121.4173	–1351	CCD	0.005313	46
51433.4128	–3804.5	vis	0.005640	38	52121.4212	–1351	CCD	0.009213	47
51433.4163	–3804.5	vis	0.009140	38	52133.766	–1307	vis	0.015634	40

Table continued on following pages

Table 3. Visual, Photographic, Photoelectric, and CCD Times of Minimum (–2,400,000) for BX Peg from 1960 to 2011. Eclipse timing residuals $(ETR)_1$ are based on the linear elements defined by Kreiner (2004).

Time of Minimum	*Cycle Mumber*	*Source*	$(ETR)_1$	*Ref.**	*Time of Minimum*	*Cycle Mumber*	*Source*	$(ETR)_1$	*Ref.**
52137.3969	–1294	CCD	0.001104	48	52521.5697	76	CCD	0.0016548	49
52137.5365	–1293.5	CCD	0.000495	48	52546.6670	165.5	CCD	0.0016006	53
52145.5289	–1265	CCD	0.000990	49	52560.9727	216.5	CCD	0.0059679	54
52194.3215	–1091	CCD	0.000911	50	52561.1123	217	CCD	0.0053591	54
52201.6134	–1065	CCD	0.001951	40	52565.5965	233	CCD	0.0028759	40
52219.558	–1001	vis	–0.000182	40	52602.6112	365	CCD	0.0024395	40
52240.5917	–926	CCD	0.002190	40	52806.7546	1093	CCD	0.001754	40
52465.473	–124	vis	–0.011505	43	52815.4469	1124	PE	0.001065	55
52465.4744	–124	vis	–0.010115	43	52815.4500	1124	PE	0.004175	55
52478.3855	–78	CCD	0.001781	40	52870.6902	1321	CCD	0.002118	40
52496.6128	–13	CCD	0.001930	40	52878.4018	1348.5	CCD	0.002232	56
52501.3783	4	CCD	0.000329	40	52878.5425	1349	CCD	0.002723	56
52501.6256	5	CCD	–0.032789	51	52886.3935	1377	CCD	0.002027	57
52504.4752	15	vis	0.0126345	43	52887.3756	1380.5	CCD	0.002665	58
52505.4453	18.5	CCD	0.0012725	52	52887.5149	1381	CCD	0.001756	58
52505.5859	19	CCD	0.0016637	52	52887.5150	1381	CCD	0.001856	59
52510.4923	36.5	CCD	0.0007540	52	52902.3758	1434	CCD	0.000518	58
52514.6663	51.5	CCD	–0.031512	51	52908.4028	1455.5	vis	–0.001462	43
52517.5164	61.5	vis	0.0143614	43	52914.7150	1478	CCD	0.001339	60
52521.4288	75.5	CCD	0.0009637	49	52914.8564	1478.5	CCD	0.002531	60

Table continued on following pages

Table 3. Visual, Photographic, Photoelectric, and CCD Times of Minimum (–2,400,000) for BX Peg from 1960 to 2011. Eclipse timing residuals $(ETR)_1$ are based on the linear elements defined by Kreiner (2004).

Time of Minimum	*Cycle Mumber*	*Source*	*$(ETR)_1$*	*Ref.**	*Time of Minimum*	*Cycle Mumber*	*Source*	*$(ETR)_1$*	*Ref.**
52920.6030	1499	CCD	0.000568	40	53228.3612	2596.5	CCD	0.000342	43
52929.4367	1530.5	CCD	0.001110	58	53233.4095	2614.5	CCD	0.001123	56
52929.5793	1531	CCD	0.003501	58	53233.5488	2615	CCD	0.000214	56
52931.3934	1537.5	vis	–0.005074	43	53236.3538	2625	CCD	0.001037	61
52941.3539	1573	vis	0.000598	43	53236.4931	2625.5	CCD	0.000129	61
52956.3592	1626.5	CCD	0.003511	43	53240.4180	2639.5	CCD	–0.000819	61
52986.5020	1734	CCD	0.001408	40	53240.5597	2640	CCD	0.000672	61
53208.4530	2525.5	CCD	0.001799	61	53250.3747	2675	CCD	0.001052	56
53209.4332	2529	CCD	0.000537	56	53250.5084	2675.5	CCD	–0.005426	62
53209.4335	2529	CCD	0.000837	61	53250.5140	2675.5	CCD	0.000144	56
53209.5743	2529.5	CCD	0.001428	61	53252.6171	2683	CCD	0.000111	63
53212.5180	2540	CCD	0.000742	61	53255.4219	2693	CCD	0.000734	56
53217.4262	2557.5	CCD	0.001632	56	53255.5628	2693.5	CCD	0.001425	56
53220.3701	2568	CCD	0.001146	61	53257.3845	2700	CCD	0.000410	56
53220.5099	2568.5	CCD	0.000738	61	53257.5226	2700.5	CCD	–0.001699	56
53220.5112	2568.5	CCD	0.002038	56	53277.5746	2772	CCD	0.000436	63
53221.4928	2572	CCD	0.002176	56	53282.3417	2789	CCD	0.000435	56
53224.4358	2582.5	CCD	0.000790	61	53282.4834	2789.5	CCD	0.001926	56
53226.5392	2590	CCD	0.001057	56	53341.2285	2999	CCD	–0.000482	64
53226.5392	2590	CCD	0.001057	61	53360.2974	3067	CCD	0.000014	65

Table continued on following pages

Table 3. Visual, Photographic, Photoelectric, and CCD Times of Minimum (–2,400,000) for BX Peg from 1960 to 2011. Eclipse timing residuals $(ETR)_1$ are based on the linear elements defined by Kreiner (2004).

Time of Minimum	*Cycle Mumber*	*Source*	*$(ETR)_1$*	*Ref.**	*Time of Minimum*	*Cycle Mumber*	*Source*	*$(ETR)_1$*	*Ref.**
53589.6777	3885	CCD	–0.001364	63	53951.2770	5174.5	CCD	–0.000689	69
53601.4569	3927	CCD	0.000292	66	53966.4203	5228.5	CCD	0.000056	70
53613.3741	3969.5	CCD	–0.000260	66	53966.5597	5229	CCD	–0.000753	70
53613.5150	3970	CCD	0.000431	65	53985.4890	5296.5	CCD	0.000352	71
53613.5159	3970	CCD	0.001331	66	53987.9119	5305	CCD	0.039701	72
53614.3566	3973	CCD	0.000778	43	53989.6960	5311.5	CCD	0.001086	72
53614.4970	3973.5	CCD	0.000969	66	53992.3574	5321	CCD	–0.001482	70
53616.4573	3980.5	CCD	–0.001655	43	53992.3628	5321	CCD	0.003908	43
53617.4407	3984	CCD	0.000283	43	54000.3487	5349.5	CCD	–0.002086	43
53632.0216	4036	CCD	–0.000537	67	54002.4524	5357	CCD	–0.001519	70
53632.1623	4036.5	CCD	–0.000046	67	54079.5669	5632	CCD	–0.001886	63
53648.4272	4094.5	CCD	0.000627	66	54279.6470	6345.5	CCD	0.000185	73
53651.3711	4105	CCD	0.000141	43	54281.7505	6353	CCD	0.000552	63
53651.3714	4105	CCD	0.000442	66	54297.4537	6409	CCD	0.000361	68
53651.5111	4105.5	CCD	–0.000067	66	54327.4581	6516	CCD	0.000067	43
53659.3629	4133.5	CCD	0.000037	66	54328.4386	6519.5	CCD	–0.000865	43
53659.5033	4134	CCD	0.000228	66	54328.4393	6519.5	CCD	–0.000195	43
53663.9891	4150	CCD	–0.000655	67	54330.5428	6527	CCD	0.000202	43
53928.4221	5093	CCD	–0.001546	68	54330.5431	6527	CCD	0.000472	43
53951.1360	5174	CCD	–0.001480	69	54359.9874	6632	CCD	0.000914	74

Table continued on following pages

Table 3. Visual, Photographic, Photoelectric, and CCD Times of Minimum (–2,400,000) for BX Peg from 1960 to 2011. Eclipse timing residuals $(ETR)_1$ are based on the linear elements defined by Kreiner (2004).

Time of Minimum	*Cycle Mumber*	*Source*	*$(ETR)_1$*	*Ref.**	*Time of Minimum*	*Cycle Mumber*	*Source*	*$(ETR)_1$*	*Ref.**
54386.6281	6727	CCD	0.001932	75	54760.7033	8061	CCD	–0.000080	78
54393.9200	6753	CCD	0.002972	74	54761.6856	8064.5	CCD	0.000758	78
54420.5567	6848	CCD	–0.000010	75	54763.5079	8071	CCD	–0.000157	79
54650.7799	7669	CCD	0.000259	76	54766.5923	8082	CCD	0.000249	79
54678.4008	7767.5	CCD	0.000015	68	54770.5184	8096	CCD	0.000101	79
54690.4604	7810.5	CCD	0.001654	68	54785.6608	8150	CCD	0.000245	78
54702.6579	7854	CCD	0.000984	76	54786.6426	8153.5	CCD	0.000583	78
54721.7261	7922	CCD	0.000781	77	55000.4587	8916	CCD	–0.001813	81
54736.7282	7975.5	CCD	0.000534	78	55000.4587	8916	CCD	–0.001813	81
54736.8681	7976	CCD	0.000225	78	55000.4590	8916	CCD	–0.001513	81
54737.7092	7979	CCD	0.000072	78	55057.3837	9119	CCD	–0.001606	82
54737.8500	7979.5	CCD	0.000663	78	55061.0300	9132	CCD	–0.000736	83
54738.6912	7982.5	CCD	0.000610	78	55061.1705	9132.5	CCD	–0.000445	83
54747.5241	8014	CCD	0.000252	79	55082.0685	9207	CCD	0.006436	83
54751.5906	8028.5	CCD	0.000396	79	55087.6684	9227	CCD	–0.002018	84
54752.5719	8032	CCD	0.000434	79	55107.2959	9297	CCD	–0.003757	84
54755.5164	8042.5	CCD	0.000548	79	55121.6025	9348	CCD	0.001540	85
54757.3391	8049	CCD	0.000733	80	55121.7390	9348.5	CCD	–0.002168	85
54759.5824	8057	CCD	0.000591	79	55146.5572	9437	CCD	–0.000935	84
54759.7225	8057.5	CCD	0.000582	78	55383.7904	10283	CCD	–0.001109	86

Table continued on next page

Table 3. Visual, Photographic, Photoelectric, and CCD Times of Minimum (–2,400,000) for BX Peg from 1960 to 2011. Eclipse timing residuals $(ETR)_1$ are based on the linear elements defined by Kreiner (2004).

Time of Minimum	*Cycle Mumber*	*Source*	*$(ETR)_1$*	*Ref.**	*Time of Minimum*	*Cycle Mumber*	*Source*	*$(ETR)_1$*	*Ref.**
55481.3719	10631	CCD	–0.004969	87	55843.6711	11923	CCD	–0.005637	79
55481.5166	10631.5	CCD	–0.000478	87	55844.6536	11926.5	CCD	–0.004499	79
55482.3561	10634.5	CCD	–0.002231	82	55849.7021	11944.5	CCD	–0.003418	88
55840.5864	11912	CCD	–0.005542	79	55850.6809	11948	CCD	–0.006080	88
55841.5692	11915.5	CCD	–0.004604	79	55856.5550	11969	vis	–0.020751	89
55841.7065	11916	CCD	–0.007013	79	55868.4891	12011.5	CCD	–0.004504	79
55842.5498	11919	CCD	–0.005266	79	55868.6284	12012	CCD	–0.005512	79
55842.6907	11919.5	CCD	–0.004475	79	55873.5372	12029.5	CCD	–0.003822	79
55843.5318	11922.5	CCD	–0.004728	79					

** References:; (1) Samec 1990; (2) Diethelm et al. 1972; (3) Baldwin and Samolyk 1995; (4) Samec 1989; (5) Samec and Bookmyer 1987; (6) Mikulášek 1985; (7) Isles 1985a; (8) Isles 1985b; (9) Hübscher and Mundry 1984; (10) Isles 1985c; (11) Mikulášek 1986; (12) Isles 1989; (13) Hübscher et al. 1986; (14) Mikulášek and Šilhán 1988; (15) BBSAG 1987; (16) Hübscher and Lichtenknecker 1988; (17) BBSAG 1988a; (18) BBSAG 1988b; (19) Mikulášek et al. 1992; (20) Hübscher et al. 1989; (21) BBSAG 1989a; (22) Hübscher et al. 1990; (23) BBSAG 1989b; (24) Isles 1992; (25) BBSAG 1990a; (26) Zejda 1995; (27) BBSAG 1990b; (28) De Young et al. 1991; (29) BBSAG 1991; (30) Hübscher et al. 1992; (31) Hübscher et al. 1993; (32) BBSAG 1992a; (33) BBSAG 1992b; (34) Hübscher et al. 1994; (35) BBSAG 1994a; (36) BBSAG 1994b; (37) BBSAG 1995; (38) Mikulášek and Zejda 2002; (39) Šafář and Zejda 2000a; (40) Baldwin and Samolyk 2004; (41) Šafář and Zejda 2000b; (42) Lee et al. 2004; (43) Brát et al. 2007; (44) Nelson 2001; (45) Nelson 2002; (46) BBSAG 2002; (47) Baldinelli and Maitan 2002; (48) Agerer and Hübscher 2002; (49) Zejda 2004; (50) BBSAG 2001; (51) Diethelm 2003; (52) Agerer and Hübscher 2003; (53) Nelson 2003; (54) Nagai 2003; (55) Gürol et al. 2003; (56) Hübscher et al. 2005; (57) Krajci 2005; (58) Hübscher 2005; (59) Diethelm 2004; (60) Maciejewski and Karska 2004; (61) Pribulla et al. 2005; (62) Bíró et al. 2006; (63) Baldwin and Samolyk 2007; (64) Diethelm 2005; (65) Zejda et al. 2006; (66) Hübscher et al. 2006; (67) Nagai 2006; (68) Parimucha et al. 2009; (69) Nagai 2007; (70) Hübscher and Walter 2007; (71) Doğru et al. 2007; (72) Ogloza et al. 2008; (73) Paschke 2007; (74) Nagai 2008; (75) Samolyk 2008a; (76) Samolyk 2008b; (77) Samolyk 2009; (78) Lee et al. 2009; (79) Alton 2013 (present study); (80) Hübscher et al. 2009; (81) Brát et al. 2011; (82) Parimucha et al. 2011; (83) Nagai 2010; (84) Samolyk 2010; (85) Diethelm 2010; (86) Diethelm 2011; (87) Hübscher 2011; (88) Diethelm 2012; (89) Nagai 2012*

Table 4. Near-term recalculated eclipse timing residuals $(ETR)_2$ for BX Peg following simple linear least squares fit of residuals $(ETR)_1$ from reference epoch and cycle number between 2008 July 03 and 2011 Nov 08.

Time of Minimum (HJD–2400000)	*Type*	*Cycle Number*	*$(ETR)_1$[a]*	*$(ETR)_2$*	*Reference**
54650.7799	p	7669	0.00025870	0.00089989	1
54678.4008	s	7767.5	0.00001525	0.00076849	2
54690.4604	s	7810.5	0.00165415	0.00071113	2
54702.6579	p	7854	0.00098420	0.00065310	1
54721.7261	p	7922	0.00078060	0.00056239	3
54736.7282	s	7975.5	0.00053365	0.00049102	4
54736.8681	p	7976	0.00022480	0.00049036	4
54737.7092	p	7979	0.00007170	0.00048635	4
54737.8500	s	7979.5	0.00066285	0.00048569	4
54738.6912	s	7982.5	0.00060975	0.00048168	4
54747.5241	p	8014	0.00036553	0.00043966	5
54751.5906	s	8028.5	0.00074555	0.00042032	5
54752.5719	p	8032	0.00061027	0.00041565	5
54755.5164	s	8042.5	0.00076442	0.00040164	5
54757.3391	p	8049	0.00073270	0.00039297	6
54759.5824	p	8057	0.00068110	0.00038230	5
54759.7225	s	8057.5	0.00058225	0.00038163	4
54760.7033	p	8061	–0.00007970	0.00037697	4
54761.6856	s	8064.5	0.00075835	0.00037230	4
54763.5079	p	8071	0.00029330	0.00036363	5
54766.5923	p	8082	0.00015527	0.00034895	5
54770.5184	p	8096	0.00043080	0.00033028	5
54785.6608	p	8150	0.00024500	0.00025824	4
54786.6426	s	8153.5	0.00058305	0.00025357	4
55000.4587	p	8916	–0.00181320	–0.00076360	7
55000.4587	p	8916	–0.00181320	–0.00076360	7
55000.4590	p	8916	–0.00151320	–0.00076360	7
55057.3837	p	9119	–0.00160630	–0.00103440	8
55061.0300	p	9132	–0.00073640	–0.00105175	9
55061.1705	s	9132.5	–0.00044525	–0.00105241	9
55087.6684	p	9227	–0.00201790	–0.00117848	10
55107.2959	p	9297	–0.00375690	–0.00127186	10
55121.6025	p	9348	0.00154040	–0.00133989	11
55121.7390	s	9348.5	–0.00216845	–0.00134056	11
55146.5572	p	9437	–0.00093490	–0.00145861	10
55383.7904	p	10283	–0.00110910	–0.00258718	12
55481.3719	p	10631	–0.00496870	–0.00305141	13

table continued on next page

Table 4. Near-term recalculated eclipse timing residuals $(ETR)_2$ for BX Peg following simple linear least squares fit of residuals $(ETR)_1$ from reference epoch and cycle number between 2008 July 03 and 2011 Nov 08, cont.

Time of Minimum (HJD–2400000)	*Type*	*Cycle Number*	*$(ETR)_1$[a]*	*$(ETR)_2$*	*Reference**
55481.5166	s	10631.5	–0.00047755	–0.00305207	13
55482.3561	s	10634.5	–0.00223065	–0.00305608	13
55840.5864	p	11912	–0.00549907	–0.00476026	5
55841.7065	p	11916	–0.00715320	–0.00476559	5
55841.5692	s	11915.5	–0.00419102	–0.00476493	5
55842.5498	p	11919	–0.00509963	–0.00476960	5
55842.6907	s	11919.5	–0.00435515	–0.00477026	5
55843.6711	p	11923	–0.00543377	–0.00477493	5
55843.5318	s	11922.5	–0.00455825	–0.00477427	5
55844.6536	s	11926.5	–0.00436905	–0.00477960	5
55849.7021	s	11944.5	–0.00341765	–0.00480361	14
55850.6809	p	11948	–0.00607960	–0.00480828	14
55868.6284	p	12012	–0.00529240	–0.00489366	5
55868.4891	s	12011.5	–0.00442688	–0.00489299	5
55873.5372	s	12029.5	–0.00380882	–0.00491700	5

Note: a. Eclipse Timing Residuals; $(ETR)_1$ from linear elements; (Kreiner 2004) for BX Peg.

** References:; (1) Samolyk 2008b; (2) Parimucha et al. 2009; (3) Samolyk 2009; (4) Lee et al. 2009; (5) Alton 2013 (present study); (6) Hübscher et al. 2009; (7) Brát et al. 2011; (8) Parimucha et al. 2011; (9) Nagai 2010; (10) Samolyk 2010; (11) Diethlem 2010; (12) Diethlem 2011; (13) Hübscher 2011; (14) Diethlem 2012.*

Table 5. Difference in BX Peg light curve magnitude at minimum and maximum light.

Bandpass (Year)	*Min I–Min II*	*Max I–Max II[a]*	*Min I–Max I*	*Min II–Max II*
B (2008)	0.119	0.016	0.724	0.621
V (2008)	0.122	0.009	0.694	0.581
I_c (2008)	0.101	0.007	0.614	0.520
B (2011)	0.199	–0.013	0.794	0.582
V (2011)	0.160	–0.024	0.747	0.563
I_c (2011)	0.101	–0.005	0.650	0.544

Note: a. Measure of asymmetry at maximum light.

Table 6. Spectral classification of BX Peg based upon data from various survey catalogs and present study.

Stellar Attribute	*Tycho-2*	*USNO-B1.0*	*USNO-A2.0*	*All Sky Combined*	*MPOSC3*	*2MASS*	*SDSS-DR8*	*Present Study*
(B–V)	0.871	0.695	0.617	0.764	0.812	0.812	0.766	0.716
Teff[a] (K)	5258	5660	5837	5503	5390	5390	5504	5613
Spectral Class[b]	G9-K0	G6V	G3V	G7-G8V	G9V	G9V	G7-G8V	G7V

Notes: a. Interpolated from Flower (1996). b. Estimated from Harmanec (1988).

Table 7. Absolute and relative system dimensions for BX Peg

Parameter	*Present Study*		*Lee et al. 2009*
	2008	*2011*	
$M_1(M_\odot)$	0.96 (0.059)[a]	0.96 (0.059)	
$M_2(M_\odot)$	0.352 (0.022)	0.356 (0.022)	
$R_1(R_\odot)$	0.9391 (0.0025)	0.9466 (0.0041)	
$R_2(R_\odot)$	0.5971 (0.0013)	0.6081 (0.0014)	
$a(R_\odot)$	1.9717 (0.0029)	1.9735 (0.0042)	
r_1(back)	0.5041 ± 0.0038	0.5084 ± 0.0037	0.5034 ± 0.0012
r_1(side)	0.4762 ± 0.0036	0.4793 ± 0.0035	0.4752 ± 0.0009
r_1(pole)	0.4442 ± 0.0034	0.4465 ± 0.0032	0.4435 ± 0.0007
r_1(volume)	0.4739 ± 0.0033	0.4767 ± 0.0035	0.4755
r_2(back)	0.3293 ± 0.0025	0.3366 ± 0.0024	0.3310 ± 0.0016
r_2(side)	0.2932 ± 0.0022	0.2978 ± 0.0022	0.2946 ± 0.0010
r_2(pole)	0.2807 ± 0.0021	0.2847 ± 0.0021	0.2820 ± 0.0009
r_2(volume)	0.3004 ± 0.0023	0.3047 ± 0.0022	0.3042

Note: *a. Formal error estimates from numerical methods according to Prša and Harmanec (2010; PHOEBE 0.32 manual).*

Table 8. A comparison of synthetic light curve parameters for BX Peg.

Parameter	*Lee et al. 2009 Group 1 Fit*[a]	*Present Study No Spot (2008)*	*Present Study Cool Spot 1 (2008)*	*Present Study No Spot (2011)*	*Present Study Cool Spot 1 (2011)*
T_1 (K)[b]	5532	5520	5520	5520	5520
T_2 (K)[c]	5300 ± 20	5957 ± 15	5858 ± 16	5978 ± 18	5998 ± 15
q (m_2/m_1)[c]	2.6897 ± 0.0045	0.3701 ± 0.0008	0.3669 ± 0.0016	0.3713 ± 0.0046	0.3705 ± 0.0015
A[b]	0.5	0.5	0.5	0.5	0.5
g[b]	0.32	0.32	0.32	0.32	0.32
$\Omega_1 = \Omega_2$[c]	6.135 ± 0.010	2.5804 ± 0.0006	2.586 ± 0.0036	2.589 ± 0.0013	2.578 ± 0.0055
i°[c]	87.693 ± 0.095	87.53 ± 0.89	88.30 ± 1.13	89.27 ± 0.35	88.92 ± 0.48
$A_{S1} = T_{S1} / T$[d]	0.828 ± 0.050	—	0.80 ± 0.01	—	0.83 ± 0.01
Θ_{S1} (spot co-latitude)[d]	66.6 ± 2.1	—	90 ± 3.2	—	90 ± 7.7
φ_{S1} (spot longitude)[d]	142.7 ± 0.4	—	143 ± 1.7	—	292 ± 3
r_{S1} (angular radius)[d]	14.1 ± 0.1	—	12.9 ± 0.13	—	15.3 ± 0.23
$\chi 2$ (B)[e]	—	0.036536	0.031770	0.023576	0.019429
$\chi 2$ (V)	—	0.054780	0.037238	0.030995	0.021960
$\chi 2$ (I_c)	—	0.140966	0.109502	0.096506	0.080949

Notes: a. Parameters and error reported by Lee et al. (2009) using m_1/m_2. b. Fixed during DC. c. Error estimates from heuristic scanning with PHOEBE *0.31a (Prša and Zwitter 2005). d. Error estimates from* WDWINT *v5.6a (Nelson 2009). e. $\chi 2$ from* PHOEBE *0.31a (Prša and Zwitter 2005).*

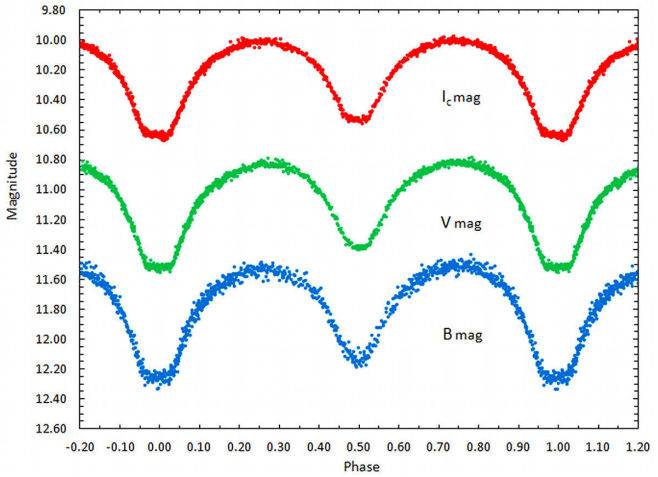

Figure 1. Folded CCD light curves for BX Peg produced from photometric data obtained between October 8 and October 31, 2008. The top (I_c), middle (V), and bottom (B) curves shown above were reduced to MPOSC3-based catalogue magnitudes using MPO CANOPUS.

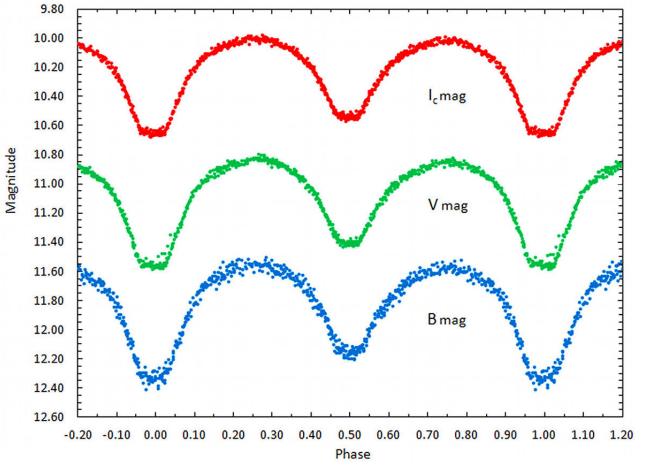

Figure 2. Folded CCD light curves for BX Peg produced from photometric data obtained between October 6 and November 8, 2011. The top (I_c), middle (V), and bottom (B) curves shown above were reduced to MPOSC3-based catalogue magnitudes using MPO CANOPUS.

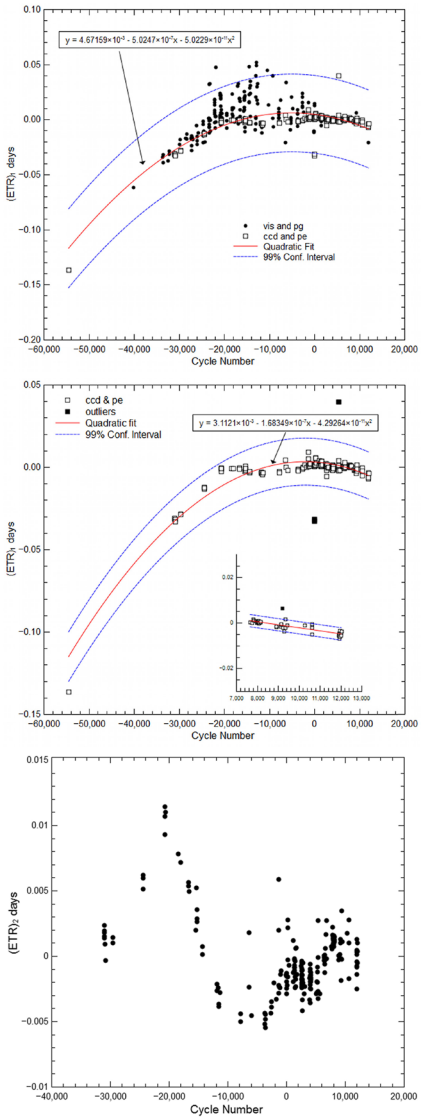

Figure 3. Non-linear regression fit (top) from visual, pg, PE, and CCD times of minimum (1960–2011) for BX Peg using a quadratic expression weighted 8:1 with respect to instrumental and non-instrument readings. The middle plot shows quadratic fit only from the CCD and PE times of minimum. The inset graph shows a straight-line fit and 99% confidence intervals of ET data between 2008 and 2011 which were used to calculate a near term linear ephemeris for BX Peg. Residuals $(ETR)_2$ from the quadratic fit of instrumental (CCD and PE) eclipse timings are shown in the bottom panel.

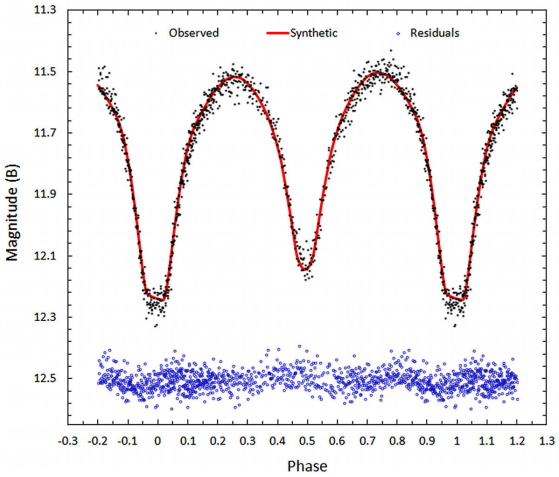

Figure 4. Synthetic fit of light curve (B mag.) for BX Peg collected at UO during 2008 using Roche model parameters (T_1, T_2, i, q, Ω, and cold spot) identical to those reported by Lee *et al.* (2009). Residuals are offset by a constant value to keep the y-axis on scale.

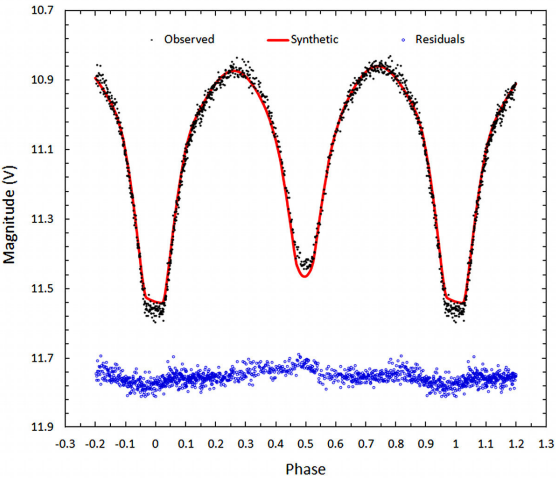

Figure 5. Synthetic fit of light curve (V mag.) for BX Peg collected at UO during 2008 using Roche model parameters (T1, T2, i, q, Ω, and cold spot) identical to those reported by Lee *et al.* (2009). Residuals are offset by a constant value to keep the y-axis on scale.

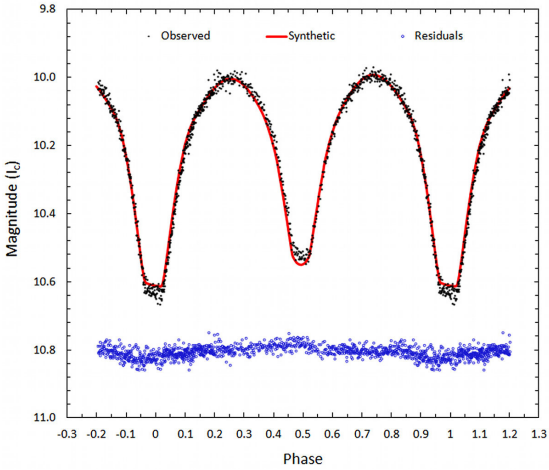

Figure 6. Synthetic fit of light curve (I_c mag.) for BX Peg collected at UO during 2008 using Roche model parameters (T_1, T_2, i, q, Ω, and cold spot) identical to those reported by Lee *et al.* (2009). Residuals are offset by a constant value to keep the y-axis on scale.

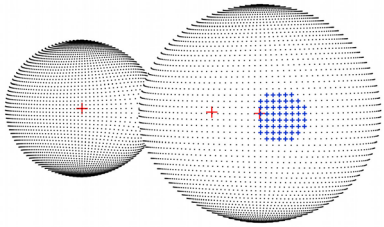

Figure 7. 3-D spatial representation (phase = 0.10) of BX Peg during October 2008 with cool spot positioned on the more massive star visible to the viewer during and slightly after Min I.

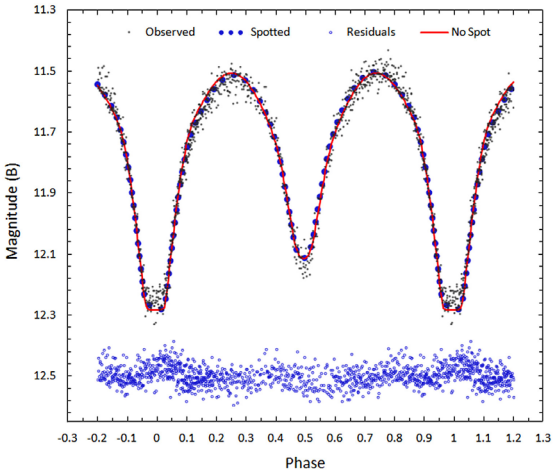

Figure 8. Synthetic fits of BX Peg light curve (B mag.) collected at UO during 2008 using an unspotted (solid-line) and a spotted (dotted-line) Roche model which incorporates a cool spot on the more massive star. Spotted residuals are offset by a constant value to keep the y-axis on scale.

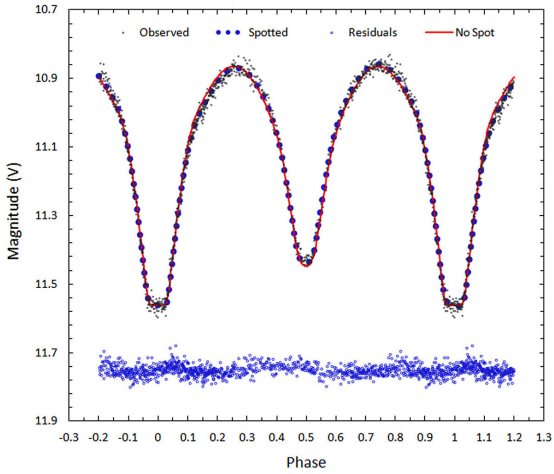

Figure 9. Synthetic fit of light curve (V mag.) for BX Peg collected at UO during 2008 using an unspotted (solid-line) and spotted (dotted-line) Roche model which incorporates a cool spot on the more massive star. Spotted residuals are offset by a constant value to keep the y-axis on scale.

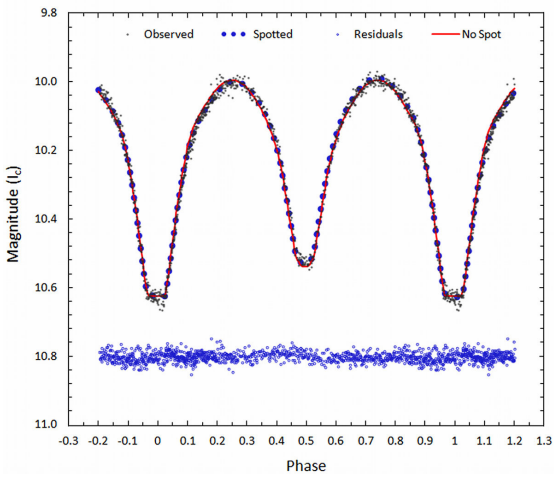

Figure 10. Synthetic fit of light curve (I_c mag.) for BX Peg collected at UO during 2008 using an unspotted (solid-line) and spotted (dotted-line) Roche model which incorporates a cool spot on the more massive star. Spotted residuals are offset by a constant value to keep the y-axis on scale.

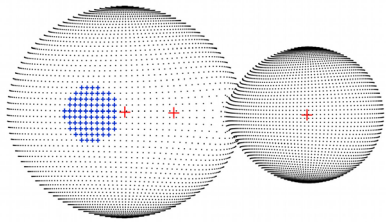

Figure 11. 3-D spatial model (phase = 0.63) of BX Peg between October and November 2011 with a cool spot positioned on the more massive star which diminishes brightness during Max II.

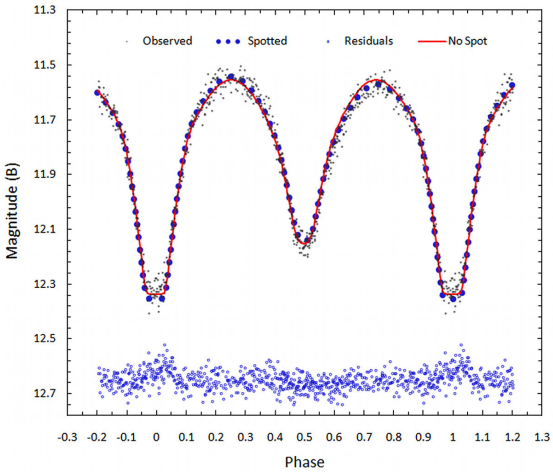

Figure 12. Synthetic fit of light curve (B mag.) for BX Peg collected at UO during 2011 using an unspotted (solid-line) and spotted (dotted-line) Roche model which incorporates a cool spot on the more massive star. Spotted residuals are offset by a constant value to keep the y-axis on scale.

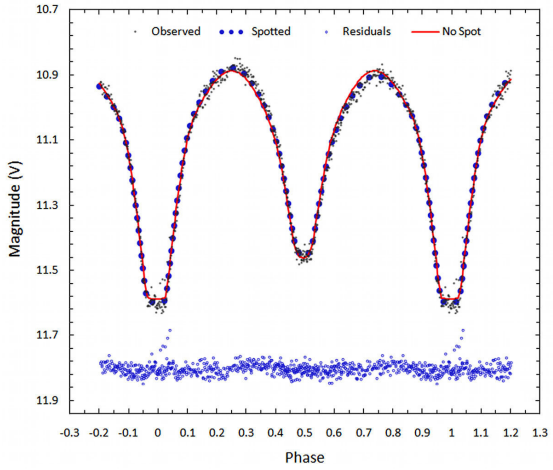

Figure 13. Synthetic fit of light curve (V mag.) for BX Peg collected at UO during 2011 using an unspotted (solid-line) and spotted (dotted-line) Roche model which incorporates a cool spot on the primary star. Spotted residuals are offset by a constant amount in order to keep the y-axis on scale.

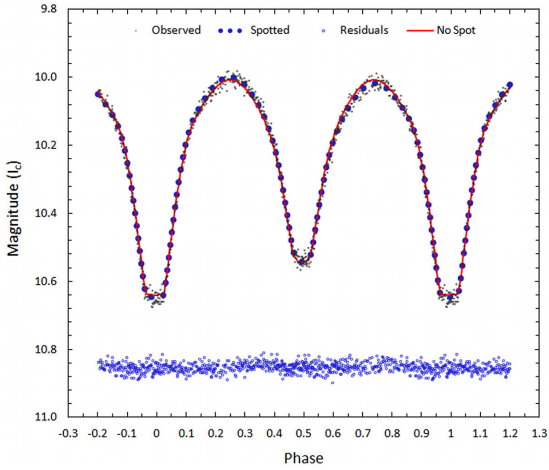

Figure 14. Synthetic fit of light curve (I_c mag.) for BX Peg collected at UO during 2011 using an unspotted (solid-line) and spotted (dotted-line) Roche model which incorporates a cool spot on the primary star. Spotted residuals are offset by a constant amount in order to keep the y-axis on scale.

V2331 Cygni is an Algol Variable With Deep Eclipses

Hans Bengtsson
Sagogången 55, SE-422 45 Hisings Backa, Sweden; hkibengtsson@gmail.com

Pierre Hallsten
Älgvägen 13, SE-137 32 Västerhaninge, Sweden; Pierre.Hallsten@yahoo.com

Anders Hemlin
Karlavägen 11, SE-802 66 Gävle, Sweden; anders@hemlin.se

Gustav Holmberg
Karl XI-gatan 8A, SE-222 20 Lund, Sweden; 5063.Gustav.Holmberg@gmail.com

Thomas Karlsson
Almers väg 19, SE-432 51 Varberg, Sweden; tkn@seaside.se

Robert Wahlström
Klintens väg 6, SE-441 41 Alingsås, Sweden; robert@alderaan.nu

Tomas Wikander
Bogservägen 8, SE-784 77 Borlänge, Sweden wikander.tomas@gmail.com

Received April 9, 2013; accepted May 1, 2013

Abstract We report the discovery that V2331 Cygni is not an L star but an eclipsing variable with deep minima, and present a determination of the elements of the star: Epoch = HJD 2456184.296 ±0.001 and Period = 1.3886 ± 0.0001 days.

1. Discovery

V2331 Cygni (R.A. 21^h 11^m 13.60^s Dec. +34° 19' 14.3") was discovered to be a variable star by Dahlmark during a systematic photographic search for new variables (Dahlmark 2001). The star, originally named LD391, was determined by Dahlmark to be a slow irregular variable, and it was classified type L when it entered the *General Catalogue of Variable Stars* (GCVS; Samus *et al.* 2013) as V2331 Cyg (Samus *et al.* 2007–2012; Kazarovets *et al.* 2003). Since then, few observers appear to have been interested in the object.

The star is close to the Mira star V2330 Cyg, which is on a program organized by SAAF/V (the variable star section of the Swedish Amateur Astronomy Association) to study fifty underobserved Miras. During the monitoring of V2330 Cyg, sudden dips in the brightness of nearby V2331 Cyg were noted on August 21 and September 4, 2012. Incompatible with the normal behavior of an L star, could these two dips be indications of V2331 Cyg being of another type?

A period of intense observations of V2331 Cyg followed, the results of which are given in this paper.

2. Observations and elements

When it became apparent that this star was an eclipsing variable and the first preliminary elements of its variations were determined, it became possible to do time-series observations around the predicted time of minimum. Three such time-series observations were made during the autumn and winter of 2012. In addition, five time-series and seventy-three individual observations were made at phases outside of primary eclipse, in order to give a picture of the full light curve. Thus, a small secondary minimum was uncovered. All in all, 1,157 observations were made. The methods used were B-, V-, and R-filtered CCD observations, on local as well as remote telescopes, and DSLR observations reduced to V. The observations are available for downloading from the SAAF/V database at http://var.astronet.se/obsar_export.php?exporttype=csv&search_fd1=v2331+cyg%25 (comma-separated file format).

The mean BVR magnitudes of the system outside of eclipse were found, by analysis of observations at phases 0.1–0.4 and 0.6–0.9, to be as shown in Table 1.

The depth of the primary minimum, in V, is 2.5 magnitudes and the secondary minimum is 0.15. The duration of the eclipse is 0.15 of the period. The V observations were analysed using PERANSO (Vanmunster 2005, methods: Lafler-Kinman and Dworetsky) and the elements for the light variations determined are:

Epoch: HJD 2456184.296 ± 0.001

Period: 1.3886 ± 0.0001 d

3. Acknowledgements

It is a pleasure to acknowledge the support of the AAVSO charts and sequences team in providing sequences of comparison stars for the program of observing fifty neglected Mira stars. This research has made use of the SIMBAD database,operated at CDS, Strasbourg, France. Remote observations were performed using the Bradford Robotic Telescope, the iTelescope network, and the Sierra Stars Observatory.

References

Dahlmark, L. 2001, *Inf. Bull. Var. Stars*, No. 5181, 1.

Kazarovets, E. V., *et al.* 2003, *Inf. Bull. Var. Stars*, No. 5422, 1.

Samus, N. N., *et al.* 2013, *General Catalogue of Variable Stars* (GCVS database, Version 2013 July, http://www.sai.msu.su/gcvs/gcvs/index.htm).

Vanmunster, T. 2005, PERANSO period analysis software (www.peranso.com).

Table 1. Mean magnitudes of V2331 Cyg outside of eclipse.

Color	*Magnitude*	*Standard Error*
V	13.422	±0.002
B	13.857	±0.006
R	13.177	±0.003
B–V	0.435	—
V–R	0.245	—

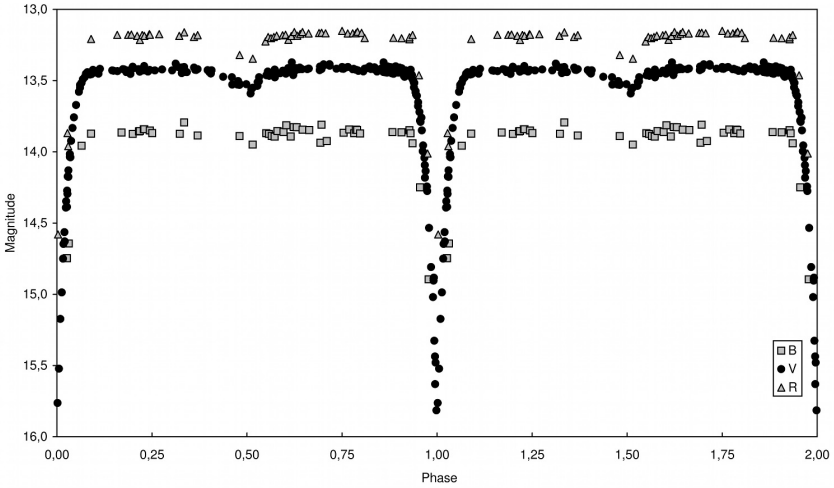

Figure 1. V2331 Cyg light curve folded according to the elements given in the text. Time-series observations during minima are here represented as averages of every fifth observation.

Data Mining the OGLE-II I-band Database for Eclipsing Binary Stars

Marco Ciocca
Department of Physics and Astronomy, Eastern Kentucky University, Richmond, KY; marco.ciocca@eku.edu

Presented at the 102nd Spring Meeting of the AAVSO, May 18, 2013. Received April 16, 2013; revised April 26, 2013; accepted April 29, 2013

Abstract The OGLE I-band database is a searchable database of quality photometric data available to the public. During Phase 2 of the experiment, known as "OGLE-II", I-band observations were made over a period of approximately 1,000 days, resulting in over 10^{10} measurements of more than 40 million stars. This was accomplished by using a filter with a passband near the standard Cousins I_c. The database of these observations is fully searchable using the MYSQL database engine, and provides the magnitude measurements and their uncertainties. In this work, a program of data mining the OGLE I-band database was performed, resulting in the discovery of 42 previously unreported eclipsing binaries. Using the software package PERANSO to analyze the light curves obtained from OGLE-II, the eclipsing types, the epochs, and the periods of these eclipsing variables were determined, to one part in 10^6. A preliminary attempt to model the physical parameters of these binaries was also performed, using the BINARY MAKER 3 software.

1. Introduction

The OGLE (Optical Gravitational Lensing Experiment) database contains over 40 million stars, with photometric data accessible to the public. By selecting the number of data points available for a particular star, the quality of the statistics, and the differences between average and median intensity, is possible to extract candidate stars that could be eclipsing binaries. The search was limited to OGLE-II stars (Udalski *et al.* 1997; Szymański 2005) in the Galactic disk (in particular in the constellation Carina) for which the data were reduced using Difference Imaging Analysis (DIA) (Szymański 2005). DIA produces more accurate photometric data, with less uncertainty. Limiting the search to just the Galactic Disk was done in order to generate a smaller sample of stars to analyze. Following the method outlined by Nicholson (2009, 2012), a search of all the data available was initiated with the following MYSQL search parameters:

```
NGOOD>=300 AND NGOOD<=3000 AND I>=13 AND I<=16.5 AND ISIG>=0.05
AND ISIG<=10 AND I>IMED
```

The search parameter constrained the results to stars with at least 300 reliable I-magnitude data points (and less than 3,000), all stars with I-magnitude between 13 and 16.5 and with a standard deviation I_{sig} of the mean I-magnitude between 0.05 and 10. This range of magnitudes was selected to try reducing the overlap with searches of other investigators (Watson *et al.* 2007; Nicholson 2010; Hümmerich 2012; Hümmerich and Bernhard 2012) which had already performed searches on OGLE-II. The upper limit was chosen, on the other hand, to avoid an extremely large number of results. OGLE-II has, in fact, data with mean magnitude I to approximately 22. Had the upper limit for I been so chosen, the returned set would have been in excess of 423,000.

The parameter I_{sig} is the standard deviation of I-magnitude, and therefore it is expected that variable stars will show a value larger than zero, but not so small to just be random noise. The upper extreme was chosen to include all possible cases. Furthermore, as the goal was to search for variable stars of the eclipsing type, stars were selected for which the mean magnitude I was larger than the median I_{med}. This was done because eclipsing variables spend more time at their highest luminosity and dim only during the eclipse, which usually has a duration that is smaller than half of the cycle. This search string netted 285 possible candidates. The same query, but on the Galactic Bulge (OGLE-II had data for that location as well), returns more than 10,000 possible candidates.

2. Data mining results

The candidates were first scrutinized by searching VSX to see if these stars had already been determined to be eclipsing variable or variable in general. This eliminated 77 candidates (Nicholson 2010; Hümmerich 2012; Hümmerich and Bernhard 2012). A smaller number, 25, of the query results were obviously corresponding to stable stars (from inspection of the light curve). These light curves had but one bad data point that created a disparity between I and I_{med} and thus were selected by the MYSQL query. Of the remaining 183, 89 had light curves that did not show an easily recognizable pattern.

To try and visualize the difference between eclipsing variable and other possibly variable stars, we plotted I_{sig} as a function of $(I–I_{med})$. It is expected that stars showing an increase in I_{sig} and also showing an increase of the difference between I and I_{med} would be more likely to be eclipsing variables. The results of such a plot is shown in Figure 1, which clearly shows that stars already identified as eclipsing variables and stars found in this work to be eclipsing variables show a fairly close correlation between I_{sig} and $(I–I_{med})$ (see the R parameters in the linear fit of Figure 1). On the other hand, the 89 stars with no readily recognizable pattern do not show this correlation (R is much smaller). At the end of this analysis, the set of stars to study further was reduced to 94.

We analyzed these data using the software package PERANSO (Vanmuster 2011). This program uses FFT routines to extract, if any, a period of variability

from the light curves obtained from the OGLE-II. In doing this analysis, the end results are phase plots, in which the light curve is folded over a single period showing clearly the eclipsing variability. From the phase plots one can determine the eclipsing types, epochs, and periods of these eclipsing variables. In particular, the results presented in this work were obtained using the routine "Anova" in PERANSO.

The analysis of these 94 candidates found using the MYSQL query is ongoing, and in this paper reports 42 newly identified eclipsing binaries, shown in Table 1. These findings have been submitted to and approved by VSX, managed by the American Association of Variable Stars Observers (AAVSO). Table I reports each star's name, coordinates, eclipsing variable type, period, and magnitude range. The remaining 52 candidates are still in the process of being analyzed and a report on the results will be presented a later date.

Figure 2 (top panel) shows a typical light curve as downloaded from OGLE-II, with the I-band magnitude of the star as a function of the Heliocentric Julian Date (HJD). The period of the star shown in Figure 2 (middle panel) is found to be 0.353095 day. The uncertainty on this period and the periods of all stars in Table 1 are of similar magnitude, approximately 1×10^{-6} d. Such uncertainties arise from the calculation routine itself, as well as the uncertainties of the photometric measurements. In Figure 2 the bottom panel shows the resulting phase plot of the binary star OGLEII CAR-SC2 236.

As is seen from Table 1, eclipsing binaries with the shortest periods are quite often identified as EW eclipsing variables. This designation originates from the star W UMa. The periods for EWs are usually shorter than one day, with the component stars being ellipsoidal in shape due to the gravitational tidal effects on their gas envelopes. EW stars are "over-contact" systems and have light curves that change continuously, so much so that it is almost impossible to specify the exact times of the onset and end of eclipses. The depths of the primary and secondary minima are equal or differ by a small percentage. The component stars generally belong to spectral types F-G. EW eclipsing variables can be described as conjoined twins revolving around each other in a tight pair.

The other types observed are EB and EA. EB (from the prototype β Lyr) are eclipsing systems with ellipsoidal components as well, with the light curves showing continuous changes, as the EW. The difference is that the secondary minimum is always observable, with a depth usually being noticeably smaller than that of the primary minimum; periods also tend to be longer than one day. This property often implies that one star is larger than the other. The components generally belong to spectral types B or A.

Different from the EW and EB types, the EA (from the prototype β Per (Algol)) has components which are mostly spherical. This is because the two stars are farther apart, and the gravitational pull on the gas envelopes is reduced. The beginning and end of the eclipses can be clearly identified in the light

curve. When not in the eclipse the light remains almost constant. EA types have an extremely wide range of periods, from 0.2 day to 10,000 days.

The star displayed in Figure 2 has been identified as an EW eclipsing variable. In Figures 3 and 4 we present two more eclipsing binaries, identified as type EB and EA, respectively.

OGLEII CAR-SC2 47145 has a period of 0.728762 day, while OGLEII CAR-SC3 59302 has a period of 3.022445 days. It should be noted how the simple imagery of the growing component separation from EWs to EBs to EAs is reflected in the period of variability for these three examples. This correlation is reinforced by observing that, in Table I, the periods seem to follow this type-period trend as well.

3. Modeling eclipsing variables

By knowing the period, the light curve shape through the phase plot, and the surface temperature, models reproducing the light curve of the binary systems can be generated. The approach is to match the observed phase plot patterns using well-known parameters of stellar properties (see for example Van Hamme 1993, for tabulated parameters of some of these stellar properties). The surface temperatures and other physical parameters necessary to have a more realistic model of the eclipsing variable identified are not known for the stars in this work, nor are any spectroscopic analyses of these stars known to exist yet in the literature.

The shape of the light curve, however, and the identified eclipsing type permit the construction of plausible models. It is fairly straightforward to match the timing of the eclipses by selecting a suitable mass ratio. The EW star OGLEII CAR-SC2 236 is a classic over-contact system (Robertson and Eggleton 1977): brightness is never constant, with eclipses of similar depth. The measured period is less than 0.4 day and since the system has been identified as a W type, the larger star is likely the cooler star (Bradstreet and Steelman 2004, page 255).

The model of OGLEII CAR-SC2 236 was then built assuming a mass ratio of 3.3 to 1 (the cooler star has a mass 3.3 times the mass of the hotter star) and with temperatures consistent with a G spectral classification. Several parameters in BINARY MAKER 3 can then be input based on this G classification (like limb darkening and reflection parameters). The results of the model are presented in Figure 5.

4. Roche lobes and Lagrangian surfaces

But what exactly is meant by “over-contact? To understand this description let us consider the following: for a single star, the gravitational equipotential lines are concentric spheres. In the case of binary system, the equipotential lines

are still somewhat spherical near the individual stars' centers, but deviate from a spherical shape as one moves away, due to both the influence of the other star's gravitational force and the Coriolis force caused by the rapid rotational motion of the two stars. For each of the two stars in the binary system, the outermost equipotential surface is called the Roche lobe. This surface is elongated and tear-drop shaped, with the long axis along the line joining the two star centers and in contact with the other star lobe precisely at the first Lagrangian point L_1. The L_1 point is where the net force (the sum of the gravitational and centrifugal forces, as a rotating system is non-inertial) is zero. The other point of interest is L_2, still located along a line joining the two stars' centers, but opposite the center of the less massive star. L_2 is where the centrifugal force (again existing because a rotating system is non-inertial) is balanced by the gravitational attraction from the two stars. The gravitational equipotential surface at L_1 is the Inner Critical Lagrangian surface. The one passing through L_2 and encompassing both stars is the outer Lagrangian surface.

As a star in a binary system evolves, it will expand and can fill the inner Lagrangian surface. If material expands beyond this surface, it can cross L_1 and leave the original star and produce mass transfer onto the companion star. Over-contact binaries are those systems where both members have expanded beyond their respective inner Lagrangian surfaces and material is being exchanged. These eclipsing binaries can continue to evolve and possibly join to become a single star.

The model presented in Figure 5 for star OGLEII CAR-SC2 236 shows the fit of the theoretical light curve to the data, the three-dimensional profiles of the two stars, and the outline of the critical equipotential lines. The model predicts that the stars have indeed expanded beyond their inner Lagrangian surfaces. On the outline L_1 (in the center) and L_2 (to the left of the smaller star) are clearly visible. The crosses indicate the star centers and the center of mass of the system. Further, as the eclipses are not total and are continually changing, the angle between the axis of star rotation and the line of sight has to be less than 90 degrees. The angle that gave the best fit to the data was found to be 66.5 degrees.

The model for star OGLEII CAR-SC2 47145 has been built in similar fashion and is shown in Figure 6. This particular system is not quite an over-contact system, but closer to a simpler contact system. The stars appear to have completely filled their inner Lagrangian surfaces but have not expanded beyond them. Systems of this type can be unstable, as the typical star evolution trend is to expand the gas envelope, eventually pushing these binaries to become over-contact systems. In some cases, it is believed that the stars will oscillate between contact and over-contact state (Bradstreet and Steelman 2004, page 241).

As shown in Figure 6, the differences in eclipse depth need to be accounted for. In particular, the flat part of the minor eclipse indicates that one star is

smaller than the other and that the angle between the line of sight and the axis of rotation is close to 90 degrees. The mass ratio that produced the best fit is 0.147 and the surface temperatures were chosen to be 12600 and 11900 K, to be consistent with the fact that EB types are usually B-A stars. The angle between the line of sight and the axis of rotation of this star giving the best fit was found to be 88.2 degrees. A more realistic model could be constructed if data (B–V color terms for example, or spectral analysis or radial velocities) were available that could allow determination of the true surface temperature. Nevertheless, the model and profile in Figure 6 fit the experimental phase plot accurately. The outline and the three-dimensional drawings also show that the hotter star is the more massive one. The Roche lobes for the components are completely filled.

The EA system (OGLEII CAR-SC3 59302) is modeled assuming stars of similar mass and temperature, with a line of sight very close to 90 degrees. The angle that gave the best fit was found to be 86 degrees. The model's results are shown in Figure 7. EA types are clearly of the detached variety, that is, where the stars are still of spherical shape and located well within the inner Lagrangian surface.

Figure 8 shows the model results for OGLEII CAR-SC2 20986. This particular system is complex, as a component of eccentricity had to be added to the orbit of the system to fit the data. Also required was a hot spot on star 1. The eccentricity can be seen by observing the phase plot, where the secondary eclipse is not occurring at phase = 0.5. The hot spot (a location of higher temperature) was needed to account for the shape of the light curve just before the eclipse. The hot spot is visible on the star's three-dimensional profile.

In an elliptical orbit, the Lagrangian inner and outer surfaces change continuously during the orbital period. In Figure 8 we show the shape of the inner Lagrangian surfaces at three points during the orbit: when the stars are at their closest proximity (top panel in Figure 8), at their farthest separation (bottom panel) and at a mid-point of the orbit.

5. Conclusions

By data mining the OGLE I-band database, 42 previously unknown eclipsing variables have been identified. The periods and epochs of these systems have been obtained from their light curves. Based on the shape of the phase plots, models of the binary system studied were constructed which fit the available data. More reliable models could be constructed if the surface temperatures and the radial velocities of the binary components were available.

6. Acknowledgements

This publication makes use of data products from the Two Micron All Sky Survey, which is a joint project of the University of Massachusetts and the

Infrared Processing and Analysis Center/California Institute of Technology, funded by the National Aeronautics and Space Administration and the National Science Foundation.

This research has made use of the VizieR databases operated at the Centre de Données Astronomiques (Strasbourg) in France and of the AAVSO International Variable Star Index (VSX).

The author wishes to thank Dr. Mark Pitts for a careful reading of the manuscript and Dr. J. Cook for securing the purchase of the software BINARY MAKER 3.

References

Bradstreet, D. H., and Steelman, D. P. 2004, BINARY MAKER 3, Contact Software (http://www.binarymaker.com).

Hümmerich, S. 2012, *BAV Rundbrief*, **61**, 10.

Hümmerich, S., and Bernhard, K. 2012, *Perem. Zvezdy, Prilozh.*, **12**, No. 11, 2012.

Nicholson, M. P. 2009, *Open Eur. J. Var. Stars*, **102**, 1.

Nicholson, M. P. 2010, *Open Eur. J. Var. Stars*, **121**, 1.

Nicholson, M. P. 2012, *Discover Your Own Variable Star (New Challenges for Amateur Astronomers*, Amazon Kindle Book (Amazon Standard Identification Number B0074IHO3W).

Robertson, J. A., and Eggleton, P. P. 1977, *Mon. Not. Roy. Astron. Soc.*, **179**, 359.

Szymański, M. K. 2005, *Acta Astron.*, **55**, 43.

Van Hamme, W. 1993, *Astron. J.*, **106**, 2096.

Vanmunster, T. 2011, PERANSO period analysis software (http://www.peranso.com).

Udalski, A., Kubiak, M., and Szymański, M. 1997, *Acta Astron.*, **47**, 319.

Watson, C. L., Henden, A. A., and Price, A. 2007, *J. Amer. Assoc. Var. Star Obs.*, **35**, 414.

Table 1. Eclipsing variables identified and uploaded to the AAVSO International Variable Star Index (VSX).

Name OGLEII CAR-	R. A. h m s	Dec. ° ′ ″	Type	Period (D)	Magnitude Range
SC1 32377	11 05 29.07	–61 13 07.4	EW	0.273914	16.02–16.32 Ic
SC1 51468	11 05 54.64	–61 43 53.9	EW	0.317607	14.50–14.80 Ic
SC1 221876	11 07 02.64	–61 39 43.4	EW	0.351361	15.68–15.90 Ic
SC2 236	11 07 16.05	–61 51 27.8	EW	0.353095	16.34–16.71 Ic
SC1 127704	11 06 20.29	–61 10 05.3	EW	0.377458	16.12–16.40 Ic
SC2 37289	11 07 04.62	–61 06 12.1	EW	0.380999	14.80–15.11 Ic
SC1 162031	11 06 53.95	–61 23 49.0	EW	0.397176	14.89–15.32 Ic
SC3 160527	11 10 25.46	–60 32 04.9	EW	0.399914	16.27–16.50 Ic
SC1 100564	11 06 22.02	–61 39 41.7	EW	0.400404	15.04–15.63 Ic
SC1 172290	11 06 56.03	–61 08 33.3	EW	0.406376	15.83–16.03 Ic
SC1 136161	11 06 19.35	–60 59 50.1	EW	0.420046	15.23–15.43 Ic
SC1 95816	11 06 03.72	–61 46 18.8	EW	0.474436	16.00–16.18 Ic
SC3 134447	11 10 43.60	–61 08 33.5	EW	0.47943	14.54–14.91 Ic
SC3 93572	11 09 55.78	–61 08 20.1	EW	0.48217	15.93–16.13 Ic
SC2 59902	11 07 40.52	–61 32 10.6	EW	0.501492	16.02–16.31 Ic
SC3 11376	11 09 14.83	–61 08 55.0	EW	0.526783	15.45–15.76 Ic
SC3 78518	11 09 32.56	–60 30 21.0	EW	0.547904	13.82–14.10 Ic
SC1 35115	11 05 09.74	–61 08 10.6	EW	0.55131	15.06–15.34 Ic
SC2 62799	11 07 37.75	–61 27 22.6	EB	0.5581	15.68–15.96 Ic
SC1 167381	11 06 37.89	–61 16 05.3	EA	0.664854	14.82–15.33 Ic
SC2 108934	11 08 03.63	–61 17 57.2	EB	0.69084	16.38–16.72 Ic
SC2 47145	11 07 33.92	–61 49 15.9	EB	0.728762	16.34–16.72 Ic
SC3 155559	11 10 47.35	–60 40 38.5	EA	0.875797	15.98–16.37 Ic
SC2 68344	11 07 37.44	–61 21 09.0	EB	1.089216	15.83–16.15 Ic
SC3 59447	11 09 48.73	–61 00 36.0	EA	1.120861	16.3–16.66 Ic
SC3 31284	11 09 04.86	–60 42 20.3	EW	1.162485	14.30–14.50 Ic
SC3 157847	11 10 41.08	–60 37 12.7	EB	1.17131	13.64–14.16 Ic
SC3 83135	11 10 13.57	–61 20 17.3	EA	1.599808	16.29–16.55 Ic
SC2 140728	11 08 37.64	–61 25 44.9	EA	1.705602	14.76–15.4 Ic
SC1 116082	11 06 10.60	–61 24 16.6	EA	1.759605	16.28–16.87 Ic
SC2 20986	11 07 13.93	–61 28 40.5	EA	1.845923	16.33–16.76 Ic
SC1 165151	11 06 43.35	–61 19 58.8	EA	2.384416	16.4–16.9 Ic
SC1 35063	11 05 12.13	–61 07 41.2	EA	2.496182	14.1–14.39 Ic
SC3 93533	11 10 09.60	–61 08 32.3	EA	2.570906	13.2–13.49 Ic
SC3 155588	11 10 37.55	–60 39 24.8	EB	2.763448	15.33–15.56 Ic
SC3 51061	11 09 36.68	–61 11 15.7	EA	2.961514	13.98–14.42 Ic
SC2 158406	11 08 43.38	–61 03 49.6	EA	2.962926	16.22–16.68 Ic
SC3 59302	11 09 39.03	–60 59 18.9	EA	3.022445	14.89–15.31 Ic

Table continued on next page

Table 1. Eclipsing variables identified and uploaded to the AAVSO International Variable Star Index (VSX), cont.

Name *OGLEII CAR-*	*R. A.* *h m s*	*Dec.* *° ′ ″*	*Type*	*Period (D)*	*Magnitude Range*
SC1 151908	11 06 44.52	–61 33 52.9	EA	3.774267	15.57–16.2 Ic
SC3 112892	11 10 05.90	–60 44 01.1	EA	7.014168	16.45–16.79 Ic
SC3 93614	11 10 13.60	–61 06 19.1	EA	7.402731	15.98–16.35 Ic
SC1 51557	11 05 46.20	–61 45 55.7	EA	8.193323	16.43–16.94 Ic

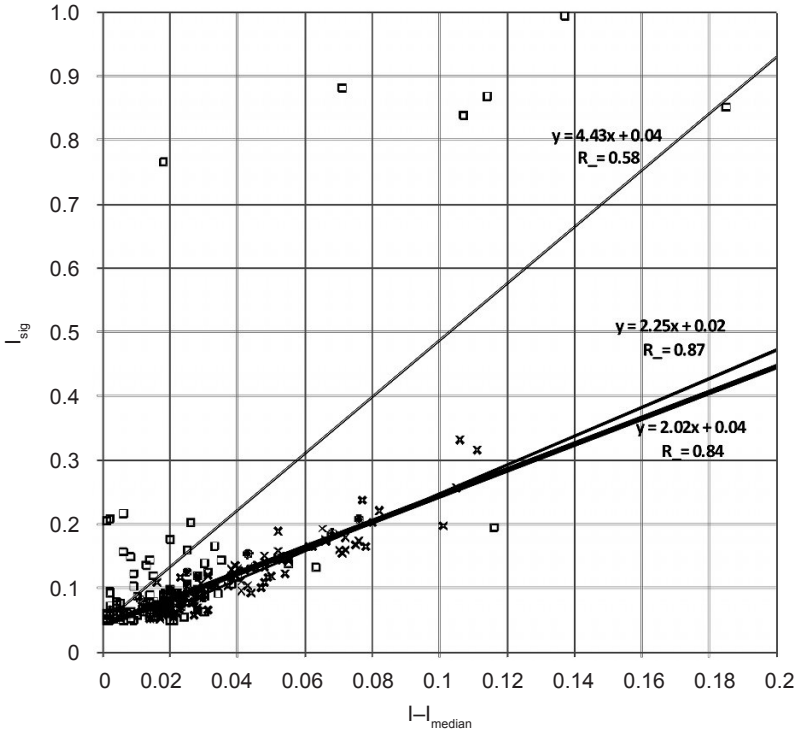

Figure 1. Plot of I_{sig} as a function of ($I–I_{med}$) for stars already identified in the literature as eclipsing variable (medium thickness line), stars identified in this work (thick line), and candidates found with our search parameters and deemed not good candidates for eclipsing variability (thin line). "×" denotes published variables; dots denote this work; open squares denote non-eclipsing.

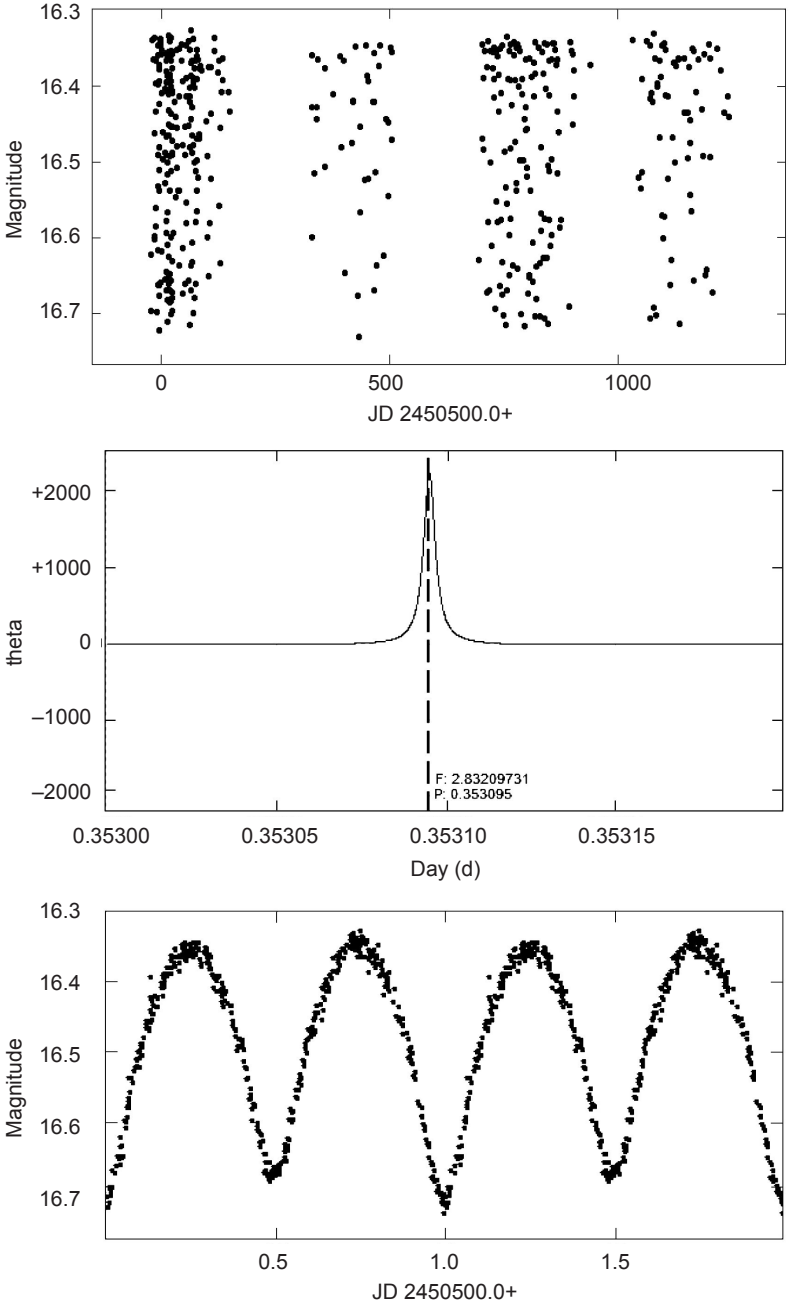

Figure 2. OGLEII CAR-SC2 236. Light curve (top), period (middle), and phase plot (bottom). Type is EW.

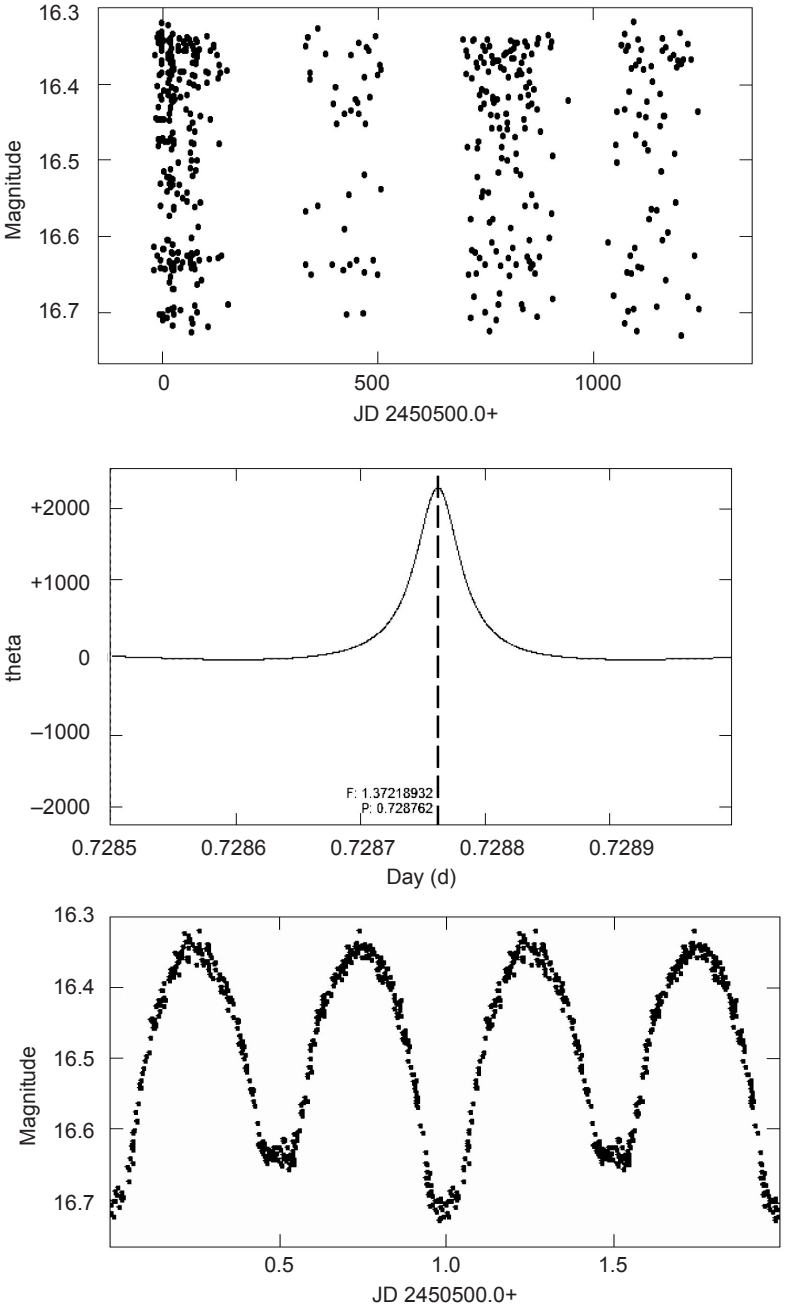

Figure 3. OGLEII CAR-SC2 47145. Light curve (top), period (middle), and phase plot (bottom). Type is EB.

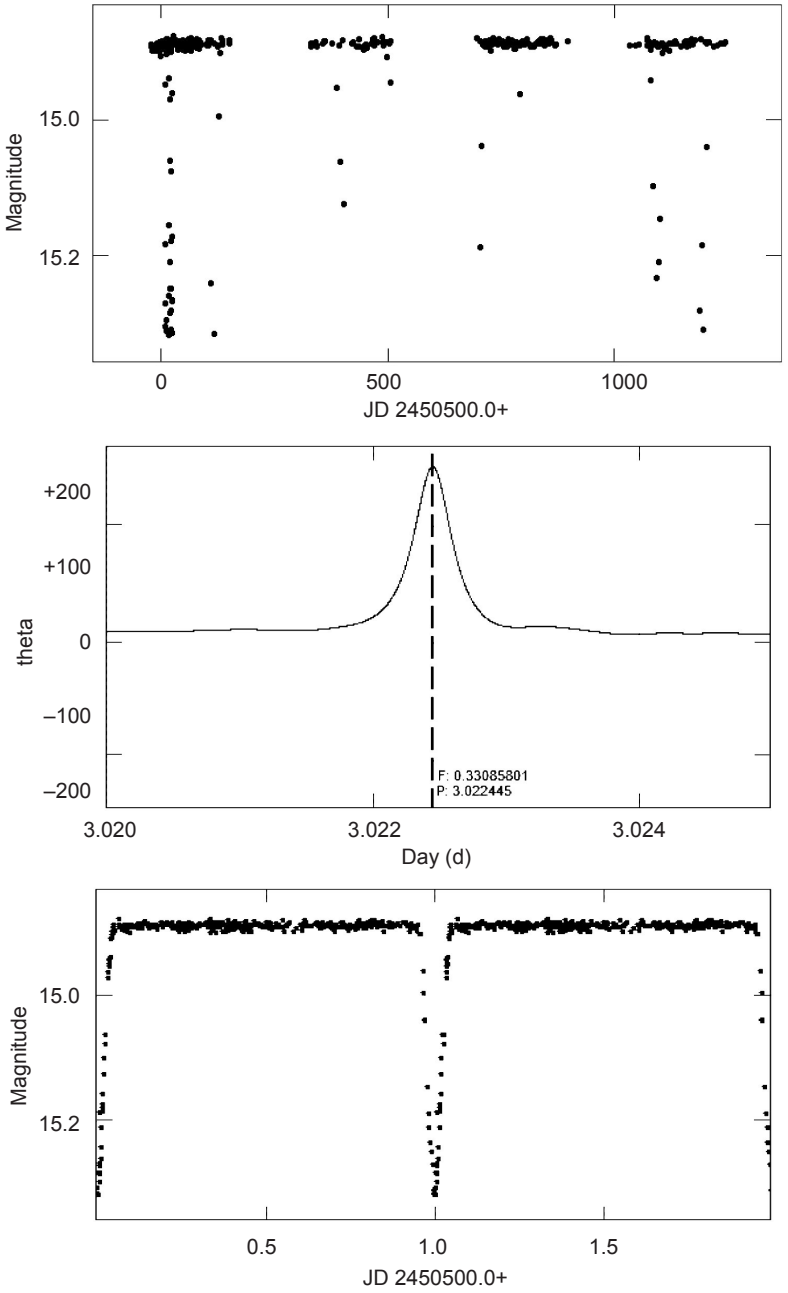

Figure 4. OGLEII CAR-SC3 59302. Light curve (top), period (middle), and phase plot (bottom). Type is EA.

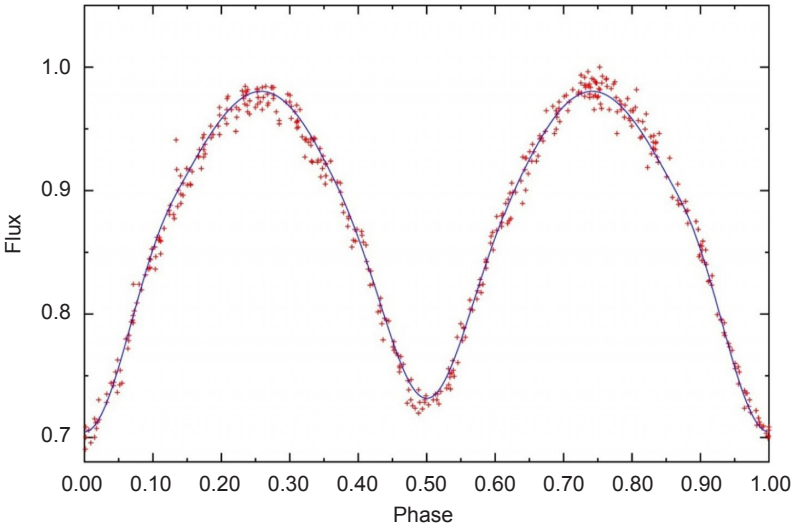

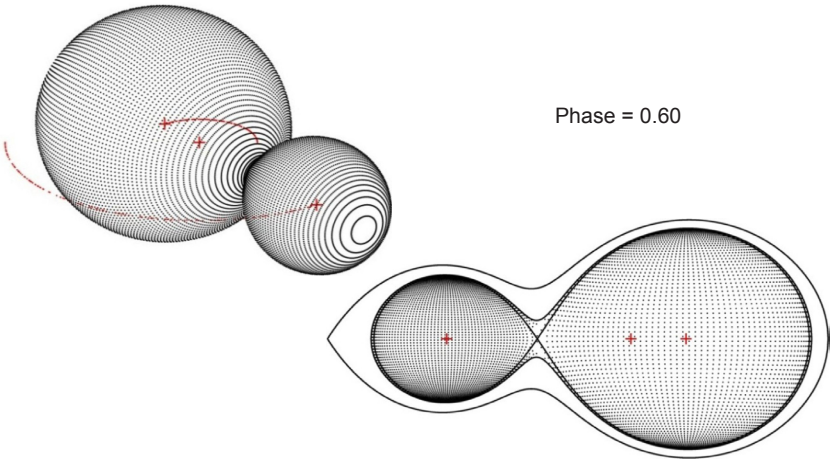

Figure 5. The over-contact binary OGLEII CAR-SC2 236. Phase plot, fit (top), three-dimensional model and equipotential profile (bottom).

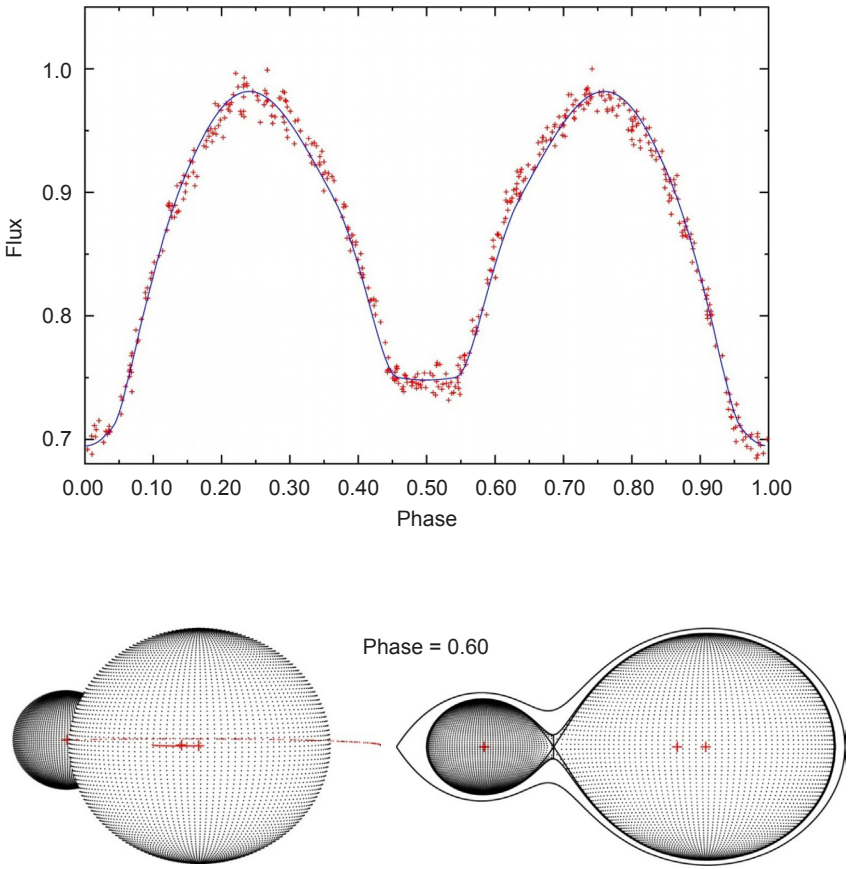

Figure 6. The contact binary OGLEII CAR-SC2 47145. Phase plot, fit (top), three-dimensional model and equipotential profile (bottom).

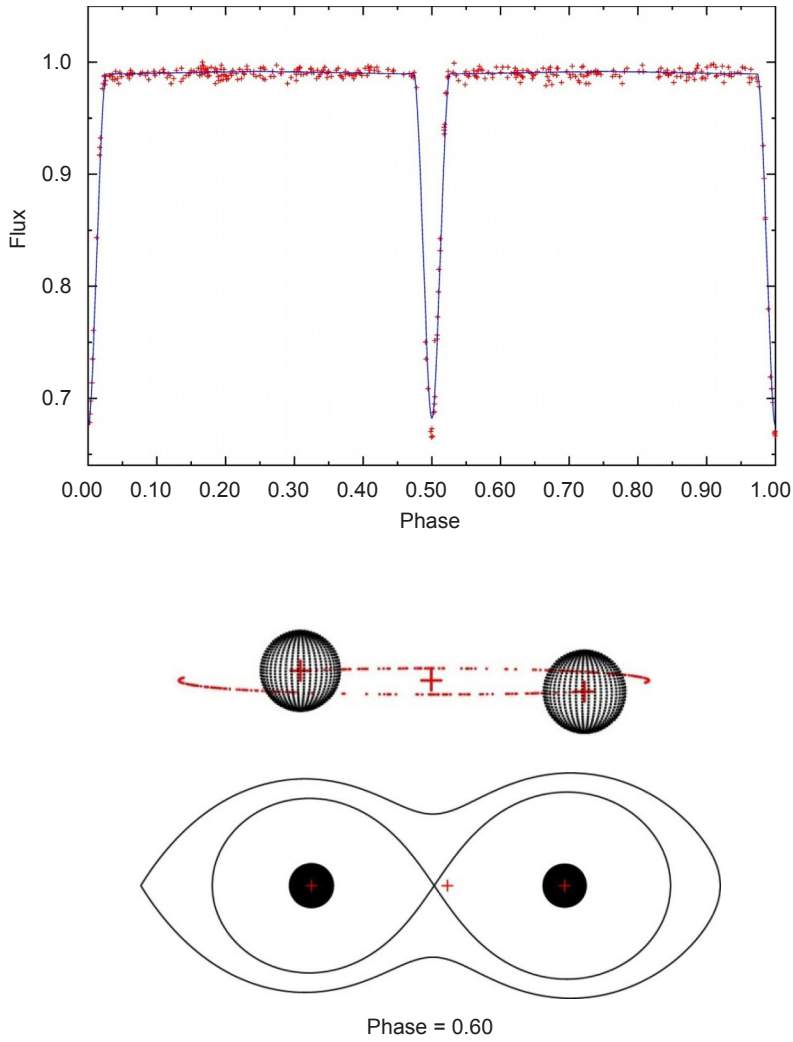

Figure 7. The detached binary OGLEII CAR-SC3 59302. Phase plot, fit (top), and profile (bottom).

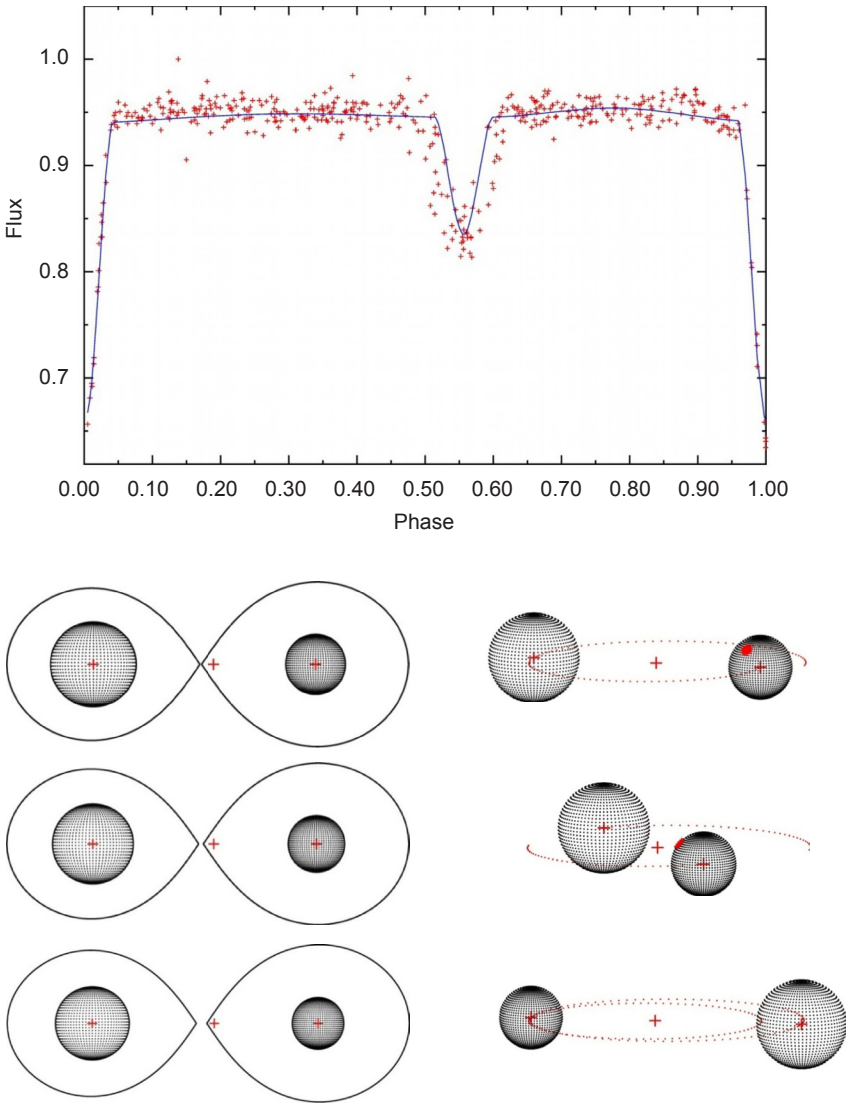

Figure 8. OGLEII CAR-SC2 20986. Phase plot (upper), three-dimensional binary model with corresponding outline (lower). Changing shape of the inner Lagrangian surfaces: at closest proximity (top), at orbital mid-point (middle), and at farthest separation (bottom).

Eighteen New Variable Stars in Cassiopeia and Variability Checking for NSV 364

Riccardo Furgoni
Keyhole Observatory MPC K48, Via Fossamana 86, S. Giorgio di Mantova (MN), Italy; riccardo.furgoni@alice.it

and

AAMN Gorgo Astronomical Observatory MPC 434, S. Benedetto Po (MN), Italy

Received June 17, 2013; revised July 19, 2013; accepted August 21, 2013

Abstract I report the discovery of eighteen new variable stars in Cassiopeia: eight pulsating (2MASS J00584964+5909260; GSC 03680-00667; GSC 03680-01320; GSC 03680-01488; 2MASS J02472793+6149024; GSC 04047-01118; GSC 04047-01418; GSC 04051-01789), six eclipsing (GSC 03680-00423; 2MASS J02443720+6143091; GSC 04047-00381; GSC 04047-00558; GSC 04051-02027; GSC 04051-02533), three rotating (ALS 6430; 2MASS J01020513+5912394; GSC 04051-01669), and one eruptive (GSC 04051-02483). The suspected variable star NSV 364 was checked for variability in six nights of observations and in the complete SuperWasp survey dataset; no variability was detected.

1. Introduction

A photometric campaign aimed at the discovery of new variable stars was carried out from the Keyhole Observatory in S. Giorgio di Mantova, Italy. Were observed two separate fields located in the constellation of Cassiopeia for a total of 21 nights, obtaining 2,329 images in the V passband with an exposure time of 2 minutes. Subsequently the light curves of all stars in the fields have been simply visually inspected in order to determine the candidate variables.

When possible the observations were combined with the SuperWASP and NSVS datasets in order to improve the precision in the determination of the period and the type of variability.

The large surface area of the sensor Kodak KAF8300 equipping the SBIG CCD ST8300m allowed us to observe a large portion of sky to a focal length suitable for areas crowded with stars.

This research shows how much work has to be done in the search for variable stars in crowded fields, especially in the area close to the Milky Way. An interesting concentration of variables was found not far from the star SAO 12415: in a radius of only 3.25' three new variables were discovered.

2. Instrumentation used

The data were obtained with a Celestron C8 Starbright, a Schmidt-Cassegrain optical configuration with aperture of 203 mm and central obstruction of 34%. The telescope was positioned at coordinates 45° 12' 33" N 10° 50' 20" E (WGS84) at the Keyhole Observatory, a roll-off roof structure managed by the author. The telescope was equipped with a focal reducer Baader Planetarium Alan Gee II able to bring the focal length from 2030 mm to 1413 mm in the optical train used. The focal ratio is also down to *f*6.96 from the original *f*10.

The pointing was maintained with a Syntha NEQ6 mount with software SYNSCAN 3.27, guided using a Baader Vario Finder telescope equipped with a Barlow lens capable of bringing the focal length of the system to 636 mm and focal ratio of *f*10.5.

The guide camera was a Magzero MZ-5 with Micron MT9M001 monochrome sensor equipped with an array of 1280 × 1024 pixels. The size of the pixels is 5.2μm × 5.2μm, for a resulting sampling of 1.68 arcsec/pixel.

The CCD camera was a SBIG ST8300m with monochrome sensor Kodak KAF8300 equipped with an array of 3352 × 2532 pixels. The pixels are provided with microlenses for improving the quantum efficiency, and the size of the pixels is 5.4μm × 5.4μm, for a resulting sampling of 0.80 arcsec/pixel.

The photometry in the Johnson V passband was performed with an Astrodon Photometrics Johnson V 50 mm round unmounted filter on a Starlight Xpress USB filterwheel.

The camera is equipped with a 1000 × antiblooming: after exhaustive testing it has been verified that the zone of linear response is between 1,000 and 20,000 ADU, although up to 60,000 ADU the loss of linearity is less than 5%. The CCD is equipped with a single-stage Peltier cell Δ-T = 35 ± 0.1° C which allows cooling at a stationary temperature.

3. Data collection

The observed fields are centered, respectively, at coordinates (J2000) R.A. $01^h01^m12^s$, Dec. +59° 05' 11" and R.A. $02^h46^m09^s$, Dec. +61° 53' 12". For both the dimensions are 44' × 33' with a position angle of 360°.

The observations were performed with the CCD at a temperature of –10° C in binning 1 × 1. The exposure time was 120 seconds with a delay of 1 second between the images and an average download time of 11 seconds per frame. The observations were conducted over twenty-one nights as presented in Table 1.

The CCD control program was CCDSOFT V5 (Software Bisque 2012). Once the images were obtained, calibration frames were taken for a total of 100 dark of 120 seconds at –10° C, 200 darkflat of 2 seconds at –10° C, and 50 flat of 2 seconds at –10° C. The darkflats and darks were taken only during the first observing session and used for all other sessions. The flat were taken for each session

as the position of the CCD camera could be varied slightly, as well as the focus point.

The calibration frames were combined with the method of the median and masterframes obtained were then used for the correction of the images taken. All images were then aligned and an astrometric reduction made to implement the astrometrical coordinate system WCS in the FITS header. These operations were conducted entirely through the use of software MAXIMDL v5.23 (Diffraction Limited 2012).

4. Finding comparison stars in the observed fields: the usefulness of the APASS data

Although the presence of an AAVSO comparison star sequence is a source of security in differential photometry, is not always possibile to have one for every observed field. In addition, since the APASS data were published (Henden *et al.* 2013) and are now available in Data Release 7, one can find a very accurate photometric reference for almost 97 percent of the sky.

I noticed that the APASS magnitudes are highly accurate and very reliable: in the various fields observed with the Johnson V filter if a single star with good SNR is taken as a reference and then the others are measured, the overall coincidence with APASS V passband was always within three hundredths of a magnitude regardless of the color index. This is definitely the result of higher quality that I have had so far in determining a star magnitude on-the-fly: the immediate reproducibility of the measurements is very high. In other words, this means that the overall instrumental response of my setup is very similar to that used in the APASS survey.

When you decide to use a star as a reference you must be certain that not only its magnitude has been measured accurately, but also that its brightness is constant over time. The APASS data are not of great help in this case: each star was observed for a few times and any changes are not easily detectable. The good news is that in this case the key factor is not accuracy but precision. You can then use the data from other surveys as NSVS (Wozniak *et al.* 2004), ASAS (Pojmański 2002), and SuperWASP (Butters *et al.* 2010) to assess whether the star has long-term variations. In this work, the comparison stars were chosen in relation to the presence of a good SNR, proximity to the variable star measured, photometric stability in the survey mentioned above, and measurement in the APASS V passband with small uncertainty. As a result all the check stars used in this work showed a photometric stability within two hundredths of a magnitude over the period considered and very good agreement with the APASS measurements.

5. Magnitude determination and period calculation

The star's brightness was measured with MAXIMDL v5.23 software (Diffraction

Limited 2012), using the aperture ring method. Since a FWHM of the observing sessions at times arrived at values of 5" it was decided to choose values providing an adequate signal-to-noise ratio and the certainty of being able to properly contain the whole flux from the star. Usually I used the following apertures: Aperture radius, 11 to 14 pixels; Gap width, 2 to 28 pixels; Annulus thickness, 8 pixels.

Before proceeding further in the analysis, the time of the light curves obtained was heliocentrically corrected (HJD) in order to ensure a perfect compatibility of the data with observations carried out even at a considerable distance in time. The determination of the period was calculated using the software PERIOD04 (Lenz and Breger 2005), using a Discrete Fourier Transform (DFT). The average zero-point (average magnitude of the object) was subtracted from the dataset to prevent the appearance of artifacts centered at a frequency 0.0 of the periodogram. The calculation of the uncertainties was carried out with PERIOD04 using the method described in Breger *et al.* (1999) .

To improve the period determination, NSVS and SWASP photometric data were used when available. However, due to the high scattering which in some cases affects them, the data with high uncertainties were eliminated. NSVS and SWASP data were also corrected in their zero-point to make them compatible with my V-band standardized data. Having the same zero-point is indeed crucial for correct calculation of the Discrete Fourier Transform operated by PERIOD04.

6. Visual inspection of the light curves: finding candidate variable stars

The search for new variable stars in the examined fields followed an approach designed to maximize the probability of success by avoiding long photometric sessions in areas without detectable variable stars. This approach distinguishes between two different ways of working: the discovery-night and the follow-up-night. In the discovery-night the chosen field is observed for the first time as long as possible, taking care to choose a night with the best photometric conditions. At the end of the session the collected data are analyzed with a classic Magnitude-RMS diagram for the presence of variables with noticeable changes. Then each light curve of the stars present in the field up to magnitude 16 V is evaluated visually for other possible variable candidates that are not immediately detectable by the Magnitude-RMS diagram. The usefulness of the proposed method will be explained below in this section.

If the field is interesting a series of follow-up night exposures is planned for the study of candidate variables, otherwise a new field is chosen. It is important to remember that in any case every follow-up-night exposure is checked again with the Magnitude-RMS diagram looking for possible new large variations not detected in the discovery night frames (such as an eclipsing variable that was not varying in the discovery-night), while the visual analysis of the light curves is performed only on the candidate variables detected in the discovery-

night, and not for all other stars because of the very long time that this analysis entails.

It is now necessary to clarify what is meant by visual analysis of the light curves, explaining the usefulness of this approach in the discovery of new variables: in Figures 1 and 2 are shown the Magnitude-RMS diagrams of the two considered fields relative to the discovery-night and the position of the variables detected in this survey. By analyzing the graphs, after having obtained all the data presented in this survey, it can be seen at once that all the discovered variables had RMS above average in the discovery-night; the suspected variable NSV 364 (point 8 in Figure 1) that was found to be constant is positioned differently from the others in Figure 1.

It is right to point out that this evidence is very different at the beginning of this survey: the graphs show indeed many other points with high RMS and many of the discovered variables are above average RMS but not so much as to be immediately identifiable. In other words, the graph is more useful to say that the variables are genuine at the end of the survey rather than to discover variables to the limit of the instrument capabilities in a photometric session.

In effect, the construction of a Magnitude-RMS diagram normally occurs with the use of automatic aperture photometry for all the stars in the field: in a field also only moderately crowded, aperture rings that are good for a star are not good for another star due to contamination phenomena.

For example, a star could present within its ring aperture only a portion of a nearby star as well for the ring relative to the sky-background. This is a great source of 5–6% flux scatter. The result is that in practice many non-variable stars have a scatter higher than other real variable stars of the same magnitude. At the end, they become indistinguishable in the diagram considered.

Visual analysis of the light curve allows instead to evaluate not only a significant change in the typical scatter but also the presence of shapes and meaningful patterns in the light curve. For every star the best aperture ring, gap ring, and sky-background ring are determined, even for the comparison stars. This type of evaluation is impossible with a diagram Magnitude-RMS: there are too many things to consider in order to be included in an automatic algorithm.

Figure 3 shows a graph that allows to understand the value of a visual assessment of one-night light curve of the variable star 2MASS J00584964 +5909260, probably the star with the most critical amplitude variation-SNR of this survey. Note that in the latter part of the night faint clouds appeared at high altitude. In Figure 3 the minimal variation coupled with a pulsation-shape of the light curve is enough to consider the star as a potential variable candidate. Of course it would also be folly to think that this is enough to consider the star as a real variable: in these cases the path of analysis must be very thorough, since the variation could also be only noise.

In order to distinguish among variables, suspected variables, and non-variables we proceeded as follows. To be considered as a variable the star

must have shown similar variations in every night and these variations must be consistent in the final phase diagram. Most importantly the variability must be confirmed in another dataset. In fact, all the stars discovered in this survey (except GSC 04051-02483, 2MASS J02472793 +6149024, GSC 04047-00381, 2MASS J02443720+6143091, and GSC 04047-01418 due to the lack of available data) were cross-checked against the SWASP and NSVS datasets in order to confirm the variability and improve the determination of the period by combining the available data with the data obtained in this survey. The phase diagrams presented at the end of this work show the superposition of the various datasets and their coincidence.

If a phase diagram highlights a variation comparable to the uncertainty and there are no other datasets available to perform a cross-check, the high cadence and the large number of measurements made in this survey allow you to make a binning to improve the SNR. If also in this case the variation is uncertain the star is only considered a potential variable. No star presented in this work is still in this condition.

7. New variable stars and variability checking of NSV 364

In this survey we discovered eighteen new variable stars and checked the suspected variable NSV 364 for variability. The population of the new variables is as follows:

- 8 pulsating (7 δ Sct and 1γ Dor)
- 6 eclipsing (1 β Lyr, 2 W UMa, and 3 β Per)
- 3 rotating (3 rotating ellipsoidal)
- 1 eruptive (1 Be with LERI variations).

The coordinates of all new variable stars discovered in this survey are reported as they appear in the UCAC4 catalogue (Zacharias *et al.* 2012) and differ from the detected positions for a value never greater than 0.5".

7.1. GSC 03680-00423

Position (UCAC4): R.A. (J2000) = $01^h03^m51.302^s$, Dec. (J2000) = +59° 18' 57.83"

Cross Identification: 1SWASP J010351.26+591858.5; 2MASS J01035130+5918577; UCAC3 299-021274; UCAC4 747-009468; USNO-B1.0 1493-0034696

Variability Type: β Lyr

Magnitude: Max. 13.10 V; Min. 13.37 V (Secondary max. 13.13 V; Secondary min. 13.28 V)

Period: 0.509944(1) d

Epoch: 2456223.2844(22) HJD

Comparison Star: UCAC4 747-009434 (APASS 12.775 V)

Check Star: UCAC4 747-009352

Finding chart, phase plot, and Fourier spectrum are shown in Figures 4, 5, and 6.

7.2. GSC 03680-00667

Position (UCAC4): R.A. (J2000) = $01^h03^m20.400^s$, Dec. (J2000) = +59° 13'45.46"

Cross Identification: 1SWASP J010320.40+591345.6;
2MASS J01032039+5913453; UCAC4 747-009355;
USNO-B1.0 1492-0033355

Variability Type: δ Sct

Magnitude: Max. 13.47 V; Min. 13.52 V

Period: 0.1584384(6) d

Epoch: 2456230.399(2) HJD

Comparison Star: UCAC4 747-009434 (APASS 12.775 V)

Check Star: UCAC4 747-009352

Notes: Despite the wide time span of the data used for the period determination (SWASP + Furgoni) the Fourier spectrum shows two significant peaks at a frequency of 6.31160976 c/d and 7.31438512 c/d that differ only by a width of 0.0007 mag. One of the two peaks is probably the alias of the other but the two very similar amplitudes do not allow determination with absolute certainty of the correct one. For this reason the period may also be P=0.1367168(4).

Finding chart, phase plot, and Fourier spectrum are shown in Figures 7, 8, and 9.

7.3. 2MASS J01020513+5912394

Position (UCAC4): R.A. (J2000) = $01^h02^m05.134^s$, Dec. (J2000) = +59° 12'39.36"

Cross Identification: 1SWASP J010205.11+591239.5;
UCAC4 747-009100; USNO-B1.0 1492-0032522

Variability Type: Rotating ellipsoidal

Magnitude: Max. 13.91 V; Min. 14.04 V

Period: 0.873754(2) d

Epoch: 2456223.4065(21) HJD

Comparison Star: UCAC4 746-009480 (APASS 11.045 V)

Check Star: UCAC4 746-009545

Finding chart, phase plot, and Fourier spectrum are shown in Figures 10, 11, and 12.

7.4. GSC 03680-01488

Position (UCAC4): R.A. (J2000) = $00^h 58^m 33.793^s$, Dec. (J2000) = +58° 57' 17.87"

Cross Identification: 1SWASP J005833.79+585717.8;
2MASS J00583378+5857178; USNO-B1.0 1489-0030192

Variability Type: δ Sct

Magnitude: Max. 11.155 V; Min. 11.180 V

Main Period: 0.046419(1) d

Secondary Period: 0.0938359(2) d

Epoch Main Period: 2456223.3449(5) HJD

Epoch Secondary Period: 2456223.3454(12) HJD

Ensemble Comparison Stars: UCAC4 745-008614 (APASS 11.006 V);
UCAC4 745-008750 (APASS 11.569 V); UCAC4 745-008771
(APASS 11.663 V)

Check Star: UCAC4 745-008825

Notes: The light curve shows an evident modulation in the different nights of observation. The Fourier spectrum shows the existence of a possible other active frequency that is very close to half the main frequency (p = 0.0938359 d).

Finding chart, phase plots, and Fourier spectrum are shown in Figures 13, 14, 15, and 16.

7.5. GSC 03680-01320

Position (UCAC4): R.A. (J2000) = $01^h 01^m 39.227^s$, Dec. (J2000) = +58° 55' 44.66"

Cross Identification: 1SWASP J010139.22+585544.8;
2MASS J01013922+5855447; UCAC4 745-008924;
USNO-B1.0 1489-0031868

Variability Type: δ Sct

Magnitude: Max. 13.035 V; Min. 13.060 V

Main Period: 0.0631941(1) d

Secondary Period: 0.0454240(1) d

Epoch Main Period: 2456223.2334(11) HJD

Epoch Secondary Period: 2456223.2798(9) HJD

Ensemble Comparison Stars: UCAC4 745-009004 (APASS 11.006 V);
UCAC4 745-009144 (APASS 11.722 V)

Check Star: UCAC4 745-008982

Notes: The continuous modulation of the light curve suggests the existence of different active frequencies. The secondary frequency corresponds to a P =

0.0454240(1) with HJD_{max} = 2456223.2798(9) and an amplitude slightly lower than that of the main period. The analysis of the Fourier spectrum shows in any case that additional frequencies are probably active.

Finding chart, phase plots and Fourier spectrum are shown in Figures 17, 18, 19, and 20.

7.6. 2MASS J00584964+5909260

Position (UCAC4): R.A. (J2000) = $00^h58^m49.657^s$, Dec. (J2000) = +59° 09' 26.09"

Cross Identification: 1SWASP J005849.66+590926.4; UCAC4 746-008985; USNO-B1.0 1491-0031750

Variability Type: δ Sct

Magnitude: Max. 14.11; Min. 14.13 V

Period: 0.193186(2) d

Epoch: 2456223.2446(38) HJD

Ensemble Comparison Stars: UCAC4 747-008816 (APASS 11.599 V); UCAC4 746-009298 (APASS 11.646 V)

Check Star: UCAC4 746-009381

Finding chart, phase plot, and Fourier spectrum are shown in Figures 21, 22, and 23.

7.7. ALS 6430

Position (UCAC4): R.A. (J2000) = $01^h00^m17.527^s$, Dec. (J2000) = +59° 08' 13.34"

Cross Identification: 1SWASP J010017.52+590813.2; 2MASS J01001753+5908133; GSC 03680-01411; LS I +58 20

Variability Type: Rotating ellipsoidal

Magnitude: Max. 11.38 V; Min. 11.41 V

Period: 1.6814956(88) d

Epoch: 2456223.4758(58) HJD

Ensemble Comparison Stars: UCAC4 747-008816 (APASS 11.599 V); UCAC4 746-009298 (APASS 11.646 V)

Check Star: UCAC4 746-009381

Notes: The APASS B-V for this star is 0.308, 2MASS J-K 0.163, redder than expected for the spectral type OB taken from the LS catalog. SPB or ACV type are possible with half the period.

Finding chart, phase plot, and Fourier spectrum are shown in Figures 24, 25, and 26.

7.8. NSV 364

Position (UCAC4): R.A. (J2000) = $01^h01^m23.856^s$, Dec. (J2000) = +59° 04' 32.88"

Cross Identification: 1SWASP J010123.84+590433.1;
2MASS J01012386+5904327; SON 10457; UCAC4 746-009503;
USNO-B1.0 1490-0032435

Variability Type: Constant; Non-Variable

Magnitude: 14.49 V

Comparison Star: UCAC4 746-009480 (APASS 11.045 V)

Check Star: UCAC4 746-009545

Notes: The star is constant both in the Furgoni dataset and the SWASP dataset. The Fourier Power Spectrum of SWASP dataset shows an equal distribution of peaks spaced by 0.5 c/d. No relevant frequencies present. The suspected variability was described in Richter (1969).

Finding chart, light curve, and Fourier spectrum are shown in Figures 27, 28, and 29.

7.9. GSC 04051-02533

Position (UCAC4): R.A. (J2000) = $02^h47^m42.288^s$, Dec. (J2000) = +61° 58' 29.35"

Cross Identification: 1SWASP J024742.26+615829.2;
2MASS J02474229+6158293; UCAC4 760-022284

Variability Type: β Per

Magnitude: Max. 12.37 V; Min. 12.72 V

Period: 1.57709(1) d

Epoch: 2456265.458(2) HJD

Comparison Star: UCAC4 760-022374 (APASS 12.081 V)

Check Star: UCAC4 761-021189

Notes: The binary system is probably included in the very small DSH J0247.7+6158=Teutsch 162 cluster of stars, involved in the HII-region Sh 2-193. The secondary minimum is probably as deep as the primary one.

Finding chart and phase plot are shown in Figures 30 and 31.

7.10. GSC 04051-02027

Position (UCAC4): R.A. (J2000) = $02^h46^m10.965^s$, Dec. (J2000) = +61° 57' 55.69"

Cross Identification: 1SWASP J024611.00+615755.8;
2MASS J02461097+6157557; UCAC4 760-022038

Variability Type: β Per

Magnitude: Max. 12.67 V; Min. 12.85 V (Secondary min. 12.83 V)

Period: 1.568639(2) d

Epoch: 2456329.1377(36) HJD

Ensemble Comparison Stars: UCAC4 760-022374 (APASS 12.081 V); UCAC4 761-021049 (APASS 12.033 V).

Check Star: UCAC4 761-021189

Finding chart, phase plot, and Fourier spectrum are shown in Figures 32, 33, and 34.

7.11. GSC 04051-01669

Position (UCAC4): R.A. (J2000) = $02^h48^m19.071^s$, Dec. (J2000) = +61° 57' 03.19"

Cross Identification: 1SWASP J024819.07+615703.2; 2MASS J02481907+6157031; UCAC4 760-022382

Variability Type: Rotating ellipsoidal

Magnitude: Max. 13.66 V; Min. 13.82 V

Period: 1.695249(6) d

Epoch: 2456266.2219(68) HJD

Ensemble Comparison Stars: UCAC4 760-022374 (APASS 12.081 V); UCAC4 761-021049 (APASS 12.033 V).

Check Star: UCAC4 761-021189

Finding chart, phase plot, and Fourier spectrum are shown in Figures 35, 36, and 37.

7.12. GSC 04051-01789

Position (UCAC4): R.A. (J2000) = $02^h47^m55.761^s$, Dec. (J2000) = +62° 09' 06.86"

Cross Identification: 1SWASP J024755.74+620906.9; 2MASS J02475576+6209069; UCAC4 761-021226

Variability Type: δ Sct

Magnitude: Max. 12.25 V; Min. 12.29 V

Period: 0.13367394(11) d

Epoch: 2456268.37961(78) HJD

Ensemble Comparison Stars: UCAC4 760-022374 (APASS 12.081 V); UCAC4 761-021049 (APASS 12.033 V).

Check Star: UCAC4 761-021189

Finding chart, phase plot, and Fourier spectrum are shown in Figures 38, 39, and 40.

7.13. GSC 04051-02483

Position (UCAC4): R.A. (J2000) = $02^h46^m06.407^s$, Dec. (J2000) = +61° 54' 23.93"

Cross Identification: 2MASS J02460641+6154239; EM* CDS 304; LS I +61 312; NSVS 1883898; UCAC4 760-022024

Variability Type: Be + LERI

Magnitude: Max. 11.52 V; Min. 11.63 V

Period: 0.25573(3) d

Epoch: 2456267.147(3) HJD

Ensemble Comparison Stars: UCAC4 760-022374 (APASS 12.081 V); UCAC4 761-021049 (APASS 12.033 V).

Check Star: UCAC4 761-021189

Notes: H-α emission-line star (the spectral type is B5IIIe (Skiff 2009–2013)). Fading event detected on 6 December 2013. The small amplitude irregular variability (Be) is coupled with quasi-periodic variations of the LERI-type. The period could be 0.51146 d with a double-waved light curve. Epoch of maximum given.

Finding chart, light curves, phase plot, and Fourier spectrum are shown in Figures 41, 42, 43, 44, and 45.

7.14. 2MASS J02472793+6149024

Position (UCAC4): R.A. (J2000) = $02^h47^m27.936^s$, Dec. (J2000) = +61° 49' 02.46"

Cross Identification: UCAC4 760-022245; USNO-B1.0 1518-0082596

Variability Type: δ Sct

Magnitude: Max. 14.85 V; Min. 14.94 V

Main Period: 0.132260(8) d

Secondary Period: 0.092002(4)

Epoch Main Period: 2456268.3360(15) HJD

Epoch Secondary Period: 2456268.3237(10) HJD

Ensemble Comparison Stars: UCAC4 760-022283 (APASS 14.465 V); UCAC4 760-022267 (APASS 14.691 V).

Check Star: UCAC4 759-022016

Notes: B–V = 0.95 (APASS) probably reddened. 2MASS J02472833+6149073 (V = 17.4) lies 5.6" away and has not been included in the photometry.

Finding chart, phase plots, and Fourier spectrum are shown in Figures 46, 47, 48, and 49.

7.15. GSC 04047-01118

Position (UCAC4): R.A. (J2000) = $02^h48^m31.004^s$, Dec. (J2000) = +61° 40' 25.48"

Cross Identification: 2MASS J02483099+6140255; IC 1848 +61 41; NSVS 1885359; TYC 4047-1118-1; UCAC4 759-022220

Variability Type: γ Dor

Magnitude: Max. 11.84 V; Min. 11.88 V

Period: 0.4065110(8) d

Epoch: 2456265.4098(29) HJD

Ensemble Comparison Stars: UCAC4 759-021947 (APASS 12.233 V); UCAC4 759-022035 (APASS 12.530 V).

Check Star: UCAC4 759-021930

Notes: B–V 0.564 (APASS). The star is in the open cluster and nebula IC 1848.

Finding chart, phase plot, and Fourier spectrum are shown in Figures 50, 51, and 52.

7.16. GSC 04047-00558

Position (UCAC4): R.A. (J2000) = $02^h46^m26.433^s$, Dec. (J2000) = +61° 36' 54.44"

Cross Identification: 2MASS J02462643+6136545; UCAC4 759-021892

Variability Type: β Per

Magnitude: Max. 14.25 V; Min. 14.62 V (Secondary min. 14.52 V)

Period: 1.96466(3) d

Epoch: Ensemble Comparison Stars: UCAC4 759-021947 (APASS 12.233 V); UCAC4 759-022035 (APASS 12.530 V).

Check Star: UCAC4 759-021930

Finding chart and phase plot are shown in Figures 53 and 54.

7.17. GSC 04047-00381

Position (UCAC4): R.A. (J2000) = $02^h44^m18.468^s$, Dec. (J2000) = +61° 45' 04.53"

Cross Identification: 2MASS J02441846+6145045; UCAC4 759-021534

Variability Type: W UMa

Magnitude: Max. 14.76 V; Min. 15.10 V

Period: 0.348687(3) d

Epoch: 2456267.3401(5) HJD

Ensemble Comparison Stars: UCAC4 760-021845 (APASS 12.487 V); UCAC4 760-021940 (APASS 12.025 V).

Check Star: UCAC4 759-021771

Finding chart, phase plot, and Fourier spectrum are shown in Figures 55, 56, and 57.

7.18. 2MASS J02443720+6143091

Position (UCAC4): R.A. (J2000) = $02^h44^m37.209s$, Dec. (J2000) = +61° 43' 09.07"

Cross Identification: UCAC4 759-021583

Variability Type: W UMa

Magnitude: Max. 15.12 V; Min. 15.49 V

Period: 0.353443(5) d

Epoch: 2456268.3037(7) HJD

Ensemble Comparison Stars: UCAC4 760-021845 (APASS 12.487 V); UCAC4 760-021940 (APASS 12.025 V).

Check Star: UCAC4 759-021771

Finding chart, phase plot, and Fourier spectrum are shown in Figures 58, 59, and 60.

7.19. GSC 04047-01418

Position (UCAC4): R.A. (J2000) = $02^h45^m11.691s$, Dec. (J2000) = +61° 43' 53.78"

Cross Identification: 2MASS J02451169+6143538; UCAC4 759-021671

Variability Type: δ Sct

Magnitude: Max. 14.13 V; Min. 14.16 V

Period: 0.17623(2) d

Epoch: 2456265.316(3) HJD

Ensemble Comparison Stars: UCAC4 760-021845 (APASS 12.487 V); UCAC4 760-021940 (APASS 12.025 V).

Check Star: UCAC4 759-021771

Finding chart, phase plot, and Fourier spectrum are shown in Figures 61, 62, and 63.

8. Acknowledgements

I wish to thank Sebastian Otero, member of the VSX team and AAVSO external consultant, for his helpful comments on the new variable stars discovered. This work has made use of the VizieR catalogue access tool, CDS, Strasbourg, France, and the International Variable Star Index (VSX) operated by the AAVSO. This work has made use of the ASAS3 Public Catalogue

(Pojmański *et al.* 2013), NSVS data obtained from the Sky Database for Objects in Time-Domain operated by the Los Alamos National Laboratory, and data obtained from the SuperWASP Public Archive operated by the WASP consortium, which consists of representatives from the Queen's University Belfast, the University of Cambridge (Wide Field Astronomy Unit), Instituto de Astrofisica de Canarias, the Isaac Newton Group of Telescopes (La Palma), the University of Keele, the University of Leicester, the Open University, the University of St. Andrews, and the South African Astronomical Observatory.

This work has made use of The Fourth U.S. Naval Observatory CCD Astrograph Catalog (UCAC4).

References

Breger M., *et al.* 1999, *Astron. Astrophys.*, **349**, 225.

Butters, O. W., *et al.* 2010, *Astron. Astrophys.*, **520**, L10.

Diffraction Limited. 2012, MAXIMDL image processing software (http://www.cyanogen.com).

Henden, A. A., *et al.* 2013, AAVSO Photometric All-Sky Survey, data release 7 (http://www.aavso.org/apass).

Lenz, P., and Breger, M. 2005, *Commun. Asteroseismology*, **146**, 53.

Pojmański, G. 2002, *Acta Astron.*, **52**,397.

Pojmański, G., Szczygiel, D., and Pilecki, B. 2013, The All-Sky Automated Survey Catalogues (ASAS3; http://www.astrouw.edu.pl/asas/?page=catalogues).

Richter, G. A. 1969, *Mitt. Veränderl. Sterne,* **5**, 69.

Skiff, B. A. 2009–2013, *General Catalogue of Stellar Spectral Classifications*, CDS/ADC Collection of Electronic Catalogues, 1, 2023 (2013), Lowell Observatory, Flagstaff, AZ (http://cdsarc.u-strasbg.fr/viz-bin/Cat?B/mk).

Software Bisque. 2013, CCDSOFT CCD control software (http://www.bisque.com).

Wozniak, P. R., *et al.* 2004, *Astron. J.*,**127**, 2436.

Zacharias, N., Finch, C., Girard, T., Henden, A., Bartlett, J., Monet, D., and Zacharias, M., 2012, *The Fourth US Naval Observatory CCD Astrograph Catalog* (UCAC4; http://arxiv.org/abs/1212.6182).

Table 1. Dates and times of observations conducted in this study.

Field R.A. 01^h 01^m 12^s Dec. +59° 05′ 11″			
Date (dd-mm-yyyy)	*UTC Start (hh:mm:ss)*	*UTC End (hh:mm:ss)*	*Useful Number of Exposures*
22-10-2012	18:13:29	22:35:31	120
23-10-2012	17:31:24	21:57:10	120
24-10-2012	17:21:23	21:53:21	120
29-10-2012	17:14:07	22:08:48	135
01-11-2012	19:28:32	22:50:03	67
05-11-2012	17:09:34	22:13:12	140
06-11-2012	17:38:27	22:11:26	126
Field R.A. 02^h 46^m 09^s Dec. +61° 53′ 12″			
Date (dd-mm-yyyy)	*UTC Start (hh:mm:ss)*	*UTC End (hh:mm:ss)*	*Useful Number of Exposures*
03-12-2012	16:56:13	22:25:51	151
05-12-2012	17:10:10	22:25:06	140
06-12-2012	17:23:53	22:25:12	135
10-12-2012	18:58:35	23:33:11	101
22-01-2013	18:04:15	23:20:00	144
26-01-2013	17:36:09	20:00:16	66
04-02-2013	18:08:29	22:50:20	129
10-02-2013	17:37:00	18:31:30	25
14-02-2013	18:38:56	21:20:30	74
18-02-2013	17:59:39	23:27:56	151
19-02-2013	17:50:28	21:48:21	103
26-02-2013	18:02:47	20:46:25	75
28-02-2013	18:00:17	21:04:39	81
04-03-2013	18:05:32	22:54:27	126

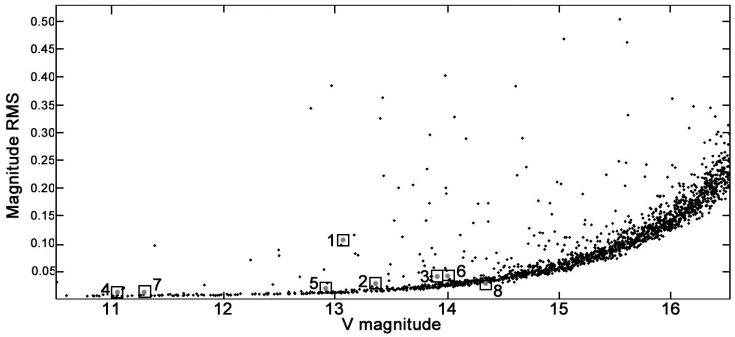

Figure 1. Magnitude-RMS diagram for the discovery-night (22-10-2012) of the field R.A. 01^h 01^m 12^s, Dec. +59° 05' 11". The squares are the variable stars detected in this survey except for No. 8 which is NSV 364 and was found to be non-variable.

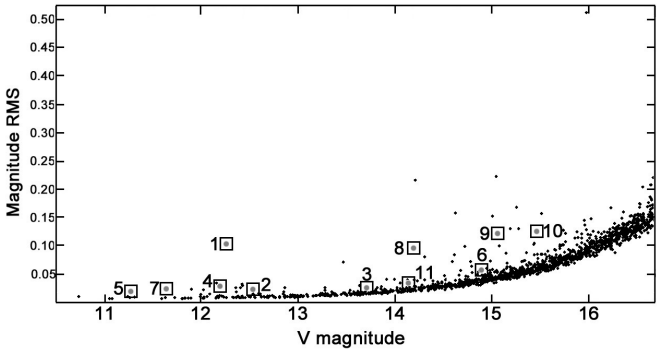

Figure 2. Magnitude-RMS diagram for the discovery-night (03-12-2012) of the field R.A. 02^h 46^m 09^s, Dec. +61° 53'1 2". The squares are the variable stars detected in this survey.

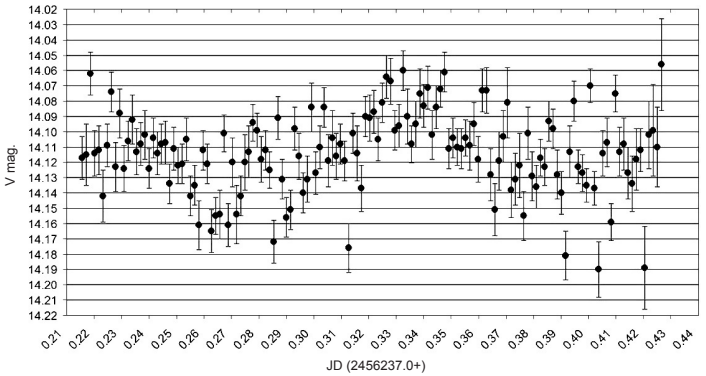

Figure 3. One night light curve of 2MASS J00584964+5909260.

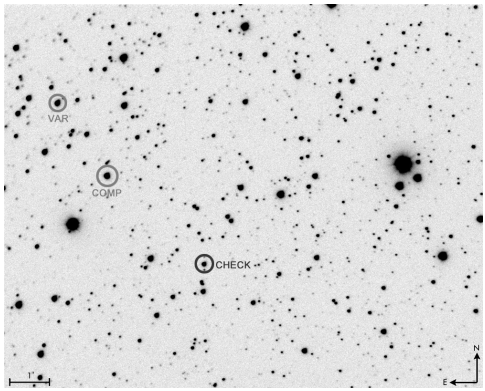

Figure 4. Finding chart of GSC 03680-00423.

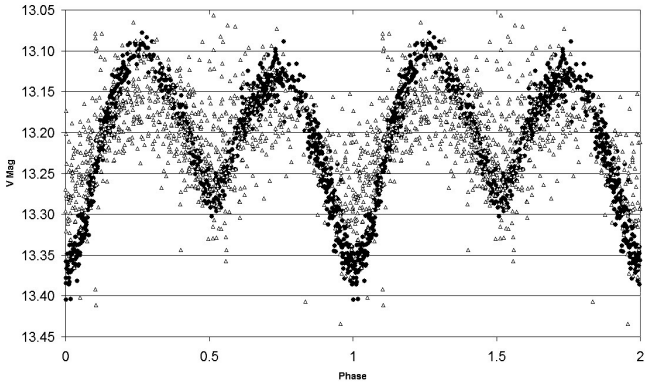

Figure 5. Phase plot of GSC 03680-00423. Filled circles denote Furgoni data; open triangles denote SWASP data (different zero-point corrections applied).

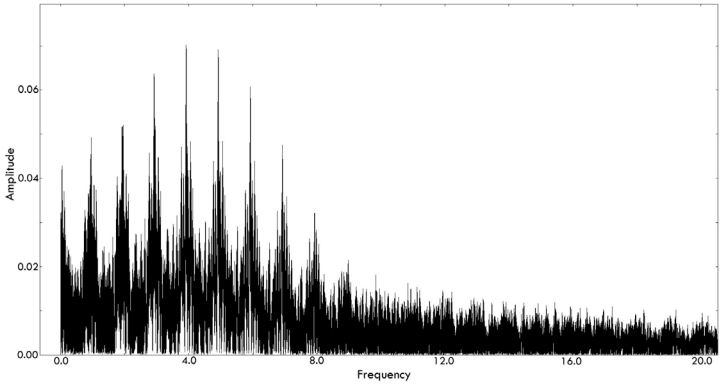

Figure 6. Fourier spectrum of GSC 03680-00423.

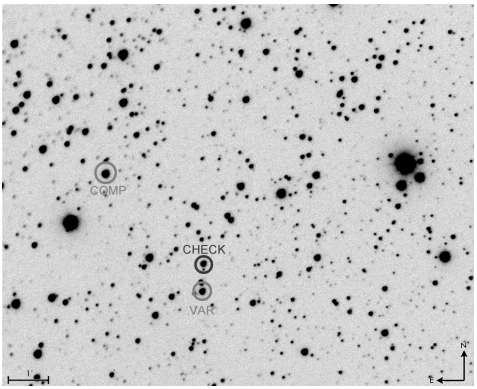

Figure 7. Finding chart of GSC 03680-00667.

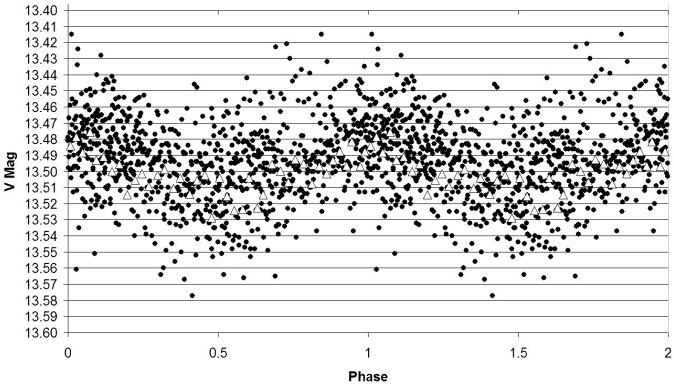

Figure 8. Phase plot of GSC 03680-00667. Filled circles denote Furgoni dataset; open triangles denote SWASP dataset with error less than 0.1 mag. +0.35 mag. offset applied.

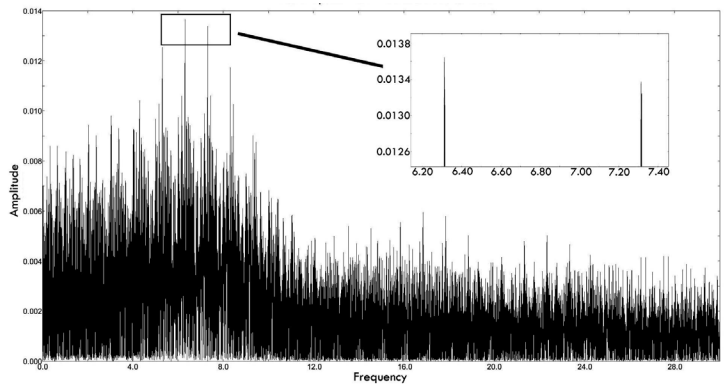

Figure 9. Fourier spectrum of GSC 03680-00667.

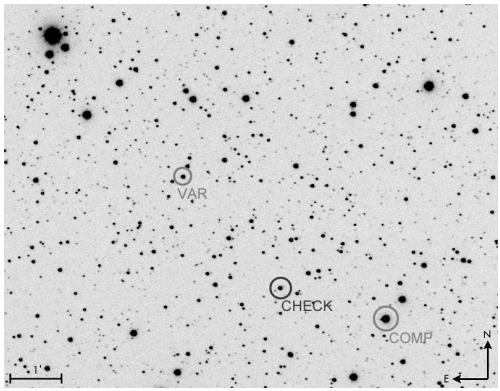

Figure 10. Finding chart of 2MASS J01020513+5912394.

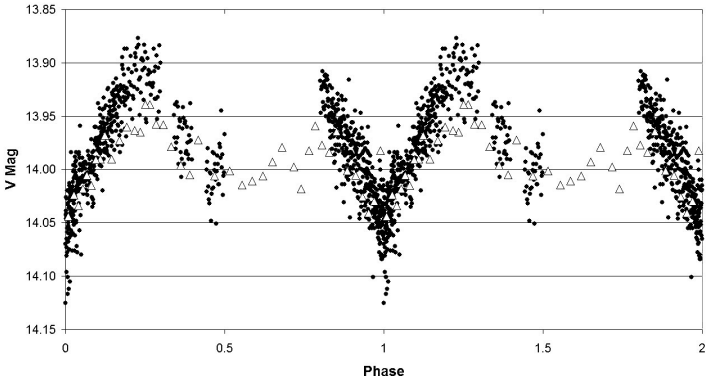

Figure 11. Phase plot of 2MASS J01020513+5912394. Filled circles denote Furgoni dataset; open triangles denote SWASP data with error less than 0.03 mag. (+0.57 mag. offset applied, 15 points binning).

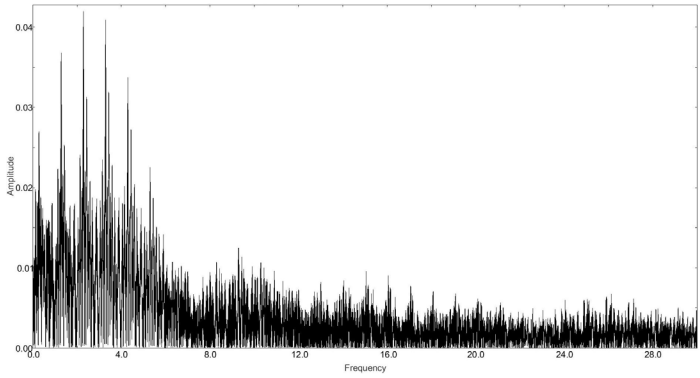

Figure 12. Fourier spectrum of 2MASS J01020513+5912394.

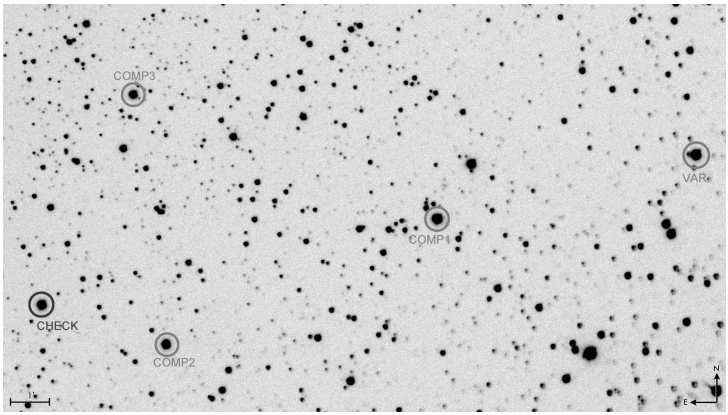

Figure 13. Finding chart of GSC 03680-01488.

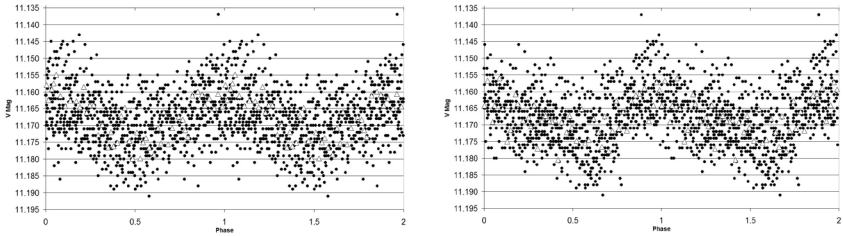

Figures 14 and 15. Main (left) and secondary (right) period phase plots of GSC 03680-01488. Filled circles denote Furgoni dataset; open triangles denote SWASP dataset with error less than or equal to 0.01 mag. Binning 15 and –0.125 mag. offset applied.

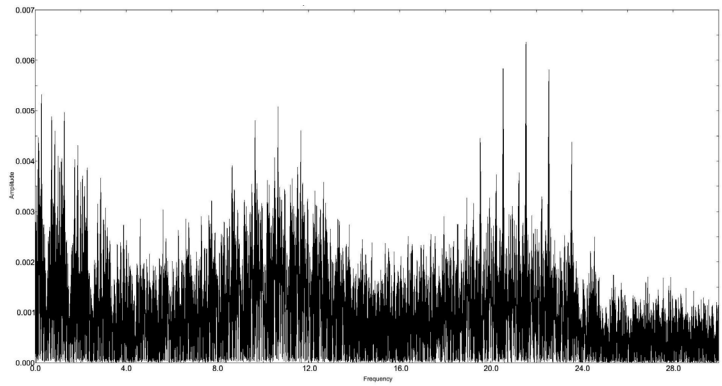

Figure 16. Fourier spectrum of GSC 03680-01488.

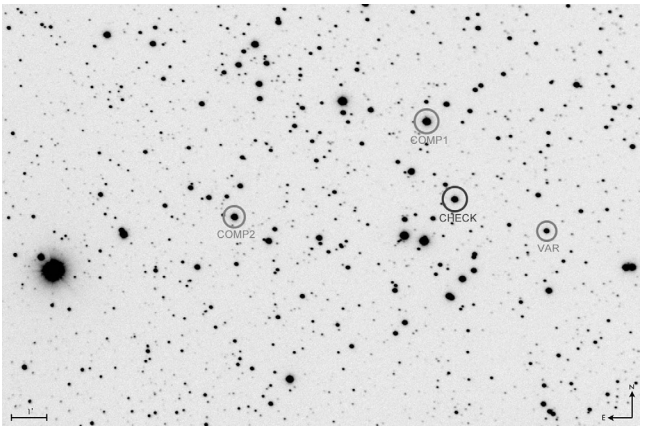

Figure 17. Finding chart of GSC 03680-01320.

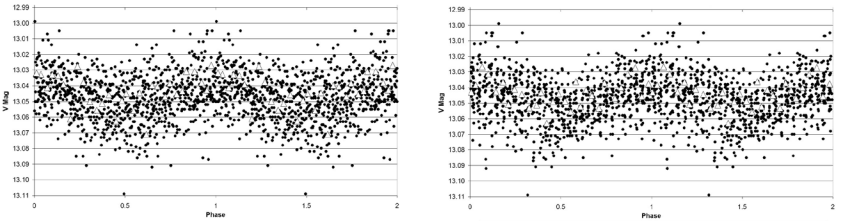

Figures 18 and 19. Main (left) and secondary (right) period phase plots of GSC 03680-01320. Filled circles denote Furgoni dataset; open triangles denote SWASP dataset with error less than 0.04 mag. and –0.35 mag. offset applied (Binning 30).

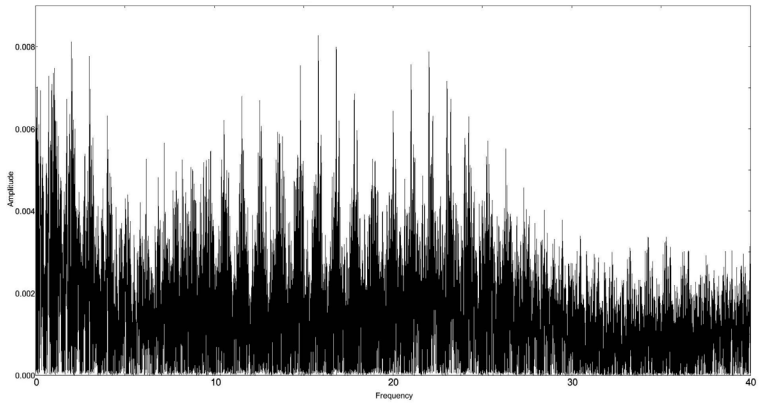

Figure 20. Fourier spectrum of GSC 03680-01320.

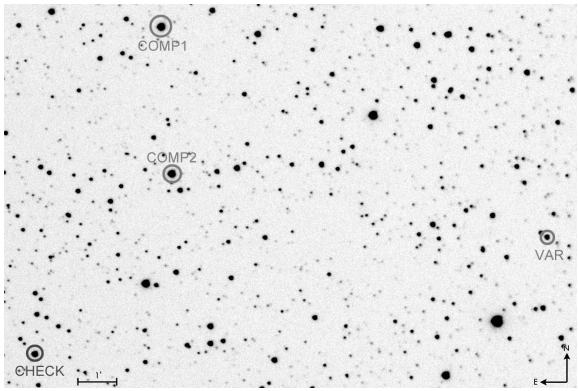

Figure 21. Finding chart of 2MASS J00584964+5909260.

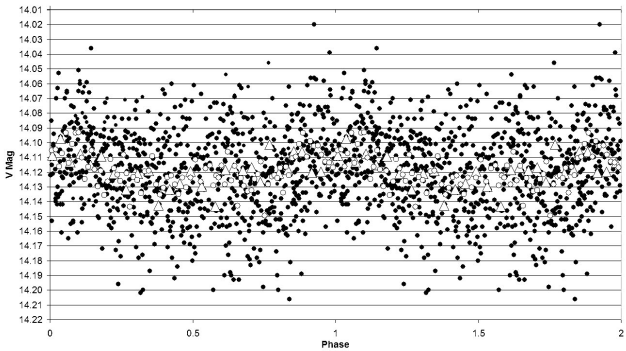

Figure 22. Phase plot of 2MASS J00584964+5909260. Filled circles denote Furgoni dataset; open triangles denote SWASP dataset with error less than 0.06 mag. Binning 30 and –0.35 mag. offset applied. Open circles denote Furgoni dataset, Binning 10.

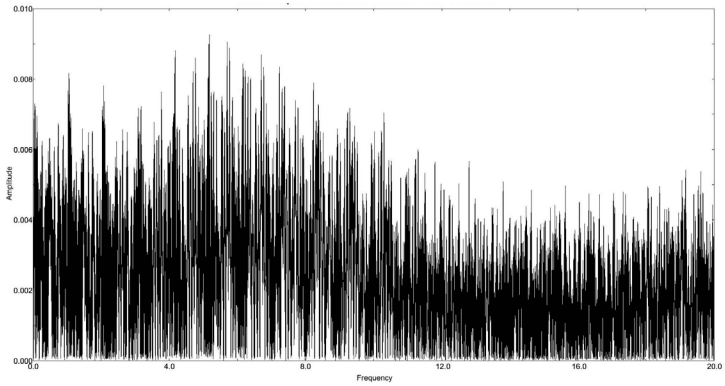

Figure 23. Fourier spectrum of 2MASS J00584964+5909260.

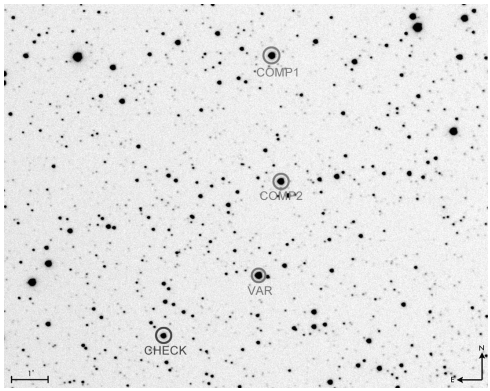

Figure 24. Finding chart of ALS 6430.

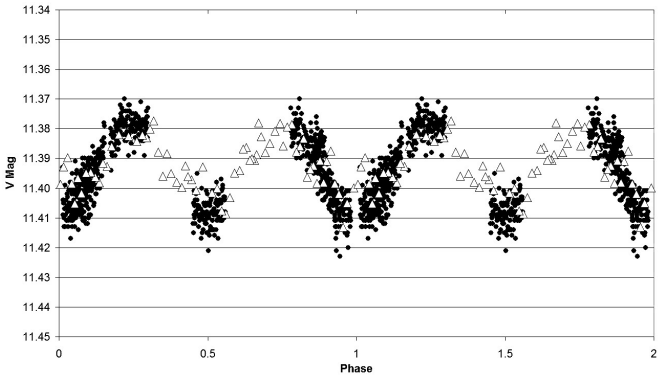

Figure 25. Phase plot of ALS 6430. Filled circles denote Furgoni dataset; open triangles denote SWASP dataset with errors less than 0.03 mag., binning 20, –0.100 mag. offset applied.

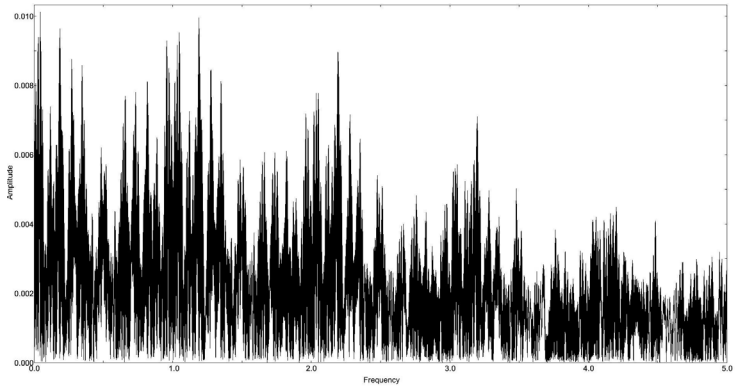

Figure 26. Fourier spectrum of ALS 6430.

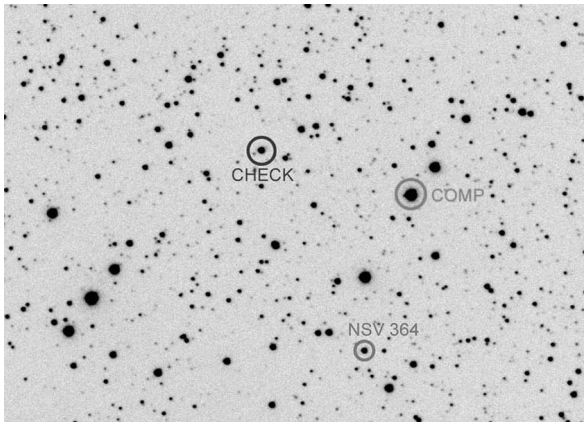

Figure 27. Finding chart of NSV 364.

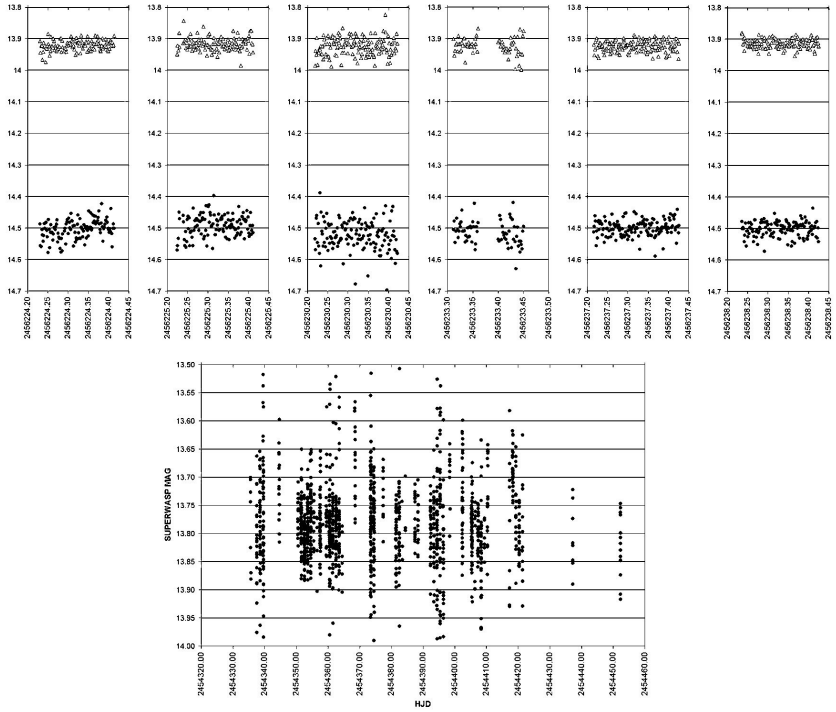

Figure 28. Light curves of NSV 364. In the Furgoni dataset (upper plot), open triangles denote the check star, and filled circles denote NSV 364; x-axis is JD, y-axis is V mag. Light curve of the SuperWasp dataset is shown in the lower plot; x-axis is HJD, y-axis is SWASP magnitude.

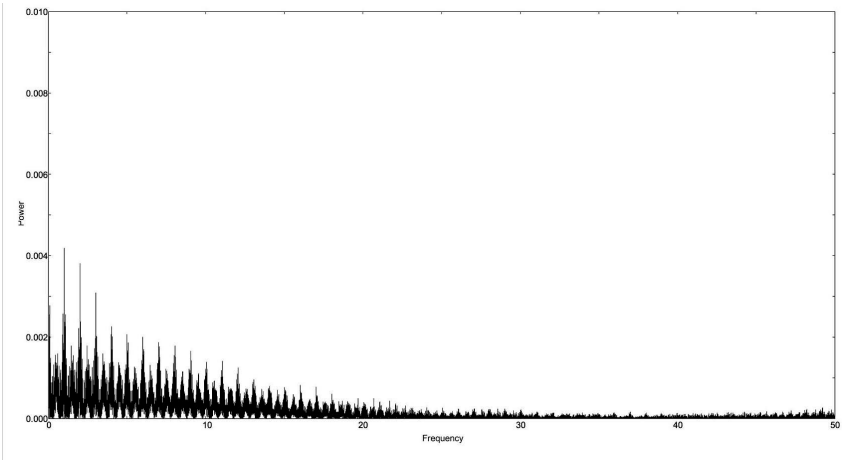

Figure 29. Fourier spectrum of NSV 364.

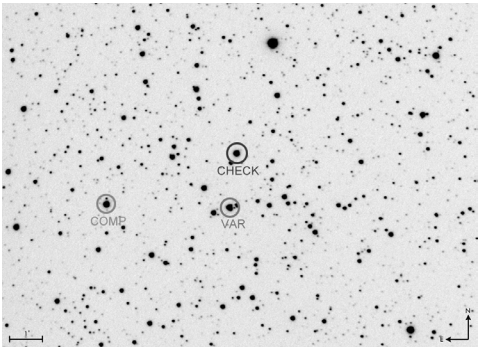

Figure 30. Finding chart of GSC 04051-02533.

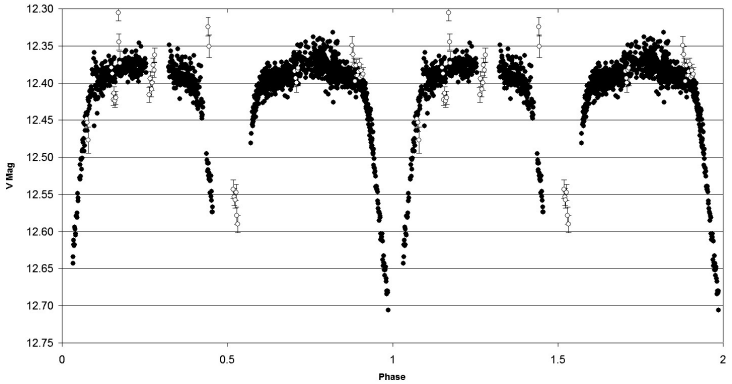

Figure 31. Phase plot of GSC 04051-02533. Filled circles denote Furgoni dataset; open circles denote SWASP dataset (−0.40 mag. offset).

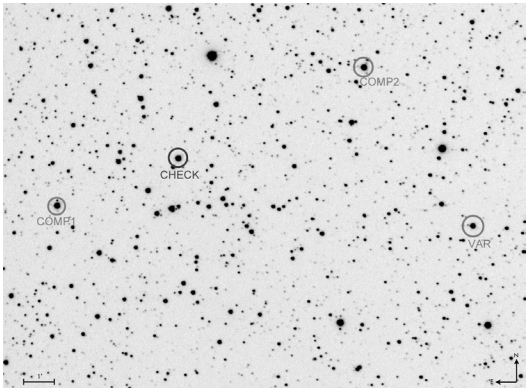

Figure 32. Finding chart of GSC 04051-02027.

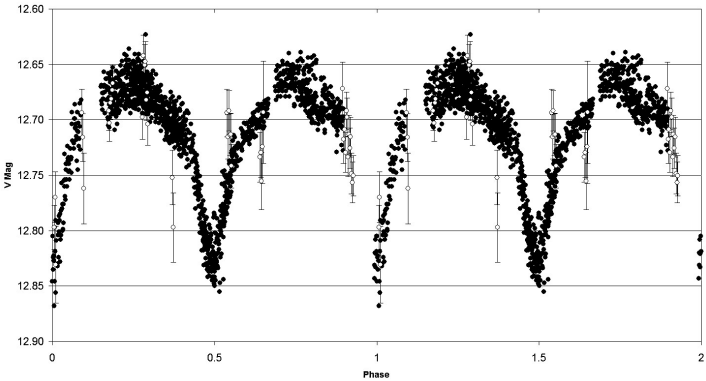

Figure 33. Phase plot of GSC 04051-02027. Filled circles denote Furgoni dataset; open circles denote SWASP dataset (–0.21 mag. offset).

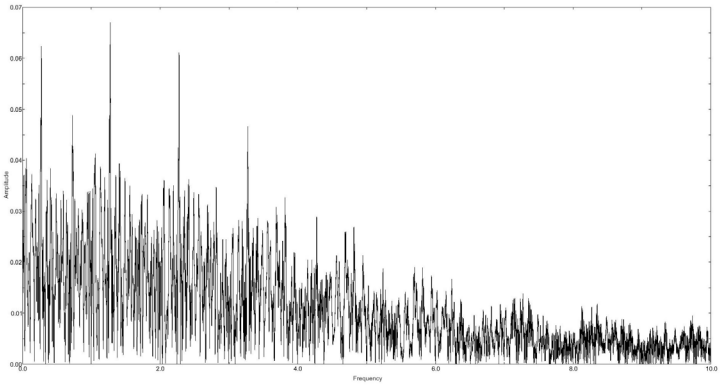

Figure 34. Fourier spectrum of GSC 04051-02027.

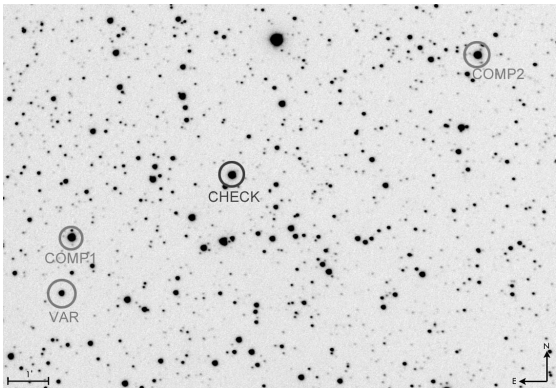

Figure 35. Finding chart of GSC 04051-01669.

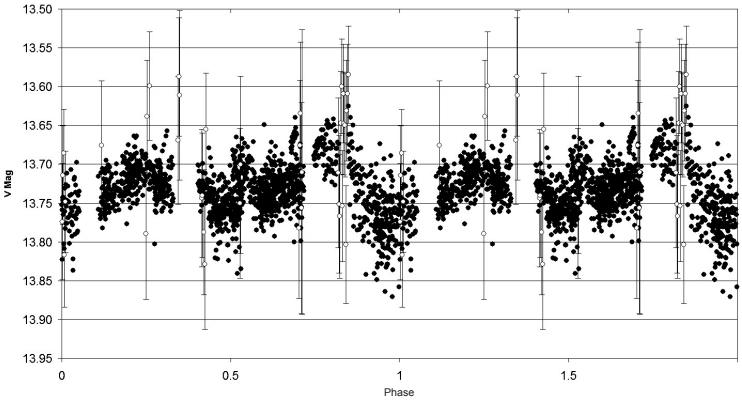

Figure 36. Phase plot of GSC 04051-01669. Filled circles denote Furgoni dataset; open circles denote SWASP dataset (–0.78 mag. offset).

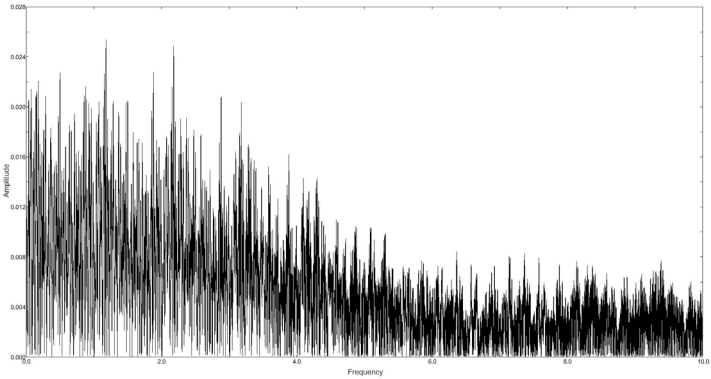

Figure 37. Fourier spectrum of GSC 04051-01669.

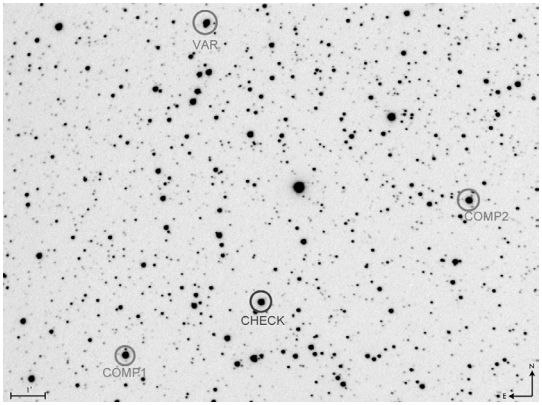

Figure 38. Finding chart of GSC 04051-01789.

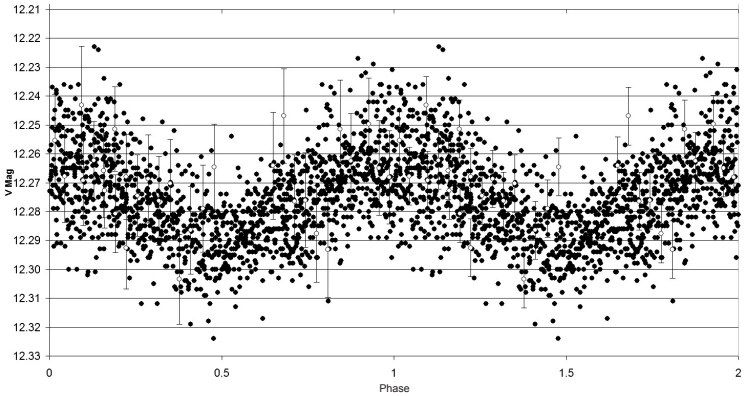

Figure 39. Phase plot of GSC 04051-01789. Filled circles denote Furgoni dataset; open circles denote SWASP dataset (–0.05 mag. offset).

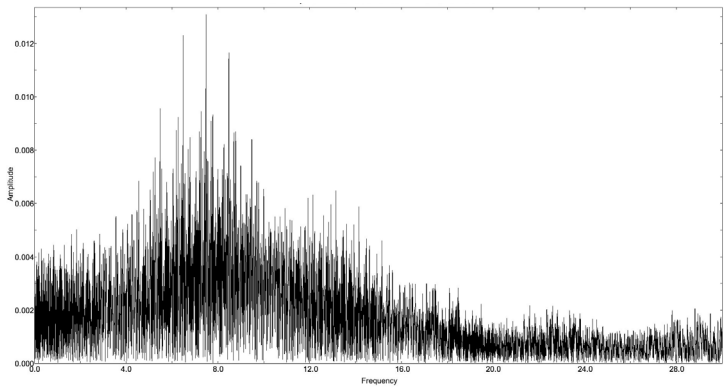

Figure 40. Fourier spectrum of GSC 04051-01789.

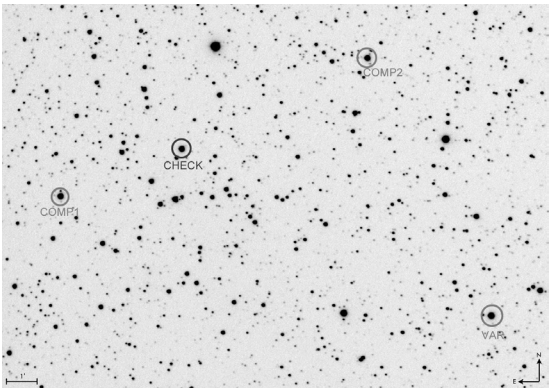

Figure 41. Finding chart of GSC 04051-02483.

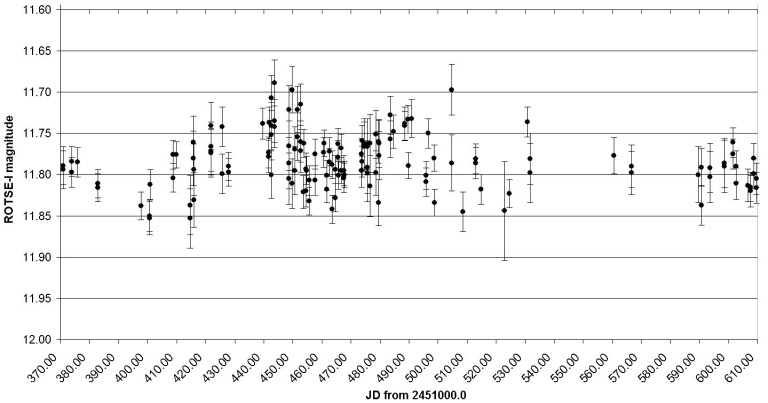

Figure 42. Light curve (NSVS dataset) of GSC 04051-02483.

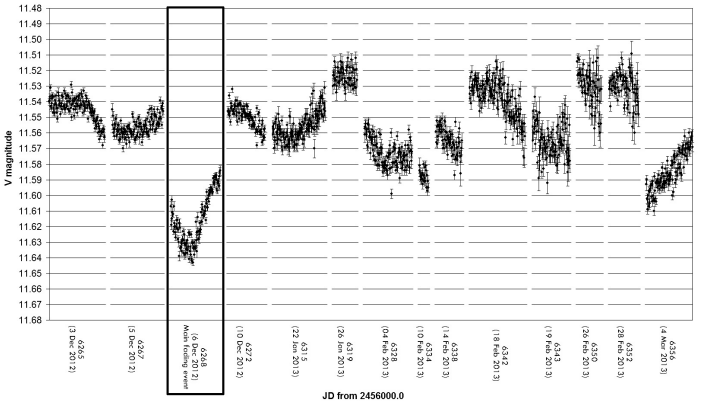

Figure 43. Light curve (Furgoni dataset) of GSC 04051-02483.

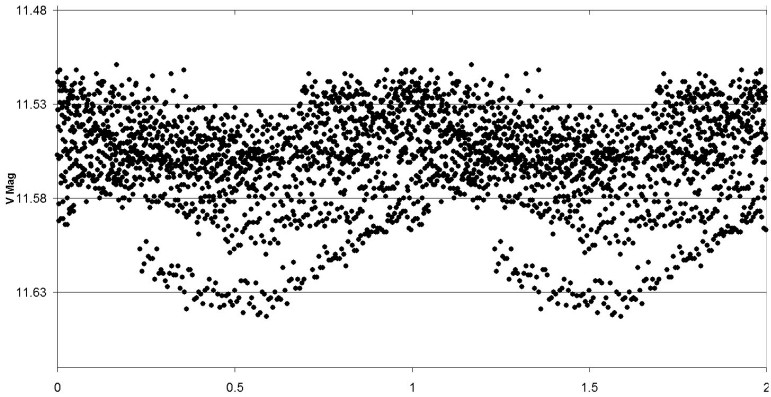

Figure 44. Phase plot of GSC 04051-02483. Furgoni dataset.

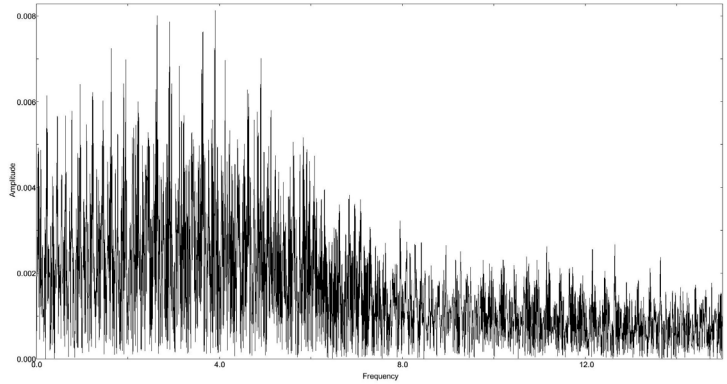

Figure 45. Fourier spectrum of GSC 04051-02483 (residuals after subtraction of frequencies (cycles per day): 0.397874538; 0.204961957; 0.834861469.

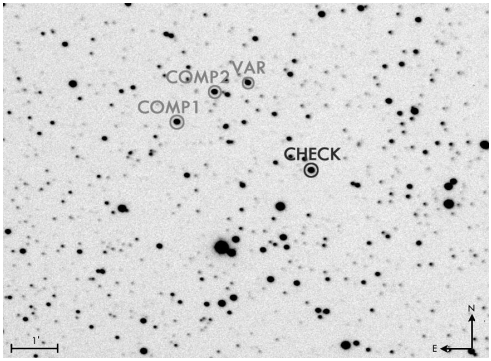

Figure 46. Finding chart of 2MASS J02472793+6149024.

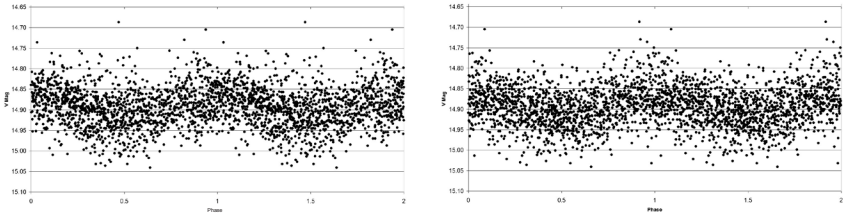

Figures 47 and 48. Main (left) and secondary (right) period phase plots of 2MASS J02472793+6149024 (Furgoni dataset).

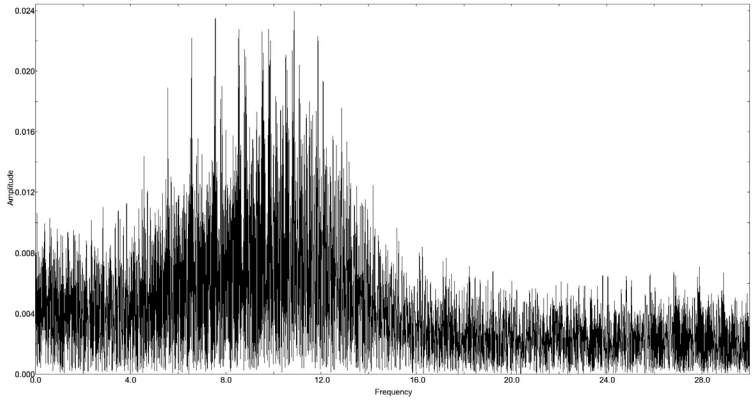

Figure 49. Fourier spectrum of 2MASS J02472793+6149024.

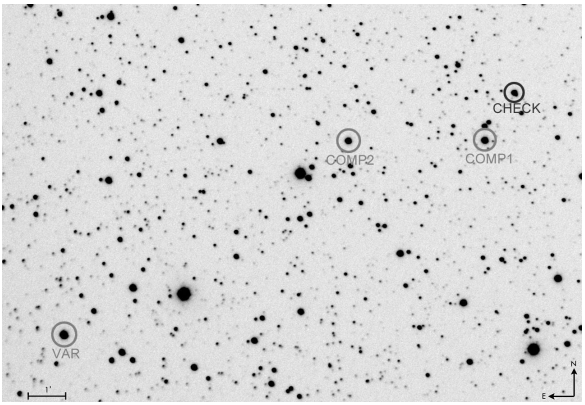

Figure 50. Finding chart of GSC 04047-01118.

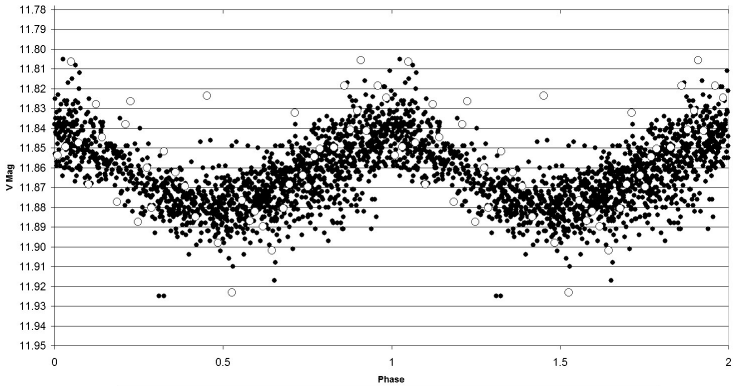

Figure 51. Phase plot of GSC 04047-01118. Filled circles denote Furgoni dataset; open circles denote NSVS dataset (–0.35 mag. offset, Binning 10).

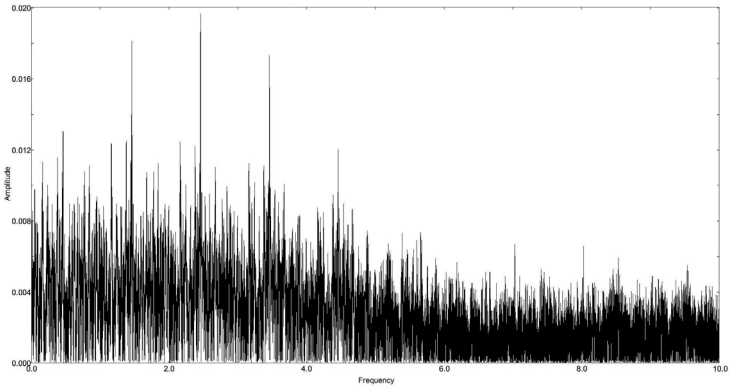

Figure 52. Fourier spectrum of GSC 04047-01118.

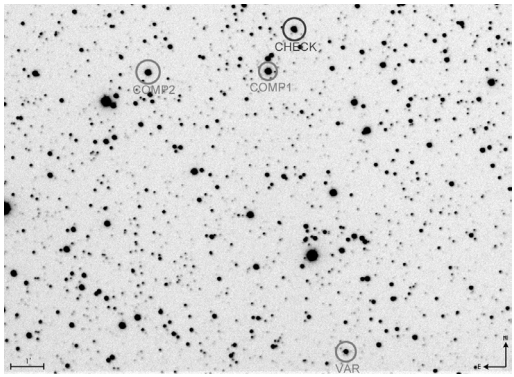

Figure 53. Finding chart of GSC 04047-00558.

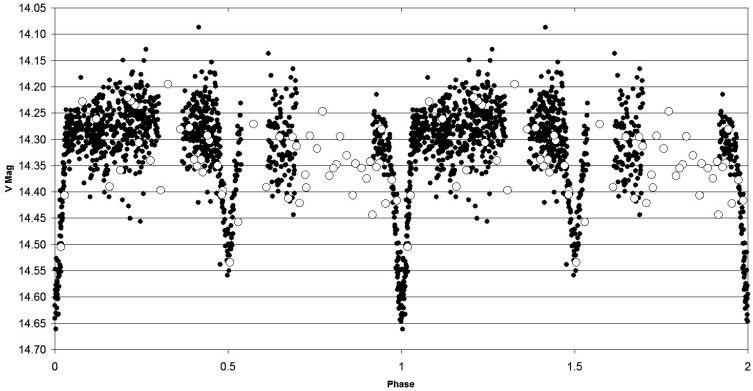

Figure 54. Phase plot of GSC 04047-00558. Filled circles denote Furgoni dataset; open circles denote NSVS dataset (0.00 mag. offset, binning 4).

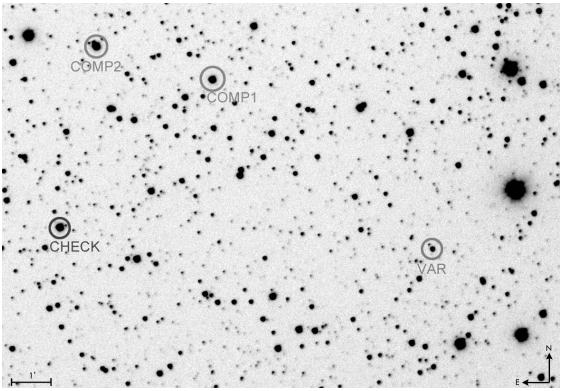

Figure 55. Light curve of GSC 04047-00381.

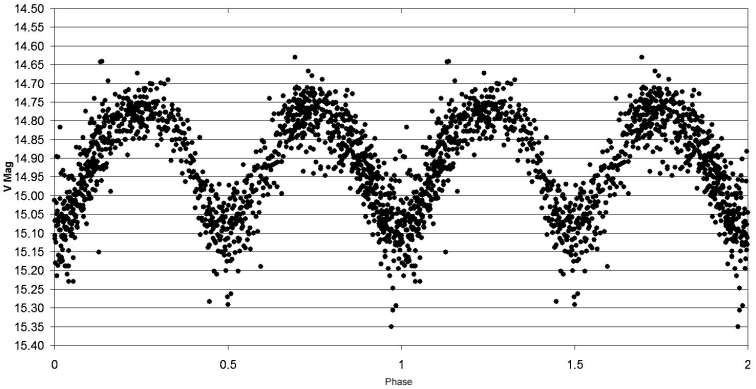

Figure 56. Phase plot of GSC 04047-00381. Furgoni dataset.

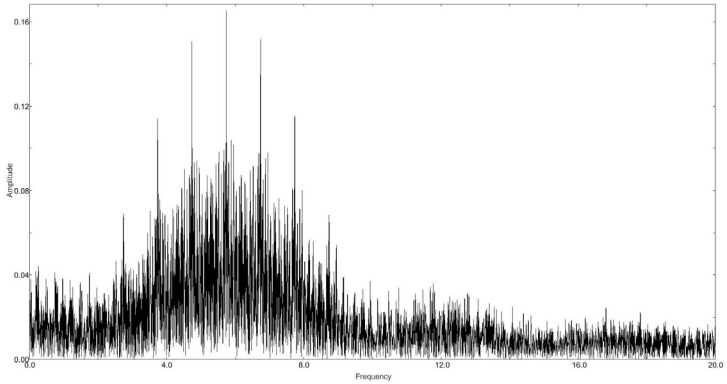

Figure 57. Fourier spectrum of GSC 04047-00381.

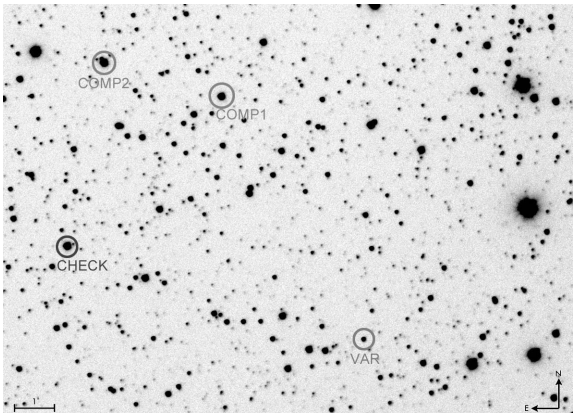

Figure 58. Finding chart of 2MASS J02443720+6143091.

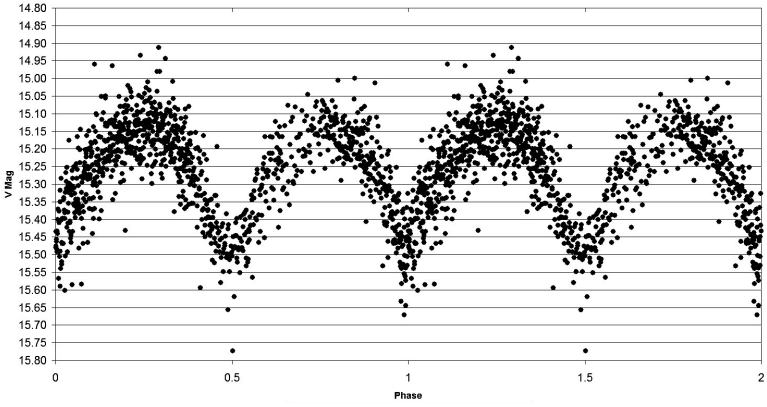

Figure 59. Phase plot of 2MASS J02443720+6143091. Furgoni dataset.

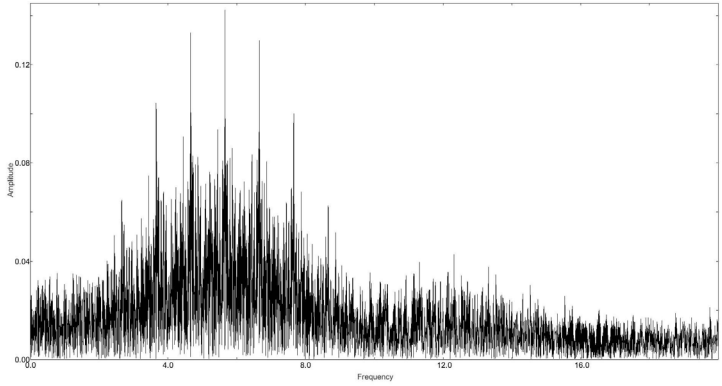

Figure 60. Fourier spectrum of 2MASS J02443720+6143091.

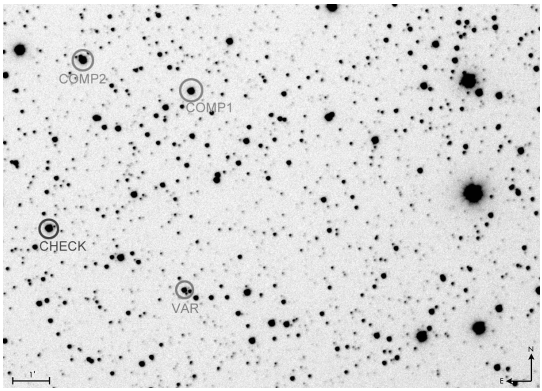

Figure 61. Finding chart of GSC 04047-01418.

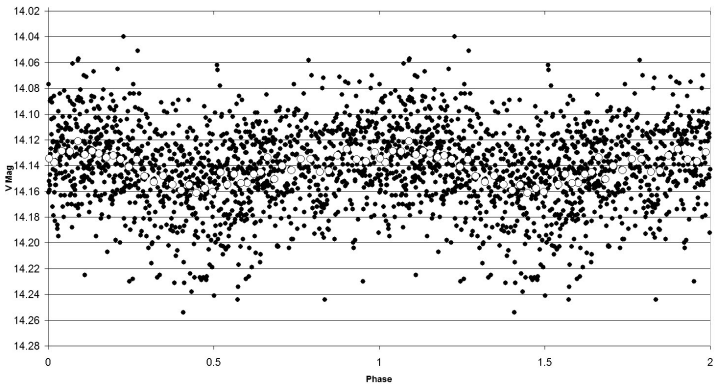

Figure 62. Phase plot of GSC 04047-01418. Filled circles denote Furgoni dataset; open circles denote Furgoni dataset, Binning 30.

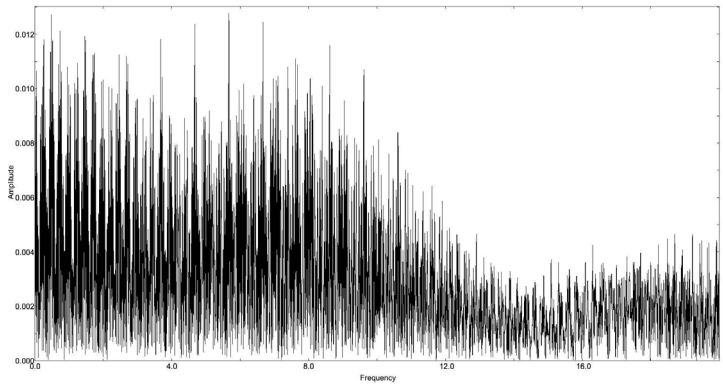

Figure 63. Fourier spectrum of GSC 04047-01418.

UV–B and B-band Optical Flare Search in AR Lacertae, II Pegasi, and UX Arietis Star Systems

Gary A. Vander Haagen
Stonegate Observatory, 825 Stonegate Road, Ann Arbor, MI; garyvh2@gmail.com

Received May 15, 2013; revised October 4, 2013; accepted November 12, 2013

Abstract A high-cadence search was conducted on the known RS CVn-type flare stars AR Lac, II Peg, and UX Ari. Two optical flares were observed in the B-band on AR Lac at 5 milliseconds (ms) resolution for a rate of 0.04 fl/hr. Flare energy of the two B-band fast-flares ranged from 0.55 to 16.7 × 10^{33} ergs. The UV–B and B-band search of II Peg for 44.5 hours at 5 and 10 ms resolution and UV–B band search of UX Ari for 25.6 hours at 10 ms resolution detected no flare activity.

1. Introduction

A flare survey was conducted on the known RS CVn-type flare stars AR Lac, II Peg, and UX Ari. This star class contains detached binaries with the more massive primary star being a G-K giant or sub-giant and the secondary a G to M spectral class sub-giant or dwarf (Berdyugina 2005). With orbital periods typically in the 1 to 14 day range, their rapid rotation and close proximity makes them "stellar dynamos," magnetically active and energetic emitters with many showing chromospheric activity, X-ray and microwave emissions, and strong X-ray, radio, and optical flares (Christian *et al.* 1996). The three stars studied were selected for their known optical flaring in the UV and B bands.

The three stars were observed from 2012-08-15 through 2012-12-28 with a total of 117.6 hours of data collection time. The objective was to collect photometric data at a minimum of 100 Hz (10 ms sampling period) for high resolution capture of the flare rise profiles, detection of possible oscillations during the flare sequences (Mathioudakis *et al.* 2003) and gathering of additional flare rate data on the star systems. The optical system was a 43-cm corrected Dall-Kirkham telescope, a high-speed silicon photomultiplier (SPM), and a data acquisition system capable of sub-millisecond data collection times.

The unique component of the optical train is the Silicon Photomultiplier, a significant divergence from standard photometric detectors. The SPM is not a conventional CCD detector, but rather a non-imaging detector with characteristics comparable to a vacuum photomultiplier (PMT). The SPM advantages versus a PMT are higher quantum efficiency over a wider spectral range, insensitivity to optical overload, very small size, low voltage, and wide bandwidth (greater than 10MHz). The SensL SPM module used (SensL 2013) has a peak photon detection efficiency (PDE) of 23%, a 1-mm square active

detection area, and 848 20-μ microcells. Higher PDEs are available with the larger microcells having greater active area fill ratios (Vander Haagen 2012). Unlike conventional CCD detectors, the SPM is insensitive to gamma-ray/particle impacts as confirmed by personal email communications with the SensL engineering organization. This eliminates the difficulty in separating high-energy impacts from photons in a non-imaging detector.

The device's 1-mm square active area is composed of an array of 848 microcells, each a silicon avalanche diode operated in the Geiger mode. The diodes are all connected electrically in parallel. When a photon strikes a single microcell with more energy than the band gap of the detector material it is absorbed, exciting a valence band electron into the conduction band. This electron is accelerated into the avalanche zone under a very high electric field and causes impact ionization. That electron in addition to the first accelerates and produces a chain reaction or "avalanche" multiplication. One photon producing one electron is multiplied through this process by ~10^6. However, the microcell is now acting as a conductor or producing a Geiger discharge. To stop the conduction process a resistor is placed in series with each of the microcell diodes such that the voltage drop during discharge is large enough to drop the junction below the breakdown voltage and reset the device. With this device, one captured photon produces one short current burst with duration of 20 to 60 ns. However, because the cell is operated at a reverse voltage well above its breakdown there is a level of spontaneous breakdown within the device causing dark counts. For a single microcell this level is 20 to 500 counts per second, depending on the active area size, junction temperature, and bias level. For the SPM used, with its 848 parallel cells, the dark count rate is approximately 20KHz at its operating temperature of –30° C.

In application the incoming light is slightly defocused to allow more than half of the microcell array to be illuminated by the incoming field. This allows an incoming stream of photons to be spread out and impinge on one of several hundred or more cells. After a cell is impacted and is in its Geiger discharge mode it takes approximately 50 ns to complete the discharge and reset. A second simultaneous photon impact on a discharging cell will not be detected. The device's linearity in photometric applications confirms multiple impacts on a single cell are not an issue.

To effectively trigger the data acquisition system for pulse counting the output of the SPM is amplified to standard logic level voltages with 0–0.8 volt for low state and 2+ volts for high state. This necessitates a 10 MHz bandwidth pulse amplifier for the narrow SPM current pulses with an amplifier voltage gain of approximately 1,000. An impedance-matching line driver takes the signal and drives a length of 50-ohm coax for connection to the data acquisition system. The data acquisition system is a PC-mounted card with bandwidth capability to 100,000 photon counts per second and integration from sub-milliseconds

to seconds, data collection triggering on count rate or event, and integrated software for real time data storage and review of events.

2. Flare search

Initial review of the data showed two categories of flares: five very short duration events among the three stars and two additional longer duration flares on AR Lac only. The five very short duration flares ranged in duration from 30 to 85 ms with peaks 0.29–0.51 mag. above the mean and were analyzed by Vander Haagen (2013). This document focuses on the flare search results and on the two longer duration flares and their parameters.

2.1. AR Lac search results

AR Lac is the brightest known totally eclipsing RS CVn binary system with a period of 1.98 days and near equal mass K0 IV+G4 IV subgiants, separated surface-to-surface by just under the diameter of the cooler larger primary (Ayres *et al.* 2005). This system has been a popular target for observers at all wavelengths (Christian *et al.* 1996). AR Lac has had flaring reported from the X-ray to the optical region (Kovari and Pagano 2000), making it a prime choice for this study.

AR Lac was observed in the B band for 47.5 hours, or 171 ksec. Photometric sampling was at 200 s/sec (5 ms sampling period). Two flares were detected and are summarized in Table 1. Given in this table are each flare's rise time (t_r, mean to peak), decay time (t_d, peak to mean at the end of decay), the flare equivalent duration (P_b), total energy (E_b), flare magnitude above the mean (b-mag), ratio t_d / t_r, and flare type.

Classification of the flares used a process described in Dal and Evren (2012) whereby a t_d / t_r ratio less than 3.5 is designated a slow flare and above 3.5 a fast flare. This classification separates those flares generating a sudden release of energy in the impulsive phase, or non-thermal process, from the longer duration thermal events. Dal and Evren conclude that the ratio defines the region between which the non-thermal and thermal events dominate the energy emitting process. Table 1, t_d / t_r data, defines flares 1 and 2 as fast flares. The flare profiles are contained in Figures 1 and 2.

The flare energy is calculated using equations (1) and (2):

$$E_b = 4\pi d^2 10^{-0.4 m_b} \Pi_b P_b \quad (1)$$

$$\textit{where } P_b = \int [(I_f - I_o) / I_o]\, dt \quad (2)$$

For AR Lac $d = 1.32 \times 10^{20}$ cm (van Leeuwen 2007), $m_b = 6.89$, $\Pi_u = 2.32 \times 10^{-6}$ erg cm^{-2} s^{-1} (Bessell 1979). The term Π_b is estimated for the B band by $E_u \simeq 1.20\, E_b$ (Mathioudakis *et al.* 1992). Equation (2) was numerically integrated

in EXCEL using the actual photometric data. The parameters for each flare are contained in Table 1. Referring to Figure 2, it is instructive to note that the initial impulse phase of flare 2 contains approximately 5.6% of the total energy in 1% of the total flare time.

The rate of flare activity was 0.04 fl/hour. Table 2 summarizes the literature showing the difficulty in comparing these results with past surveys. Two of the surveys reported at least one flare in the UV but there is insufficient data to calculate the rates. The third survey was focused on spectroscopy, Chandra HEG in UV, but did report flare rate data at 0.07 fl/hour.

A FFT analysis was run on flare 2 data for possible oscillation detection. Mathioudakis *et al.* (2003) identified intensity variations in II Peg after the impulsive phase. These intensity variations in a much longer flare were analyzed using FFT and Wavelet analysis and found to have a high confidence period of 220 s. The FFT analysis of AR Lac showed no evidence of oscillations.

There is concern that the flares are not real but rather a gamma-ray impact(s) or an instrumental or a reduction issue. This concern is heightened by the considerably shorter event duration than typical of RS CVn type flares, particularly flare 1. As noted previously the SPM does not response to gamma-ray impacts. The data were further reviewed for instrumental and reduction issues and the S/N were also confirmed at 18 or greater for these events. A literature review does reveal observations of short duration RS CVn flares. Mathioudakis *et al.* (1992) describes an II Peg flare with $(t_r + t_d) \sim 245$ sec. Byrne *et al.* (1998) also describes an II Peg flare with duration of 59 seconds. Both of these are comparable to flare 2 described in Table 1. No short duration references were found for AR Lac. The brief description of five very short duration flares from the same study is described in section 2 of this paper. Their intensity profile is significantly different and 2 to 3^+ orders shorter in duration. Additional observations are needed to verify these and the flare 1 results.

2.2. II Peg and UX Ari search results

Two similar RS CVn type stars, II Peg and UX Ari, were studied, having demonstrated optical flaring activity (Henry and Newsom 1996). II Peg is a 6.72-day single-line spectroscopic binary system with spectral type K2 IV-V star and an as yet unseen M-dwarf companion (Gu and Tan 2003). This system has been widely studied with reported flares from X-ray through optical wavelengths (Mathioudakis *et al.* 1992). UX Ari is a less studied 6.4 day double-line spectroscopic binary system with G5 V and K0 IV components and optical UBV flaring reported by Henry and Newsom (1996).

II Peg had a varied sampling plan; 15.6 hours in B band at 200 s/sec, 14.6 hours in B band at 100 s/sec, and 14.3 hours in UV–B band at 100 s/sec for a total of 44.5 hours. Photometric measurements at 200 s/sec and 100 s/sec resulted in sampling periods of 5 ms and 10 ms, respectively. UV–B-band observations used an Edmund 500 nm short pass filter. When combined with the response of

the SPM the resultant band pass was approximately 380 to 500 nm. This gave some added sensitivity to any UV flare component. The UX Ari search was conducted for 25.6 hours in the UV–B band at 100 s/sec.

No flares were detected in either system over the sampling period. Table 2 summarizes the current search and historical rate data. II Peg has a range of reported rates from 0.225 fl/hour to 0. As noted in the cited references the system seems to vary widely in activity from a highly energetic period (Byrne *et al.* 1994) to a quiet state.

Definitive flare rate data on UX Ari were limited to Henry and Newsom (1996), where a single flare just after maximum resulted in a flare rate of 0.034 fl/hr. Data from the Advanced Satellite for Cosmology and Astrophysics (ASCA) and the Extreme Ultraviolet Explorer (EUVE) campaigns were analyzed by Gudel *et al.* (1999) where UV flares were detected. However, no flare rates were calculated or could be accurately inferred from the information.

3. Discussion

Inspection of the AR Lac flare rise time data indicates under-sampling at 200 s/sec with the true profile not characterized. Figure 3 shows the rise time portion of flare 1 in 5 ms intervals. With the actual flare rise time unknown, it is important to understand what sampling options are needed and possible to better characterize the flare waveform. Equation (3) describes the relationship between the measurement system's bandwidth (BW) and the rise time (t_r) of a signal under study:

$$\mathrm{BW} = \frac{0.35}{t_r} \tag{3}$$

To avoid signal aliasing, the sampling rate f_s must exceed the Nyquist Rate f_n, thereby equation (4):

$$f_s > f_n \text{ where } f_n = 2\,\mathrm{BW} \text{ (minimum)} \tag{4}$$

Assume the actual flare rise time is 2 ms; the equivalent minimum system BW requirement would be 175 Hz, necessitating a sampling rate of 350 s/sec. With the limited light from the optical system an additional search at 500 s/sec in the B band should be possible. With the shorter sampling duration the S/N would degrade from approximately 18 to 12 and provide adequate BW for t_r as short as 1.5 ms. Sampling at 1,000 s/sec using the UV–B filter should also result in S/N above 10. Either sampling rate would improve the rise profile resolution under energetic impulse conditions.

The lack of flare detection on either II Peg or UX Ari was disappointing but typical of the results from other studies. Note again the large variability in

Table 2 on the searches (Mathioudakis *et al.* 1992), (Henry and Newsom 1996), and (Byrne *et al.* 1994). There is clear evidence of long-term variability in the level of optical flaring. While two of the searches were in the UV band, where flare energy is at least 1.2 times greater than B band (Mathioudakis et al. 1992) the S/N should be sufficient for all but low level flares, such as < 0.05 mag. This limitation is exacerbated by both the telescope aperture and more importantly by the lack of a second SPM monitoring a reference star for optical transmission correction. Fast occurring transmission variations can mask low level flares and make positive discrimination of these events difficult. A two-sensor system has been designed but has not been constructed due to its complexity and difficulty in alignment.

This study provided the highest reported sampling rates found for study of these three stars. An additional search, at the higher sampling rates, is planned to further refine the rise time profiles. In addition, further observations may serendipitously discover other short duration flares to verify these results.

4. Acknowledgements

The author thanks the referee for input and concern over the very short-duration flare events atypical of RS CVn stars. Additional supporting information was included as was the need for more observations to confirm results.

References

Ayres, T. R., Brown, A., Harper, G. M., Korhonen, H., Redfield, S., Hawley, S. L., and Optical Support Team. 2005, *Bull. Amer. Astron. Soc.*, **37**, 1445.

Berdyugina, S. V. 2005, *Living Rev. Solar Phys.*, **2**, 8.

Bessell, M. S. 1979, *Publ. Astron. Soc. Pacific*, **91**, 589.

Byrne, P. B., Lanzafame, A. C., Sarro, L. M., and Ryans, R. 1994, *Mon. Not. Roy. Astron. Soc.*, **270**, 427.

Byrne, P. B., *et al.* 1998, *Astron. Astrophys., Suppl. Ser.*, **127**, 505.

Christian, D. J., Drake, J.J., Patterer, R.J., Vedder, P.W., and Bowyer, S. 1996, *Astron. J.*, **112**, 751.

Dal, H. A., and Evren, S. 2012, *New Astron.*, **17**, 399.

Gu, S., and Tan, H. 2003, in *The Future of Cool-Star Astrophysics: 12th Cambridge Workshop on Cool Stars, Stellar Systems, and the Sun*, eds. A. Brown, G. M. Harper, and T. R. Ayres, Univ. Colorado, Boulder, 986.

Gudel, M., Linsky, J. L., Brown, A., and Nagase, F. 1999, *Astrophys. J.*, **511**, 405.

Henry, G. W., and Newsom, M. S. 1996, *Publ. Astron. Soc. Pacific*, **108**, 242.

Huenemoerder, D., Canizares, C., and Tibbetts, K. 2003, in *The Future of Cool-Star Astrophysics: 12th Cambridge Workshop on Cool Stars, Stellar Systems, and the Sun*, eds. A. Brown, G. M. Harper, and T. R. Ayres, Univ. Colorado, Boulder, 1002.

Kovari, Zs., and Pagano, I. 2000, in *Workshop on the Sun and Sun-like Stars*, eds. I. Jankovics, J. Kovács, and I. J. Vincze, Gothard Astrophysical Observatory, Szombathely, Hungary, 7.

Kreiner, J. M. 2004, *Acta Astron.*, **54**, 207.

Mathioudakis, M., Doyle, J. G., Avgoloupis, S., Mavridis, L. N., and Seiradakis, J. H. 1992, *Mon. Not. Roy. Astron. Soc.*, **255**, 48.

Mathioudakis, M., Seiradakis, J. H., Williams, D. R., Avgoloupis, S., Bloomfield, D. S., and McAteer, R. T. J. 2003, *Astron. Astrophys.*, **403**, 1101.

SensL Technologies Ltd. 2013, manufacturers of silicon photomultipliers (http://sensl.com/products/silicon-photomultipliers/spmmini/).

van Leeuwen, F. 2007, *Astron. Astrophys.*, **474**, 653.

Vander Haagen, G. A. 2012, in *The Society for Astronomical Sciences 31st Annual Symposium on Telescope Science*, eds. B. D. Warner, R. K. Buchleim, J. L. Foote, and D. Mais, Society for Astronomical Sciences, Rancho Cucamonga, CA, 165.

Vander Haagen, G. A. 2013, *J. Amer. Assoc. Var. Star Obs.*, **41**, 114.

Table 1. AR Lac flare characteristics in the B-band.

Date	*Flare*	t_r *(sec)*	t_d *(sec)*	P_b *(sec)*	E_b *(10^{33} ergs)*	*Flare (b-mag)*	t_d/t_r	*Flare Type*
Aug 23, 2012	1	0.010	2.55	0.62	0.55	0.51	255	fast
Aug 23, 2012	2	0.015	203.1	18.8	16.7	0.49	13540	fast

Table 2. Flare rate comparison between current flare search and historical data.

Star System	*Search Time (hours)*	*Search Flare Rate (fl/hour)*	*Historical Rates (fl/hour)*
AR Lac	47.5	0.04 B-band	X[a] X[b] 0.07[c]
II Peg	44.5	0	0.17[d] 0.225[e] 0[f] X[g]
UX Ari	25.6	0	0.034[e] X[h]

a) (Christian et al. 1996), EUVE study, rate not reported. b) (Kovari and Pagano 2000), UV flares, rate not reported. c) (Huenemoerder, Canizares, and Tibbetts 2003), Chandra HEG in UV. d) (Mathioudakis et al. 1992), UV- band. e) (Henry and Newsom 1996), UBV search. f) (Byrne et al. 1994), UV–Band. g) (Byrne et al. 1998), UV–Band, 1-large flare, rate not reported. h) (Gudel et al. 1999), ASCA and EUVE data, UV flares, rate not reported.

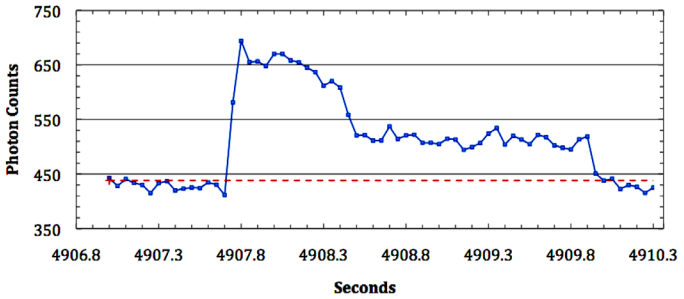

Figure 1. Flare 1, August 23, 2012, 4:21 UTC, resampled at 50 ms, orbital phase 0.26 (Kreiner 2004).

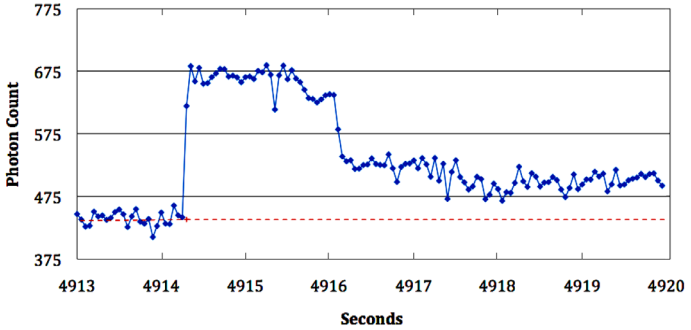

Figure 2. Flare 2, August 23, 2012, 4:21 UTC, early impulse portion only, resampled at 50 ms, orbital phase 0.26.

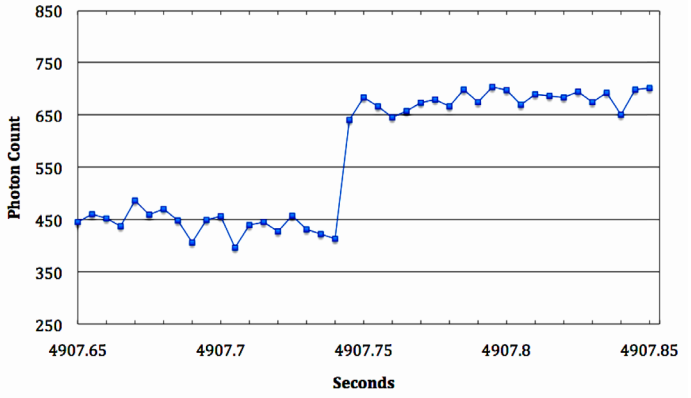

Figure 3. Flare 1, August 23, 2012, 4:21 UTC, original photometric data sampled at 200 s/sec (5 ms sampling period), noting under-sampling of signal during the impulsive rise time portion.

Recent Minima of 199 Eclipsing Binary Stars

Gerard Samolyk
P.O. Box 20677; Greenfield, WI 53220; gsamolyk@wi.rr.com

Received October 4, 2013; accepted October 4, 2013

Abstract This paper continues the publication of times of minima for eclipsing binary stars from observations reported to the AAVSO EB section. Times or minima from observations received from December 2012 through September 2013 are presented.

1. Recent Observations

The accompanying list contains times of minima calculated from recent CCD observations made by participants in the AAVSO's eclipsing binary program. This list will be web-archived and made available through the AAVSO ftp site at ftp://ftp.aavso.org/public/datasets/gsamoj412.txt. This list, along with the eclipsing binary data from earlier AAVSO publications, is also included in the Lichtenknecker database (Kreiner 2011) administrated by the Bundesdeutsche Arbeitsgemeinschaft für Veränderliche Sterne e. V. (BAV) at: http://www.bav-astro.de/LkDB/index.php?lang=en. These observations were reduced by the observers or the writer using the method of Kwee and Van Worden (1956). Column F in Table 1 indicates the filter used. A "C" indicates a clear filter. The standard error is included when available.

The linear elements in the *General Catalogue of Variable Stars* (GCVS, Kholopov *et al.* 1985) were used to compute the O–C values for most stars. For a few exceptions where the GCVS elements are missing or are in significant error, light elements from another source are used: AC CMi (Samolyk 2008), CW Cas (Samolyk 1992a), DV Cep (Frank and Lichtenknecker 1987), DF Hya (Samolyk 1992b), DK Hya (Samolyk 1990), GU Ori (Samolyk 1985). The light elements for QX And, V952 Cas, EX Leo, and CU Tau are from Kreiner (2013). O–C values listed in this paper can be directly compared with values published in the *AAVSO Observed Minima Timimgs of Eclipsing Binaries* series.

References

Frank, P., and Lichtenknecker, D. 1987, *BAV Mitt.,* No. 47, 1.

Kreiner, J. M. 2011, Lichtenknecker-Database of the BAV (http://www.bavdata-astro.de/~tl/cgi-bin/varstars_cgi).

Kreiner J. M. 2013, Up-to-date linear elements of eclipsing binaries (http://www.as.up.krakow.pl/ephem/), Cracow Pedagogical Univ., Cracow.

Kholopov, P. N., *et al.* 1985, *General Catalogue of Variable Stars*, 4th ed., Moscow.

Kwee, K. K., and Van Woerden, H. 1956, *Bull. Astron. Inst. Netherlands*, **12**, 327.
Samolyk, G. 1985, *J. Amer. Assoc. Var. Star Obs.*, **14**, 12.
Samolyk, G. 1990, *J. Amer. Assoc. Var. Star Obs.*, **19**, 5.
Samolyk, G. 1992a, *J. Amer. Assoc. Var. Star Obs.*, **21**, 34.
Samolyk, G. 1992b, *J. Amer. Assoc. Var. Star Obs.*, **21**, 111.
Samolyk, G. 2008, *J. Amer. Assoc. Var. Star Obs.,* **36**, 171.

Table 1. Recent times of minima of stars in the AAVSO eclipsing binary program.

Star	*HJD 2400000+*	*Cycle*	*O–C (day)*	*F*	*Observer*	*Standard Error (day)*
RT And	56528.6388	24465	–0.0108	V	G. Samolyk	0.0001
TW And	56529.7862	4247	–0.0454	V	N. Simmons	0.0001
UU And	56511.8822	9999	0.0685	V	R. Sabo	0.0005
WZ And	56528.8240	22506	0.0641	V	G. Samolyk	0.0002
XZ And	56520.8205	23977	0.1744	V	G. Samolyk	0.0001
AB And	56535.5162	61544	–0.0336	V	L. Corp	0.0001
AD And	56508.8608	17751.5	–0.0455	V	G. Samolyk	0.0003
BD And	56538.7545	46611	0.0154	V	N. Simmons	0.0001
BX And	56536.8311	32794	–0.0691	V	G. Samolyk	0.0002
BX And	56536.8330	32794	–0.0672	V	R. Sabo	0.0002
BX And	56566.7303	32843	–0.0655	V	K. Menzies	0.0003
DS And	56542.7617	20188	0.0031	V	K. Menzies	0.0002
QX And	56297.5709	9213.5	0.0002	V	N. Simmons	0.0002
QX And	56536.8342	9794	–0.0024	V	G. Samolyk	0.0003
RY Aqr	56515.7494	7979	–0.1181	V	G. Samolyk	0.0001
CX Aqr	56481.8576	36023	0.0117	V	G. Samolyk	0.0002
CX Aqr	56564.7000	36172	0.0122	V	R. Poklar	0.0001
CZ Aqr	56512.8830	15232	–0.0549	V	R. Sabo	0.0001
XZ Aql	56492.8472	6820	0.1718	V	G. Samolyk	0.0002
KP Aql	56521.6449	4788.5	–0.0223	V	G. Samolyk	0.0002
OO Aql	56493.7911	35282	0.0577	V	B. Manske	0.0001
OO Aql	56495.8175	35286	0.0570	V	R. Sabo	0.0001
OO Aql	56519.6369	35333	0.0573	V	G. Samolyk	0.0001
OO Aql	56521.6641	35337	0.0574	V	N. Simmons	0.0001
V342 Aql	56523.7409	5074	–0.1754	V	G. Samolyk	0.0002
V343 Aql	56523.7576	15223	–0.0509	V	G. Samolyk	0.0001
V343 Aql	56525.6021	15224	–0.0510	V	K. Menzies	0.0001
V346 Aql	56505.7692	13185	–0.0110	V	G. Samolyk	0.0001
SS Ari	56534.9273	43121	–0.3177	V	R. Sabo	0.0001
SX Aur	56229.7954	13278	0.0150	V	N. Simmons	0.0001
SX Aur	56263.6786	13306	0.0160	V	R. Poklar	0.0002

Table continued on following pages

Table 1. Recent times of minima of stars in the AAVSO eclipsing binary program, cont.

Star	HJD 2400000+	Cycle	O–C (day)	F	Observer	Standard Error (day)
AP Aur	56388.6403	24492	1.4296	V	K. Menzies	0.0002
CL Aur	56336.5848	18780	0.1575	V	G. Samolyk	0.0001
HP Aur	56549.8718	9694.5	0.0617	V	G. Samolyk	0.0002
HP Aur	56559.8303	9701.5	0.0605	V	K. Menzies	0.0001
IM Aur	56283.7443	12642	–0.1182	V	G. Samolyk	0.0002
TU Boo	56336.9210	71759.5	–0.1416	V	G. Samolyk	0.0002
TU Boo	56369.8361	71861	–0.1416	V	K. Menzies	0.0001
TU Boo	56411.8305	71990.5	–0.1424	V	R. Sabo	0.0006
TY Boo	56382.7256	69060	0.0804	V	K. Menzies	0.0001
TY Boo	56399.6930	69113.5	0.0804	V	R. Poklar	0.0002
TY Boo	56419.8319	69177	0.0805	V	K. Menzies	0.0001
TZ Boo	56287.9452	56047	0.0648	V	K. Menzies	0.0001
TZ Boo	56316.9177	56144.5	0.0640	V	K. Menzies	0.0004
TZ Boo	56462.6750	56635	0.0633	V	G. Samolyk	0.0003
UW Boo	56303.8770	13834	–0.0052	V	K. Menzies	0.0001
VW Boo	56424.6441	73764.5	–0.2165	V	N. Simmons	0.0001
AD Boo	56475.7121	14541	0.0333	V	G. Samolyk	0.0005
Y Cam	56541.8563	4108	0.4237	V	G. Samolyk	0.0001
SV Cam	56283.9110	23082	0.0552	V	N. Simmons	0.0001
AL Cam	56552.7012	22691	–0.0338	V	N. Simmons	0.0001
R CMa	56340.6575	10609	0.1037	V	G. Samolyk	0.0001
TU CMa	56329.6642	26026	–0.0103	V	R. Poklar	0.0002
UU CMa	56340.6578	5420	–0.0986	V	R. Poklar	0.0002
XZ CMi	56323.6730	23979	–0.0017	V	R. Poklar	0.0001
YY CMi	56283.8794	25832	0.0155	V	G. Samolyk	0.0003
AC CMi	56328.7129	5016	0.0036	V	R. Poklar	0.0002
AK CMi	56284.7981	23296	–0.0221	V	G. Samolyk	0.0001
AK CMi	56330.6365	23377	–0.0214	V	R. Poklar	0.0002
AM CMi	56337.6863	30507.5	0.2164	V	R. Poklar	0.0008
TY Cap	56552.6509	8261	0.0801	V	G. Samolyk	0.0003
RZ Cas	56529.7656	11152	0.0648	V	N. Simmons	0.0001
TV Cas	56436.8627	6529	–0.0274	V	G. Samolyk	0.0001
TV Cas	56505.7417	6567	–0.0270	V	K. Menzies	0.0003
TV Cas	56534.7438	6583	–0.0264	V	N. Simmons	0.0005
TW Cas	56528.7356	10166	0.0065	V	G. Samolyk	0.0004
AB Cas	53258.6038	7714	0.0766	R	G. Lubcke	0.0001
AB Cas	56541.8783	10116	0.1202	V	G. Samolyk	0.0001
AX Cas	56292.2687	46081	–0.0998	C	Y. Ogmen	0.0001

Table continued on following pages

Table 1. Recent times of minima of stars in the AAVSO eclipsing binary program, cont.

Star	*HJD 2400000+*	*Cycle*	*O–C (day)*	*F*	*Observer*	*Standard Error (day)*
CW Cas	53269.5788	36496.5	–0.0298	R	G. Lubcke	0.0001
CW Cas	56172.3179	45600	–0.0701	V	Y. Ogmen	0.0001
CW Cas	56528.6410	46717.5	–0.0776	V	N. Simmons	0.0001
CW Cas	56528.7985	46718	–0.0795	V	N. Simmons	0.0001
CW Cas	56538.6836	46749	–0.0792	V	B. Manske	0.0001
CW Cas	56544.7424	46768	–0.0788	V	K. Menzies	0.0001
CW Cas	56558.6138	46811.5	–0.0780	V	B. Manske	0.0002
CW Cas	56558.7717	46812	–0.0795	V	K. Menzies	0.0001
DP Cas	56258.2533	23512	–0.0032	C	Y. Ogmen	0.0001
DZ Cas	54004.5875	32578	–0.1670	V	G. Lubcke	0.0004
DZ Cas	56536.6235	35804	–0.1913	V	G. Samolyk	0.0004
DZ Cas	56558.6013	35832	–0.1905	V	N. Simmons	0.0007
IR Cas	53993.5750	17085	0.0110	R	G. Lubcke	0.0004
IR Cas	56521.6390	20799	0.0094	V	G. Samolyk	0.0001
IS Cas	56229.5971	14908	0.0672	V	N. Simmons	0.0001
IT Cas	56541.6315	7129	0.0652	V	G. Samolyk	0.0001
KR Cas	51133.568	7360	–0.1471	C	S. Cook	—
MM Cas	56515.8613	18226	0.1041	V	G. Samolyk	0.0003
PV Cas	56562.7599	9332	–0.0292	V	G. Samolyk	0.0007
V364 Cas	53314.5557	12301	–0.0218	R	G. Lubcke	0.0002
V364 Cas	56521.8210	14379.5	–0.0233	V	G. Samolyk	0.0003
V366 Cas	56215.3183	28987	0.3846	V	Y. Ogmen	0.0001
V375 Cas	56554.6248	14872	0.1983	V	G. Samolyk	0.0002
V380 Cas	56528.8256	22754	–0.0692	V	G. Samolyk	0.0006
V952 Cas	56202.2819	1629	0.0136	V	Y. Ogmen	0.0001
V1115 Cas	55934.5451	7876	–0.0560	V	G. Lubcke	0.00064
V1115 Cas	55934.5458	7876	–0.0552	I	G. Lubcke	0.00043
V1115 Cas	55935.5155	7879	–0.0554	I	G. Lubcke	0.00104
V1115 Cas	55935.5162	7879	–0.0547	V	G. Lubcke	0.00017
SU Cep	56565.6755	33548	0.0064	V	G. Samolyk	0.0002
WZ Cep	53270.5847	60439	–0.0566	R	G. Lubcke	0.0001
WZ Cep	56460.8533	68081.5	–0.1274	V	G. Samolyk	0.0005
XX Cep	56222.5805	4870	–0.0022	V	N. Simmons	0.0002
DK Cep	56530.6668	23268	0.0337	V	G. Samolyk	0.0001
DL Cep	54001.5746	12300	0.0503	R	G. Lubcke	0.0003
DL Cep	56497.8494	13831	0.0587	V	G. Samolyk	0.0002
DV Cep	56493.7250	8374	–0.0050	V	G. Samolyk	0.0001
EG Cep	56446.8518	25435	0.0131	V	G. Samolyk	0.0002

Table continued on following pages

Table 1. Recent times of minima of stars in the AAVSO eclipsing binary program, cont.

Star	HJD 2400000+	Cycle	O–C (day)	F	Observer	Standard Error (day)
EG Cep	56529.6341	25587	0.0128	V	N. Simmons	0.0001
SS Cet	56565.8710	4746	0.0519	V	G. Samolyk	0.0001
TT Cet	56271.6154	48823	–0.0688	V	R. Poklar	0.0001
TT Cet	56538.8898	49373	–0.0705	V	N. Simmons	0.0001
RW Com	53110.5951	55144	–0.0236	R	G. Lubcke	0.0001
RW Com	53830.5882	58177.5	–0.0192	R	G. Lubcke	0.0001
RW Com	56336.7388	68736.5	–0.0040	V	G. Samolyk	0.0002
RW Com	56386.7013	68947	–0.0028	V	R. Poklar	0.0002
RW Com	56413.6396	69060.5	–0.0032	V	K. Menzies	0.0001
RW Com	56427.6433	69119.5	–0.0029	V	K. Menzies	0.0001
RZ Com	56384.7296	63654	0.0463	V	K. Menzies	0.0001
SS Com	56336.8914	75906.5	0.7930	V	G. Samolyk	0.0002
SS Com	56376.7290	76003	0.7962	V	R. Poklar	0.0003
SS Com	56414.7086	76095	0.7990	V	K. Menzies	0.0001
SS Com	56451.6560	76184.5	0.8015	V	G. Samolyk	0.0002
CC Com	56316.7551	76050	–0.0195	V	K. Menzies	0.0002
CC Com	56384.6165	76357.5	–0.0191	V	K. Menzies	0.0001
RW CrB	56451.6582	21613	–0.0016	V	G. Samolyk	0.0002
W Crv	56385.7100	43130	0.0178	V	R. Poklar	0.0002
RV Crv	56340.8718	20490.5	–0.0814	V	G. Samolyk	0.0003
Y Cyg	56498.6980	15701	–0.1425	V	G. Samolyk	0.0004
SW Cyg	56487.7893	3197	–0.3377	V	G. Samolyk	0.0001
WW Cyg	56515.6272	4864	0.1128	V	G. Samolyk	0.0002
ZZ Cyg	56488.8867	18276	–0.0644	V	R. Sabo	0.0001
ZZ Cyg	56526.6040	18336	–0.0640	V	K. Menzies	0.0001
AE Cyg	56525.6411	12319	–0.0048	V	G. Samolyk	0.0002
CG Cyg	56176.3073	26541	0.0719	V	Y. Ogmen	0.0001
CG Cyg	56462.8438	26995	0.0704	V	G. Samolyk	0.0001
DK Cyg	56565.6045	39444	0.1026	V	G. Samolyk	0.0002
KR Cyg	53300.5788	28627	0.0081	R	G. Lubcke	0.0001
KR Cyg	56487.6559	32398	0.0181	V	G. Samolyk	0.0001
KV Cyg	56492.8251	9519	0.0560	V	G. Samolyk	0.0002
V346 Cyg	56527.6329	7597	0.1695	V	G. Samolyk	0.0004
V387 Cyg	56558.6428	44604	0.0200	V	G. Samolyk	0.0001
V388 Cyg	56515.6363	16952	–0.0996	V	G. Samolyk	0.0003
V401 Cyg	53283.5671	16214	0.0536	R	G. Lubcke	0.0002
V401 Cyg	56541.5867	21805	0.0745	V	K. Menzies	0.0001
V401 Cyg	56555.5733	21829	0.0758	V	K. Menzies	0.0001

Table continued on following pages

Table 1. Recent times of minima of stars in the AAVSO eclipsing binary program, cont.

Star	*HJD 2400000+*	*Cycle*	*O–C (day)*	*F*	*Observer*	*Standard Error (day)*
V456 Cyg	56490.6622	12993	0.0489	V	G. Samolyk	0.0001
V466 Cyg	53584.6296	17829	0.0052	R	G. Lubcke	0.0003
V466 Cyg	56511.7906	19932.5	0.0065	V	K. Menzies	0.0001
V466 Cyg	56562.5831	19969	0.0069	V	G. Samolyk	0.0002
V477 Cyg	56522.6688	5255	–0.0307	V	G. Samolyk	0.0002
V548 Cyg	53251.5955	4872	0.0045	R	G. Lubcke	0.0003
V548 Cyg	56522.7040	6684	0.0308	V	G. Samolyk	0.0003
V548 Cyg	56522.7048	6684	0.0316	V	N. Simmons	0.0001
V704 Cyg	56498.7353	32520	0.0322	V	G. Samolyk	0.0002
V1034 Cyg	56523.6664	13906	0.0049	V	N. Simmons	0.0002
V1034 Cyg	56525.6209	13908	0.0056	V	G. Samolyk	0.0003
TT Del	54003.6168	3055	–0.0707	V	G. Lubcke	0.0001
TT Del	56515.8116	3930	–0.1051	V	G. Samolyk	0.0002
TY Del	56497.8528	11366	0.0596	V	G. Samolyk	0.0001
YY Del	56488.8818	17059	0.0100	V	G. Samolyk	0.0003
YY Del	56508.7090	17084	0.0099	V	R. Sabo	0.0001
YY Del	56539.6395	17123	0.0098	V	G. Samolyk	0.0001
YY Del	56562.6389	17152	0.0095	V	N. Simmons	0.0001
YY Del	56562.6391	17152	0.0097	V	B. Manske	0.0001
FZ Del	56521.8106	32172	–0.0342	V	G. Samolyk	0.0001
RZ Dra	56446.6745	22272	0.0577	V	G. Samolyk	0.0002
TW Dra	56424.6753	4378	0.0041	V	G. Samolyk	0.0003
UZ Dra	56428.7796	4556	0.0029	V	G. Samolyk	0.0001
AI Dra	56436.6585	10965	0.0294	V	G. Samolyk	0.0001
BV Eri	56285.3244	25284	–0.1852	V	L. Corp	0.0005
TX Gem	56284.9589	13013	–0.0353	V	G. Samolyk	0.0003
WW Gem	56274.7584	24471	0.0284	V	N. Simmons	0.0001
SZ Her	56451.7910	17831	–0.0246	V	G. Samolyk	0.0001
SZ Her	56479.6060	17865	–0.0249	V	K. Menzies	0.0001
TT Her	56492.6565	18087	0.0397	V	G. Samolyk	0.0002
TU Her	56436.7956	5459	–0.2221	V	G. Samolyk	0.0001
AK Her	56506.4228	33972	0.0171	V	L. Corp	0.0001
CC Her	56460.6944	9684	0.2402	V	G. Samolyk	0.0001
DQ Her	51000.6959	82872	0.0021	C	J. Hannon	—
DQ Her	51005.7307	82898	0.0027	C	J. Hannon	—
DQ Her	51006.6992	82903	0.0031	C	J. Hannon	—
DQ Her	56178.3156	109613	0.0059	C	Y. Ogmen	0.0001
DQ Her	56184.3188	109644	0.0069	C	Y. Ogmen	0.0001

Table continued on following pages

Table 1. Recent times of minima of stars in the AAVSO eclipsing binary program, cont.

Star	HJD 2400000+	Cycle	O–C (day)	F	Observer	Standard Error (day)
DQ Her	56192.2576	109685	0.0072	C	Y. Ogmen	0.0001
HS Her	56500.4891	6925.5	–0.0010	V	L. Corp	0.0005
V450 Her	56440.7002	33694	–0.356	V	K. Menzies	0.0009
WY Hya	56283.7705	21945	0.0324	V	N. Simmons	0.0001
WY Hya	56364.6796	22058	0.0327	V	R. Poklar	0.0001
AV Hya	56284.9805	28697	–0.1032	V	G. Samolyk	0.0002
DF Hya	56336.7983	40982.5	–0.0068	V	G. Samolyk	0.0001
DF Hya	56349.6917	41021.5	–0.0070	V	R. Poklar	0.0001
DK Hya	56366.6866	25910	0.0033	V	R. Poklar	0.0002
SW Lac	54013.6122	27246	–0.0972	R	G. Lubcke	0.0005
SW Lac	56508.6617	35025.5	–0.0959	V	G. Samolyk	0.0001
SW Lac	56519.5655	35059.5	–0.0966	V	L. Corp	0.0003
SW Lac	56534.8004	35107	–0.0959	V	R. Sabo	0.0001
SW Lac	56563.6657	35197	–0.0955	V	G. Samolyk	0.0001
SW Lac	56564.7885	35200.5	–0.0952	V	K. Menzies	0.0001
VX Lac	56527.8435	10488	0.0823	V	G. Samolyk	0.0001
AW Lac	56539.6516	26176	0.1932	V	G. Samolyk	0.0005
CM Lac	53999.5748	16809	–0.0024	V	G. Lubcke	0.0002
CM Lac	56552.6377	18400	–0.0037	V	G. Samolyk	0.0001
DG Lac	56554.6288	5459	–0.2273	V	K. Menzies	0.0001
Y Leo	56284.7997	6434	–0.0316	V	G. Samolyk	0.0001
UV Leo	56284.8859	29736	0.0386	V	N. Simmons	0.0001
UV Leo	56397.7022	29924	0.0389	V	K. Menzies	0.0001
XY Leo	56408.6368	39895	0.1004	V	N. Simmons	0.0002
EX Leo	56354.3966	9432.5	0.0059	R	L. Corp	0.0008
UW LMi	56015.3613	1332	0.010	R	L. Corp	0.0008
SS Lib	56428.7870	10621	0.1471	V	G. Samolyk	0.0002
δ Lib	56447.6820	5795	–0.0356	V	G. Samolyk	0.0004
EW Lyr	56451.8217	15370	0.2522	V	G. Samolyk	0.0001
EW Lyr	56459.6166	15374	0.2522	V	K. Menzies	0.0001
FL Lyr	56537.6505	8409	–0.0023	V	G. Samolyk	0.0001
RU Mon	56336.6083	4071	–0.0996	V	G. Samolyk	0.0001
RW Mon	56284.7431	11859	–0.0752	V	N. Simmons	0.0001
AT Mon	56334.6813	14651	0.0093	V	R. Poklar	0.0002
BB Mon	56331.6811	40467	–0.0040	V	R. Poklar	0.0001
V753 Mon	56340.3866	5374.5	–0.0038	V	L. Corp	0.0004
U Oph	56464.7631	7183	–0.0008	V	G. Samolyk	0.0010
SX Oph	56481.7345	11187	–0.0021	V	G. Samolyk	0.0004

Table continued on following pages

Table 1. Recent times of minima of stars in the AAVSO eclipsing binary program, cont.

Star	*HJD 2400000+*	*Cycle*	*O–C (day)*	*F*	*Observer*	*Standard Error (day)*
V508 Oph	56486.6926	33075.5	–0.0225	V	B. Manske	0.0003
V508 Oph	56520.6555	33174	–0.0216	V	G. Samolyk	0.0002
V839 Oph	56451.8575	39128	0.2757	V	G. Samolyk	0.0002
V1010 Oph	56462.7595	26496	–0.1562	V	N. Simmons	0.0003
ER Ori	53043.6078	26965.5	0.0352	R	G. Lubcke	0.0001
ER Ori	56283.7372	34618	0.1060	V	G. Samolyk	0.0001
ER Ori	56297.7105	34651	0.1071	V	N. Simmons	0.0001
FR Ori	56310.6118	32212	0.0330	V	N. Simmons	0.0001
FZ Ori	56340.5949	30791.5	–0.0508	V	N. Simmons	0.0001
FZ Ori	56340.5954	30791.5	–0.0503	V	G. Samolyk	0.0002
FZ Ori	56355.5943	30829	–0.0509	V	N. Simmons	0.0003
GU Ori	56309.6355	28129	–0.0533	V	R. Sabo	0.0002
GU Ori	56325.6381	28163	–0.0539	V	R. Poklar	0.0003
U Peg	56506.4828	53351	–0.1500	R	L. Corp	0.0003
U Peg	56535.9037	53429.5	–0.1494	V	R. Sabo	0.0004
TY Peg	56283.5847	5120	–0.3657	V	G. Samolyk	0.0001
TY Peg	56558.7808	5209	–0.3772	V	G. Samolyk	0.0001
UX Peg	56549.7275	10439	–0.0084	V	G. Samolyk	0.0001
BB Peg	56490.8255	35204.5	–0.0086	V	G. Samolyk	0.0001
BB Peg	56552.6414	35375.5	–0.0095	V	B. Manske	0.0004
BB Peg	56552.8218	35376	–0.0099	V	B. Manske	0.0004
BB Peg	56562.5820	35403	–0.0102	V	G. Samolyk	0.0002
BG Peg	56539.8421	5638	–2.1113	V	B. Manske	0.0005
BX Peg	56487.7941	43836	–0.1092	V	G. Samolyk	0.0001
BX Peg	56554.5350	44074	–0.1084	V	K. Menzies	0.0001
DI Peg	53285.5554	11364	–0.0187	R	G. Lubcke	0.0001
DI Peg	53317.5875	11409	–0.0184	R	G. Lubcke	0.0001
DI Peg	56537.8635	15933	–0.0016	V	G. Samolyk	0.0001
DI Peg	56557.7934	15961	–0.0025	V	B. Manske	0.0003
DI Peg	56565.6246	15972	–0.0013	V	B. Manske	0.0001
GP Peg	56498.8932	15642	–0.0500	V	R. Sabo	0.0002
GP Peg	56541.8199	15686	–0.0505	V	K. Menzies	0.0001
GP Peg	56560.3557	15705	–0.0514	V	L. Corp	0.0005
Z Per	56557.7713	3566	–0.2630	V	G. Samolyk	0.0002
RT Per	56266.6281	26949	0.0806	V	N. Simmons	0.0001
RT Per	56552.8805	27286	0.0851	V	G. Samolyk	0.0001
RV Per	56565.8969	7357	–0.0018	V	G. Samolyk	0.0002
XZ Per	56520.8743	11300	–0.0687	V	G. Samolyk	0.0001

Table continued on following pages

Table 1. Recent times of minima of stars in the AAVSO eclipsing binary program, cont.

Star	HJD 2400000+	Cycle	O–C (day)	F	Observer	Standard Error (day)
KW Per	56287.5545	14908	0.0157	V	K. Menzies	0.0002
V432 Per	56284.6404	63480	0.3652	V	G. Samolyk	0.0001
V432 Per	56284.6409	63480	0.3657	V	N. Simmons	0.0002
V432 Per	56522.8653	64221	0.3460	V	G. Samolyk	0.0002
RV Psc	56303.5199	57622	–0.0554	V	K. Menzies	0.0001
RV Psc	56521.7909	58016	–0.0571	V	N. Simmons	0.0002
RV Psc	56557.8007	58081	–0.0567	V	G. Samolyk	0.0001
RV Psc	56566.6651	58097	–0.0562	V	R. Poklar	0.0002
U Sge	56541.6704	11658	–0.0011	V	G. Samolyk	0.0001
V505 Sgr	56474.7542	10156	–0.0801	V	G. Samolyk	0.0007
RS Ser	56492.6302	36063	0.0561	V	G. Samolyk	0.0004
AO Ser	56462.7196	25393	–0.0142	V	G. Samolyk	0.0001
CC Ser	56382.8559	36628	1.0108	V	K. Menzies	0.0001
CC Ser	56417.6879	36695.5	1.0124	V	K. Menzies	0.0001
RZ Tau	56266.8561	44723	0.0695	V	B. Manske	0.0002
RZ Tau	56562.8190	45435	0.0720	V	B. Manske	0.0002
SV Tau	46131.521	5403	–0.016	C	S. Cook	—
SV Tau	49028.701	6740	0.012	C	S. Cook	—
SV Tau	50092.629	7231	–0.011	C	S. Cook	—
TY Tau	56316.5998	32602	0.2608	V	K. Menzies	0.0002
WY Tau	56348.5674	27349	0.0599	V	N. Simmons	0.0002
CT Tau	56283.6360	16315	–0.0593	V	N. Simmons	0.0001
CU Tau	52306.5962	–469.5	–0.0344	V	S. Dvorak	0.0003
CU Tau	52332.5859	–406.5	–0.0334	V	S. Dvorak	0.0003
CU Tau	52644.6572	350	–0.0324	V	S. Dvorak	0.0002
EQ Tau	56276.6458	47058.5	–0.0266	V	K. Menzies	0.0001
V Tri	56523.9654	54766.5	–0.0076	V	R. Sabo	0.0003
V Tri	56558.7864	54826	–0.0063	V	G. Samolyk	0.0003
X Tri	56294.5515	14196	–0.0832	V	N. Simmons	0.0001
X Tri	56522.8611	14431	–0.0844	V	G. Samolyk	0.0001
X Tri	56558.8077	14468	–0.0846	V	G. Samolyk	0.0001
RS Tri	56565.8068	9757	–0.0488	V	N. Simmons	0.0001
RS Tri	56565.8069	9757	–0.0487	V	B. Manske	0.0001
RS Tri	56565.8071	9757	–0.0485	V	G. Samolyk	0.0003
RV Tri	56287.6574	13606	–0.0367	V	K. Menzies	0.0001
RV Tri	56525.8145	13922	–0.0382	V	G. Samolyk	0.0001
RV Tri	56562.7438	13971	–0.0386	V	G. Samolyk	0.0001
TY UMa	53115.6091	38311.5	0.2071	R	G. Lubcke	0.0001

Table continued on next page

Table 1. Recent times of minima of stars in the AAVSO eclipsing binary program, cont.

Star	*HJD 2400000+*	*Cycle*	*O–C (day)*	*F*	*Observer*	*Standard Error (day)*
TY UMa	56358.6950	47458.5	0.3284	V	R. Poklar	0.0002
TY UMa	56463.6424	47754.5	0.3323	V	K. Menzies	0.0003
UX UMa	53890.6679	83682	0.0015	R	G. Lubcke	0.0002
UX UMa	56400.7815	96445	–0.0005	V	K. Menzies	0.0001
UX UMa	56454.6692	96719	–0.0007	V	G. Samolyk	0.0001
W UMi	56431.7247	13373	–0.1789	V	G. Samolyk	0.0005
VV Vir	56428.7366	56502	–0.0447	V	G. Samolyk	0.0001
AH Vir	56340.9062	25830	0.2538	V	G. Samolyk	0.0003
AH Vir	56400.6098	25976.5	0.2555	V	K. Menzies	0.0001
AW Vir	56398.7174	32136	0.0264	V	R. Poklar	0.0001
AW Vir	56451.6414	32285.5	0.0279	V	G. Samolyk	0.0002
AX Vir	56393.7064	41028	0.0175	V	R. Poklar	0.0002
AZ Vir	56418.6491	35583	–0.0245	V	K. Menzies	0.0001
AZ Vir	56447.6718	35666	–0.0240	V	G. Samolyk	0.0004
BH Vir	56406.7384	16130	–0.0097	V	R. Poklar	0.0001
AW Vul	56563.6713	12745	–0.0169	V	G. Samolyk	0.0001
AX Vul	56536.6754	5770	–0.0333	V	G. Samolyk	0.0002
AY Vul	56520.6497	5735	–0.1097	V	G. Samolyk	0.0004
AY Vul	56549.5992	5747	–0.1096	V	G. Samolyk	0.0001
BE Vul	56508.8140	10565	0.0881	V	G. Samolyk	0.0001
BO Vul	56463.8274	10522	–0.0372	V	G. Samolyk	0.0001
BS Vul	56457.8622	27704	–0.0294	V	G. Samolyk	0.0002
BT Vul	56508.6790	18495	0.0050	V	G. Samolyk	0.0002
BU Vul	56497.6865	40359	0.0150	V	G. Samolyk	0.0001
BU Vul	56558.5678	40466	0.0141	V	G. Samolyk	0.0002
CD Vul	56528.6967	14962	–0.0010	V	G. Samolyk	0.0002

The Naked-eye Optical Transient OT 120926

Yue Zhao
Cuiying Honors College, Lanzhou University, Lanzhou, Gansu, China

and

Department of Physics and Astronomy, York University, 128 Petrie Science and Engineering Building, 4700 Keele Street, Toronto, Ontario, M3J 1P3, Canada; zhao.yue32012@gmail.com

Patrick B. Hall
Paul Delaney
J. Sandal
Department of Physics and Astronomy, York University, 128 Petrie Science and Engineering Building, 4700 Keele Street, Toronto, Ontario, M3J 1P3, Canada

Received October 21, 2013; revised November 6, 2013; accepted November 6, 2013

Abstract A previously unknown optical transient has been observed in the constellation Bootes. The transient flared to brighter than 5th magnitude, which is comparable to the visual magnitudes of the nearby stars π Boo and ο Boo. This article describes the relative astrometry and photometry work we have done regarding the transient.

1. Introduction

Distant astronomical sources normally invisible to the naked eye which transiently brighten by more than a magnitude to naked-eye visibility ($V < 6$) are of considerable scientific interest. Specific examples include a flare on the Be star HD 160202 (peak $V \sim 1$, Bakos 1969), SN 1987A (peak $V = 2.96$, Hamuy *et al.* 1988), GRB 080319B (peak $V = 5.3$, Cwiok *et al.* 2008, Bloom *et al.* 2009), and possibly OT 060420 (apparent peak $V = 4.7$, Shamir and Nemiroff 2006). Cataclysmic variable eruptions and flares on M dwarf stars can also in principle create naked-eye transients. M dwarf flares can have peak brightenings, in units of magnitudes of $\Delta V = 6$ (Stelzer *et al.* 2006, Kowalski *et al.* 2013) and even $\Delta V = 9$ (Stanek *et al.* 2013, Schmidt *et al.* 2013) or $\Delta B = 9.5$ (Schaefer 1990). Cataclysmic variables such as classical novae or dwarf novae of the WZ Sge subtype can brighten by up to $\Delta V = 7.5$ magnitudes (Harrison *et al.* 2004). Superflares on main sequence stars usually have $\Delta V < 1$ magnitude (Schaefer *et al.* 2000), though examples of increases up to $\Delta V = 7$ are known (Schaefer 1989). Superflares may be due to reconnection events between the magnetic fields of the star and a close-in giant planet (Rubenstein and Schaefer 2000, Rubenstein 2001).

In part, because of the rarity of reports of naked-eye transients, current limits on the rate of their occurrence on the sky are not strong (Shamir and Nemiroff 2009). Current and future large-area sky surveys will reveal more and more of these bright transients. Until then, studies of the transient naked-eye sky must rely on whatever images are available.

At York University, students in the introductory Natural Sciences course on Astronomy have taken photographs of assigned constellations each fall for over a decade. Here we report the details of our discovery (Zhao *et al.* 2013) of a naked-eye transient in photographs taken by one of those students.

2. Discovery

The constellation Bootes was observed from Brampton, Ontario, Canada (79.7667 W, 43.6833 N), by J. Sandal on the evening of 2012 September 25 local time (MJD 56195; UTC 2012 September 26) using a Sony DSC-W570 18.2 Mpix handheld digital camera. These unfiltered observations reveal an optical transient (hereafter referred to as OT 120926) flaring to brighter than 5th magnitude, close in brightness to π Bootes and ο Bootes. The transient's altitude was between 20 and 30 degrees at the times of observation.

There are two photographs taken on the night of observation suitable for analyzing the properties of the transient. Image DSC1875 (Figure 1) had an exposure time of 0.125 second, and stars in it possess a slightly elongated point spread function with a FWHM of about 10 pixels. Image DSC1861 had an exposure time of 2 seconds, and stars in it appear as complicated trails (spanning approximately 13 by 18 pixels) due to camera motion (Figure 2). Information on the two images is given in Table 1; the pixel scale was determined from the separation of π Boo and ο Boo. OT 120926, π Boo, and ο Boo are approximately equally spaced in a straight line on the sky with π Boo in the middle and OT 120926 to the west, as seen in the close-up images in Figure 3.

A third photograph (DSC1864), taken in between the other two at 00:23:14 (UTC), does also show the transient to be present. However, its poor point spread function and low resolution of about 300 arc seconds per pixel makes it useless for detailed analysis. All we can conclude from that image is that the transient is not brighter than π Boo in it. All three images of this transient are available on nova.astrometry.net by searching for "Bootes flare."

The two pictures taken at different time with different rotation angles of the camera on the sky show that OT 120926 has an unchanged position relative to π Boo and ο Boo. That excludes the possibility that OT 120926 is a reflection of Arcturus: if OT 120926 was such an artifact, it would have appeared at a different location on the sky when the camera was rotated. Prof. Bradley Schaefer (2013), who has considerable experience investigating flare phenomena in non-flare stars, also agrees with our assessment based on the identity in the shape, size, and orientation of the hand-held jitter, and also the fact that positions of the

transient in both images agree to good accuracy. Including the transient, eighteen objects are visible in DSC1861 (one very faintly) and fourteen in DSC1875. Inspection of the images reveals no other objects which cannot be identified with known stars.

3. All-sky camera searches

We searched for the transient on images from the all-sky camera operated by The Liverpool Telescope Project (Steele *et al.* 2004) on the island of La Palma, Spain. We scrutinized images taken between 19:41:14 and 20:05:14 on September 25th 2012 (UTC), which is several hours before the transient was observed in Ontario. Because of moonlight, we smoothed, shifted, and combined several images together before seeking around Bootes for the transient. We did not find any object at the anticipated position with brightness comparable to π Boo and ο Boo, from which we concluded that those images were taken before the transient brightened to the magnitude observed later.

We also examined images from other all-sky cameras. Images from the West Acton Observatory in Acton, Massachusetts, spanning the time of the transient's appearance in our images do not show the transient. However, its brightness is limited to $V > 2.2$ (fainter than α CrB) at best. Images are also available from the Kitt Peak National Observatory and MMT Observatory (Pickering 2006) beginning approximately UTC 02:00 on September 26th 2012. They do not show the transient, but the limit on its brightness is only $V > 2.2$ from Kitt Peak and worse on the lower-resolution MMTO images.

Scrutiny of the Liverpool all-sky camera images taken the next night (UTC September 26th 2012 between 19:40:13 and 20:04:15) also shows no sign of the transient.

4. Position measurement

In image DSC1861, the stars have the shape of a seeing disk trailed in a complicated pattern due to camera motion. We used IRAF (Image Reduction and Analysis Facility) task "imedit" to isolate only the sharpest part of each object trail, which is shown in Figure 2.

We calculated the coordinates of OT 120926 via a local linear transformation between pixel and equatorial coordinate systems, using the known coordinates of π Boo and ο Boo. Our approach assumes the two coordinate systems are locally Cartesian near π Boo, with the equatorial system having only a rotation angle and a scale difference relative to the pixel system. We solved for the coordinates of OT 120926 on the processed image DSC1861 and the image DSC1875 separately using the IRAF task "geomap" with the parameter "fitgeo=rscale." These coordinates and their weighted average are given in Table 2.

5. Magnitude of the transient

On our unfiltered images, the transient OT 120926 was of similar brightness to o Boo but not as bright as π Boo (which is a blended binary). o Boo and π Boo have nearly identical V-band magnitudes (V=4.61 and V=4.51, respectively), but in the B band, o Boo (B=5.56) is fainter than π Boo (B=4.59).

The unfiltered relative magnitudes of o Boo and π Boo in our images are consistent with the camera responding to the average flux in the B and V bands. We used those average fluxes with the V band zeropoint to calculate "BV" magnitudes for o Boo and π Boo (4.98 and 4.55, respectively). In both of our images, we measured the magnitude of OT 120926 relative to o Boo and π Boo and averaged to obtain the "BV" magnitude and associated RMS uncertainty of OT 120926 shown in Table 3.

The decline of about one magnitude in the half an hour between our images is less steep than observed in gamma-ray bursts (Bloom *et al.* 2009). The decline is consistent with the range seen in flares on M dwarfs during the gradual decay phase after peak brightness (Kowalski *et al.* 2013). If OT 120926 was an M dwarf flare, a fast rise phase may have been missed wherein it could have up to 2.5 magnitudes brighter than in our first image.

We obtain an upper limit to the magnitude of the transient approximately four hours before its detection based on an average image from the Liverpool all-sky camera. We shifted ten images to align π Boo in all of them, subtracted a heavily smoothed version of each image from itself, and then averaged those background-subtracted images together. OT 120926 is not detected in the average image, and because o Boo is the faintest object detected on the average image, the magnitude of OT 120926 must be larger than that of o Boo. This magnitude limit is shown in Figure 4 with an error bar extending off the plot, while the two measured magnitudes of OT 120926 are shown as points with error bars.

6. Candidate identifications for OT 120926 in quiescence

No known variable star is listed in the *General Catalogue of Variable Stars* (GCVS; Samus *et al.* 2010) within one degree of the transient. There are three stars that may be responsible for the transient when we search for candidates on SIMBAD centered on the calculated coordinates within a radius of 5 arcmin. Information on these three candidates, plus one other identified in the SDSS, is listed in Table 4, including their distance from OT 120926 in units of the random uncertainty (sigma) on the position of OT 120926. Objects labeled in Table 3 are shown in a finding chart in Figure 5.

We used the databases of the CRTS (Catalina Real-time Transient Survey; Drake *et al.* 2009) and the ASAS (All-sky Automated Survey; Pojmański 1997) to search for photometric light curves of these objects.

The object SDSS J1436+1553 (SDSS J143627.19+155326.8 = ASAS 143627+1553.5) was taken into consideration because of its relative proximity to OT 120926. In the CRTS, this object has a constant magnitude around 14.0, which is consistent within the errors with the result given by the ASAS.

The red, high proper motion star LP 440-48 (Luyten 1981) has a magnitude of 15.9 in the CRTS, with no sign of variability. It is not found in the ASAS.

When comparing the photometry results from the CRTS and ASAS on the objects BD +16 2617 and TYC 1477-341-1, there emerged a large discrepancy. There are no conspicuous changes in their magnitudes judging from the ASAS light curves, but the CRTS results suggest three to four magnitudes of variability in both objects. In fact, CRTS photometry data for these objects are untrustworthy because the objects are often saturated.

We also searched for variable objects within a radius of 5 arcmin around OT 120926. We found one object (CSS J143625.1+155102) with apparent variability which, however, is due to its proximity to a much brighter star. There are no useful data available in ASAS for this object.

We examined cutouts of the CRTS images at the location of OT 120926 (kindly provided by A. Drake), but found no evidence for an uncatalogued variable object in them.

Examination of the POSS-I and POSS-II plates within a 6 arc minute radius of the transient's coordinates did not reveal any objects with dramatic variability. (Note that the POSS-I O plate has at least six point-like defects within a 6 arc minute radius which are spurious, as they do not correspond to the positions of any objects in the SDSS images of the region.)

Examination of GALEX images of the field did not reveal any objects with unusual ultraviolet-optical colors. The star BD +16 2617 is much brighter in the UV than TYC 1477-341-1, but both stars have UV-optical colors consistent with expectations for stars with their optical colors. The star LP 440-48 is not detected by GALEX, and the star SDSS J1436+1553 is barely detected.

Examination of the HEASARC X-ray and gamma-ray satellite databases did not reveal any X-ray sources near the position of the transient, nor any gamma-ray burst consistent with its location and time of appearance.

7. Conclusion

The optical transient OT 120926 flared to naked-eye brightness for at least half an hour, but was not at naked-eye brightness several hours before the observation. Database searches at its position yield no unambiguous identification of a quiescent counterpart of this transient, but do identify several candidates. A flare on the high proper motion, probable M dwarf star LP 440-48 could have produced OT 120926, but the amplitude of the flare would be an unprecedented 11.3 magnitudes, as compared to the previous record amplitude of 9.5 magnitudes (Schaefer 1990). OT 120926 could be an

outburst from a previously unrecognized cataclysmic variable identified with LP 440-48 or one of two brighter stars in our error circle. If the latter is the case, the outburst would be 6.8 to 7.3 magnitudes, consistent with the known range of CV outburst amplitudes (Harrison *et al.* 2004). However, none of the candidate stellar counterparts of OT 120926 have shown any credible evidence of previous variability in the ASAS or CRTS. Spectroscopy of the possible counterparts of OT 120926 is needed as a next step to identifying its quiescent counterpart and determining the nature of this remarkable event.

8. Acknowledgements

We thank K. Stanek, A. Drake, C. Kochanek, and J. L. Prieto for archival searches and suggestions, P. Lloyd for initial conversations regarding this object, Joe Kristl for all-sky images from West Acton Observatory, and the referee for a thorough and speedy review.

Y. Zhao was supported at York University by the MITACS Globalink program. P. Hall thanks NSERC for research support.

The Liverpool Telescope is operated on the island of La Palma by Liverpool John Moores University in the Spanish Observatorio del Roque de los Muchachos of the Instituto de Astrofisica de Canarias with financial support from the UK Science and Technology Facilities Council. Kitt Peak National Observatory, National Optical Astronomy Observatory, is operated by the Association of Universities for Research in Astronomy (AURA) under cooperative agreement with the National Science Foundation. The Image Reduction and Analysis Facility (IRAF) is also distributed by NOAO. MMT Observatory is a joint facility of the University of Arizona and the Smithsonian Institution.

References

Bakos, G. 1969, in *Non-Periodic Phenomena in Variable Stars*, ed. L. Detre, Reidel, Dordrecht, 159.

Bloom, J. S., *et al.* 2009, *Astrophys. J.*, **691**, 723.

Cwiok, M., *et al.* 2008, *GRB Coordinates Network, Circular Service*, No. 7445, 1.

Drake, A. J., *et al.* 2009, *Astrophys. J.*, **696**, 870.

Hamuy, M., Suntzeff, N. B., Gonzalez, R., and Martin, G. 1988, *Astron. J.*, **95**, 63.

Harrison, T. E., Johnson, J. J., McArthur, B. E., Benedict, G. F., Szkody, P., Howell, S. B., and Gelino, D. M. 2004, *Astron. J.*, **127**, 460.

Kowalski, A. F., Hawley, A. L., Wisniewski, J. P., Osten, R. A., Hilton, E. J., Holtzman, J. A., Schmidt, S. J., and Davenport, J. R. A. 2013, *Astrophys. J., Suppl. Ser.*, **207**, 15.

Luyten, W. J. 1981, *Proper motion survey with the 48-inch Schmidt telescope. LVII. The stars of large proper motion*, Univ. Minnesota, Minneapolis.

Pickering, T. E. 2006, in *Ground-based and Airborne Telescopes*, ed. L. M. Stepp, Proc. SPIE, 6267A, 42.

Pojmański, G. 1997, *Acta Astron.*, **47**, 467.
Rubenstein, E. P. 2001, *Amer. Sci.*, **89**, 38.
Rubenstein, E. P., and Schaefer, B. E. 2000, *Astrophys. J.*, **529**, 1031.
Samus, N. N., Kazarovets, E. V., Kireeva, N. N., Pastukhova, E. N., and Durlevich, O. V. 2010, *General Catalogue of Variable Stars: Current Status and New Name-Lists*, *Odessa Astron. Publ.*, **23**, 102.
Schaefer, B. E. 1989, *Astrophys. J.*, **337**, 927.
Schaefer, B. E. 1990, *Astrophys. J., Lett.*, **353**, L25.
Schaefer, B. E. 2013, private communication.
Schaefer, B. E., King, J. R., and Deliyannis, C. P. 2000, *Astrophys. J.*, **529**, 1026.
Schmidt, S. J., *et al.* 2013, *Astrophys. J., Lett.*, submitted (arXiv:1310.4515).
Shamir, L., and Nemiroff, R. J. 2006, *Publ. Astr. Soc. Pacific*, **118**, 1180.
Shamir, L., and Nemiroff, R. J. 2009, *Astron. J.*, **138**, 956.
Stanek, K. Z., *et al.* 2013, *Astron. Telegram*, 5276, 1.
Steele, I. A., *et al.* 2004, in *Ground-based Telescopes*, ed. J. M. Oschmann, Jr., Proc. SPIE, 5489, 679.
Stelzer, B., Schmitt, J. H. M. M., Micela, G., and Liefke, C. 2006, *Astron. Astrophys.*, 460, L35.
Zhao, Y., Hall, P. B., Delaney, P., and Sandal, J. 2013, *Astron. Telegram*, 5287, 1.

Table 1. Information on images DSC1861 and DSC1875.

Image Name	*UTC of Observation*	*Exposure Time (seconds)*	*Pixel Scale (arcsec/pixel)*
DSC1861	2012-09-26 00:17:54	2	146.49±1.94
DSC1875	2012-09-26 00:45:50	0.125	83.67±1.74

Table 2. Coordinates of OT 120926 derived from images DSC1861 and DSC1875.

Image	*R.A./degrees*	*Dec./degrees*	*R.A. (2000) h m s*	*Dec. (2000) ° ′ ″*
DSC1861	219.1299	15.8928	14 36 31.2	+15 53 34
	±0.0122	±0.0122	±0 02.9	±0 44
DSC1875	219.1359	15.8778	14 36 32.6	+15 52 40
	±0.0116	±0.0232	±0 02.8	±1 24
Average	219.1331	15.8896	14 36 31.9	+15 53 22
	±0.0084	±0.0108	±0 02.0	±0 39

Table 3. The magnitude of OT 120926 relative to π Boo and ο Boo and averaged to obtain the "BV" magnitude and associated RMS uncertainty of OT 120926.

Image	*UTC*	*Magnitude*
Liverpool	2012-09-25 19:51:14–20:00:03	>5
DSC1861	2012-09-26 00:17:54	4.7±0.2
DSC1875	2012-09-26 00:45:50	5.6±0.3

Table 4. Candidate identifications for OT 120926 in quiescence.

Object	*V Magnitude*	*Distance (arcsec)*	*Distance (sigma)*	*R.A. (2000) h m s*	*Dec. (2000) ° ′ ″*
OT 120926	4.70	0.00	0.00	14 36 31.9	+15 53 22
				±0 02.0	±0 39
SDSS J1436+1553	13.99	70.81	2.05	14 36 27.19	+15 53 26.83
BD +16 2671	11.49	132.90	3.85	14 36 21.97	+15 51 09.47
LP 440-48	15.96	182.06	5.27	14 36 41.59	+15 50 20.20
TYC 1477-341-1	12.03	247.51	7.16	14 36 29.56	+15 57 29.50

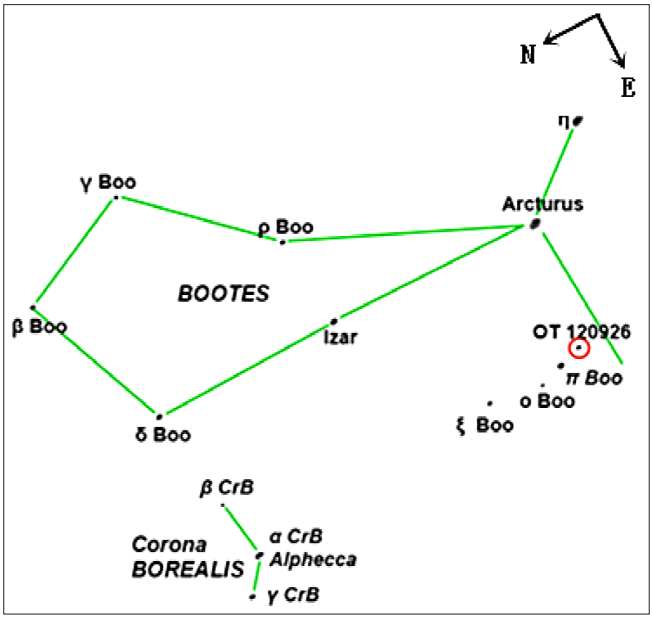

Figure 1. Unfiltered image DSC1875, with constellations sketched. Stars visible in the photo are annotated. The labeled circle indicates the position of OT 120926 near the right edge of the figure.

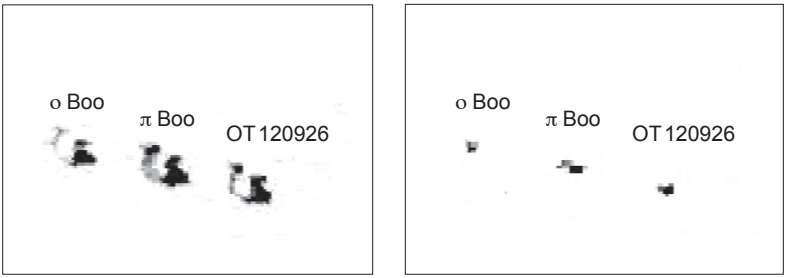

Figure 2. Both unfiltered images above show o Boo (left), π Boo (middle), and OT 120926 (right). The left image is the original version of DSC1861, in which each object has a complicated trail by virtue of camera motion. The region occupied by the trail is approximately 13 × 18 pixels in size. The right image is a processed version in which the unresolved peak at one end of the trail has been isolated.

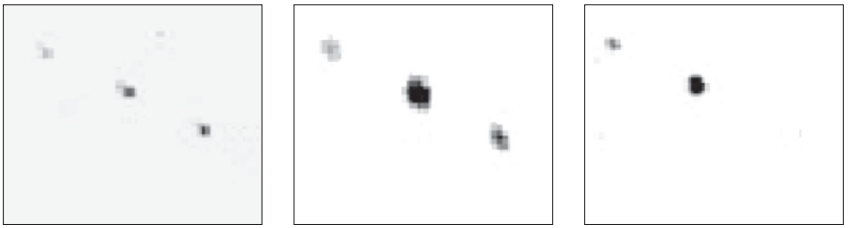

Figure 3. We show o Boo, π Boo, and OT 120926 in our two unfiltered images side by side (DSC1861 on the left, and DSC1875 in the middle), rotated and rebinned to the same pixel scale, with north up and east left. The third image of the same region (right) is from the Palomar Observatory Sky Survey blue plate, magnified to the same scale.

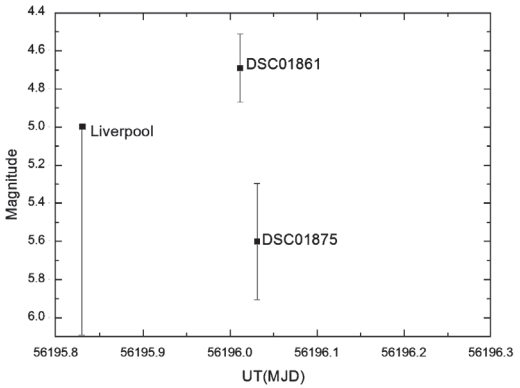

Figure 4. The magnitude of the transient at three different times. Note that the downward error bar on the Liverpool point means the transient's magnitude can be any value larger than 5.

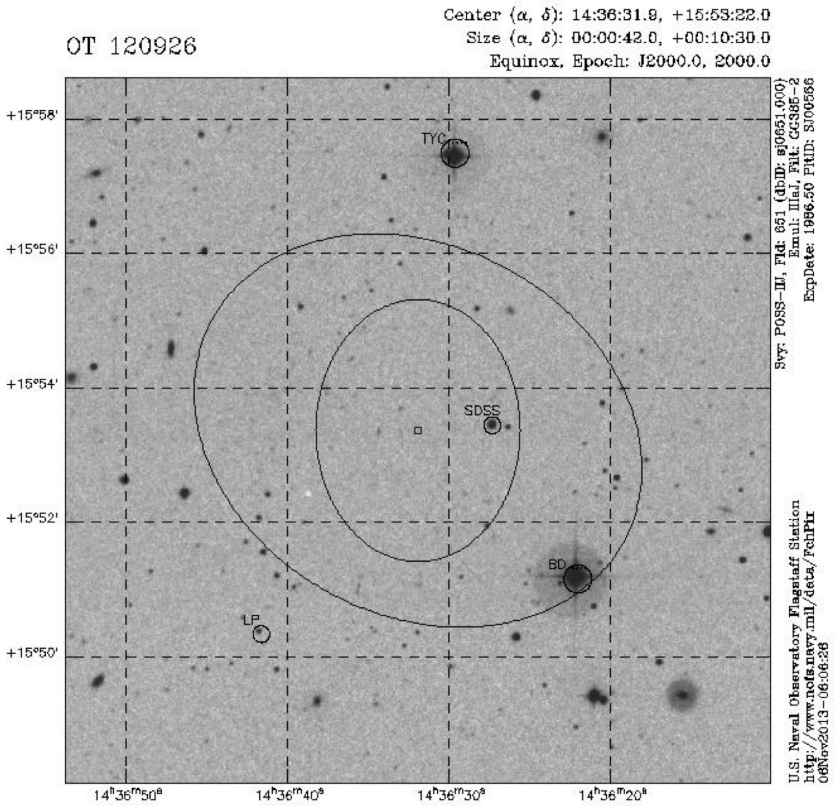

Figure 5. The box on this finding chart shows the weighted average position of OT 120926. The inner ellipse shows the 3-sigma random uncertainty on that position. The outer ellipse incorporates both the 3-sigma random uncertainty and the 3-sigma systematic uncertainty (from the uncertainty on the pixel scale) on the position of OT 120926, added together linearly (not in quadrature). The four objects discussed in the text as possible counterparts are labeled by their IAU prefix.

Maxima and O–C Diagrams for 489 Mira Stars

Thomas Karlsson
Almers väg 19, 432 51 Varberg, Sweden; tkn@seaside.se

Received June 12, 2012; revised November 19, 2012, June 14, 2013, October 23, 2013; accepted October 24, 2013

Abstract Maxima for 489 Mira stars have been compiled. They were computed with data from AAVSO, AFOEV, VSOLJ, and BAA-VSS and collected from published maxima. The result is presented in a MYSQL database and on web pages with O–C diagrams, periods and some statistical information for each star.

1. Introduction

The O(bserved) minus C(alculated) diagram is a well-established technique to study changes in the periods of variable stars. O–C diagrams are sensitive to small changes in a star's period that can be signs of evolutionary changes. For long period variables of the Mira type the O–C method has been used for over 100 years; Cannon and Pickering (1909), for example, published O–C values for the maxima in their large catalogue. But it is only for a few stars certain changes have been noted. Among them are the stars R Aql, R Cen, BH Cru, LX Cyg, W Dra, R Hya, Z Tau, and T UMi (Templeton *et al.* 2005). Zijlstra and Bedding (2002) identified three types of real variations of the periods of Miras: continuously changing, where the period increases or decreases with a steady pace; sudden change, where the period dramatically changes after a long period of stability; and meandering Miras, where the period changes forth and back by up to 10% within fifty years.

A disadvantage with the O–C technique is that random intrinsic changes in the period are added over time and can create random-walk patterns, with a deviation proportional to the square root of N after N cycles. Mira stars are well known for such random cycle-to-cycle variations that make O–C diagrams for these stars hard to interpret (Eddington and Plakidis 1929; Sterne 1934). The recorded time of maximum (or whatever point in the light curve that is used for the O–C) can also differ from the true time of maximum because of sparse or inaccurate data. This type of deviation causes noise but no drift in the diagram. Given these types of noise, a baseline as long as possible is preferred to be able to see real secular or periodic changes.

For this purpose times for maximum of 489 selected Miras have been computed and collected as far back as possible. This collection is in the form of a MYSQL database and presented on web pages in the form of O–C diagrams and period diagrams together with some statistical data. The database and website is

hosted at Astronet.se and can be found at http://var.astronet.se/Mirainfooc.php or can be provided upon request to the author.

The O–C technique was chosen because it is a method that is easy to implement and works well for the older material, where the time of maximum often is the only available information, and it gives a good basic understanding of the star's behavior.

AAVSO has published a similar collection, "AAVSO Maxima and Minima of Long Period Variables, 1900–2008" (Waagen *et al.* 2010), that is also included in the database. The technique used was similar to the one used in this paper, with mean curves fitted to the observations.

2. Data collection

Of the stars in *The General Catalogue of Variable Stars* (GCVS; Kholopov *et al.* 1985) that are of type M, those were selected that were found to have enough combined data for at least twenty maxima to be determined. Two stars that fulfilled this criterion were discarded, Y Per and RZ Sco; both have a more semiregular than Mira-like behavior.

The database contains maxima of two types, those computed from and fitted to individual observations (hereafter fitted maxima) and those collected from published sources (hereafter published maxima). For the fitted maxima, data from the following organizations were used: The American Association of Variable Star Observers (AAVSO); Association Française des Observateurs d'Étoiles Variables (AFOEV); Variable Star Observers League in Japan (VSOLJ); and The British Astronomical Association-Variable Star Section (BAA-VSS).

The published maxima were used to complement the fitted to extend the timeline backward and fill in gaps among the fitted.

2.1. Published maxima

For the published maxima the main data sources are:

- "AAVSO Maxima and Minima of Long Period Variables, 1900–2008" (Waagen *et al.* 2010). This collection has information of date and magnitude for maxima and minima of 394 stars, most Miras but also some semiregulars, from observations made within AAVSO. Hereafter AAVSO maxima.

- *Annals of Harvard College Observatory*, volume 55 (Cannon and Pickering 1909). This paper contains published maxima from many different sources as they were known by 1909.

- *Annals of Harvard College Observatory*, volumes 115 and 118 (Gaposchkin and Payne-Gaposchkin 1952a, 1952b). Maxima determined from photographic plates at Harvard from 1886 to 1947, with the majority

between 1901 and 1940. Variables with a photographic magnitude brighter than 10 and known by 1936 were considered. The time for the maximum is generally rounded to nearest 5 or 10 JD.

Maxima published by various other observers found in *Astronomische Nachrichten*, *Peremennye Zvezdy*, *Mitteilungen über Veränderliche Sterne*, *Geschichte und Literatur des Lichtwechsels der Veränderlichen Sterne*, and other publications are also included.

The maxima were collected from the sources in the order above. For each source all maxima for the selected stars that were not among the fitted or in a previous source were collected. Among the lesser sources the median date was used if the same maximum was found in several sources. The same is for Cannon and Pickering (1909) where the median date was used for the maxima that have dates from several observers. AAVSO maxima use mean curves to determine the maxima; in the other sources the time for maximum light is probably the most common method.

For the AAVSO maxima a mean offset per star was calculated from the maxima that are common between the fitted and AAVSO and added to the AAVSO maxima in the database to make the two sets more consistent.

For stars with double maxima, R Cen and R Nor for example, dates for both primary and secondary maxima are sometimes published. In such cases the date that best matched the fitted was selected.

2.2. Fitted maxima

For the fitted maxima a computer program was developed in VISUAL BASIC 6. The program processes the observations and determines the time and magnitude for the maxima. The output is in form of text files that were imported to a MYSQL database. Here follows a short description of the program.

The periods from GCVS were used as preliminary periods for the stars. For each star, the two points on the mean curve where the rising and falling magnitude were equal and at a distance of 0.8 period were determined (hereafter RP and FP). RP and FP are expressed in number of days before and after maximum. They define the interval around each maximum used in the further process. Several iterations of the fitting were sometimes needed to find these points.

All available data for the selected stars were collected from the AAVSO, AFOEV, VSOLJ, and BAA-VSS. The visual and V-band data were selected and combined, and duplicate observations were removed (many observations were reported to two or more of the organizations). The remaining observations were grouped in one-day bins that were used in the further process. The times for the maxima were then determined in two steps.

For both steps the same algorithm was used to identify the individual maxima. A window with a width of one-third cycle was stepwise moved along the light curve. The brightest observation in the window was found and the

time between when the curve rose above and fell below 0.3 magnitude below this point was used as a preliminary maximum point (PM). The window width was chosen so that adjacent cycles should not interfere when looking for the PM. The observations in the interval PM–RP and PM+FP were then checked for outliers. An eighth-order polynomial was fitted to the observations and all observations 1.5 magnitudes over or under the curve were removed, except for the first and last five observations that always were retained to fix the ends of the curve. The remaining observations were then checked against a set of criteria.

In the first step a maximum had to fulfill the following criteria to be further processed:

- at least a total of fifteen points found;
- at least six points exist both before and after PM;
- the interval includes points at least 1.5 magnitudes below PM, both before and after PM;
- the gap between any two points is not greater than 0.2 of the period.

For the maxima thus detected a new eighth-order polynomial was fitted and a new PM was calculated as the maximum of the fitted curve. The observations in the PM–RP to PM+FP interval were then saved in a new collection with their offset from maximum and magnitude. After all maxima were detected the mean magnitude per day was calculated for this collection and a twelfth-order polynomial was fitted to get the mean light curve for the star, representing a stacked mean from all maxima. These mean light curves are also published and can be found on the web at http://var.astronet.se/Mirainfomax.php.

In the second step the same detection algorithm as in step one was used, but with fewer restrictions. In the first step only well documented maxima are used to build the mean curve; in the second the priority was to find as many, but still well defined, maxima as possible. The criteria for detecting maxima in the second step were:

- at least a total of twelve points found;
- at least five points exist both before and after PM;
- the interval includes points at least 1.4 magnitudes below PM, both before and after PM;
- the gap between any two points is not greater than 0.4 of the period.

The mean light curve from the first step was overlaid on each individual maximum and fitted to the observations in seven iterations. This was done by letting the observations slide step-wise alternately horizontally and vertically

against the mean curve by applying an offset to the time or magnitude. The observations that thus fell outside the RP to FP interval of the mean curve were discarded and for the rest the mean square sum of the differences between the observations and the curve was calculated. In each horizontal turn the best offset was kept and used for the next vertical turn. It was empirically tested that after seven such iterations it was generally not possible to find any better fit. The time and magnitude for the maximum point on the mean curve after the last fit was then recorded as the maximum. Figure 1 shows an example of the fitting process.

A mean curve that covers 80% of the maximum was chosen for several reasons. As a polynomial was used, it is appropriate to have a curve with not too many bends, therefore the curve was truncated before the inflection points around the minima were reached but still covering as much as possible of the curve. Maxima are usually better covered with observations than minima, hence that part of the cycle often forms the best basis for the curve. And in the cases where the period varies it is easier to fit a curve that only contains a part of a single cycle than a curve that also covers parts of the prior or next cycle. The drawback is that the fitting is not possible, or can go wrong, if the observations mainly cover only the falling or rising branch for a specific maximum. This is possible with a curve that covers more than one cycle. Examples of mean light curves are shown in Figure 2.

2.3. The database

All maxima are kept in a MYSQL database with information on cycle number (E), JD, and date for observed maximum (O), JD and date for calculated maximum (C), O–C, a reference to the source for the maximum, and magnitude at maximum (for the fitted and AAVSO maxima only). E, C, and O–C were calculated by using the elements from GCVS. In some cases manual corrections were needed to map the maxima to the right cycle number for stars with the wrong period in GCVS or having large period variations.

Finally all maxima were inspected and individual maxima that differed >40 days from their neighbors were checked. If an explanation could be found, such as a misprint in the source or the fitting was obviously wrong compared to the observations, it was corrected if possible or else that maximum was removed.

The span between the first and last maximum per star is tabulated in Tables 1 and 2.

2.4. Evaluation and analysis

A test was done to investigate possible offsets between the fitted and the datasets Canon and Pickering (1909) and Gaposchkin and Payne-Gaposchkin (1952a, 1952b). In all cases where a maximum in the fitted dataset was surrounded within five cycles before and after by maxima from one of the other datasets, or vice versa, the date for maximum was interpolated from the

surrounding maxima and compared to the surrounded maximum. The result as the mean deviation per star is presented in Figure 3. The scatter seen is probably mainly caused by the rather small number of data points per star; no significant overall trend is noticed for any of the papers, but can be present for specific stars.

The outlying stars with an offset >20 days were investigated further and are listed below. The number after each star is the number of data points.

Cannon and Pickering (1909): S Del –35 days (1), R Lyn –26 (5), and S Cas +29 (9). S Cas has five fitted maxima that coincide with a local minimum in the O–C diagram. The rejected maxima from Cannon and Pickering (1909) are near the corresponding fitted and no real offset is present. The same, but a local maximum, seems to be the case for R Lyn. S Del has one odd point.

Gaposchkin and Payne-Gaposchkin (1952a, 1952b): RX Sgr –25 (3), V Oph +24 (5), RS Sco +24 (1), S Psc –23 (1), Z Oph –23 (2), S Ori –23 (1), R Del –21 (1). The offsets are due to one or a few odd points for all stars except the carbon star V Oph where an offset is plausible.

A comparison was also made to the AAVSO maxima. Elizabeth Waagen has kindly provided the following description on how these maxima (and minima) are determined:

> For the stars with mean curves, the mean curve is superimposed on the light curve of observations, fitted to the observations by eye, and the dates and magnitudes of maximum and minimum marked. The mean curve covers one cycle and is repeated once, making a curve that shows the mean maximum and minimum twice. We find this presentation of the mean curve most helpful in fitting the mean curve to the observations, especially as we are determining both maxima and minima. Although we fit the overall curve to the data as best as is reasonable, we do not try to fit a minimum at the same time as a maximum, or two maxima at the same time. We fit only one extremum at a time.
>
> The mean curve is created by gathering many well-observed cycles of data of a reasonably well-behaved star, superimposing them on one another, and determining the best mean fit through the stacked data. Obviously, stars that are reasonably well-behaved from cycle to cycle will yield a more representative mean curve. It usually takes many cycles to determine how well-behaved a star is, so it is usually many years before we can determine a mean curve for a star....
>
> For this work to have the best outcome from year to year, it is best to have the same person doing the fitting of the mean curve and the "eyeballing" of the non-mean-curve stars. That way there is more consistency in executing the process and the smallest number of judgment errors because the person gets to know the stars by working with them year after year. (Waagen 2012)

Figure 4 shows the mean difference/P per star between the fitted and AAVSO datasets for maxima that are in both collections. The offset is in most cases rather small, less than 2% of the period for 89% of the stars or in absolute terms less than five days for 82% of the stars. The stars with an offset larger than ten days are: V Aur (–14), R Vol (–13), V Del (+12), S Cep (–12), T CVn (–12), R For (–12), RR Vir (+11), W Cas (+11), T Dra (–11), S PsA (–11), U Per (+10), and T Ari (–10). An example of a star with a large offset is shown in Figure 5.

The offsets could to some degree be explained by different shapes of the mean curves used. The mean curves for a star with a large offset and no offset are shown in Figure 2. Although the offsets for most stars are rather small, they are significant to > 2 times the standard error of the mean for 73% of the stars.

There are some other stars where the published maxima don't seem to connect very well with the fitted, including: ZZ Dra, UV Her, AZ Her, AI Per, and X Psc. These stars usually have large gaps in their sequence of maxima, so it is hard to determine if the star has had an unusual change in its period or something else is wrong.

For common stars and with date before 2008, 68.1% of the maxima are common between the AAVSO and fitted collections, 29.7% are only in the AAVSO, and 2.2% are only in the fitted collection.

3. Presentation

The data for the stars are presented on web pages and dynamically linked to the database. The main page is at http://var.astronet.se/Mirainfooc.php. For each star there is an O–C diagram with the cycle number, linked to the GCVS epoch, plotted on the x-axis and O–C in days on the y-axis. The fitted maxima are plotted with red dots, the published with blue. Under each star are some facts and statistics. By clicking on the diagrams a table with the underlying data for that star are presented with information of mean period, AAVSO offset, and all maxima with their source. An example of a diagram is found in Figure 6.

For C in the O–C, elements with $P = P_{GCVS} + \Delta P$ and $Epoch = Epoch_{GCVS} + \Delta Epoch$ were used.

The data under the diagrams contain the following information:

- The period and epoch from GCVS4.
- LC, Avg, and Per are links to the mean light curve, smoothened O–C diagram, and a period diagram.
- Mean magnitude at maximum, standard deviation, and extreme values. Only the fitted and AAVSO maxima are used for the magnitude.
- Spectral type from GCVS.
- ΔP and ΔEpoch are the linear components in the diagram, in days, when

using the elements from GCVS. These are what the GCVS elements are adjusted with in the formula above.

- ΔP/C is the parabolic component in days/cycle. This is the average change of the period each cycle during the time span of the diagram.

- E/P shows the result from the Eddington and Plakidis (1929) test. The E/P method helps to distinguish real changes from random fluctuations. Two cases are shown, with $X \leq 5$ and $X \leq 15$.

ΔP and ΔP/C also shows the standard error, SE, for the coefficients (±), t-statistics (t), and the coefficient of determination (r^2). t is ΔP or ΔP/C divided by SE. r^2 tells how well a linear or parabolic curve fit the O–C values, SE and t tell the significance of the coefficients. This provided that the deviations from the fit are normally distributed, which may not be the case for most Miras where the deviations probably have a combination of random and physical causes.

The color of ΔP and ΔP/C is green if $t \geq 5$, otherwise is it red. This is to point out stars that likely have a period that differs from that in GCVS or could be candidates for having a secular change in their period.

ΔP is clickable to show the O–C diagram with the original period elements from GCVS.

ΔP/C is also clickable to show a diagram of the residuals with the parabolic component removed. If the resulting diagram only has evenly distributed points with small amplitude it could be a sign of a star with secular change in its period.

For a discussion of the method of Eddington and Plakidis (1929), see Percy and Colivas (1999). In short, ε^2 reflects the average size of the random cycle-to-cycle variation and $2a^2$ the average difference between the true time of maximum and the recorded time. If the variation in the diagram only consists of normal distributed noise then ε^2 and $2a^2$ should be positive and r^2 near 1. If the star has secular and/or periodic changes one would expect ε^2 to have a big positive value, $2a^2$ to have a big negative value and r^2 to deviate significantly from 1.

4. Conclusions

It is demonstrated that a computer algorithm as the one described in this paper can determine maxima from observations of Mira stars with almost the same quality as those manually determined and with huge time savings. 35,000 maxima were calculated in a few hours, then a few weeks were needed to check and validate the material. The AAVSO collection, however, contains 24% more maxima for common stars. The manual method and the use of mean curves of two cycles, width seems in this aspect to be more effective. A modelling of mean curves different from that given in this paper could be a future improvement for computer-generated maxima.

In most cases the collections with older published maxima integrate well together with the fitted maxima and extend the history for the earliest discovered stars several decades or in some cases centuries back in time compared to the AAVSO collection. Also, some stars that are poorly monitored by AAVSO observers benefit from maxima published in other sources to show their earlier history.

For many stars there are gaps in the sequence of maxima, both for the fitted and other collections. This has to be accounted for when analyzing the material. The Eddington and Plakidis (1929) method, for example, is sensible for gaps in the series of maxima and can give results that do not reflect the true nature of the stars in such cases.

5. Acknowledgements

I thank the organizations AAVSO, AFOEV, VSOLJ, and BAA-VSS and their observers for their long-term persistent work and for making their data publicly available, and Gustav Holmberg and Hans Bengtsson for ideas and help with the writing, and Elizabeth Waagen for the description of how maxima/minima are determined at AAVSO.

References

Campbell, L. 1955, *Studies of Long Period Variables*, AAVSO, Cambridge, MA.

Cannon, A. J., and Pickering, E. C. 1909, *Ann. Harvard Coll. Obs.*, **55**, 95.

Eddington, A. S., and Plakidis, S. 1929, *Mon. Not. Roy. Astron. Soc.*, **90**, 65.

Gaposchkin, S., and Payne-Gaposchkin, C., 1952a, *Ann. Harvard Coll. Obs.*, **115**, 1–273.

Gaposchkin, S., and Payne-Gaposchkin, C., 1952b, *Ann. Harvard Coll. Obs.*, **118**, 1–217.

Kholopov, P. N., *et al.* 1985, *General Catalogue of Variable Stars*, 4th ed., Moscow.

Percy, J. R., and Colivas, T. 1999, *Publ. Astron. Soc. Pacific*, **111**, 94.

Sterne, T. E. 1934, *Popular Astron*, **42**, 558.

Templeton, M. R., Mattei, J. A., and Willson, L. A. 2005, *Astron. J.*, **130**, 776.

Waagen, E. O. 2012, private communication.

Waagen, E. O., Mattei, J. A., and Templeton, M. R. 2010, "AAVSO Maxima and Minima of Long Period Variables, 1900–2008" (http://www.aavso.org/maxmin).

Zijlstra, A. A., and Bedding, T. R. 2002, *J. Amer. Assoc. Var. Star Obs.*, **31**, 2.

Table 1. Number of years between the first and last maximum.

Years	*Number of Stars*
< 40	10
40–79	45
80–119	259
120–159	159
≥160	16

Table 2. Number of cycles between the first and last maximum.

Cycles	*Number of Stars*
< 50	12
50–99	71
100–149	194
150–199	123
200–249	54
250–299	18
≥ 300	17

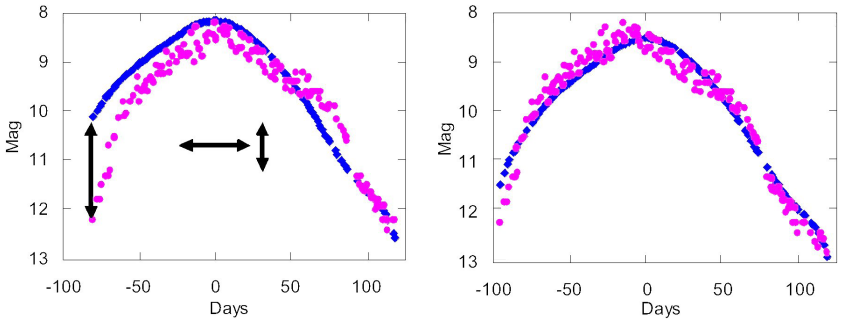

Figure 1. The fitting of the mean curve to observations of R Cam. The observations are pushed alternately left-right and up-down on the mean curve and the square sum of the deviations is calculated. To the right is the best fit. The observations are pushed 15 days to the left and the curve 0.035 magnitude down from the left image.

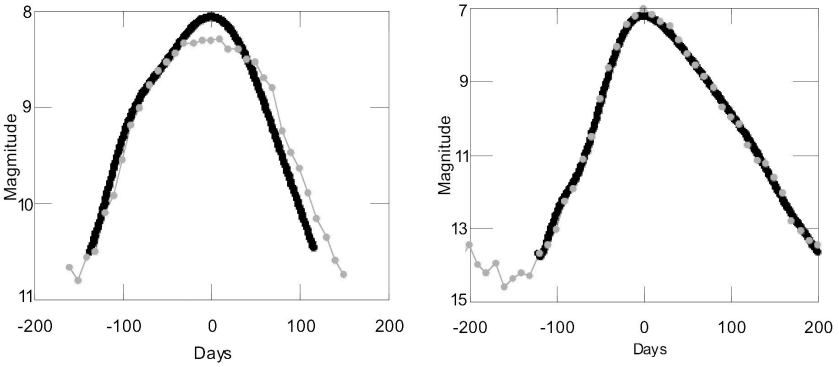

Figure 2. Two examples of mean light curves: U Per (left plot) and R And (right plot). The black lines were used for the fitted maxima, the dotted gray lines are from AAVSO data (Campbell 1955). For U Per the mean offset between the curves for the rising and falling branches is 7 days.

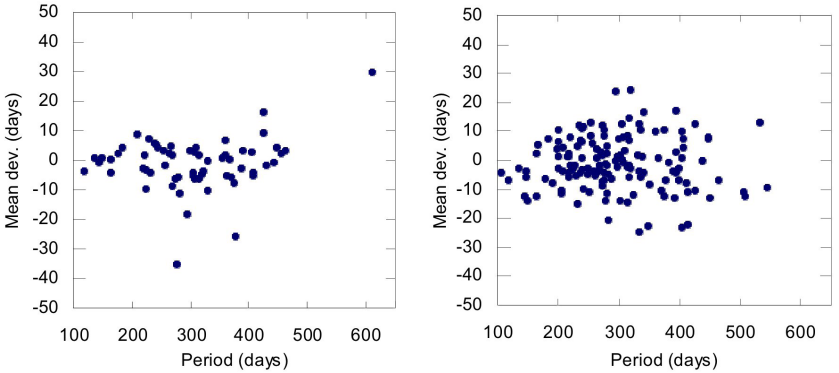

Figure 3. The mean offset for O–C values between the fitted maxima and two of the main papers. Cannon and Pickering (1909; left plot): Average offset –1.4 from 62 stars with 7.6 data points/star. Gaposchkin and Payne-Gaposchkin (1952a; right plot): Average offset –1.4 from 142 stars with 5.6 data points/star.

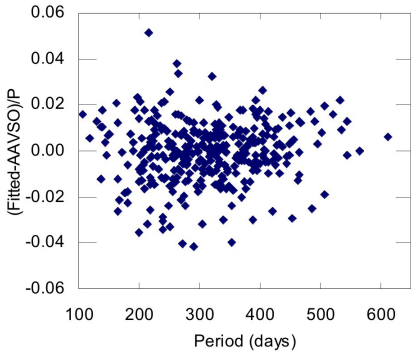

Figure 4. Average difference/P per star between the fitted and AAVSO maxima. The overall average is –0.0005 or –0.1 day from 352 stars, with on average 77.7 maxima/star.

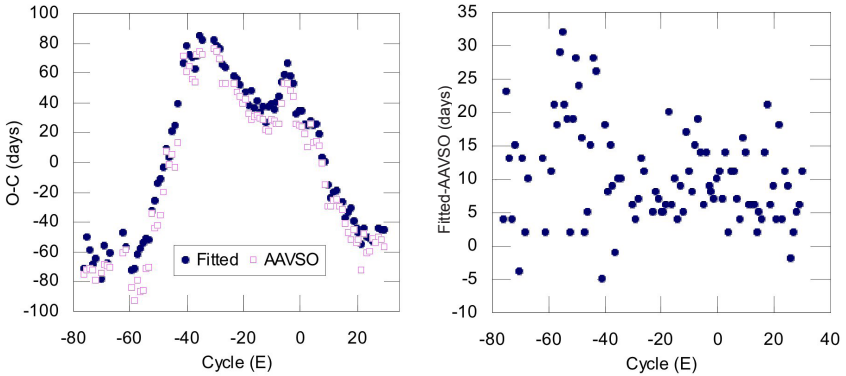

Figure 5. An example of a star (U Per) with an offset between the fitted and AAVSO maxima. The offset is 10.4 days with SEM 1.5 from 95 maxima. On the left is the O–C diagram, on the right a plot of the difference between the times of maxima. See Figure 2 for the corresponding mean curves of this star.

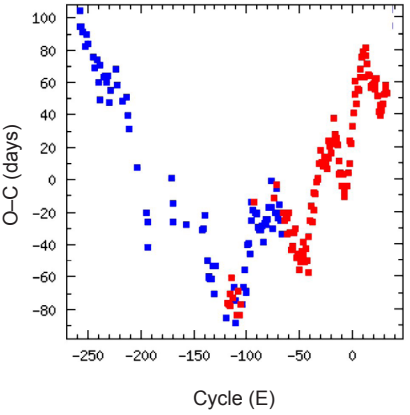

Period: 408.05, Epoch: 2442140 LC Avg Per
Mag at max: 5 ±0.5 (4.0-6.4)
Spectral type: S6,2e-S10,4e(MSe)
ΔP: -0.84 ±0.04 (t:19.3, r^2:0.659) ΔEpoch: -33.4
ΔP/C: 0.013 ±0 (t:31.1, r^2:0.834)
E/P (X=15) ε^2: 46.2, $2a^2$: -19.8, r^2: 0.995
E/P (X=5) ε^2: 35.7, $2a^2$: 11.4, r^2: 0.965

Figure 6. An example of an O–C diagram (χCyg) with corresponding statistics. The x-axis shows cycle number and the y-axis O–C in days. Blue dots are published maxima. Red dots are fitted from observations.

I-band Measurements of Red Giant Variables: Methods and Photometry of 66 Stars

Terry T. Moon
Sydney Institute for Astronomy, School of Physics, University of Sydney, NSW 2006, Australia

Received April 11, 2013; revised May 16, 2013; accepted May 16, 2013

Abstract New measurements of I_C and $V–I_C$ are presented for 66 bright red giant variables. This is the first stage of a program to measure sufficient numbers of such stars that also have well-determined Hipparcos parallaxes with a view to calibrating the TRGB in the I_C band as a tool for accurately measuring distances to nearby galaxies.

1. Introduction

The evolutionary paths of red giant variables follow a two-stage ascent on the HR diagram. In the first stage, they ascend the Red Giant Branch (RGB) burning hydrogen in a shell around the core. Their luminosity increases over time until they reach the point where helium burning commences. After the depletion of helium in the core, a second ascent on a parallel path, the Asymptotic Giant Branch (AGB), occurs. Measuring the end of the first ascent, that is, the Tip of the Red Giant Branch (TRGB), has been shown by Madore and Freedman (1995) to provide a means of determining the distance to nearby galaxies comparable in accuracy to using Cepheid variables. Through generating synthetic *I* magnitudes as a function of *V–I* color index (for Population II stars) their computer simulations indicated that this discontinuity as measured at *I*-band could be used as a primary distance indicator for galaxies to an accuracy of ±10% out to 3 Mpc.

The TRGB represents the maximum luminosity reached by red giants during their first ascent, and is associated with the sudden onset of helium burning in the core, providing a well-defined discontinuity that can be readily observed (Tabur *et al.* 2009a). As red giant variables are both bright and abundant, measurement of the TRGB offers both high utility for, and accuracy in, measuring cosmic distances. The TRGB method purportedly continues to grow in popularity owing to its "low cost in observing time, its conceptual simplicity, and its wide range of application" (Madore *et al.* 2009). Tabur *et al.* (2009a) extended the TRGB method to red giant variables in the solar neighbourhood using photometry from the 2MASS and DIRBE catalogs together with revised Hipparcos parallaxes. Madore *et al.* (2009) introduced a modified detection method for measuring the luminosity of the TRGB based on composite *I* magnitudes modified using a scaling of the *V–I* color index to account for known systematic variations due to metallicity.

For locating the TRGB, near-infrared—that is, *I*-band—measurements are preferred to measurements in other bands as:

- *I*-band magnitudes provide a better indicator of luminosity for red giants than *V* magnitudes. In M giants large variations in *V* arise from a substantial change in temperature as they pulsate. At their cooler phase, red giants emit a smaller fraction of their total energy in the visual portion of the spectrum. Additionally TiO molecules that form during the cooler phase absorb light preferentially in *V*-band (Percy 2007).
- Interstellar reddening corrections are reduced in the near infrared (Tabur *et al.* 2009a).
- *I*-band measurements are less sensitive to metallicity (Tabur *et al.* 2009a).

Additionally, Bedding (2009) has suggested that single-epoch *I*-band measurements may be sufficient to calibrate the TRGB as a tool for measuring cosmic distances.

Unfortunately there is a paucity of *I*-band measurements for those M giants with well-determined Hipparcos parallaxes (Tabur *et al.* 2009a). The available *I*-band data are a mixture of measurements using different systems. For the 261 M giants listed by Tabur *et al.* (2009b), the *General Catalogue of Photometric Data* (GCPD; Mermilliod *et al.* 1997) gives Johnson *I*-band (I_J) values for only 56 of them; 24 of these also have Cousins *I*-band (I_C) values listed. There are an additional 6 stars for which only Cousins values are available. For the remaining 199 bright M giants in this list no *I*-band values are given in the GCPD. A program of systematic *I*-band measurements of bright, nearby M giants was thus started.

2. Which *I*-band?

Bessell (2005) discusses the different *RI* systems that arose as extensions of the well-defined *UBV* photometric system. Early on, a variety of photomultiplier tube and filter combinations were used which gave rise to substantially different *R* and *I* bands. In particular the Johnson *R* and *I* bands (Johnson *et al.* 1967) had significantly longer effective wavelengths than those defined by Kron and Smith (1951) or Cousins (1976).

Precise southern *UBVRI* standards established by Cousins (1976, 1980) provided a good representation of the Johnson and Morgan *UBV* system (1953) and were related linearly to Kron's *RI* system (Kron and Smith 1951). As a result, the $UBV(RI)_C$ system emerged with well-defined passbands (Bessell 1979, 1990) and precisely measured standards (Menzies *et al.* 1989). This instantiation of a *UBVRI* system has been extended to CCD photometry (Bessell 1995), becoming the modern standard in which many new *UBVRI*

measurements are made. It was thus decided that near-infrared measurements of the M giants listed by Tabur *et al.* (2009b) would be made in the Cousins *I*-band (I_C).

3. Equipment

3.1. Photometers and telescopes

An Optec SSP-3 (Gen 1) photometer (Persha and Sanders 1983) was used for measuring about fifty of the brighter M giants listed by Tabur *et al.* (2009b). As this is a solid-state photometer with a photodiode detector it is less sensitive than photometers with photomultiplier tubes or those based on CCD cameras. It does, however, have a relatively good sensitivity in the near-infrared. Measurement methods followed were those suggested in the SSP-3 manual (Optec 2006).

For other M giants in the list of Tabur *et al.* (2009b), a system using a Meade DSI Pro II camera with its supplied software (Meade 2005) was developed. To use it as a photometer a filter wheel and a flip-mirror assembly with an illuminated-reticle eyepiece were added. A cooling fan was also attached. For data acquisition and processing, the techniques described by Hopkins and Lucas (2007) are followed. Telescopes used include a 15-cm f/12 Maksutov (for the SSP-3 photometer and Meade camera) and 12-cm f/5 and 7-cm f/7 refractors (camera only). All three telescopes are operated on equatorial mounts so as to avoid field rotation during CCD measurements.

3.2. Filters

Unfortunately the red and infrared filters originally supplied with the SSP-3 match the Johnson *RI* system. As the focus was on measuring I_C and $V - I_C$, a spare filter slide was fitted with the supplied Optec *V* filter and an I_C filter constructed using a Hoya RT-830 filter cemented between two optically-flat borosilicate windows (used as fill glass to bring the filter to the same thickness as the supplied *V* filter). As shown in Figure 1, the Hoya RT-830 filter has essentially the same spectral transmission characteristics as a Schott RG9, which is the filter usually specified for I_C band measurements (Bessell 1995).

The differences may be regarded as minor when it is noted that a filter's spectral transmission varies with changes in temperature (Young 1967) and, even for a specific filter make and type, from one manufactured batch to another. Subsequent measurements of standard stars over 24 nights confirmed that measurements made through this filter can be linearly transformed to standard I_C magnitudes and $V - I_C$ colors.

The advantage of the I_C filter described is that it is made from inexpensive and readily-available components supplied (such as by Edmunds Scientific) in a diameter that fits SSP-3 filter slides. For convenience (that is, having one of

the SSP-3's two-filter slides fitted with *B* and *V* filters and another with *V* and *I*) a new V filter was subsequently purchased. The new *V* filter was used for all $V–I_C$ measurements taken after July 30, 2011. For the Meade camera a larger diameter of the same type of Hoya filter was used but without the fill glass. For the *V*-filter an inexpensive Wratten #12 long-pass filter of the type supplied for visual astronomy applications (similar to Schott GG495) was cemented to a Schott BG39 visual band-pass filter.

4. Reduction and transformation of measurements

4.1. Standard stars

The standard stars chosen for calibrating the VI_C system described above were selected from the list of Menzies *et al.* (1989). For measurements with the less sensitive SSP-3 photometer attached to small telescopes only bright stars (Hoffleit and Warren 1991) can be used. This limits the choice of standard stars from the list of Menzies *et al.*, making it sometimes difficult to select standard stars with a wide spread of colors that could, at the time of observing, be measured at low air masses. The use of other bright stars as secondary standards was thus investigated.

Mean values of *V*, *B–V*, and *U–B* can be readily retrieved from the GCPD. For many bright stars such values are weighted means derived from multiple sources. Of the standards listed by Menzies *et al.* (1989), 100 are also listed as bright stars by Hoffleit and Warren (1991). Figure 2 shows that there is an excellent correspondence between the GCPD and Menzies *et al.* values for *V*, *B–V*, and *U–B*, with no apparent systematic variations with color index. The average difference between the GCPD and Menzies *et al.* (1989) values for the *V* band and *B–V* and *U–B* color indices were 0.001, 0.000, and –0.001, respectively, with standard deviations of 0.007, 0.003, and 0.005.

There are fewer sources of $V–R_C$ and $V–I_C$ colors and the GCPD lists individual values from each source rather than a weighted mean. Where the star is also a standard, its value given by Menzies *et al.* (1989) is listed separately in the GCPD and denoted as "STD." These standard values were not included in the values adopted from the GCPD for this analysis. Where there were multiple values the mean was calculated. Figure 3 shows the difference between GCPD and Menzies *et al.* (1989) values of $V–R_C$ and $V–I_C$ for those $UBV(RI)_C$ standards that are also bright stars. Again there is excellent agreement. For the $V–R_C$ and $V–I_C$ color indices the average difference between GCPD and standard values was +0.001, with a standard deviation in both cases of 0.002. It is, however, noted that some of the GCPD values are measurements by Cousins and co-workers.

For measurements of I_C and $V–I_C$ it is concluded that GCPD values for bright stars can be used as secondary standards.

4.2. Transformation to I_C and $V–I_C$

Atmospheric extinction coefficients were measured on most nights and applied to the data on a night-by-night basis. Average values for the atmospheric extinction coefficients measured on 24 nights (spread across seasons) were 0.20 and 0.12 for the V and I_C bands, respectively, which are in good agreement with mean values given by Allen (1973), Cousins (1976), Minniti *et al.* (1989), and Sung and Bessell (2000). The average value for I_C-band atmospheric extinction was used on those few nights for which no suitably accurate determination was made. (For the smaller number of CCD measurements average extinction coefficients were used.)

As shown in Figure 4, a linear relationship suffices for transforming the instrumental ($v–i$) indices measured with the SSP-3 photometer to standard $V–I_C$ colors. A small difference in the transformation constant does, however, occur from one V filter to another. Preliminary calibrations show that similar linear relationships apply to V and I_C magnitudes and the $V–I_C$ color index when using the CCD camera.

Measurements of M giants were made relative to selected comparison stars. In most cases the comparison stars used were the same as used previously by the author (see Tabur *et al.* 2009b). Typically, a chosen comparison star was close in the sky to the M giant and measured just before or just after it, keeping corrections for air mass differences to a minimum. An average value of the coefficient for transforming i to I_C magnitudes sufficed as comparison stars chosen were typically late K giants, minimizing the magnitude of the color corrections applied.

5. New I_C and $V–I_C$ measurements of red giant variables

Table 1 lists the new measurements made. Some stars were measured on more than one night to test the suggestion that single-epoch I-band measurements may be sufficient. Measurements made with the SSP-3 photometer are shown in normal type while recent CCD measurements are in italics. In the bottom portion of the table are measurements of several southern, bright M giants that are not included in the list of Tabur *et al.* (2009b). All but one of these is listed in the Hipparcos catalogue.

Of the M giants measured, seventeen have Cousins $V(RI)_C$ values listed in the GCPD. Using the forty-eight measurements of these seventeen stars, an average difference between measured and listed values of +0.01 ±0.10 magnitude was calculated. Considering that all M giants vary in light to some extent, and standard magnitudes are determined through extrapolating transformations established for earlier-type stars, the agreement is good. Similarly, the colors measured deviated only a few hundredths of a magnitude from listed values, which is within known variations that occur for transforming measurements of M giants to the $UBV(RI)_C$ system (Moon *et al.* 2008). The magnitudes and colors

measured may thus be considered to have been well transformed to standard I_C and $V–I_C$ values.

The CCD measurements included are early results in the extension of this program to fainter magnitudes and were made at a new observing site (Scottsdale, Tasmania). They were transformed using a preliminary calibration based on only a dozen standard stars. Also, a series of measurements of BQ Oct on one night show a larger scatter than for the SSP-3 measurements. This may in part be due to inadequate flat-field corrections or the observing conditions on the night. More data will be acquired to better define the transformation coefficients and to understand variations in atmospheric extinction at the new site. The challenges of all-sky CCD photometry are discussed further in Hopkins and Lucas (2007).

6. Conclusion

A program is underway to make I_C band measurements of those bright red giant variables for which there are also well-determined Hipparcos parallaxes. New data for the brighter M giants in the list of Tabur *et al.* (2009b) were gathered that are well transformed to standard VI_C magnitudes and color. This provides a basis for further work to measure sufficient numbers of red giant variables (with known parallaxes) in an effort to calibrate the TRGB in the I_C band as a tool for accurately measuring distances to nearby galaxies.

7. Acknowledgements

The continued support of the Astronomical Society of South Australia is appreciated. In particular, thank you to the Instrument Officer, Blair Lade, for his repairs of and modifications to the SSP-3 photometer. Thanks also to Professor Tim Bedding, Head of School of Physics, University of Sydney, for suggesting this project and his continued support.

References

Allen, C. W. 1973, *Astrophysical Quantities*, 3rd ed., Univ. London, Athlone Press, London.

Bedding, T. 2009, private communication (email of August 21).

Bessell, M. S. 1979, *Publ. Astron. Soc. Pacific*, **91**, 589.

Bessell, M. S. 1990, *Publ. Astron. Soc. Pacific*, **102**, 1181.

Bessell, M. S. 1995, in *New Developments in Array Technology and Applications*, eds. A. G. D. Philip, K. A. Janes, and A. R. Upgren, IAU Symp. 167, Kluwer, Dordrecht, 175.

Bessell, M. S. 2005, *Annu. Rev. Astron. Astrophys.*, **43**, 293.

Cousins, A. W. J. 1976, *Mem. Roy. Astron. Soc.*, **81**, 25.

Cousins, A. W. J. 1980, *South African Astron. Obs. Circ.*, **1**, 234.
Hoffleit, D., and Warren, W. H., Jr. 1991, *The Bright Star Catalogue*, 5th rev. ed., online-only reference (http://cdsarc.u-strasbg.fr/viz-bin/Cat?V/50).
Hopkins, J. L., and Lucas, G. A. 2007, *AutoStar CCD Photometry* (http://www.hposoft.com), Hopkins Phoenix Observatory, Phoenix, AZ.
Johnson, H. L., Mitchell, R. I., and Latham, A. S. 1967, *Commun. Lunar Planet. Lab.*, **6**, 85.
Johnson, H. L., and Morgan, W. W. 1953, *Astrophys. J.*, **117**, 313.
Kron, G. E., and Smith, J. L. 1951, *Astrophys J.*, **113**, 324.
Madore, B. F., and Freedman, W. J. 1995, *Astron. J.*, **100**, 1645.
Madore, B. F., Mager, V., and Freedman, W. J. 2009, *Astrophys. J.*, **690**, 389.
Meade Instruments Corp. 2005, AUTOSTAR SUITE software, Version 3.0 (www.meade.com).
Menzies, J. W., Cousins, A. W. J., Banfield, R. M., and Laing, J. D. 1989, *South African Astron. Obs. Circ.*, **13**, 1.
Mermilliod, J. C., Hauck, B., and Mermilliod, M. 1997, *Astron. Astrophys., Suppl. Ser.*, **124**, 349 (*General Catalogue of Photometric Data (GCPD) II*, http://obswww.unige.ch/gcpd/gcpd.html).
Minniti, D., Clariá, J. J., and Gómez, M. N. 1989, *Astrophys. Space Sci.*, **158**, 9.
Moon, T. T., Otero, S. A., and Kiss, L. L. 2008, *J. Amer. Assoc. Var. Star Obs.*, **36**, 77.
Optec 2006, *Model SSP-3 Solid-State Stellar Photometer* (Technical Manual), Optec Inc., Lowell, MI.
Percy, J. R. 2007, *Understanding Variable Stars*, Cambridge Univ. Press, Cambridge.
Persha, G., and Sanders, W. 1983, in *Advances in Photoelectric Photometry, Vol. 1.*, eds. R. C. Wolpert, R. M. Genet, and J. Wolpert, Fairborn Observatory, Fairborn, OH, p.130.
Sung, H., and Bessell, M. S. 2000, *Publ. Astron. Soc. Australia*, **17**, 244.
Tabur, V., Bedding, T. R., Kiss, L. L., Moon, T. T., Szeidl, B., and Kjeldsen, H. 2009b, *Mon. Not. Roy. Astron. Soc.*, **400**, 1945.
Tabur, V., Kiss, L. L., and Bedding, T. R. 2009a, *Astrophys. J., Lett.*, **703**, L72.
Young, A. T. 1967, *Mon. Not. Roy. Astron. Soc.*, **135**, 175.

Table 1. Measurements of I_C and $V–I_C$ for bright red giant variables.

*Star**	*HIP*	*JD*	I_C	$V–I_C$
U Ant	51821	2455653.981	2.70	2.73
		2455675.998	2.73	2.73
OO Aps	74999	2455312.083	4.29	2.19
		2456217.926	4.53	2.28
		2456232.933	4.56	2.47
delta[1] Aps	80047	2455677.003	2.01	2.81
theta Aps	68815	2455654.081	1.33	4.27
		2455676.992	1.18	4.11
EN Aqr	102624	2455898.953	2.22	2.18
V626 Ara	86628	2455821.920	3.69	2.46
		2456241.942	3.78	2.52
V854 Ara	84105	2455821.928	3.46	2.43
		2456241.944	3.50	2.35
RV Cae	*20856*	*2456365.938*	*4.77*	*1.68*
V505 Car	51141	2455676.979	4.29	2.25
		2455968.990	4.38	2.23
		2456003.963	4.36	2.23
V744 Cen	66666	2455676.006	2.26	3.49
V763 Cen	56518	2455654.023	3.26	2.33
		2455675.971	3.32	2.38
2 Cen	67457	2455654.085	1.08	2.99
		2455676.073	1.04	3.06
AD Cet	1158	2455898.989	2.84	2.20
AE Cet	1170	2455923.969	2.44	1.98
AR Cet	9372	2455923.990	2.39	3.04
BL Cru	60781	2455676.038	2.51	2.97
		2456003.993	2.54	2.91
gamma Cru	61084	2455654.031	-0.72	2.32
		2455676.028	-0.77	2.37
		2456003.985	-0.75	2.34
R Dor	21479	2455577.003	0.16	5.01
		2455677.925	-0.04	5.13
		2455899.069	0.25	5.18
		2455996.963	-0.09	4.91
WZ Dor	23840	2455577.029	2.79	2.42
		2455676.939	2.80	2.47
		2455924.019	2.81	2.35
eta[2] Dor	29353	2455577.043	2.76	2.12
		2455676.922	2.79	2.17
		2455923.053	2.85	2.12

Table 1 continued on following pages

Table 1. Measurements of I_C and $V–I_C$ for bright red giant variables, cont.

*Star**	*HIP*	*JD*	I_C	$V–I_C$
DM Eri	21763	2455923.019	2.03	2.27
		2455941.028	2.01	2.27
		2455996.933	1.85	2.30
FH Eri	*12016*	*2456259.976*	*4.36*	*2.73*
		2456312.022	*4.31*	*2.71*
tau[4] Eri	15474	2455923.003	1.24	2.36
		2455941.019	1.25	2.35
		2456003.926	1.27	2.41
DL Gru	114407	2455478.976	3.29	2.65
		2455801.021	3.31	2.51
		2455940.967	3.27	
beta Gru	112122	2455478.940	-0.61	2.77
		2455800.997	-0.56	2.58
		2455822.041	-0.60	2.69
delta[2] Gru	111043	2455470.940	1.61	2.51
		2455478.933	1.61	2.55
		2455801.005	1.63	2.51
		2455822.034	1.62	2.53
		2455898.969	1.60	2.43
pi[1] Gru	110478	2455478.958	1.88	4.72
		2455822.024	1.69	4.44
TV Hor	*11648*	*2456312.012*	*3.98*	*2.67*
TW Hor	14930	2455941.008	3.27	2.46
TZ Hor	11293	2455822.010	3.49	2.92
		2455899.051	3.47	2.88
		2455924.010	3.49	2.86
WX Hor	*17889*	*2456312.028*	*3.75*	*3.09*
gamma Hyi	17678	2455923.042	1.33	1.91
		2455940.988	1.31	1.91
		2456003.934	1.30	1.95
T Ind	105334	2455800.977	3.71	2.25
WX Men	26169	2455676.961	3.21	2.52
		2455969.000	3.29	2.57
		2455996.972	3.25	2.46
BO Mus	61404	2455676.047	2.29	3.55
epsilon Mus	59929	2455654.052	1.25	2.92
		2455676.064	1.28	2.92
V367 Nor	79490	2455677.038	3.74	2.08
		2455821.913	3.76	2.14
		2456232.944	3.75	2.37

Table 1 continued on following pages

Table 1. Measurements of I_C and $V–I_C$ for bright red giant variables, cont.

*Star**	*HIP*	*JD*	I_C	$V–I_C$
BQ Oct	*71348*	*2456232.970*	*4.29*	*2.60*
		2456319.987	*4.19*	*2.71*
		2456319.989	*4.20*	*2.70*
		2456319.990	*4.21*	*2.68*
		2456319.992	*4.23*	*2.68*
		2456319.992	*4.21*	*2.70*
		2456351.917	*4.12*	*2.70*
		2456351.918	*4.12*	*2.71*
		2456353.000	*4.20*	*2.64*
		2456354.951	*4.21*	*2.67*
		2456365.910	*4.27*	*2.72*
		2456382.887	4.16	2.75
epsilon Oct	110256	2455654.068	1.73	3.32
		2455677.903	1.78	3.30
		2455836.956	1.79	3.27
		2455925.036	1.77	3.26
omicron[1] Ori	22667	2455923.028	2.14	2.56
Y Pav	105678	2455821.975	3.62	2.70
		2455836.947	3.59	2.62
SX Pav	106044	2455821.971	2.15	3.24
		2455836.940	2.22	3.40
		2455924.992	2.09	3.17
NU Pav	98608	2455492.960	1.66	3.73
		2455821.958	1.65	3.62
		2455836.913	1.61	3.49
omicron Pav	104755	2455836.931	3.05	2.02
		2455924.985	3.02	1.99
SW Pic	28596	2455940.997	3.73	2.67
		2456303.997	4.00	2.35
WW Pic	*24943*	*2456382.920*	*4.44*	*2.14*
AC Pic	*30237*	*2456354.987*	*4.73*	*2.14*
TV Psc	2219	2455898.999	2.42	2.50
YY Psc	154	2455898.960	1.99	2.42
57 Psc	3632	2455923.981	2.71	2.52
AL Phe		*2456301.994*	*5.23*	*3.10*
		2456352.919	*5.26*	*2.86*
		2456352.949	*5.25*	*2.88*
AW Phe	*6952*	*2456301.986*	*3.63*	*2.65*
BU Phe	*3894*	*2456311.964*	*4.54*	*2.55*
		2456312.004	*4.58*	*2.48*

Table 1 continued on next page

Table 1. Measurements of I_C and $V–I_C$ for bright red giant variables, cont.

*Star**	*HIP*	*JD*	I_C	$V–I_C$
psi Phe	8837	2455478.999	1.88	2.56
		2455576.979	1.88	2.48
		2455821.999	1.90	2.41
l[2] Pup	34922	2455675.915	2.96	3.41
		2455925.049	3.14	3.05
		2455968.969	3.21	3.60
		2456003.949	3.40	4.07
gamma Ret	18744	2455576.953	2.01	2.44
		2455677.933	2.03	2.45
		2455899.062	1.97	2.40
X TrA	74582	2455312.075	3.01	2.45
		2455677.022	2.85	2.74
		2456232.940	3.02	2.99
BQ Tuc	4200	2455479.028	2.91	2.92
		2455899.021	2.89	2.81
		2455925.024	2.90	2.79
CC Tuc	4879	2455899.028	3.97	2.24
		2455925.015	4.03	2.29
		2455940.979	4.02	2.31
CV Tuc	*3634*	*2456311.960*	*5.47*	*1.72*
		2456311.994	*5.45*	*1.74*
DR Tuc	115433	2455837.010	3.80	2.27
		2455925.004	3.82	2.25
nu Tuc	111310	2455478.968	2.36	2.49
		2455801.013	2.33	2.51
		2455821.991	2.41	2.47
		2455836.922	2.37	2.51
HR 935	14456	2455924.000	2.90	2.33
		2455968.960	2.91	2.30
HD 31754	*22737*	*2456365.945*	*4.92*	*1.49*
HD 33116	*23653*	*2456365.983*	*4.46*	*1.90*
HD 46742	*31221*	*2456354.924*	*5.77*	*2.21*

**Note: Stars having CCD measurements are given in italics.*

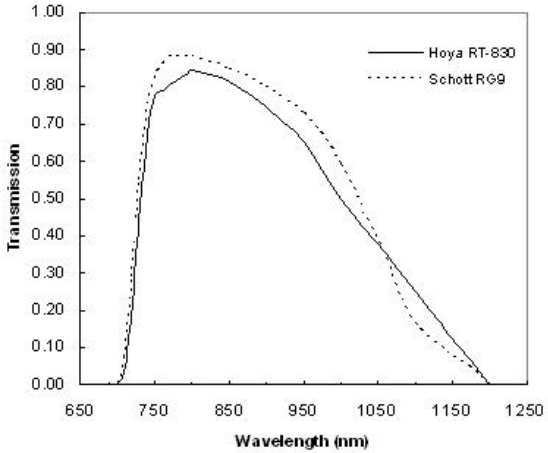

Figure 1. Spectral transmission of the Hoya RT-830 filter compared to a Schott RG9.

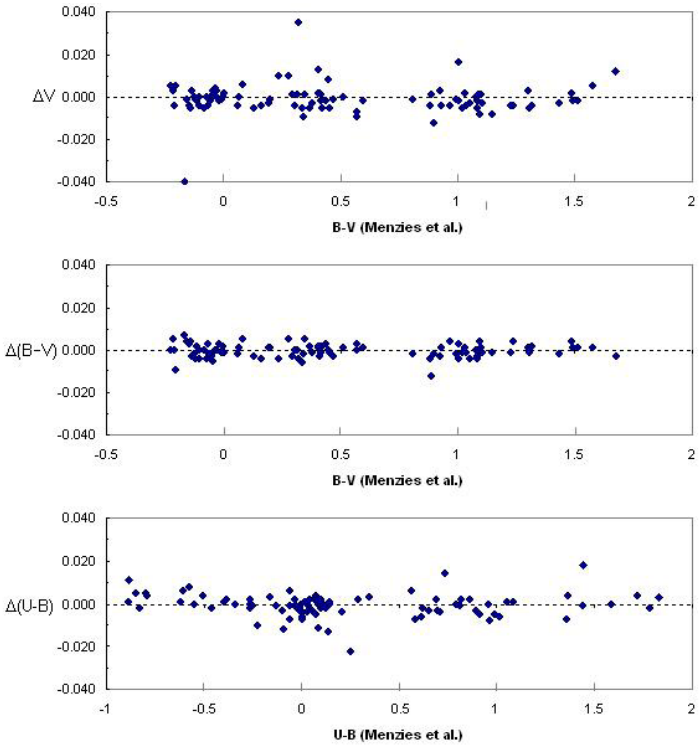

Figure 2. The differences between GCPD (Mermilliod *et al.* 1997) and Menzies *et al.* (1989) *V*, *B–V*, and *U–B* values as a function of the Menzies *et al. B–V* and *U–B* color indices.

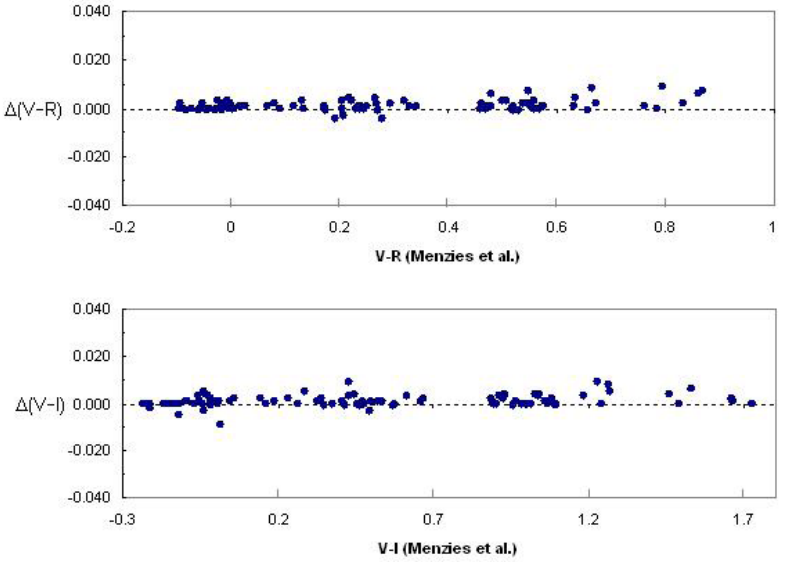

Figure 3. The differences between GCPD (Mermilliod *et al.* 1997) and Menzies *et al.* (1989) $V–R_C$ and $V–I_C$ values as a function of the Menzies *et al.* and $V–I_C$ color indices.

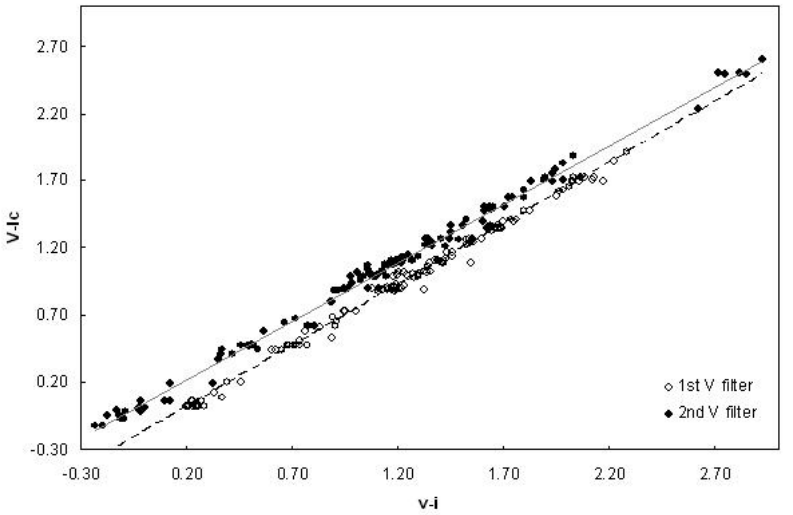

Figure 4. Transformation of $v–i$ to $V–I_C$ indices using standard stars (different V filters) indicating linearity over the range of $V–I_C$ measured.

Monitoring Solar Activity Trends With a Simple Sunspotter

Kristine Larsen
Physics and Earth Sciences, Central Connecticut State University, 1615 Stanley Street, New Britain, CT 06053; larsen@ccsu.edu

Presented at the 101st Annual Meeting of the AAVSO, November 11, 2012; received May 7, 2013; revised November 12, 2013; accepted November 13, 2013

Abstract With the Sun now in solar maximum, solar observations are a timely means to interest students and the general public in astronomy in general and variable stars in particular. The commercially produced Sunspotter is a solar projection system that allows for safer solar observations by several individuals simultaneously. Educational uses for the Sunspotter are reviewed, and the ability of the instrument to track trends in the sunspot cycle (compared to a standard telescope and the American Relative Sunspot Number (R_a)) is examined.

1. Introduction

One of the areas where students and amateur astronomers have provided a valuable service to the discipline is in the field of solar observing. For example, Elizabeth Brown led the Solar Section of the Liverpool Astronomical Society in the 1880s, and then the British Astronomical Association in the 1890s. She aggregated the sunspot counts and drawings of other amateurs for use by the Greenwich Royal Observatory and other scientists interested in the growing field of solar astronomy (Brück 2009). In the United States, Vassar College astronomy professor Maria Mitchell set her students to work at first observing and then photographing the Sun as early as 1874 (Mitchell 1890). These observations were published in *Scientific American* nearly monthly between January 1875 and January 1881.

The most commonly used protocol for reporting sunspot activity is the Wolf Number, defined in 1848 by Bern Observatory Director Rudolf Wolf as $10g+s$, where g is the number of groups of sunspots (distinct areas of sunspot activity) and s is the total number of spots. Currently there are several different sunspot indices based on the Wolf Number, including the International Index and Boulder Index. The American Index (also termed the Relative American Sunspot Number) traces its origin to World War II when there was difficulty in communicating official sunspot counts from Europe to the United States, and the AAVSO Solar Division (now Solar Section) was formed. A more detailed discussion of these different solar indices can be found in Feehrer (2000a).

The greater weight given to groups means that slight variations in the total number of spots between one observer and the next do not result in large variations in R_a. This is important because observers with different size

apertures contribute observations to the AAVSO. In addition, some observers directly observe the Sun using a filter while others project the image onto a screen. In order to compensate for these differences (and others), it has become customary to assign each observer a K-factor which is multiplied by his or her Wolf Number to correct for these differences (Feehrer 2000a). The projection method is popular with solar observers who conduct outreach, because more than one person can simultaneously view the Sun, and since no one is looking through the telescope itself there is an added layer of safety (assuming the finder scope is properly covered or removed). Identifying sunspot groups (areas of activity) is relatively straightforward when the Sun is quiet, as there are fewer sunspot groups, but becomes increasingly challenging when the Sun becomes more "crowded." A group most often either consists of a series of small spots clustered together, or demonstrates a bipolar structure, consisting of two larger spots (generally aligned parallel with the Sun's equator) and a variety of other spots and structures (including grayish-appearing areas called penumbra surrounding and encompassing sunspots). On average, sunspot groups extend over only a few degrees of longitude, although the largest groups can stretch over fifteen degrees of longitude or more. Information on the classification of sunspot groups (using the Zurich system) can be found on the AAVSO website (http://www.aavso.org/zurich-classification-system-sunspot-groups), while an exercise for older students (middle school or higher) on identifying and classifying sunspot groups is available on the NOAA website (http://www.esrl.noaa.gov/gsd/outreach/education/sam1/Activity10.html).

2. Using the Sunspotter to monitor R_a

The Sunspotter is a commercially produced solar projection system (available at http://www.scientificsonline.com/sunspotter.html). Its optical system consists of a 57-mm f/11 folded refractor that produces a 3.25-inch diameter image of the solar disk magnified 56 times (Sadler and West 2002). It is quicker to set up than a regular telescope, and the Sun is easily located by minimizing the shadow of its built-in gnomon. With the solar maximum then an estimated two years away, in late 2011 the author began observing with the Sunspotter in addition to her regular solar observing system, a 6-inch filtered SCT used at a magnification of 48 times. The goal of this experiment was to ascertain whether the Sunspotter could be effectively used in schools or long-term outreach programs to monitor the solar cycle over many months in sufficient detail to unequivocally demonstrate the trends of the American Relative Sunspot number, as published each month in the AAVSO *Solar Bulletin* (http://www.aavso.org/solar-bulletin).

Between October 2011 and September 2012 sixty-seven sets of data from both instruments were collected by the author. Observations with the Sunspotter were limited by time constraints, as it was only used on days on which

sufficient time could be allotted to careful observations with both instruments. On these days the Sunspotter was the first instrument used, in order to not have observations from the larger SCT bias the observer. Groups were identified and the total number of sunspots counted, then the Wolf number formula was applied (10g+s) to determine the sunspot activity visible with each instrument for that date. Representative results are shown in Figures 1 and 2, where the sunspot activity for the Sunspotter and telescope are compared to the published R_a value for the same date.

As expected, observations with the SCT typically resulted in higher Wolf numbers, as small spots were more difficult to view (partially due to lower contrast) with the Sunspotter. Groups consisting of a single small spot were sometimes missed, resulting in a difference in one fewer group being reported with the Sunspotter, and therefore a Wolf Number that was 11 lower than that obtained with the SCT. It was also sometimes difficult to count the numbers of spots in crowded groups with the Sunspotter, also resulting in lower Wolf numbers. However, despite these difficulties, Figures 1 and 2 demonstrate that the Sunspotter does track the overall trends in R_a. Therefore, the Sunspotter system would be useful in a school or long-term outreach program to safely monitor solar activity and allow children and others to compare their observations to those of seasoned amateur astronomers.

3. Additional uses of the Sunspotter in education and outreach

The Sunspotter is not inexpensive; therefore, in order to justify the expense there need to be additional pedagogical and outreach uses besides sunspot counts and monitoring trends in sunspot activity. Fortunately there are a number of different types of both short-term and long-term activities that can be completed using this equipment. For example, the built-in gnomon used to align the Sunspotter can be utilized as a mini-sundial to show the movement of shadows (and the changing angle of the Sun) over an hour. The rotation of the Earth can also be demonstrated by watching the Sun's image drift out of the field of view. Over several consecutive days changes can be seen in individual sunspot groups, and the rotation rate of the Sun can be measured. During the course of a season (or longer) the changing angle of the Sun at noon can be noted by keeping track of changes in the vertical angle the Sunspotter must be set at in its cradle. Sadler and West's manual (2002) for the Sunspotter describes a number of these activities, and George Roberts (2013) has produced a website with downloadable templates and Stonyhurst grids for detailed sunspot observations (http://gr5.org/sunspotter/).

Another argument in favor of including the Sunspotter in science education and outreach is that the types of activities listed above align with state and school district science standards. For example, the Connecticut Grade 6–8 Core Scientific Inquiry, Literacy, and Numeracy Standards include the ability

of students to "use appropriate tools and techniques to make observations and gather data; use mathematical operations to analyze and interpret data; identify and present relationships between variables in appropriate graphs; [and] draw conclusions and identify sources of error" (CT DOE 2011). Grade 1 students are expected to be able to "describe the apparent movement of the Sun across the sky and the changes in the length and direction of shadows during the day" while Grade 5 students are expected to "describe the uses of different instruments, such as eye glasses, magnifiers, periscopes and telescopes, to enhance our vision" (CT DOE 2011). Science standards for other states can often be readily found online through a simple Google search, and in general are fairly consistent from state to state in terms of overall content. The Sunspotter also aligns with the National Research Council's Standards and the AAAS Benchmarks in Astronomy (Sadler and West 2002). The recently published Next Generation Science Standards (Achieve Inc. 2013) highlight patterns involving the Sun within its progression of Earth Science standards from Kindergarten through grade 12. While younger students may have some difficulty manipulating the Sunspotter to properly align it to the Sun, students in Grades 5 and higher should have little difficulty (especially considering that this will, of course, be done under close teacher supervision). Students who are interested in comparing their observations with the published results beyond the level of general trends can compute an "observatory constant" each month by comparing their observations with those published by the AAVSO, using a method described by Feehrer (2000b). Therefore, sunspot observations in general and those utilizing the Sunspotter in particular can play an important role in astronomy education and outreach and introduce students and the general public to the importance of amateur astronomy.

4. Conclusion

With solar maximum now upon us, this is the time to interest students and the general public in observing the nearest variable star, the Sun (Hathaway 2013). The Sunspotter is an easy-to-use commercially produced instrument designed exactly for this task, and which can be used for both one-off events as well as longer term observing programs.

References

Achieve Inc. 2013, "Next Generation Science Standards" (http://www.nextgenscience.org/next-generation-science-standards), Appendix E.

Brück, M. 2009, *Women in Early British and Irish Astronomy*, Springer, Dordrecht.

Connecticut State Department of Education. 2011, "Prekindergarten—Grade 8 Science Curriculum Standards" (http://www.sde.ct.gov/sde/lib/sde/pdf/curriculum/science/pk8_science_curriculumstandards2011.pdf

Feehrer, C. E. 2000a, "Dances with Wolf's" (http://www.aavso.org/dances-wolfs-short-history-sunspot-indices#american).

Feehrer, C. E. 2000b, "Accuracy and Consistency in the Production of the American Sunspot Number (Ra): Addendum" (http://www.aavso.org/accuracy-and-consistency-production-american-sunspot-number-ra).

Hathaway, D. H. 2013, "Solar Cycle Prediction" (http://solarscience.msfc.nasa.gov/predict.shtml).

Mitchell, H. 1890, *Proc. Amer. Acad. Arts Sci.*, **25**, 331.

Roberts, G. 2013, "Sunspotter Telescope Measure Sunspots and Measure Rotation of Sun" (http://gr5.org/sunspotter/).

Sadler, P., and West, M. L. 2002, *A Manual for the Care and Use of the Sunspotter*, Contact Learning Technologies, Inc., Somerville, MA.

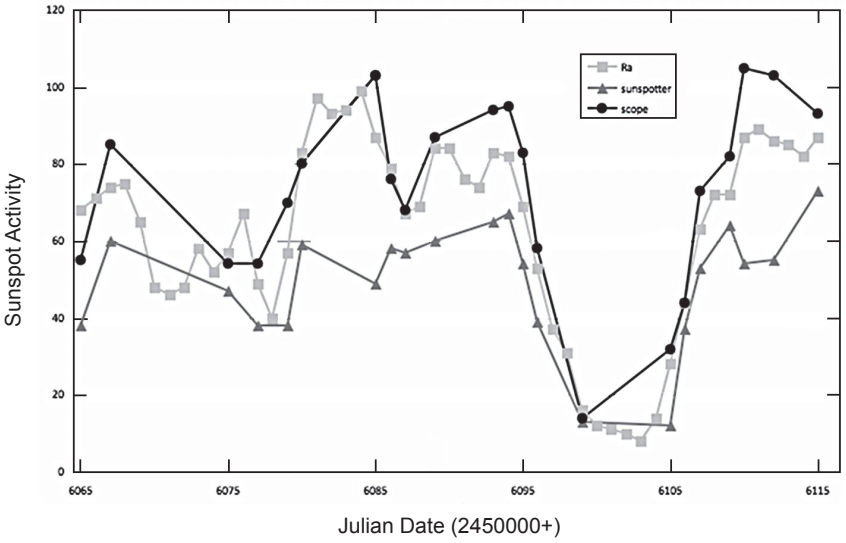

Figure 1. Sunspot activity as measured by the SCT, Sunspotter, and published R_a for May–July 2012.

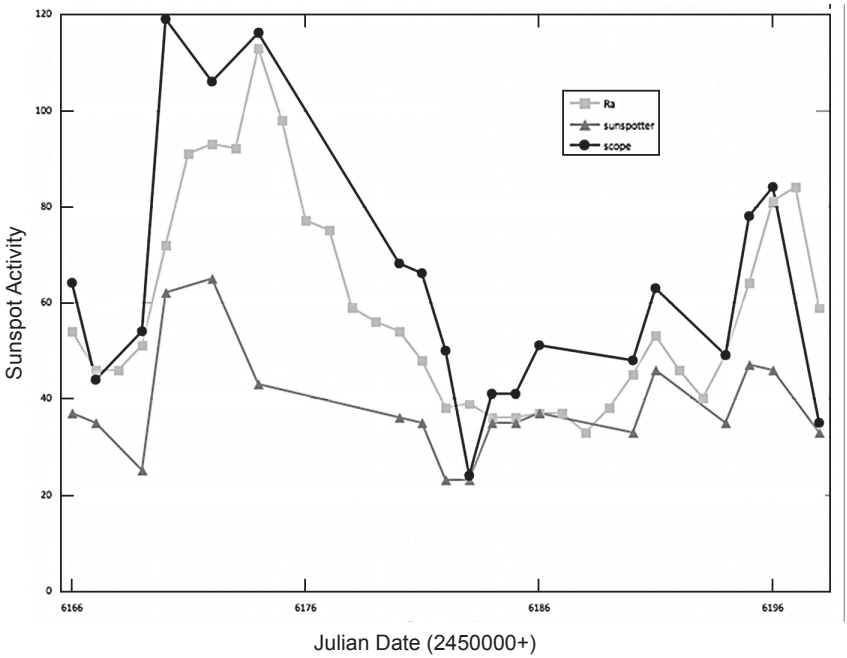

Figure 2. Sunspot activity as measured by the SCT, Sunspotter, and published R_a for August–September 2012.

Book Review

Received September 9, 2013

The Life and Death of Stars

Kenneth R. Lang, 2013, 332 pages, quotation references, author index, subject index, ISBN 978-1-107-01638-5. Price $39.99, hardcover. Published by Cambridge University Press.

The Life and Death of Stars by Kenneth R. Lang describes in great detail the formation, life stages, and final states of the stars. Its approach is even more thorough than a standard introductory textbook, but it avoids using any equations, often describing in many sentences what the equation would show in a single line. While entirely descriptive, it is not a breathless, gushing, glossy portrayal of what we have learned about the stars.

The first few chapters concentrate on the fundamental physics of light, gravity, motion, atomic structure, and spectral lines, and the basic nuclear reactions that create the heat and light of the stars. After this foundation, Lang turns his attention to the Sun, starting in its core with the production of its energy, then moving out through the interior and photosphere to the outer atmosphere, and then to the realm of space plasma that permeates the solar system and produces various forms of space weather. There are numerous figures illustrating the concepts being described, as well as Focus boxes where more detailed descriptions are provided. The coverage is up-to-date, describing results from solar seismology as well as presenting continuing questions such as the faint-young-Sun paradox.

After this extensive treatment of the Sun, Lang turns to the other stars, first concentrating on the range of basic properties of distance, diameter, luminosity, colors, temperatures, and masses, and ending with a description of stellar motions and star clusters. The ranges of these quantities are collected in numerous tables as well as being displayed in fundamental diagrams such as the mass-luminosity relation and the Hertzsprung-Russell diagram.

With the basics of stellar structure and evolution covered, the focus shifts to the interstellar material from which the stars formed, first just the physical properties of the gas and dust, and then on to the process of stellar formation. As part of this descripton, Lang also covers the detections of planets that form with these stars.

After this Lang switches to the various ways that stars come to the end of their lives, depending on stellar mass and the influence of stellar companions. Again, there are numerous tables and figures to amplify the descriptions in the text.

The next to last chapter broadens the focus from stars and star clusters to the Milky Way that contains all the stars we see. In some ways this was a natural

progression because the stars form, live, and die in the Milky Way, but in other ways this chapter seemed inappropriate for the book's primary focus on stars. The massive black hole at the galactic center, the different kinds of galaxy clusters, and the expanding Universe seemed out of place.

The final chapter, titled "Birth, Life, and Death of the Universe" continued the trend of the previous chapter to reach the ultimate distance from the theme of stars. In fact, in some places it almost seemed to become un-scientific, such as when it stated that "conservation of energy or momentum, which are valid within a restricted range of conditions" or "equations sometimes are disconnected from the observable world."

In addition to the diversion in the final chapter from the primary theme of the book, I also found a lack of uniformity in some of the numerical values, a tendency to repeat things in different chapters that seemed to fragment the flow, and I would have preferred to have the color images incorportated into the flow of the text instead of having black and white versions there and the color versions collected in the middle of the book. Overall, however, *The Life and Death of Stars* was a rewarding and stimulating book that gives an in-depth description of our understanding of all aspects of stars. I particularly liked the many historical foundations that were provided, some of which were new to me and that I plan to incorporate into my courses, as well as the many literary quotations that show the central place of astronomy, and stars in particular, in the life of the human mind.

John B. Lester
Professor, Astronomy and Astrophysics
Mississauga Campus
University of Toronto
Mississauga, Ontario L5L 1C6, Canada

e-mail: john.lester@utoronto.ca

Book Review

Received August 7, 2013

Meeting Venus—a Collection of Papers Presented at the Venus Transit Conference, Tromsø 2012

Christiaan Sterken and Per Pippin Aspaas, eds., 2013, 256 pages, paperback, ISBN 978-82-8244-094-3, Vrije Universiteit Brussel, and University of Tromsø, available in open access (http://www.vub.ac.be/STER/JAD/JAD19/jad19_1/jad19_1.htm).

On June 6, 2012, the planet Venus passed across the face of the Sun, as seen from the Earth. The brightness of the Sun (if you could measure it precisely) would have decreased by about 0.001 magnitude, adding to the Sun's status as a variable star. More to the point: a transit of Venus (or Mercury) is a graphic demonstration of what an exoplanet transit would look like, if we had sufficient power to resolve it.

Transits of Venus are brief and rare. Kepler's and Newton's laws made it possible to predict them. Jeremiah Horrocks was the first to observe one, in 1639, based on Kepler's prediction, and his own refinement thereof. Edmond Halley, building on a suggestion by James Gregory, showed that it would be possible to measure the absolute size scale of the solar system by observing a transit of Venus from multiple sites across the Earth, and this led to a number of expeditions to observe the 1761 and 1769 transits, notably James Cook's expedition to Tahiti in 1769. It was the "space race" of its day. Specifically, the project was to measure the *solar parallax*—the angle subtended at the Sun by the mean radius of the Earth, now known to be 8.794143 arc seconds. The solar parallax is inversely proportional to the *astronomical unit*, the average distance between the Earth and Sun, in km. Nowadays, there are still some scientific benefits to observing transits of Venus—mostly related to the interpretation of observations of exoplanet transits—but their main appeals are their rarity, and their many historical and cultural connections. The parallax observations were repeated at the 2004 transit, but as an educational project.

This book is the proceedings of a symposium, held in the city of Tromsø, Norway, on June 2–3, 2012, just before the 2012 transit—the last one until December 10–11, 2117. I looked forward to receiving this book, because we also held a transit of Venus symposium here in Toronto. Ours was just one day, April 28, and was a partnership with our Institute for the History and Philosophy of Science and Technology. We did not publish a proceedings, but the lectures can be found on *YouTube* (http://transitofvenus.nl/wp/2012/05/17/toronto-transit-talks/). The symposium was broad in scope, including a keynote address by Jay Pasachoff,

and papers on transits of Venus across the centuries; the astronomical politics in the UK at the transit of 1874; comments by Victor Davies, composer of the opera *Transit of Venus*; educational applications of transits; observing transits safely; and transits in the modern (exoplanet) era. The symposium was accompanied by a talk on, and exhibit of historical astronomical instruments from the University of Toronto Scientific Instrument Collection (www.utsic.org).

The viewing on June 6 was extraordinarily successful; over 5,000 people gathered in the University's Varsity Stadium, and viewed the first two hours of the transit with suitable solar glasses, as well as on the stadium jumbotron. Many smaller telescopes were set up for solar viewing, including one dating from 1830. There was extensive local and national media coverage. The event won two awards from the Council for Advancement and Support of Education (CASE).

The problem with conference proceedings is that their content usually depends on who attends, and what they present. In this case, the contributions provide a very interesting account of both a rare astronomical event, and a part of the world that most of us are not familar with. Collectively, they are well focussed; there are none which are off-topic.

Why Tromsø? First: because northern Norway figured prominently in early transit expeditions, especially that of the Viennese Jesuit astronomer Maximilian Hell, who travelled to Vardø, in Norway. Halley's method for determining the solar parallax depended on getting observations from a very wide range of latitudes and longitudes. Second: because, on June 6, the Sun is circumpolar as seen from Tromsø, and the entire transit could be viewed, including the onset at the time of "the midnight Sun"—weather permitting. Was it clear? Find out in Section 3 of this review!

I am reviewing the present book as an astronomer with an interest in transits of Venus, and the history of astronomy in general. I specifically mention topics which I find particularly interesting. I am not qualified to judge the fine details of the scholarly work in the historical chapters.

The book begins with a useful, exhaustive overview of the geography of Scandinavia, and the political organization in the 18th and 19th centuries. The editors provide a complete list of those who observed the historical transits from Scandinavia, plus those, mentioned in the book, who observed them from elsewhere. The book ends with a brief remembrance of astronomer Hilmar Duerbeck, who was to have been a speaker at the conference, but passed away on January 5, 2012. The rest of the book is divided into the following three sections.

1. Historical observations of transits from Scandinavia

Editor Per Pippin Aspaas reviews the state of astronomy in Denmark-Norway in the 18th century; they were a single Kingdom at that time. Denmark had a long tradition in astronomy, dating from the work of Tycho Brahe, through

the establishment of Copenhagen's Round Tower Observatory in 1642. By the 18th century, Denmark-Norway was scientifically isolated, and a second-rate power in astronomy, as compared with Sweden and Russia. But Denmark-Norway made the interesting decision to contract Maximilian Hell, the Jesuit "Imperial and Royal Astronomer of Vienna," to observe the 1769 transit from Vardø, in northern Norway (latitude +70.4 degrees). His observatory was the first state-funded observatory in Norway. Hell was eminently successful, though, at one point, it was suggested—incorrectly—that he had faked his results. Nevertheless, it was still clear that Denmark-Norway lagged behind their neighbors, astronomically speaking.

Hell's expedition was scientifically successful; he observed the transit, and also gathered much useful information about the natural and cultural history of the "northern fringes of the realm." But it was also controversial, and this topic is well described by László Kontler. Hell was born in what is now Slovakia; he worked in Austria, which was part of the Austro-Hungarian Empire. He was a servant of two masters: Christian VII of Denmark-Norway, who had contracted him to lead the expedition, and his regular employer Empress Maria Theresa. One of the objectives of the expedition was to study the language and culture of the Sami (Lappian) people, and the results of that part of the expedition were published by Hell's associate János Sajnovics in his *Demonstratio*. Unfortunately, the possible linguistic and cultural connection between the Sami and the Hungarians was politically sensitive, and Sajnovics's book opened a "can of worms" among the various factions in the Empire—especially the Hungarian nobility.

By contrast, Sweden (which included Finland at the time) was becoming a major power in astronomy, and in science in general, in the 18th century. Sven Widmalm outlines how this was part of an "enlightenment research policy," and makes some interesting parallels with science policy today, including the motives for state funding of research. These new policies were in part due to the influence of a new political party—the "Hat Party." The Swedish Royal Academy of Sciences was founded in 1739, the Uppsala University Observatory in 1741, and the Stockholm Academy Observatory in 1753. Celsius and Linnaeus were familiar names in these developments. Pehr Wilhelm Wargentin, the most notable Swedish astronomer of the time, was important, but is less well known today. Sweden participated in the observation of both the 1761 and 1769 transits in a significant way. Wargentin's ability to network was a major contributor to their success. By the end of the 18th century, however, science in Sweden was on the decline.

Osmo Pekonen describes the work of Anders Hellant, a Swedish amateur astronomer who set out to observe the 1761 and 1769 transits. He was well-educated and, in his "day job," played an important administrative and economic role in northern Sweden. He had broad interests as an amateur scientist, had an excellent library, and established a small observatory in Tornio—at the time,

the northernmost permanent observatory in the world. Among other things, he observed the variable star Mira, and made important studies of the aurora. His observations of the 1761 transit were successful, and were sent to Wargentin who forwarded them to Paris for analysis. But they proved "scattered, unreliable and virtually worthless." In 1769, he and Frederik Mallet, a professional astronomer, attempted to observe the transit from north of the Arctic circle, but were clouded out.

As described by Gudrun Bucher, Tsarina Catherine II of Russia made a special effort to encourage and support transit expeditions in 1769, in part to re-establish the reputation of Russian scientists, and the Russian Academy of Sciences. Though the expeditions were complicated by the fact that they had significant natural-history and ethnographic objectives as well as astronomical ones, they generated a large output of scientific knowledge and publications. (It's interesting that, as I write this review, the Russian Academy of Sciences is under threat of dissolution by the current Russian government!)

Nils Voje Johansen describes an expedition sent by the Royal Society of London to observe the 1769 transit at the North Cape of Norway (latitude +71.5 degrees), with astronomers William Bayly and Jeremiah Dixon (of Mason-Dixon line fame) aboard the Admiralty's *HMS Emerald*, commanded by Captain Charles Douglas. Dixon and Mason had observed the 1761 transit from the Cape of Good Hope. Observations of the transit from the two portable observatories were only partially successful, but Douglas also took some novel measurements of the temperature of the sea water at different depths, and was enquiring about the possible existence of giant "sea worms" (the locals claimed to have seen them). He also kept a "spying log," reporting on his observations of defences, commercial information, charts and soundings of ports, and supply possibilities ("watering and wooding") for territories that they were visiting. And apparently the locals were spying on the English as well. So surveillance is not just a "today" thing!

Swedish astronomer Anders Lexell is perhaps best known for his study of the orbit of Comet Lexell, discovered by Messier in 1770. Lexell showed that the comet had made a close approach to Jupiter in 1767, which drastically changed its orbit. A second close approach to Jupiter in 1779 further changed its orbit, and it was never seen again. Johan Stén and Per Pippin Aspaas describe Lexell's role in analyzing the large and diverse set of observations of the 1769 transit, in competition and debate with astronomers much more senior (but not necessarily more competent) than him— including Hell. The authors usefully describe how the observations were actually used to derive the solar parallax, and hence the solar distance.

2. Historical observations of transits from elsewhere

This section opens with a chapter, by Steinar Thorvaldsen, which addresses the transition from Kepler's Laws, to precise predictions of transits of Mercury

and Venus. Kepler's *Rudolphine Tables* enabled the prediction of the 1631 transit of Mercury, and the 1639 transit of Venus and, although these were not widely observed, the few observations that were made validated and refined Kepler's predictions. One of the most remarkable things about Kepler's and Newton's Laws is that they allow for the prediction of the exact circumstances for phenomena such as eclipses and transits—something that should constantly amaze both us and the public.

This section also includes an interesting and fundamental chapter, by Suzanne Débarbat, which reviews the methods by which the solar parallax (or the average distance from the Earth to the Sun, in km) has been determined over the ages, and how the accuracy has improved. Prior to the 17th century, the accepted values were an order of magnitude too small! Improvement was helped by Napier's invention of logarithms in the early 17th century. It continued with a measurement of the parallax of Mars at close approach, in 1672–1673, and with the measurements of the 1761 and 1769 transits of Venus (with observations of transits of Mercury as useful "practice"), and with continued measurements of the parallaxes of Mars and Venus at close approach. The accuracy gradually improved from 10% to 5% to about 3%. Observations of the 1874 and 1882 transits improved the accuracy to 1–2%, though the *black-drop effect* always limited the accuracy which could be obtained. For the next few decades, several strategies were used, but the best was to measure the parallax of near-Earth asteroids, notably Eros in 1930–1931. Now, the scale of the solar system is determined by bouncing radar waves off the inner planets. This chapter ends by reprinting IAU Resolution B2, passed at the 2012 IAU General Assembly in Beijing: the average distance of the Sun (the Astronomical Unit) is *adopted* to be 149,597,870,700 meters.

Désbarbat's chapter emphasizes the role of French astronomers. That theme is continued in a chapter by Simone Dumont and Monique Gros, who describe the important role of Joseph-Nicolas Delisle and Joseph-Jérôme Lalande in organizing the international observations of the 1761 and 1769 transits. Halley suggested how these could be used, but passed away in 1742. Guy Ratier and Sylvain Rondi describe observations of Venus and Mercury transits from the Pic-du-Midi Observatory in the Pyrenees. It was founded in 1882, but clouded out for the transit that year but, with its excellent seeing conditions, went on to make many other important contributions to solar and planetary astronomy, including the discovery of the 4-day retrograde rotation of the atmosphere of Venus. I had always assumed that this discovery was made from space, by *Mariner 10*.

Co-editor Christiaan Sterken describes the work of his countryman Jean-Charles Houzeau, who developed a new approach to measuring the solar parallax: a "heliometer with unequal focal lengths." He used one such instrument to observe the 1882 transit from San Antonio, Texas, and sent another to Santiago de Chile. These were the first major expeditions in the

history of Belgian science. Both expeditions were at least partially successful, and produced a value of the solar parallax which was within 1.3% of the true value. Parts of the heliometers still survive, and are on display at the Royal Observatory, Belgium. A slightly-inaccurate plaque marks the site of Houzeau's observations in Texas.

Thomas Posch and colleagues provide more information on five Jesuit observatories in central Europe, and on the work of Maximilian Hell who observed the 1769 transit from northern Norway. Three of the observatories were in present-day Austria, one in Slovakia, and one in Romania. The Jesuits were well known for their efforts to support scientific research and teaching, and they still operate the Vatican Observatory (with branches in Italy and Arizona) today. Hell observed the 1761 transit, measured the angular diameter of Venus, and analyzed some of the international observations of the 1761 transit, obtaining a solar parallax only a few percent different from the true value.

David Dunér contributes a fascinating chapter on the evolution of the belief that Venus might be inhabited. Galileo observed mountains and valleys on the moon; might it be inhabited? The heliocentric theory showed that the Earth and planets all orbited the Sun; were they not all "worlds"? Dunér is especially interested in the cognitive processes which lead to "belief"—a topic that is still relevant today. In his paper, he discusses the impact of two kinds observations of Venus: (1) the *ashen light*, a supposed glow on the dark side of Venus, and the *black drop effect* which is observed at transits; these suggest that Venus might have an atmosphere (which it does, though the historical observations of the black-drop effect continue to be controversial); and (2) supposed observations of markings on the planet (which, like the "canals" on Mars, are an optical illusion). Even Percival Lowell (of Mars canals fame) claimed to see markings on Venus, though he believed them to be natural features. Many eminent astronomers and writers of the 17th, 18th, and 19th century weighed in on the "plurality of worlds" debate, and Dunér does an excellent job of reviewing and commenting on them.

3. Observing the 2012 transit from Tromsø, and beyond

Aside from the historical connections to earlier transit expeditions, June transits have the advantage that the Sun is circumpolar in Tromsø. The whole transit can be observed (weather permitting), even at midnight.

Three observers planned to observe the transit over North Cape, from a small plane; they could observe from above the clouds if necessary. Sadly, their camera malfunctioned, even though they had double-checked it. Lesson learned: always take a spare camera.

A larger group set out to follow in the footsteps of Maximilian Hell, who observed the 1769 transit from Vardø. Their expedition is described at length, in vivid detail, and profusely illustrated, in "A Voyage to Vardø. A Scientific Account of an Unscientific Expedition." The purpose was *not* to make scientific

observations, but to commemorate and re-enact historically-significant observations—a growing trend for historians of science. The expedition was undertaken by boat (*MS Lofoten*—a national historical monument!), with stopovers at Hammerfest and North Cape, both of which figured in expeditions, 250 years earlier, and have other historical, cultural, and scientific significance. The 2012 trip was ten times faster than Hell's! In Vardø, many dignitaries and visitors gathered; there were public lectures and demonstrations, television interviews, a concert, banquet, and religious service, and finally the viewing of the transit. Sadly, only the last hour or two of the transit was visible, through partly cloudy sky. Weather is always a factor. Otherwise, a good time was had by all.

The main viewing of the transit was from Tromsø, and the conditions were perfect. Visitors came from across Europe. Observing sites included a cable car station, an auroral observatory, a soccer field on the Island of Tromsø, and in the case of one observer, a nearby mountain peak. At the soccer field, there was a big screen, about a thousand people, and a film crew from Norwegian national television. On television, about 160,000 people followed the entire 6-hour transit, almost 900,000 watched some part of it, and 50,000 followed the live stream in the Internet. First contact was about midnight, with the Sun only about two degrees above the horizon. But the times of first and second contact could still be measured on the projection screen. Real-time comparison between the local image and the image streamed in from Hawaii showed the parallax effect clearly.

4. Commentary

This book can be enjoyed at several levels: as an account of the challenge of making astronomical observations over the centuries, or as an introduction to the history of astronomy in northern Europe, or simply as a travelogue in an interesting but out-of-the way part of the world. The chapters are scholarly, rather than "popular," and assume some understanding of world history and politics. But that's part of the strength and appeal of the book; it demonstrates that astronomy is not done in isolation, but is embedded in and connected to world affairs.

I commend the organizers of this conference for conceiving and planning it, and the editors for their excellent work in producing an interesting, attractive, and well-organized book. The chapters are edited to a common format; they are profusely illustrated with maps (both historical and modern), images of historical documents, buildings, instruments, and observations and, in the third section, formal and informal pictures of the participants enjoying their surroundings. The chapters are extensively referenced, and there are good name, subject, and author indexes.

I especially applaud the editors' willingness to make the book freely available as an open-source document. The on-line document is set up so that

you can download whichever chapters you are interested in. Everyone will find something of interest in this book.

John R. Percy
Department of Astronomy and
Astrophysics, University of Toronto,
Toronto, ON M5S 3H4, Canada;
john.percy@utoronto.ca

Abstracts of Papers Presented at the 102nd Spring Meeting of the American Association of Variable Star Observers, Held in Boone, North Carolina, May 16–18, 2013

Working Together to Understand Novae

Jennifer L. Solokoski
Columbia Astrophysics Lab, 1027 Pupin Hall, Mail Code 5247, 550 West 120th Street, New York, NY 10027; jeno@astro.columbia.edu

Abstract In ancient times, people occasionally looked up to find a "nova," or new star, in the sky. With about thirty-five per year in our galaxy, novae are the most common major stellar explosions. Although researchers now understand what causes a white dwarf to suddenly brighten into a nova, many puzzles remain, such as why novae appear to eject orders of magnitude more material than predicted by theory, and how a uniform eruption on a spherical white dwarf can expel matter in the form of jets, clumps, and rings. Coordinated observations at radio, optical, and X-ray wavelengths can answer these questions. I will describe a new opportunity for amateur astronomers to work with professional astronomers who are using X-ray and newly upgraded radio telescopes to observe novae. Participants will have the opportunity to learn about novae, share their own expertise, and participate in the process of scientific discovery.

AAVSO High Energy Network: Past and Present

Matthew R. Templeton
AAVSO, 49 Bay State Road, Cambridge, MA 02138; matthewt@aavso.org

Abstract The AAVSO High Energy Network grew out of several initiatives in Pro-Am cooperation on gamma-ray burst localizations at the end of the 20th Century, and continues today as an informal "Section" within the AAVSO. A number of observers and groups continue to receive GRB alerts from the AAVSO's automatic service, and the amateur community remains involved in GRB followups. I'll highlight a few recent bursts with amateur followups, both within AAVSO HEN, and on their own, and make suggestions for how the amateur community could expand its pursuit of this field.

Late-time Observations of Novae

Arne A. Henden
AAVSO, 49 Bay State Road, Cambridge, MA 02138; arne@aavso.org

Abstract The 61-cm telescopes of the AAVSO's robotic telescope network have been used to obtain multi-wavelength photometry of many recent novae. Few novae have been previously followed more than 100 days after outburst. We are systematically imaging all novae from the past decade. This paper is an interim report, giving results for the most recent novae, and highlighting where amateurs can contribute to the project.

Deriving Definitive Parameters for the Long Period Cepheid S Vulpeculae

David G. Turner
Saint Mary's University, Halifax, NS B3h 3C3, Canada; turner@ap.smu.ca

Abstract The long-period variable S Vul is now recognized to be a classical Cepheid, following a period a century ago when its status was less well established. Its pulsation period of 68.5 days makes S Vul the longest period Cepheid recognized in the Galaxy. Possible membership in an OB association was considered briefly thirty years ago, until it was discovered to be surrounded by a sparse cluster of faint stars designated as Turner 1. Membership of S Vul in the cluster was considered unlikely in the original photometric study of Turner 1 because of contradictory implications regarding the reddening and distance of S Vul with that of cluster stars, but a recent revisiting of the data supplemented by APASS observations indicates that the cluster and Cepheid are indeed related. The implications for the implied parameters of S Vul, its reddening, distance, age, and evolutionary mass, are discussed in light of our refined knowledge of the cluster in which the Cepheid resides.

The Z CamPaign Year Four

Mike Simonsen
AAVSO, 49 Bay State Road, Cambridge, MA 02138; mikesimonsen@aavso.org

Abstract Z Cam stars are a small subset of dwarf novae that exhibit standstills in their light curves. Most modern literature and catalogs of cataclysmic variables quote the number of known Z Cams to be on the order of thirty or so systems. After a three-year observing campaign and an exhaustive examination of the data in the AAVSO International Database we have trimmed that number by a third. One of the reasons for the misclassification of some systems is the fact that the definition of a Z Cam has evolved over the last eighty-five years to what it is today. We present the results of our investigation into sixty-four CVs listed at one time or another in the literature as Z Cams or possible Z Cams.

Periodic Brightness Fluctuations in the 2012 Ouburst of SN 2009ip

John Martin
Universtiy of Illinois at Springfield Observatory, One University Plaza, MS HSB 314, Springfield, IL 62704; jmart5@uis.edu

Abstract In September 2012, the supernova impostor SN 2009ip in NGC 7259 had what some have theorized was its final outburst and terminal explosion as a type II-n supernova. Our Pro-Am collaboration observed this event with high temporal cadence in V, R, and I bands. Analysis of our data reveals a periodic fluctuation on the order of weeks (with several harmonics) in the de-trended light curve after peak brightness. We have verified that this is not an instrumental effect in that it also appears in data from other unrelated instruments. In this talk will present our data and findings.

Observations of an Eclipse of Bright Star b Persei by the Third Star in February 2013

Donald F. Collins
138 College View Drive, Swannanoa, NC 28778; dcollins@warren-wilson.edu

Abstract b Persei (SAO 24531 = HD 26961, V ~4.52) is a multiple star system consisting of a close ellipsoidal binary with a 1.5-day period and a third star with a 702-day orbit. b Per is a non-thermal radio source, and the evolutionary stage of the close binary is unclear. It may be a non-eclipsing Algol or a precursor to the Algol stage. Observations with the Navy Precision Optical Interferometer showed that the third star has a nearly edge-on orbit about the close binary. Based on this orbit an eclipse of the close binary by the third star was predicted for late January 2013. A call for observations—especially those with equipment to observe bright stars instrumentally—was made via the AAVSO. With the "back yard" convenience of a DSLR camera on a fixed tripod, DFC obtained an observation of the V magnitude of b Persei nearly every clear night in January–February 2013. The DSLR clearly detected the expected eclipse with a drop in of 0.12 V on JD 2456329 and JD 2456330 (Feb 5–6, 2013 and Feb 6–7, 2013). The eclipse was also detected by other AAVSO observers extending to JD 2456331 inclusive. The estimated duration of the eclipse (FWHM) is 2.0 ± 0.3 d. The DSLR also detects the 1.53-day orbital period of the A and B components of b Persei—a variation of 0.05 V magnitude due to the non-eclipsing ellipsoidal star shapes. A concerted campaign should recruit many AAVSO observers to detect the next predicted eclipses in mid-January 2014 (secondary) and early January 2015 (primary) assuming a 702-day cycle. Future photometric

observations may aid the understanding of the evolutionary stage of the close binary.

The Astronomer Who Came in from the Cold: the Evolution of Observing Variable Stars Over Three Decades at Appalachian State's Dark Sky Observatory

Daniel B. Caton
133 Thompson Hollow Road, Vilas, NC 28692; catondb@appstate.edu

Abstract Variable star research has been my main work from my Ph.D. dissertation work through three decades of research at our Appalachian State University Dark Sky Observatory. I will present a review of that work and the evolution of technology that took me from in situ observing with a photometer in a cold dome to remote and automatic CCD observing today. The research targets included RS CVn stars, apsidal motion eclipsing binaries, Trojan planets, and exoplanets in binaries.

Color of the Night Sky

Gary Walker
Maria Mitchell Association Observatory, 4 Vestal Street, Nantucket, MA 02554; bailyhill14@gmail.com

Abstract The author presents the results of all-night monitoring of the sky brightness in BVRI filters. The measuring equipment used was Unihendron SQM's and KNIGHTWARE software. Results from four observatories are presented, along with implications of twilight flats.

Kalman Filtering and Variable Stars

Gary Walker
Maria Mitchell Association Observatory, 4 Vestal Street, Nantucket, MA 02554; bailyhill14@gmail.com

Abstract The Kalman Filter (also known as linear quadratic estimation (LGE)) is used extensively in Navigation Systems to estimate the state in the presence of noise. The author explores the use of Kalman Filtering to estimate the magnitude of Variable Stars in the presence of Noise.

Astronomy: Hobby or Obsession?

Mike Simonsen
AAVSO, 49 Bay State Road, Cambridge, MA 02138; mikesimonsen@aavso.org

Abstract A humorous look at amateur astronomers and the lengths, extent, and expenses they are willing to go to realize their celestial dreams.

Index to Volume 40

Author

Subject

CEPHEID VARIABLES [See also VARIABLE STARS (GENERAL)]

CHARTS, VARIABLE STAR

PHOTOMETRY, CCD

SU URSAE MAJORIS STARS [See CATACLYSMIC VARIABLES]

VARIABLE STARS (GENERAL)

VARIABLE STARS (INDIVIDUAL); OBSERVING TARGETS

The AAVSO CENTENNIAL HISTORY

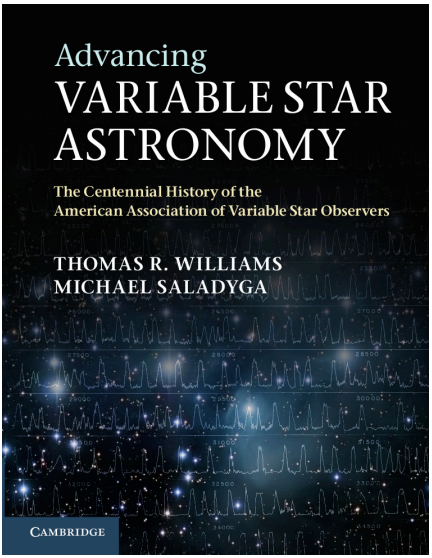

Advancing Variable Star Astronomy: The Centennial History of The American Association of Variable Star Observers

by Thomas R. Williams and Michael Saladyga,
published by Cambridge University Press,
is available through the AAVSO at a special reduced price of $80

Thanks to the generosity of a donor, the purchase price of each book sold through the AAVSO online store will go to benefit the AAVSO

To order, visit the AAVSO online store:

http://www.aavso.org/aavso-online-store

or contact the AAVSO,
49 Bay State Road, Cambridge, MA 02138, USA
phone: 617-354-0484 email: aavso@aavso.org

Now also available as a Kindle e-book through Amazon.com

NOTES